Contactless Human Activity Recognition and Vitals Sensing for Next Generation Smart Homes and Healthcare Centers

Muhammad Farooq

Submitted in fulfilment of the requirements for the
Degree of Doctor of Philosophy

James Watt School of Engineering
College of Science and Engineering
University of Glasgow

June 2025

To Ayesha, Fatima, and Ibrahim,
for filling my journey with wonder, adventure, and love beyond measure.

Abstract

According to the House of Commons Library United Kingdom Parliament, approximately 7.9 million people live alone in the UK. Out of 7.9 million,over 3.1 million adults aged 65 and above live alone in the UK. The older population in the UK is projected to grow, with people aged 65 and over making up 24% of the population by 2043 (17.4 million people). Given this background, the development of a monitoring system that can recognize an emergency or health condition is desired by healthcare providers and families of individuals living alone. Unusual changes in a lonely living person's regular daily mobility routine at home can indicate early symptoms of developing health problems.

This thesis paves the way to develop a novel system that exploit Energy, LoRa, WiFi, RF and radar based technologies to monitor human activity, including presence detection, postural transitions such as walking, sitting, standing, lying, and fall detection. Additionally, it introduces a robust framework for contactless vital signs monitoring, enabling accurate measurement of breath rate, pulse, heart rate, and heart sounds. The integration of AI-driven anomaly detection enhances the system's ability to identify potential health risks in real-time. The research further explores the fusion of human activity recognition with vital signs monitoring to develop a complete, scalable, and privacy preserving solution for both general well-being and clinical healthcare applications. By developing advanced signal processing techniques and machine learning models, the proposed system aims to provide an efficient, non-invasive alternative to conventional health monitoring methods.

Further contributions include a contactless framework for sleep pattern recognition, utilizing micro doppler radar signals to classify sleep postures and detect abnormalities associated with autism spectrum disorder. The study also advances non-invasive health monitoring through radar systems for vital signs detection, achieving high accuracy in respiration and heart rate variability assessment. Moreover, heart sound detection and analysis enhance cardiac monitoring, improving pulse detection, heart rate estimation, and overall reliability of vital signs monitoring.

This work contributes to the future of smart living by ensuring continuous, real time health monitoring without compromising user's comfort and privacy. Future research will focus on improving system adaptability, enhancing multimodal sensing capabilities, and addressing data security challenges to facilitate widespread deployment in next generation smart homes and medical facilities.

Contents

List of Tables

List of Figures

List of Abbreviations

AC - Alternating Current
AI - Artificial Intelligence
AR - Augmented Reality
BPM - Beats Per Minute
CFR - Contactless Frequency Radar
DNN - Deep Neural Network
ECG - Electrocardiogram
FMCW - Frequency-Modulated Continuous-Wave
HR - Heart Rate
HS - Heart Sounds
IoT - Internet of Things
ML - Machine Learning
NLP - Natural Language Processing
RF - Radio Frequency
SFCW - Step Frequency Modulated Continuous Wave
STFT - Short-Time Fourier Transform
UWB - Ultra-Wideband
VGG - Visual Geometry Group
VR - Virtual Reality
WHO - World Health Organization
SDG - Sustainable Development Goals
AIoT - Artificial Intelligence of Things
RNN - Recurrent Neural Network
CNN - Convolutional Neural Network
SNR - Signal-to-Noise Ratio
FFT - Fast Fourier Transform
MSE - Mean Squared Error
TPR - True Positive Rate
FPR - False Positive Rate

List of Publications

Journal Papers

1. **Farooq, Muhammad,** Syed Aziz Shah, Dingchang Zheng, Ahmad Taha, Muhammad Imran, Qammer H. Abbasi, and Hasan Tahir Abbas. "Contactless Heart Sound Detection Using Advanced Signal Processing Exploiting Radar Signals," in IEEE Journal of Biomedical and Health Informatics, vol. 29, no. 2, pp. 1009-1020, Feb. 2025, doi: 10.1109/JBHI.2024.3490992.

2. **Farooq, Muhammad,** Hira Hameed, Balal Saleemi, Ahmad Taha, Dena Al-Thani, Marwa Qaraqe, Muhammad Ali Imran, Hasan Abbas, and Qammer H. Abbasi. "Contactless Sleep Monitoring for Early Autism Detection." Nature Scientific Report (2025). (Under Review)

3. **Farooq, Muhammad,** Syed Aziz Shah, Ahmad Taha, Muhammad Ali Imran, Qammer H. Abbasi, Hasan Tahir Abbas "Contactless Snores Apnea Detection During Sleep by Exploiting Radar Signal." Nature Communications Medicine (2025). (Under Review)

4. **Farooq, Muhammad,** Ahmad Taha, Muhammad Ali Imran, Qammer H. Abbasi, Hasan Tahir Abbas "Contactless Stethoscope Exploiting Radar Based Heart Sounds." IEEE Internet of Things Journal (2025). (Submitted)

5. **Farooq, Muhammad,** Ahmad Taha, Muhammad Ali Imran, Qammer H. Abbasi, Hasan Tahir Abbas "Contactless Blood Pressure Monitoring Exploiting PPG and Radar Signal." Nature Communications Engineering (2025). (Writing Up)

6. Ge, Yao, Wenda Li, **Muhammad Farooq,** Adnan Qayyum, Jingyan Wang, Zikang Chen, Jonathan Cooper, Muhammad Ali Imran, and Qammer H. Abbasi. "LoGait: LoRa sensing system of human gait recognition using dynamic time wraping." in IEEE Sensors Journal, vol. 23, no. 18, pp. 21687-21697, 15 Sept.15, 2023, doi: 10.1109/JSEN.2023.3297438. (Published)

7. Khan, Muhammad Zakir, Muhammad Usman, Ahsen Tahir, **Muhammad Farooq,** Adnan Qayyum, Jawad Ahmad, Hasan Abbas, Muhammad Imran, and Qammer H. Abbasi.

"Transparent RFID tag wall enabled by artificial intelligence for assisted living." Scientific Reports 14, 18896 (2024). https://doi.org/10.1038/s41598-024-64411-y (Published)

8. Prisila Ishabakaki, **Muhammad Farooq,** Muhammad Ali Imran, Qammer H. Abbasi, and Hasan Tahir Abbas. "Non-Invasive Vital Signs Sensing: Advances, Challenges, and Future Directions in Radio Frequency-Based Techniques."IEEE Open Journal of Antennas and Propagation, (2025). (Under Review)

Book Chapters

1. Muhammad Zakir, **Muhammad Farooq,** Ahmad Taha, Adnan Qayyum, Fehaid Alqahtani, Adnan Nadeem Al Hasan, Kamran Arshad et al. “Chapter three - indoor localization technologies for activity-assisted living: Opportunities, challenges, and future directions,” in Internet of Things: Architectures for Enhanced Living Environments, ser. Advances in Computers, G. Marques, Ed. Elsevier, 2024, vol. 133, pp. 59–98.

Conference Papers

1. **Farooq, Muhammad,** Prisila Ishabakaki, Syed Aziz Shah, Ahmad Taha, Muhammad Ali Imran, Qammer H. Abbasi, and Hasan Tahir Abbas. "Contactless Sleep Quality and Vital Signs Monitoring for Autism Spectrum Disorder Detection" IEEE International Symposium on Antennas and Propagation and USNC-URSI Radio Science Meeting (USNC-URSI), 2025. (Accepted)

2. **Farooq, Muhammad,** Balal Saleemi, Prisila Ishabakaki, Syed Aziz Shah, Ahmad Taha, Muhammad Ali Imran, Qammer H. Abbasi, and Hasan Tahir Abbas. "Contactless Sleep Quality Monitoring Exploiting Radar Signal" IEEE MICROWAVE, ANTENNAS & CIRCUITS (ICMAC 2025), 2025. (Accepted)

3. **Farooq, Muhammad,** Hira Hameed, Prisila Ishabakaki, Syed Aziz Shah, Ahmad Taha, Muhammad Imran, Qammer H. Abbasi, and Hasan Tahir Abbas. "Breathing Rate Variability Impact on Heart Rate Estimation Through Radar Sensing," 2024 IEEE International Symposium on Antennas and Propagation and INC/USNC-URSI Radio Science Meeting (AP-S/INC-USNC-URSI), Firenze, Italy, 2024, pp. 2799-2800, doi: 10.1109/AP-S/INC-USNC-URSI52054.2024.10734335.

4. **Farooq, Muhammad,** Hira Hameed, Ahmad Taha, Muhammad Imran, Qammer H. Abbasi, and Hasan Tahir Abbas. "Contactless Respiration Variability Detection and Accuracy Test Using UWB Radar," 2024 18th European Conference on Antennas and Propa-

gation (EuCAP), Glasgow, United Kingdom, 2024, pp. 1-4, doi: 10.23919/EuCAP60739.2024.10501651.

5. **Farooq, Muhammad,** Yao Ge, Adnan Qayyum, Chong Tang, Amir Hussain, Muhammad Ali Imran, Ahmad Taha, Qammer H. Abbasi, and Hasan Tahir Abbas. "Privacy-Preserving Speaker Recognition Using Radars for Context Estimation in Future Multi-Modal Hearing Assistive Technologies," 2023 IEEE International Radar Conference (RADAR), Sydney, Australia, 2023, pp. 1-5, doi: 10.1109/RADAR54928.2023.10371189.

6. **Farooq, Muhammad,** Adnan Qayyum, Yao Ge, Muhammad Zakir Khan, Ahmad Taha, Muhammad Ali Imran, Qammer H. Abbasi, and Hasan Tahir Abbas. "LoRa-based Privacy-Aware and Contactless Surveillance in Next-generation Smart Homes," 2023 IEEE International Symposium on Antennas and Propagation and USNC-URSI Radio Science Meeting (USNC-URSI), Portland, OR, USA, 2023, pp. 1751-1752, doi: 10.1109/USNC-URSI52151.2023.10238314.

7. **Farooq, Muhammad,** Mahmoud A. Shawky, Aisha Fatima, Ahsen Tahir, Muhammad Z. Khan, Hasan T. Abbas, Muhammad Imran, Qammer H. Abbasi, and Ahmad Taha. "Room-Level Activity Classification from Contextual Electricity Usage Data in a Residential Home," 2023 International Telecommunications Conference (ITC-Egypt), Alexandria, Egypt, 2023, pp. 96-100, doi: 10.1109/ITC-Egypt58155.2023.10206425.

8. Prisila Ishabakaki, **Muhammad Farooq,** Muhammad Ali Imran, Qammer H. Abbasi, and Hasan Tahir Abbas. "RF Sensing for Automated Classification of Stimming Behaviors in ASD: A First Step Toward Contactless Screening" IEEE MICROWAVE, ANTENNAS & CIRCUITS (ICMAC 2025), 2025. (Accepted)

9. Balal Saleemi, **Muhammad Farooq,** Muhammad Ali Imran, Qammer H. Abbasi, and Hasan Tahir Abbas. "RF Sensing for Automated Classification of Stimming Behaviors in ASD: A First Step Toward Contactless Screening" IEEE MICROWAVE, ANTENNAS & CIRCUITS (ICMAC 2025), 2025. (Accepted)

10. Prisila Ishabakaki, **Muhammad Farooq,** Muhammad Ali Imran, Qammer H. Abbasi, and Hasan Tahir Abbas. "'A Two-Stage Deep Learning Framework for Enhanced Radio Frequency Sensing Reliability" IEEE International Symposium on Antennas and Propagation and USNC-URSI Radio Science Meeting (USNC-URSI), 2025. (Accepted)

11. Zaidi, Fatima, Hira Hameed, **Muhamamd Farooq,** Aisha Fatima, Kamran Arshad, Khaled Assaleh, and Qammer H. Abbasi. "Privacy-Preserving Visual Cues Communication for Hearing-Impaired People Using Deep Learning," 2024 IEEE International Conference on Image Processing (ICIP), Abu Dhabi, United Arab Emirates, 2024, pp. 2885-2888, doi: 10.1109/ICIP51287.2024.10647125.

12. Ishabakaki, Prisila, Hira Hameed, **Muhammad Farooq,** Umer Saeed, Syed Aziz Shah, Muhammad Ali Imran, and Qammer H. Abbasi. "RF-Based Respiration Disorders Sensing and Classification Using Machine Algorithms," 2024 IEEE International Symposium on Antennas and Propagation and INC/USNC-URSI Radio Science Meeting (AP-S/INC-USNC-URSI), Firenze, Italy, 2024, pp. 1881-1882, doi: 10.1109/AP-S/INC-USNC-URSI52054.2024.10686093.

13. Hameed, Hira, Prisila Alex Ishabakaki, **Muhammad Farooq,** Aisha Fatima, Kamran Arshad, Khaled Assaleh, Muhammad Ali Imran, and Qammer H. Abbasi. "BSLR: Bridging Communication Gaps with Wi-Fi Enabled British Sign Language Recognition," 2024 IEEE International Symposium on Antennas and Propagation and INC/USNC-URSI Radio Science Meeting (AP-S/INC-USNC-URSI), Firenze, Italy, 2024, pp. 345-346, doi: 10.1109/AP-S/INC-USNC-URSI52054.2024.10686089.

14. Hameed, Hira, Mostafa Elsayed, **Muhammad Farooq,** Jaspreet Kaur, Muhammad Usman, Amir Hussain, Abd El-Latif, A. Ahmed, Muhammad Imran, and Qammer H. Abbasi. "Exploring Hand Gesture Recognition: Trends, Technologies, and Application," 2025 3rd International Conference on Intelligent Data Communication Technologies and Internet of Things (IDCIoT), Bengaluru, India, 2025, pp. 1809-1812, doi: 10.1109/IDCIOT64235.2025.10914713.

15. Khan, Muhammad Zakir, **Muhammad Farooq,** Ahmad Taha, Naeem Ramazan, Muhammad Ali Imran, and Qammer H. Abbasi. "Localization using wireless sensing for future healthcare," 2022 29th IEEE International Conference on Electronics, Circuits and Systems (ICECS), Glasgow, United Kingdom, 2022, pp. 1-4, doi: 10.1109/ICECS202256217.2022.9971116.

16. Khan, Muhammad Zakir, Ahmad Taha, **Muhammad Farooq,** Mahmoud A. Shawky, Muhammad Imran, and Qammer H. Abbasi. "Comparative Analysis of Artificial Intelligence on Contactless Human Activity localization," 2022 International Telecommunications Conference (ITC-Egypt), Alexandria, Egypt, 2022, pp. 1-3, doi: 10.1109/ITC-Egypt55520.2022.9855712.

Acknowledgements

During the course of my academic journey, I have been truly fortunate to be surrounded by exceptional mentors, supportive colleagues, and a loving family. The work presented in this thesis is not the result of my efforts alone; it is the culmination of the collective encouragement, patience, and unwavering belief of those who stood beside me through each step of this long and challenging journey.

I would like to take this opportunity to express my deepest gratitude to my supervisors, Dr. Hasan Abbas, Prof. Qammer H. Abbasi, Prof. Muhammad Ali Imran, and Dr. Ahmed Taha, for their invaluable guidance, continuous support, and insightful feedback throughout the course of my PhD. Their mentorship has been instrumental in shaping my research and enabling me to overcome the many challenges along the way.

A special note of heartfelt appreciation to Prof. Qammer H. Abbasi, whose unwavering mentorship, visionary guidance, and steadfast support have been central to my academic development. His constant encouragement, timely advice, and ability to challenge my thinking have helped me grow not only as a researcher but also as a person. I am immensely grateful for his belief in my work and the many opportunities he provided to push the boundaries of my potential.
My sincere appreciation also extends to my colleagues Muhammad Zakir Khan, Yao Gi, Aziz Shah, and fellow researchers in CSI Group, and those, whose names are not mentioned here, and whose collaboration and stimulating discussions played a crucial role in refining my ideas and enhancing the quality of my work.

I owe a great deal of appreciation to my all other colleagues and friends within the lab and research community; those with whom I shared brainstorming sessions, academic discussions, long hours of experiments, and the occasional much-needed laughter. Their companionship and intellectual camaraderie made the process not only more productive but also more enjoyable. I am especially grateful to those who reviewed my work, challenged my assumptions, and supported me in both professional and personal capacities during this time.

I would also like to sincerely thank the College of Science and Engineering at the University of Glasgow for awarding me a School Scholarship, which made it possible for me to pursue this research. Their support provided not just financial relief but also the resources and platform

necessary to conduct meaningful work in the field of contactless sensing for healthcare. This

PhD journey would have been incomplete without the love and support of my family. To my parents, I express my deepest gratitude. Their prayers, sacrifices, and quiet strength have been the foundation of everything I have achieved. They have always supported my ambitions, even when it meant enduring the emotional strain of separation during my extended stays abroad. It is because of their values and encouragement that I have reached this milestone.

Thank you mother for everything.

A heartfelt thank you to my wife Mehtab Rehman, who has been my pillar of support, offering endless patience, love, and understanding. Her encouragement, sacrifices, and unwavering belief in my abilities have made this achievement possible. She has been my source of motivation, ensuring that I remain focused and determined despite the challenges along the way.

A very special thanks to my beloved children; Ayesha Farooq, Fatima Farooq, and Muhammad Ibrahim, who endured my long absences and the disruption caused by my extended stays abroad for research. I am deeply aware of the time I missed with them during crucial years of their growth. Despite the challenges, they have shown immense strength, resilience, and understanding. I am especially thankful for the joy and motivation they brought when they joined me later during my PhD journey. Their love and presence gave me renewed energy and a constant reminder of why this journey matters.

Finally, I extend my gratitude to my friends and well-wishers, who have stood by me, offering their encouragement and support in both academic and personal capacities. This PhD journey has been a challenging yet rewarding experience, and I am truly grateful to everyone who has been a part of it.

To all my teachers, mentors, and friends, whether mentioned by name or not, who have played a role in shaping my academic and personal development, I thank you with all my heart.

This thesis is a shared accomplishment, and I dedicate it to all those who walked with me on this path. Thank you!

Muhammad Farooq
University of Glasgow, 2025

Declaration

University of Glasgow

College of Science & Engineering

Statement of Originality to Accompany Thesis Submission

Name: Muhammad Farooq
Registration Number: xxxxxxx

I certify that the thesis presented here for examination for a PhD degree of the University of Glasgow is solely my own work other than where I have clearly indicated that it is the work of others (in which case the extent of any work carried out jointly by me and any other person is clearly identified in it) and that the thesis has not been edited by a third party beyond what is permitted by the University's PGR Code of Practice.

The copyright of this thesis rests with the author. No quotation from it is permitted without full acknowledgement.

I declare that the thesis does not include work forming part of a thesis presented successfully for another degree.

I declare that this thesis has been produced in accordance with the University of Glasgow's Code of Good Practice in Research.

I acknowledge that if any issues are raised regarding good research practice based on review of the thesis, the examination may be postponed pending the outcome of any investigation of the issues.

Signature: Muhammad Farooq

Date: 18 March 2025

Statement of Copyright

Chapter 1

Foundations and Background

1.1 Background and Motivation

The number of single-person households is gradually increasing worldwide [2]. In the United Kingdom alone, as of Jun 2021, according to the House of Commons Library [3], approximately 7.9 million people live alone, with over 3.1 million of them aged 65 or older [3, 4]. In England alone, there were an estimated 24.7 million households in self-contained accommodation in 2023-24. These 24.7 million exclude those in institutional settings such as nursing homes or student accommodations. Notably, 30% of these households (approximately 7.4 million) were occupied by individuals aged 65 or older, while 3% of households were in the 16-24 age group and 15-18% in the 25-64 age group, reflecting the growing aging population living alone. This older population (65 or older) is projected to grow significantly, reaching 24% of the total population (17.4 million people) by 2043.

Older adults are particularly susceptible to health risks such as cardiovascular diseases, respiratory disorders, and mobility impairments. Given this trend, there is a growing need for remote health monitoring systems capable of detecting emergencies, deteriorating health conditions, and abnormal changes in daily routines. Traditional healthcare systems have primarily relied on sensor-based technologies to track physical activity and vital signs [5]. Wearable devices can monitor heart rate, blood pressure, breathing rate, and sleep patterns, but they often suffer from user compliance issues, discomfort, privacy concerns, and high operational costs [6, 7]. Recent studies demonstrate the efficacy of contactless sensing methods, such as radar-based heart sound detection, respiration monitoring, and energy consumption analysis, to provide continuous and unobtrusive health tracking [8]. As a result, healthcare providers and families are increasingly interested in non-invasive monitoring systems that can detect health emergencies or early signs of deteriorating health conditions among individuals living alone.

While detecting deviations in daily activity patterns can indicate emerging health problems, integrating physiological monitoring can provide deeper insights into an individual's well-being. Abnormalities in vital signs such as irregular heartbeats, fluctuating blood pressure, or breath-

ing difficulties are early indicators of cardiovascular diseases, respiratory disorders, and sleep-related conditions. Recent advancements in radio frequency (RF) sensing, radar, and AI-driven signal processing have demonstrated the feasibility of monitoring vital signs without requiring direct physical contact. For instance, radar-based sensing can track heart sounds, pulse, heart rate, respiration variability, and snore-induced apnea episodes, key areas explored in recent studies. Furthermore, WiFi, LoRa, radar, and RFID-based localization technologies offer potential solutions for non-intrusive, real-time health monitoring in smart homes.
Despite their potential, traditional sensor-based monitoring systems face adoption challenges due to privacy concerns, device complexity, and maintenance costs. A more practical and widely accepted approach involves leveraging existing smart home infrastructure, such as:

- Radar based monitoring for contactless tracking of activities and vital signs.
- WiFi and LoRa enabled health detection for seamless, privacy-preserving surveillance.
- Energy consumption data to infer activity and detect anomalies in behaviour.

Moreover, optimizing energy usage patterns can not only support health monitoring but also contribute to net-zero carbon emission goals, aligning with broader sustainable development initiatives.

1.2 Problem Description

The problem of finding unusual changes in the daily behavior of an adult who lives independently at home has been widely investigated in the literature [9]. Most of the solutions are sensor-based systems categorized as wearable and nonwearable sensors that track the day-to-day activities of the lonely living adults and notify when detecting an anomaly behavior [10].

Some past research show that elderly adults do not appreciate camera-based and wearable sensors due to discomfort in wearing sensors all the time, and sometimes they don't remember to wear sensors [11]. Camera-based sensors are computationally complex and lose the user's privacy when monitoring at home [12]. Moreover, most of the existing systems require an explicit explanation or labeling process, which is offline to manually configure the typical behavior of the monitored persons before using the system [11, 12].

A contactless human activities and vitals monitoring system can help identify unusual happenings leading to serious health issues with lonely living people [13]. Besides, eliminating unwanted energy and economic load identified from energy usage patterns and unwanted health issues will help achieve sustainable development goals related to net zero, good health and well being.

1.3 Problem Statement

This research focuses on the development of a contactless human activity recognition and vital signs detection portable system which can help the betterment of health and wellbeing of lonely living people in the next generation smart houses and healthcare centres.

1.4 Research Aim and Objective

Research Aim

Development of human activity recognition and vital detection system using contactless sensors that will contribute towards the betterment of humans living in the next generation smart homes and healthcare centres.

Objective

- Research and development of contactless human activity detection system which identifies presence, walking, sitting, standing, lying, and fall detection of human targets in confined and open spaces.
- Research and development of a vital signs detection system that can accurately identify the breath rate, heart rate, and heart sounds of human targets in confined spaces.
- Development of combined human activity and vitals detection systems for clinical healthcare applications.

1.5 Contributions

This thesis builds upon recent advancements in contactless health monitoring and privacy-aware surveillance to develop a robust, non-invasive system that integrates:

- Contactless monitoring of sleep, autistic behaviours, apnea, hypopnea and snores monitoring system.
- Human activity recognition through behaviour and sleep analysis.
- Contactless vital sign monitoring, including pulse, heart rate, respiration rate, heart sounds, and blood pressure using RF and radar-based techniques.
- AI-powered anomaly detection to identify potential health risks using radar, RF, LoRa, and WiFi.

- Smart home energy analytics to enhance monitoring accuracy while promoting sustainability.

By combining physiological sensing, activity tracking, and AI-driven analysis, this research aims to provide a scalable and privacy-preserving solution to improve the quality of life for individuals living alone.

1.6 Thesis Organisation

This thesis is organized into seven chapters. Chapter 1 introduces the study, outlining its motivation and objectives. Chapter 2 provides a detailed overview of research prevalence, a literature survey, identified gaps, and potential research opportunities. Chapters 3 and 4 present various contactless human activity detection techniques, while Chapters 5 focus on novel RF and radar-based methods for human vital signs detection in smart homes and healthcare centres. Chapter 6 explores contactless heart sounds detection, emphasizing its significance in real time vital sign monitoring and its contribution towards the development of contactless blood pressure monitoring systems. Chapter 7 focuses on applications derived from the integration of human activity detection and vital signs monitoring. These applications include the detection of autistic behaviours, apnea, hypopnea, and snoring by combining contactless sleep monitoring with vital sign analysis. Each chapter systematically addresses critical aspects of the research problem, methodology, findings, and conclusions, ensuring a clear and coherent presentation of the research. Further, apart from the groups of chapters mentioned above, a high-level detail of all chapters is given in below paragraphs.

Chapter 1 introduces the research problem, objectives, and significance of the study. It provides an overview of the research background and the motivation behind conducting the research. Additionally, this chapter outlines the key research questions and hypotheses that direct the investigation.

Chapter 2 presents a systematic literature review, validate relevant theoretical frameworks and previous research in the field. This chapter critically evaluates existing studies, identifies gaps in research, and establishes the foundation for the research.

Chapter 3 details the research methodologies for human activities recognition from electricity and LoRa sensing, describing the study design, data collection techniques, and analytical methods. It explains the foundation behind selecting specific methodologies and discusses ethical considerations related to the research.

Chapter 4 focuses on the results and analysis for human activity detection by using software radio defined and Radar systems. This chapter illustrates the findings of the study using tables, figures, and statistical analyses. The results are interpreted in relation to the research questions and hypotheses.

Chapter 5 discusses the implications of the findings from human vital signs detection, com-

paring them with previous studies and theoretical perspectives. This chapter also illustrates practical applications, limitations of the study, and potential foundation for future heart sounds based vital signs monitoring.

Chapter 6 focuses on radar based contactless heart sounds detection, limitations and gaps in conventional radar based vital signs detection, identifies key situations in which contactless conventional pulse and heart rate detection fails but our state-of-the-art heart sounds based pulse and heart rate detection system shows high accuracy and reliability.

Chapter 7 focuses on applications derived from the integration of human activity detection and vital signs monitoring. These applications include the detection of autistic behaviours, apnea, hypopnea, and snoring by combining contactless sleep monitoring with vital sign analysis.

Chapter 8 concludes the thesis by summarizing the key findings, highlighting their significance, and providing final reflections on the research contributions. It also offers recommendations for policymakers, practitioners, and researchers in the field.

This thesis organization ensures a systematic and comprehensive presentation of the research, demonstrates a clear understanding of the research process and its outcomes.

Chapter 2

Eyeing Human Activity and Vitals from The Contactless Sensing Perspective

2.1 Contactless Sensing: Enabling Technologies and Applications

Different from traditional sensor-based sensing, wireless sensing does not need any sensors but relies on the signal itself for sensing. The sensor-free and contact-free nature makes wireless sensing appealing in many real-life scenarios. Diverse wireless sensors have been employed for sensing including contactless sensors such as WiFi [14, 15] , LoRa [16], FMCW radars [17], 60GHz radar [18, 19], Ultra-wide-band (UWB) radars [20], ultrasonic [21, 22], RFID [23, 24], visible light [25, 26], Occupancy sensors, smart energy meters, smart energy plugs, location sensing and camera-based sensors had been deployed for sensing purpose. The underlying principle of wireless sensing is that wireless signals get reflected from the target and the reflection signals vary with target movements. By carefully analyzing the movement-induced signal variation, rich context information of the target can be obtained.

In recent years, joint sensing and communication using wireless signals have been widely studied for different future smart home systems and other sensing applications [27–29]. Using ambient wireless signals like LoRa and WiFi rather than a camera provides three advantages. First, it preserves the users' privacy without requiring to record videos of daily life activities. Secondly, it resolves the limitations of video-based analysis by allowing sensing through-wall and dark spaces. Last but not the least, the utilisation of ambient signals like LoRa and WiFi reduces the cost. Although it requires computation resources to support the sensing algorithm like edge computing, the system's transceiver units are provided by current communication facilities.

The problem of recognising humans from their walking patterns is known as gait recognition. It has many potential applications in surveillance, healthcare, and human-computer interaction. In the literature, WiFi-based sensing has provided various solutions for gait recognition [30, 31].

However, the nature of the WiFi signal restricts the sensing range [16, 32]. Therefore, WiFi-based systems cannot be adopted in long-range spaces, e.g., corridors.

Contactless sensing has been employed in many complex health and wellbeing monitoring applications [33, 34] such as security and survival in life saving operations [35, 36], intrusion detection [37], indoor and outdoor human activity recognition [38], localization [39], key stroke detection [40] and vitals monitoring [33] in the past few years.

2.2 WiFi-based sensing

The research community has gained significant interest in human activity detection in indoor environments due to its potential uses in independent living, remote healthcare monitoring, and intrusion detection. In fact, the UK's national strategy for 2030 includes independent living as part of its policy of healthy communities [41]. The United Nations estimates that there were 901 million people over 59 years old globally in 2015, and that number will increase to 2.1 billion by 2050 [42]. The growing number of elderly people with chronic diseases, medical emergencies, and disabilities have an effect on the social and economic situations of all nations and ultimately raise the cost of healthcare systems substantially [43].

To address these challenges, some countries and nonprofit organizations began to advocate for ambient computing. Its primary objective is to extend the period of time that older people can live freely in their homes. During the last decade, human activity detection (HAD), vital sign monitoring, and location tracking have attracted the most interest in ambient computing [44]. Since it can provide doctors access to clinical information and people to health management, HAD is an important indicator for evaluating the health of the elderly.

Due to the GPS's (Global Positioning System) low accuracy and signal attenuation imposed by various physical infrastructures, localization in this type of environment is not practical [44]. However, as of right now, there isn't a de facto system like GPS for outside localization. Instead, there are many different kinds of indoor localization systems.

In the literature, a number of human activity detection systems that make use of wearable, cameras, and ambient sensors have been presented. However, these methods either cause discomfort or are cumbersome from wearing wearable all the time or privacy concerns. Using a system for wireless HAD can help with these issues. Numerous wireless sensing alternatives are suggested in the literature in this area, using doppler fingerprints from radar systems [45] or CSI from WiFi [46] and 5G wireless networks [47].

Many applications use RF-based Wi-Fi sensing due to the usage of existing WiFi infrastructure already installed in many homes, eliminating the need to introduce extra sensing equipment. Different RF-sensing-based systems have different hardware requirements, operating radio frequencies, classification algorithms, quantities of monitored activities, and quantities of subjects. Available tracking methods for RF signal activity detection can use either the Received Signal

Strength Indicator (RSSI) [48] or CSI [46]. According to studies such as [49], although RSSI gives coarse information, CSI is fine-grained and measured each Orthogonal Frequency Division Multiplexing (OFDM) packet. CSI is thus a better option for activity detection and localization due to its increased attention to detail.

2.3 LoRa-based sensing

Applications that already have used LoRa networks so far include vehicle tracking [50], facility management [51], intelligent building control [52], environment monitoring [53, 54], and smart agriculture [55]. Prior LoRa network research has mostly been focused on empowering the Internet of Things (IoT) applications with LoRa's long-range capacity. [56,57] has transferred data from IoT-based sensors using the LoRa network. LoRaMote is attached to a person's arm with a band equipped with a set of sensors (e.g., temperature and pressure) to monitor the human target's health condition [34]. [52] deployed LoRa sensors on corridors, windows, and roofs to form a mesh network to send data collected from LoRa sensors for campus monitoring. [51] collected data from IoT based LoRa sensors from different industrial application. [58] has employed LoRa sensors for indoor human activity recognition by using received signal strength indicator (RSSI) measurement and found that high energy and long-range LoRa sensors have better results than WiFi, Bluetooth and Bluetooth low energy sensors. Despite being useful for localisation, we observe that the RSSI measurement is still a piece of coarse information that cannot detect fine-grained human activity. A multi-band backscatter system for localization with sub-centimetre-sized devices is developed in the most recent work suggested by [59]. For comparison, we use standard LoRa devices in this work to explore the passive sensing capability of the LoRa signal without relying on specialised sensors. Other popular wireless technologies for sensing include Examining the passive sensing capabilities of the LoRa signal instead of relying on specialised sensors. More wireless sensing methods such as FMCW radar [33, 60], Doppler radar [61], millimeter wave radar [62], UWB radar [20], commodity RFID [23], Zigbee [63] and WiFi [14], are frequently used for sensing. Adib et al. detect users' breathing rate by using specialised equipment like FMCW radar and UWB radar, and the sensing accuracy is pretty high even at a distance of up to 8 metres from the device [33]. Among all the specialized device-based solutions, such as Zigbee, RFID, WiFi, and WiFi-based human activity recognition is the most popular one and has found many practical applications such as human respiration detection [64], gesture recognition [65] and localization [66]. For example, [64, 67] has leveraged commodity-based WiFi devices to detect respiration rate for different people who are 2-4 meter away from each other IndoTrack used existing Wi-Fi devices to sense human activity in a short range of 6-8 meters [68]. Short range sensing capabilities of WiFi and radar is good however long range and high-energy capabilities of LoRa sensing are still unmatched in all other sensing technologies. However for short range sensing, existing WiFi devices has good results.

2.4 Energy-based Sensing

IoT devices have been used to monitor individual households in several ways. IoT devices include cameras, wearable technology, specialized sensors, and smart plugs. The highest levels of accuracy are now possible with vision-based activity recognition systems such as in [69, 70]. Still, most users are unwilling to install cameras in their homes out of privacy concerns. Since they need people to wear and charge wearable devices at home, many believe that methods like those in [71] are intrusive and increase the daily burden. [72, 73] presented a method of determining household activities by observing how much power each device uses in a home. However, these devices also have a cost and need maintenance services, including installation, calibration, power supply, and site monitoring. Despite achieving greater context awareness, the IoT device usage method has an issue with the cost involved. Smartphone applications are not just expensive but also inconvenient for households with more than one person. As a result, utilizing utility data provides benefits over using other IoT-based technologies. The residential sector's continuous rise in energy consumption has opened the door for the emergence of new technologies that promise to transform the way electricity is generated, managed, and consumed. The literature has shown there is great interest in using utility data, such as electricity, water, and gas, for activity recognition [74, 75]. This non-invasive approach is helpful because it makes it easy to get the needed information without invading privacy or causing discomfort to individuals. The anomaly detection approach includes using historical data to predict daily consumption and then determining if the actual consumption differs noticeably from the expected amount. It is considered an abnormality if the difference is too high. The prior work's activity detection-based approach using energy consumption data used power disaggregation technology, commonly known as non-intrusive load monitoring (NILM) [76]. Since NILM generally requires one second of sampling data and is only partially applied to commercialization, providing a cost-effective elderly people daily activity monitoring service within a room is not practical. Recently, activity monitoring technologies have been suggested as a valuable way to assist decision-making and reduce the burden on caretakers to detect emergencies concerning elderly people [77, 78]. Most of these technologies use internet of things (IoT) devices or smartphone applications to monitor individual health in real-time [2, 79].

Based on prior work, our approach focuses on activity detection utilizing electricity usage data. The proposed solutions using data on electricity consumption are preferred among all the utility data. Since utility data and electricity usage are personal information, privacy is crucial for this study. Artificial intelligence (AI) technology shouldn't invade people's privacy, even if it's used for good reasons, like keeping an eye on older adults, which is one of the applications discussed in this work. This study aims to create a monitoring system that can automatically evaluate daily activities inside the house. The proposed methodology attempts to improve on non-invasive technologies that target providing assisted living to elderly people. Furthermore, the long-term goal is to see such a technique utilised in nursing homes for elderly adults, in the

United Kingdom.

2.5 Radar-based Sensing

Different from traditional sensor-based sensing, contactless sensing does not require any sensors but relies on the signal itself for detection. The sensor-free and contact-free nature make contactless sensing appealing in many real-life applications including security and survival in life-saving operations, intrusion detection, indoor and outdoor human activity recognition and vitals monitoring. Diverse contactless sensors such as WiFi [80], long range radio (LoRa) [81], RFID [82], radars [83], ultrasonic and visible light have been deployed for sensing purposes.

The underlying principle of contactless sensing is that wireless signals get reflected from the target and the reflection signals vary with target movements [84]. By carefully analysing the movement-induced signal variations, rich contextual information regarding the target's movements can be obtained. As compared to other contactless sensing technologies such as WiFi, RFID, FMCW radars, and ultrasounds, which have a few meters sensing range, LoRa has a relatively very high range and high energy signal which can easily pass through obstacles and brick walls. This makes it highly suitable for applications where low range, low energy, and high power consumption signals do not work.

In one of our APS paper [85]; we presented a LoRa signal by using a pair of universal software radio peripherals (USRP), one as a transmitter having one antenna and another as a receiver have two antennas to detect people from their walking patterns through a thick brick wall. Human activity include strolling outside the room wall and the resulting information is person detection from their walking patterns. Below sections include experimental setup, data collection, pre-processing of the complex I/Q signal data and walking patterns results for the strolling activities of six different people.

Speaker recognition is the process of identifying or verifying the identity of an individual based on their voice [86]. It has a wide range of applications including security, authentication, and access control. Traditional SR systems rely on audio signals captured by microphones, which can be affected by background noise, distance, and some environmental factors [87, 88]. SR using audio-visual signals, which involves combining information from both audio and visual cues to identify or verify the speaker's identity, has gained increasing attention in recent years [89, 90]. While SR using audio-visual signals has the potential to improve the accuracy and reliability of SR systems [91–93], it is important to consider the limitations of this technology [94]. These limitations include lighting conditions, environmental noise, occlusions, facial expressions, privacy concerns, equipment costs, and algorithmic bias. By understanding these limitations, researchers and practitioners can develop more effective and reliable SR systems [95–97]. In recent years, ultra-wideband (UWB) radar technology has emerged as a promising alternative to traditional microphone-based SR systems. UWB radar technology is

Table 2.1: Summary of contactless sensors used for corpus detection and speaker recognition other than audio-visual techniques.

Reference	Year	Sensing technology	Language	Corpus size	Speakers diversity	Speaker/words recognition	Accuracy
[98]	2022	FMCW radar	European Portuguese words	13	Four speakers	Words	84.50% (average)
[99]	2022	SFCW radar	German words	40	Five male speakers 28 to 36 years old	Words	76.50%
[100]	2022	SFCW radar	Forty German words and digits zero to nine	50	Two individual speakers	Words	94.02% (average)
[101]	2016	Impulse radio ultra-wideband radar	English	5	Five Korean speakers	Words	85%
[102]	2021	RFID	N/A	0	Fifty dynamic and static users	Person	95.05% (average)
[103]	2018	Microwave	German	25	Two male native German speakers	Words	89% (average)

capable of detecting and tracking human movements and can provide information about the individual's vocal tract and speech characteristics, which can be used to identify or verify the speaker's identity. UWB radar technology has several advantages over traditional microphone-based systems. One of the main advantages is its ability to operate in noisy environments, as it is not affected by background noise. It can also penetrate through walls and other obstacles, making it suitable for use in surveillance and security applications. Another advantage of UWB radar is its ability to detect small movements and vibrations, such as those caused by the human vocal tract during speech. Overall, non-invasive radar-based SR technology offers a number of advantages over traditional invasive methods of SR. It is non-invasive, accurate, contactless, versatile, cost-effective, portable, and capable of providing real-time results, making it an attractive option for a wide range of applications. UWB radar technology uses short pulses of electromagnetic waves with a very wide frequency spectrum to detect different changes in objects. The pulses are typically in the range of a few nanoseconds to a few microseconds and are transmitted from an antenna [104–106]. The pulses reflect off objects and are received by a receiver antenna. The time delay between the transmitted and received pulses is used to calculate the distance to the object, while the amplitude and phase of the received pulse provide information about the object's properties, such as lips and vocal tract movements, shape of face and speech characteristics. While exploring silent speech interfaces based on frequency-modulated continuous-wave (FMCW) radar in [98], the author recognized 13 words spoken by four different speakers of Portuguese origin with 84.5% average accuracy. Another step frequency modulated continuous wave (SFCW) radar used for silent speech recognition, total of forty German words including

nouns, adjectives, verbs, and digits spoken by five male native German speakers aged between 28 and 36 years old. Results accuracy for word recognition is 76.50% and 68.18% obtained using the headset and the tape, respectively [99]. While recognizing forty German words and zero to nine German digits from two persons with the help of SFCW radar, author obtained recognition accuracies of 99.17% and 88.87% for the speaker-dependent multi-session and inter-session accuracy respectively (average accuracy 94.02%) [100]. RFID tags have been used for the identification of people for static and dynamic users [102], author collected walking and body information for identification purposes. Other studies includes microwave sensors [103] and Radars [107, 108], details provided in Table 2.1.

The goal of this study is to collect CSI data on a single human subject performing seven different activities (sitting, standing, no-activity, leaning forward, walkingTx-Rx and walkingRx-Tx) in two separate locations in a single room using two USRP devices, one acting as a Transmitter (Tx) and the other as the Receiver (Rx). The amplitude shifts in the CSI distinguish between the activities carried out at each location. As the human movement affects radio signals differently depending on where the activity occurs, this enables CSI to be used to locate a target.

Machine learning (ML) is used to categorize seven separate human activities that are carried out in two different locations apart one meter from each other. The main contribution of this work is the use of ML and Deep Learning (DL) algorithms, namely Random Forest (RF), Support Vector Machine (SVM), K-Nearest Neighbor (KNN), Artificial Neural Networks (ANN), Convolutional Neural Networks (CNN) and Recurrent Neural Networks (RNN), to provide predictions on CSI, collected from USRP devices, to accurately identify and localize seven different activities inside a room. Additionally, the system is capable to identify the direction of the walking in the designated area. Radar, Wi-Fi, and GSM technologies can be used to detect and identify activities without the need of cameras or wearable sensors. Radar-based approaches exhibited accurate localization and continual medical monitoring [109] when there are several targets present by using large antenna arrays and bandwidths. However, such solutions are not yet available or widely accessible, are costly, and need a lot of energy. Since RF sensing is becoming more and more popular in the security and healthcare industries due to the extensive use of low-power sensors. A deep-learning-based approach was used by [110] to categorise various user movement states, such as forward, backward, and no movement. Their system was trained using data from Wi-Fi sensors. According to their research, the model has an accuracy of 89% at a distance of 1.5 meters, but as the distance increases to 2 meters, the accuracy decreases to 74%. As a result, the model's accuracy decreased as the position of motions shifted away from the passive sensing system. Nipu et al. [111] attempted to distinguish between various participants using CSI data. Different participants crossed two devices throughout the experiment while data was being transferred, saving the CSI data they picked up in the process. After that, ML algorithms such as RF and decision tree were applied to the data. Their study demonstrates how a human's movements vary from the CSI patterns. In the research [38], USRP N210

devices were utilized to accurately identify activity with 95%. The authors in [112] evaluated classifiers using a range of features and classification techniques such RF, SVM, KNN, and Linear Discriminant Analysis on the HAR dataset. Highest accuracy was achieved by the classifier RF was 98.16 %. Similar to this, [27] achieved high accuracy of 93.75% on a single subject in line of sight scenario of a corridor having a distance of 20 metres by using USRPs X300 and X310 to distinguish between sitting, standing, and walking activities using the RF, Extra Tree, and Multilayer Perceptrons algorithms.

2.6 Contactless Sensing: Limitations

2.6.1 Installation issues

The sensing range is substantially narrower than the signal communication range in wireless sensing because the information is gathered through reflected signals. The problem is present in all wireless communications. In contrast to RFID and mm Wave-based systems, which have to sense ranges of only 1-3 metres, WiFi, for instance, has a transmission range of 20–50 metres but a sensing range of only 6–12 metres. Due to its extensive communication range, the deployment of LoRa gateways outside may be limited.

LoRa indoor gateways can be denser, and many LoRa nodes are anticipated to be connected to each LoRa gateway. We don't need the gateway and the node to be close to the destination for LoRa sensing to function (10-20m). LoRa signal can be used for sensing as long as one of the nodes is close to the target.

In contrast to an in-door or confined space, LoRa sensing needs to monitor in the outdoor environment with a sparser deployment. We believe there is still space to increase the sensing range further. We expect to achieve around 80-120m sensing range with advanced signal processing in an outdoor environment.

2.6.2 Security Concern

Be aware that long-range sensing may cause privacy and insecurity concerns. The privacy concern is diminished when compared to current video-based monitoring, though sensorless technology, in our opinion, is an intriguing answer to the problem. LoRa devices can use an interference signal to track the signal reflecting from the receiver. It will be challenging to detect the target since the interfering and target-reflected signals would be mixed.

Chapter 3

LoRa Signal and Energy Driven Human Gait Dynamics

3.1 LoRa Based Human Gait Recognition using Dynamic Time Warping

In recent years, joint sensing and communication (JSAC) using wireless signals have been widely studied for different future smart home systems and other sensing applications [27–29, 89]. Sensing with such RF signals is not in itself a new concept in research. The phenomena depend upon the analysis using the radio signal transmission and reception parameters, using the same principles developed to detect the presence of objects in aircraft radar and sonar systems. In wireless transmission systems, the transmission signal's attenuation is inevitable due to path loss, shadowing, and multi-path fading [113]. On the other hand, these attenuations on the wireless channel can be used to map the physical environment where the RF signals are propagating, providing the theoretical underpinning principle for contactless sensing. Using a communication wireless signal is the most cost-efficient way to perform RF sensing since it is easily accessible in most indoor spaces.

The growing interest in JSAC-based sensing systems is due to their practical deployments in indoor settings, as well as their ability to gain responses from monitored persons. Using ambient wireless signals like LoRa and WiFi rather than a camera provides three advantages. First, it preserves the users' privacy—without requiring them to record videos of daily life activities. Secondly, it resolves the limitations of video-based analysis by allowing sensing through-wall and dark spaces. Last but not the least, the utilisation of ambient signals like LoRa and WiFi reduces the cost. Although it requires computation resources to support the sensing algorithm like edge computing, the system's transceiver units are provided by current communication facilities.

This section gives an overview of previous researches in JSAC and gait recognition respectively

with the listed works shown in Table. 3.1. Gait recognition is one of the human recognition methods as gait provide features that are highly related to specific person [121]. The gait recognition method nowadays is vision based mostly. However, recording video or picture can cause privacy issues. In addition, vision based gait recognition is limited with the working scenery. To address these problems, gait recognition based on different sensors is proposed [122].

JSAC is a concept that involves combining sensing and communication functions in a single device or system. This approach can lead to increased efficiency of communication and cost savings, as well as improved performance of sensing. This concept is becoming increasingly important as the Internet of Things (IoT) and other connected devices continue to grow in popularity. Typically, WiFi is one of popular topic in this field due to the high cost-effectiveness compared to other sensors. In [114, 115], two WiFi based human activity recognition system are proposed. Both systems achieved over 95% accuracy in recognizing human activities. WiFi is also used in gait recognition [116, 117], the WiDIGR proposed in [116] achieved 78.28% accuracy in 6 subjects gait recognition. FMCW radar and UWB radar are also commonly used in different situation, including gesture recognition [118], gait recognition [119] and human ac-

Table 3.1: Review of RF sensing works

Reference	**Protocol**	**Carrier Frequency**	**Bandwidth**	**Application**	**Experimental Setup Range and Subjects**	**Performance**
CARM [114]	WiFi	5 GHz	20 MHz* & 30 subcarriers	human activity recognition	7.7*6.5 m and 25 subjects	8 activities recognition with over 96.5% accuracy in average
HARNN [115]	WiFi	5 GHz	20 MHz* and 30 subcarriers	human activity recognition	indoor 5*6m, 8*6m and 10 subjects	6 activities recognition with over 95% accuracy in average.
WiDIGR [116]	WiFi	5.825 GHz	20MHz* and 30 subcarriers	gait recognition	5*5m and 60 subjects	78.28% accuracy for 6 subjects recognition
CAUTION [117]	WiFi	5 GHz	40MHz* 114 subcarriers	gait recognition	5.8*6.3 m, 7.2*5.2 m/ 20 subjects	88% accuracy in 15 subjects identification
latern [118]	FMCW radar	24 GHz	4 GHz	gesture recognition	1.5m, 2m, 3m / 5 subjects	8 gestures recognition with 96% accuracy
[119]	FMCW and UWB radar	25 GHz FMCW 7.5 GHz/ UWB	2GHz FMCW/ 1.5GHz UWB	gait recognition	2.7*1.8m / 14 subjects	Gait recognition in 14 subjects with 84% accuracy in average
citeUWB	UWB	5.2 GHz	8.7 GHz	human activity recognition	2.5m / 13 subjects	12 non-in-situ motions recognition with an average of 88.9% accuracy, in-situ motions 89.7% average accuracy.
[120]	UHF RFID	865 MHz	3 MHz	gestures recognition	2.5m / 15 subjects	87% accuracy for recognition of drinking episodes for young volunteers and 79% for older volunteers
[16]	LoRa	915 MHz	125 kHz	respiration sensing/ human tracking	25m(respiration)/ 35m(tracking)	Achieve long-range through-wall respiration sensing with 0.25bpm mean absolute error, human tracking with 4.27cm average absolute error.
(Ours)	LoRa	868.1 MHz	125 kHz	gait recognition	5m, 20m (LOS) & 6m(NLOS) /10 subjects	Adopt LoRa signals to extend the gait recognition in various environment including 20m corridor, with 82.8% accuracy.

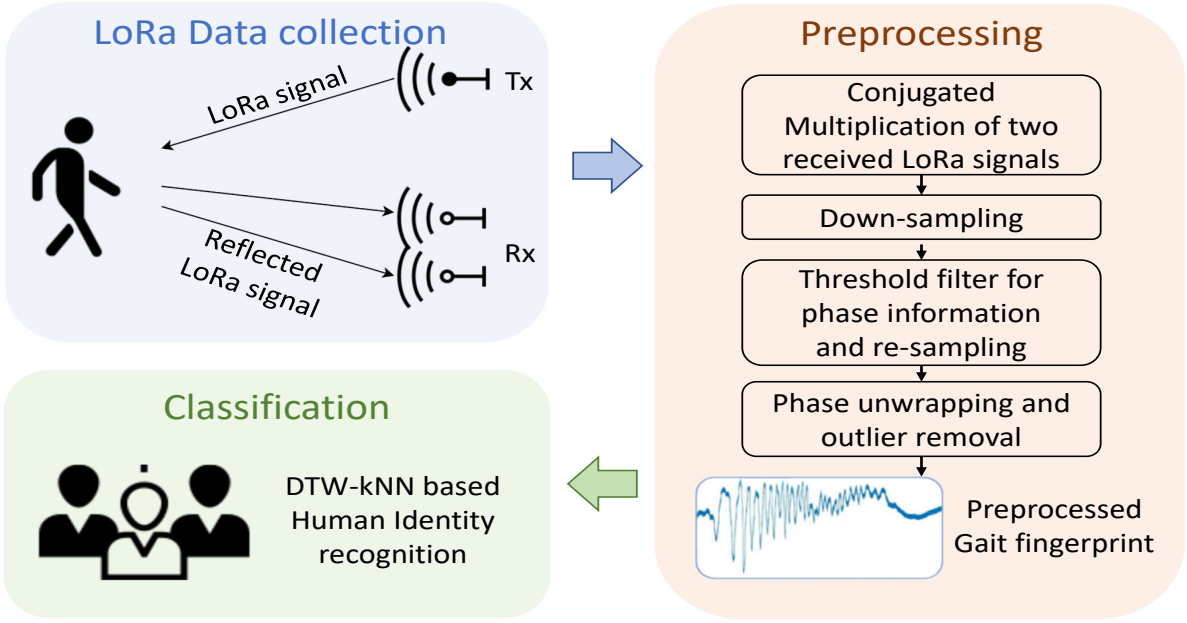

Figure 3.1: Overview of the proposed LoGait system that consists of three components. (1) LoRa Data Collection. (2) Preprocessing. (3) Classification using DTW and kNN.

tivity recognition [123]. In [120], RFID is also used in recognizing the fluid taking gesture. However, all systems mentioned above are limited with the sensing distance. As shown in Table. 3.1, the sensing range of WiFi, radar and RFID system is limited in 8m, 3m and 2.5m respectively. In comparison, LoRa system proposed in [16] extend the sensing range to 35m for human tracking and 25m for respiration monitor.

Contributions

The problem of recognising humans from their walking patterns is known as gait recognition. It has many potential applications in surveillance, healthcare, and human-computer interaction. In the literature, WiFi-based sensing has provided various solutions for gait recognition [30, 31]. However, the nature of the WiFi signal restricts the sensing range [16, 32]. Therefore, WiFi-based systems cannot be adopted in long-range spaces, e.g., corridors. Inspired by the previous LoRa-based sensing work [124–127], we attempt to analyse the feasibility of adopting LoRa sensing in long and narrow environments. We propose LoRa system to push the range of gait recognition to multiple indoor scenarios including a corridor of 20m length. The proposed LoRa system is shown in Fig. 3.1. In summary, the following are the major contributions of this work.

1. To the best of our knowledge, this study is the first attempt toward using LoRa signals for gait recognition in a 20 meters range.

2. We propose a pipeline for performing preprocessing of LoRa signals for gait feature extraction and classification.

3. We collect LoRa signals containing the gait patterns of different subjects in various scenarios. Our experimental results in different settings validate the effectiveness of our proposed LoRa system in performing gait recognition. Our work fills an absence in this field.

3.1.1 Methodology

Preliminaries

Unlike WiFi which applies OFDM to divide channel bandwidth into different subcarriers, LoRa adopts full bandwidth for Chirp Spread Spectrum technology, which encodes information on radio waves using chirp pulses. The technology operates in a fixed-bandwidth channel of 125 kHz for up-link. The frequency of linear chirps increases from $f_c - \frac{B}{2}$ to $f_c + \frac{B}{2}$ over the the sampling period of $-\frac{T_s}{2} < t \leq \frac{T_s}{2}$, where the f_c and T_s represent carrier frequency and sampling time, respectively. The exponential representation of LoRa transmitting signal is composed of two elements, chirp signal and carrier frequency modulation:

$$Tx(t) = e^{j\pi f_s(t) + j2\pi f_c(t)}, \text{ with } f_s(t) = \pm\frac{B}{T_s}t \tag{3.1}$$

where, $f_s(t)$ represents the chirp signal with sweep rate. Existing literature on LoRa-based sensing suggests that the channel response at the receiver end can be represented without considering the chirp signal [16]:

$$H(t) = \frac{Rx(t)}{Tx(t)} = e^{-j2\pi\Delta t}(H_s + H_a(t)) + N(t) \tag{3.2}$$

where, $e^{-j2\pi\Delta ft}$ is due to the sampling frequency offset (SFO) and carrier frequency offset (CFO); $H_s$and $H_a(t)$ represents the LoRa signals from the time-invariant static paths (including the signals in line of sight (LOS) path and those reflected off the stationary objects) and time-variant dynamic paths (including signals reflected from the dynamic objects). $N(t)$ represents the free space transmission noise. LoRa signals in active paths can be expressed as:

$$H_a(t) = \sum_{i=1}^{N_d} a_i(t) e^{-j2\pi\frac{d_i(t)}{\lambda}} \tag{3.3}$$

where, N_d is the index of path that signal passes through, $a_i(t)$ represents the complex attenuation factor of the i^{th} path; $e^{-j2\pi\frac{d_i(t)}{\lambda}}$ represents the phase change of i^{th} path, with the changing distance of $d_i(t)$ in i^{th} path. λ represents the wavelength of the LoRa signal.

However, the channel response cannot be calculated directly with reference data. In this case, we replicate the setup from previous work with two receiver antennas to get the conjugate multiplication (CM) signal [16, 128]. There are various parameters that correlate with signal

ratio. However, to find the dominant dynamic path for estimation, we select two directional antennas which perform better in the reduction of the multipath effect ($N_d = 1$). So we assume in the ideal situation, that there is a single path with relatively less noise ($d_i(t) = d(t)$).

$$\begin{aligned} R_{CM}(t) &= Rx_1(t)\overline{Rx_2(t)} = Tx(t)\overline{Tx(t)}H_1(t)\overline{H_2(t)} \\ &= Tx(t)\overline{Tx(t)}(e^{-j2\pi\Delta t}(H_{s1}+H_{a1}(t))) \\ &(e^{j2\pi\Delta t}(\overline{H_{s2}}+\overline{H_{a2}(t)})) \\ &= \|Tx\|^2(H_{s1}+H_{a1}(t))(\overline{H_{s2}}+\overline{H_{a2}(t)}) \\ &= \overbrace{\|Tx\|^2}^{(1)}(\overbrace{H_{s1}\overline{H_{s2}}}^{(2)}+\overbrace{H_{s1}\overline{H_{a2}(t)}}^{(3)}+\overbrace{\overline{H_{s2}}H_{a1}(t)}^{(4)} \\ &+\overbrace{H_{a1}(t)\overline{H_{a2}(t)}}^{(5)}) \end{aligned} \tag{3.4}$$

From the representation, the components of chirp signal, CFO and SFO are removed. On the other hand, the equation are divided into five parts for analysis: the transmission part of (1) and product of static components of (2) can be regarded as constant value, and the product of active components of (5) is small that can be ignored. Meanwhile, we consider the extended changing path, ΔS, which is caused from the different physical locations of two receiver antennas. This value is assumed as the constant value due to the setup receiver antennas are close to each other. Next we can rewrite the superposition of rest components.

$$\begin{aligned} (2)+(3) &= H_{s1}\overline{H_{a2}(t)}+\overline{H_{s2}}H_{a1}(t) \\ &= H_{s1}(a_2(t)e^{j2\pi\frac{d(t)+\Delta S}{\lambda}})+\overline{H_{s2}}(a_1(t)e^{-j2\pi\frac{d(t)}{\lambda}}) \\ &= (H_{s1}a_2(t)e^{j2\pi\frac{\Delta S}{\lambda}})e^{j2\pi\frac{d(t)}{\lambda}}+(\overline{H_{s2}}a_1(t))e^{-j2\pi\frac{d(t)}{\lambda}} \end{aligned} \tag{3.5}$$

In this case, we can adopt the analysis methods proposed in [128] to prove that the phase variation of CM result is mainly influenced by components from the dynamic path of $d(t)$, which is available to be adopted for gait feature extraction.

Preprocessing stages

The inference provided in Section 3.1.1 shows that human motion can be indicated by the phase variance of CM results. However, to extract any relevant data related to the motion, it is necessary to go through a series of preprocessing steps before using the Dynamic Time Warping (DTW) recognition. This section outlines all of the steps that we proposed which need to be taken prior to the DTW recognition.

Conjugated multiplication of two antennas signal The Fig. 3.2 shows the different amplitude of raw LoRa signals with/without dynamic physical interference. Although the envelope

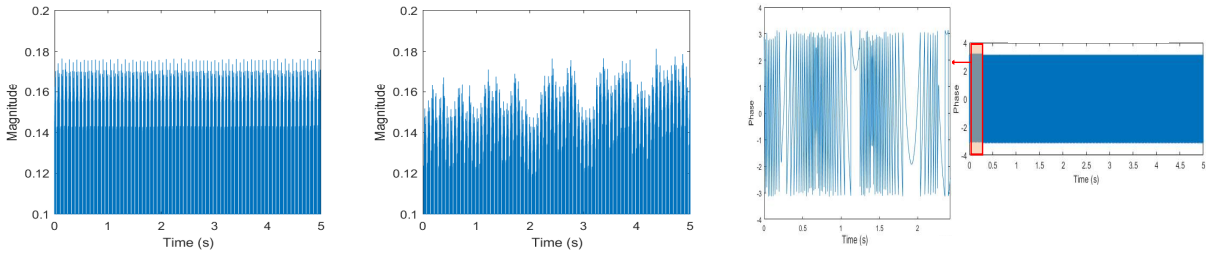

(a) Amplitude of static person (b) Amplitude of a single person walking within line-of-sight (LOS) (c) Raw phase signal of LoRa signal

Figure 3.2: Amplitude and phase plots of raw LoRa signals.

shape of LoRa amplitude is explicit, it is required to transform these perturbations into measurable values. Compared to visible variation from amplitude information, phase information shown in Fig. 3.2c provides random information that cannot be intuitively observed. In the next step, we observed a considerable number of blank interpolations inside the recieved envelope, which represents the receiver end collected noise during packet duration. Removal of this blank information is important to extract accurate gait features. Firstly, we calculated the CM result from raw LoRa signals of dual antennas, which is shown in Equation. 3.4. Demonstrated by the Equation, the gain of $\|Tx\|^2$ can determinately increase the amplitude of the received signal, which differentiates the meaningful LoRa signal from noise. From this point of view, the noise duration can be removed by setting the low amplitude threshold of CM result. In Fig. 3.3a, the red dashed line represents signal components from noise and the green one from the LoRa chirp signal. Meanwhile, we assume the transmitted power of LoRa signals and free space attenuation is stable. In this case, the threshold was set to the mean value of the first second's receiving signals.

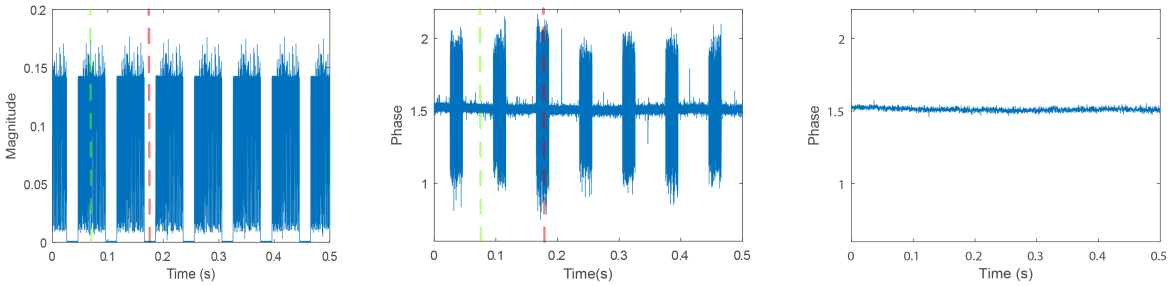

(a) Amplitude plot (b) Phase plot (c) Phase plot after threshold filter

Figure 3.3: Plot of CM results under static environment with the red dashed line labelled for noise components and green one for LoRa chirp signals in (a) and (b).

Threshold filter for phase information and down-sampling Meanwhile, there are two down-sample operations executed before and after threshold filtering. For amplitude threshold, it is a

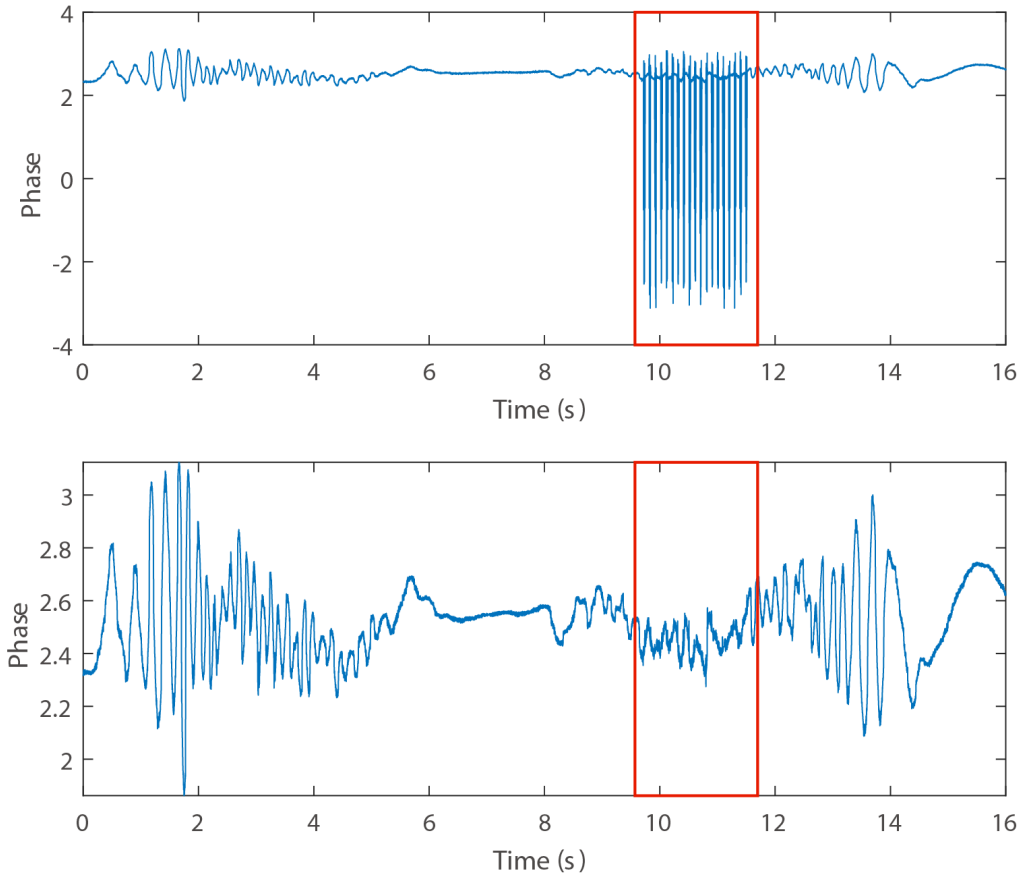

Figure 3.4: Comparison plots with/without Hampel filter and phase unwrapping, with circled outliers in red boxes. The first graph shows original gait signals and the second shows Hampel filtered and phase-unwrapped gait signals.

waste of computational resources for searching and comparing all $800k$ samples per second. On the other hand, the Doppler shift frequency range that human activity can generate is limited to $60Hz$ [129], $800kHz$ sampling rate is highly redundant. Therefore, we set the first downsample of $1k$ sample rate ahead of threshold operation. After performing thresholds filtering, we discovered that the length of the LoRa chirp signal is not constant. Then, we resample the filtered data to $1kHz$ for unifying constant sampling frequency among different profiles. Fig. 3.2c shows the LoRa signal after threshold filtering with twice downsampling.

Phase unwrapping and outlier removal In this stage, we acquire meaningful phase information that can reflect the channel environment. However, the outliers and mismatched phase data appear. We adopt the Hampel filter and unwrap operation to denoise the signals, with the shown comparison figures shown in Fig. 3.4. The signal components that are framed out by a red box represent the recovered parts by the methods.

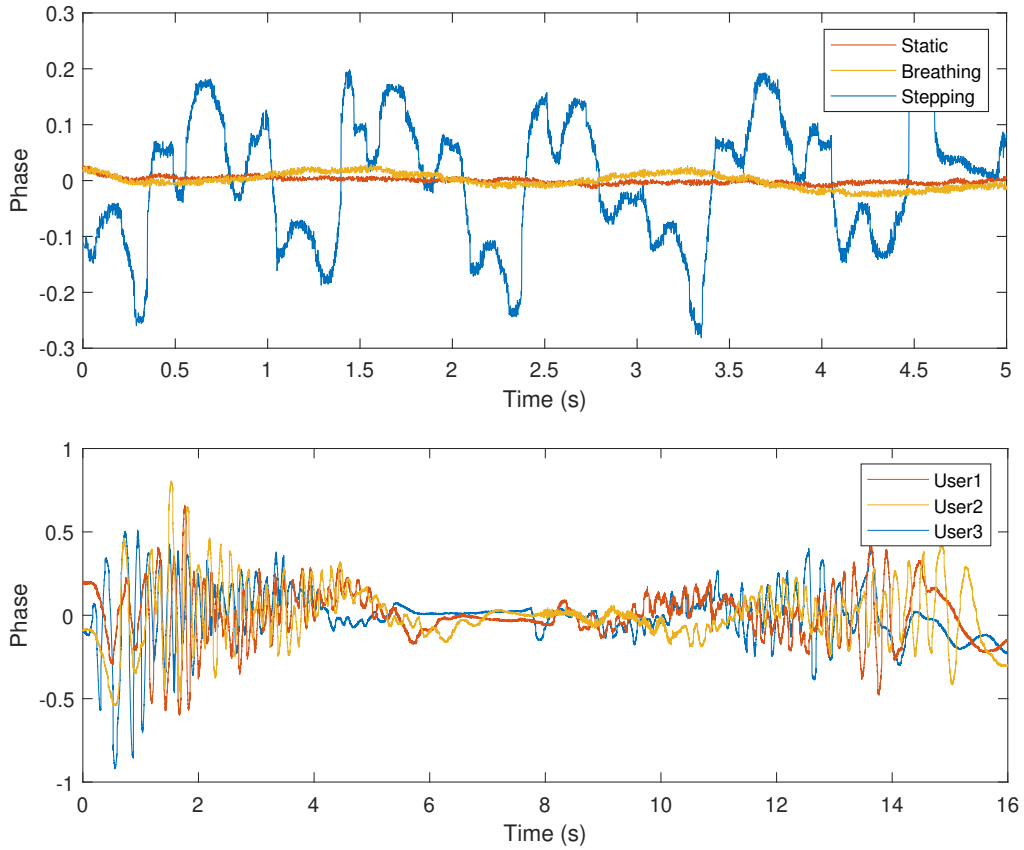

Figure 3.5: Comparison of LoRa signals under different scenarios of no-person, a person standing still, a person stepping shown in the first figure; and gait profiles of three users in the second figure.

DTW-based Gait Recognition

After preprocessing of LoRa signals, we compared the signals collected from different activities and gait signals, shown in Fig. 3.5. The gait experiment setup is the same as LOS experiment that mentions in Section. 3.1.2.

From the intuitive view, we observed the collected activity signals under three different scenarios that match our normal experiences: the human presence scene only contains chest motion of respiration, and stepping signals contains multiple signal peaks from human skeleton motion. From the gait profiles of three users, we found that the human behaviour patterns of different identities are highly overlapping compared to human activity recognition. Besides, there are two main challenges that were observed in the comparison:

1. Variation of motion speed can result in various lengths of gait signals from a single subject.

2. Temporal gait signal can not be completely aligned while the data collection, which causes the distortion of information.

The general method of measuring the similarity of two-time series signals is to calculate the Euclidean distance. However, lock-step Euclidean distance measurement refers to those

distances that compare the ith point of one series to the ith point of another, which is significantly influenced by incomplete alignment [130]. To solve the alignment problem and improve the recognition performance, DTW based method was adopted.

DTW is a similarity measurement method, which exhausts all the correspondences with restrictions and finds the one with the smallest distance. Then the cumulative distance of the selected path is used for their similarity judgement. The Equation. 3.6 describes the algorithm of DTW distance.

$$D_{min}(i,j) = M(i,j) + min \begin{cases} D(i-1,j-1) \\ D(i-1,j) \\ D(i,j-1) \end{cases} \quad i,j \geq 1 \tag{3.6}$$

To align the two sequences, a matrix with two dimensions of sequences' length is required. The matrix element $M(i,j)$ denote the Euclidean distance $d(x_i,y_j)$ between the two points x_i and y_j. The shortest distance of the current element $D_{min}(i,j)$ is necessarily the length of the shortest path of the previous element plus the value of the current element. There are three possible directions for the previous element, so we take the minimum value of three possibilities into DTW distance.

For initial validation of DTW, we calculated the DTW distance of gait profiles of different identities and the same identity respectively to verify the algorithm's availability. The comparison graph is shown in Fig. 3.6 which illustrated the distance between the same user and different users. The larger DTW distance verified our assumption that the gait profiles of different identities have mismatched information and the data from a single identity has similar features. Therefore, we adopted a K-nearest neighbour (KNN) cluster-based algorithm to classify different identities of gait signals.

3.1.2 Evaluation

Experimental Setup

Devices

Our implementation considers one pair of devices to imitate the general LoRa link. We select one USRP b205mini and one USRP x310 as transmitter and receiver, respectively. They are equipped with one Aaronia Ag vertical polarized antenna for the transmitter and two SlimLine A5010 Circular Polarized Antenna with 8.5 dBi gain for the receiver. The LoRa signal is generated by an open-source project of LoRa communication in the physical layer [131]. On the receiver side, we configured Labview based system to collect LoRa signal. The experimental setup can be viewed in Fig. 3.9. The sampling rate and packet duration are set to $800kHz$ and $20ms$, respectively.

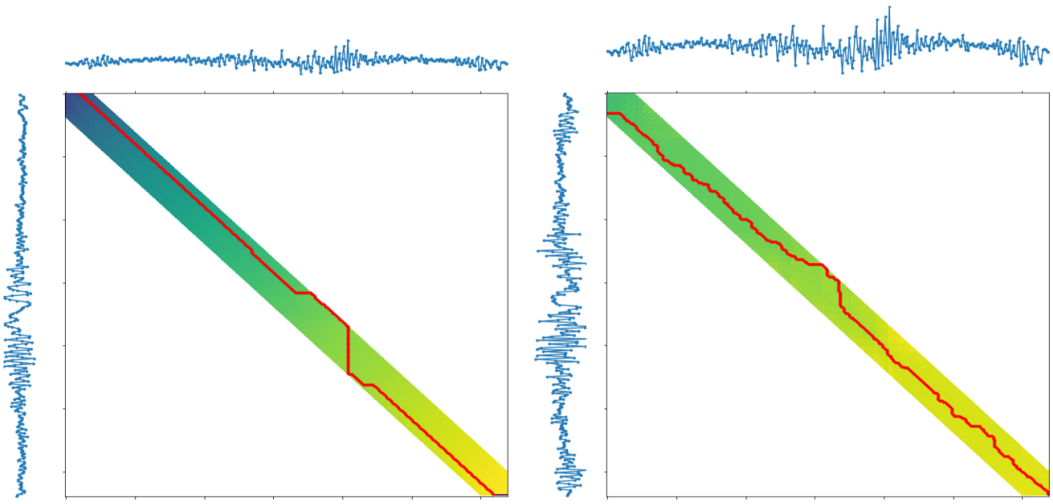

(a) DTW distance: 5.81 (b) DTW distance: 0.36

Figure 3.6: Comparison of DTW distance matrix of (a) gait profiles from the first user and second user; (b) gait profiles from the first user.

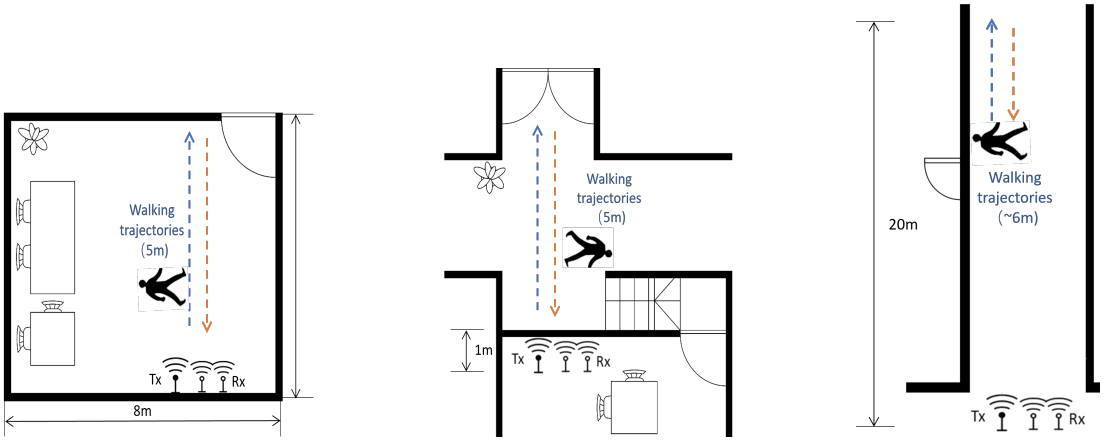

(a) Line of Sight (LOS) (b) Non Line of Sight (NLOS) (c) Long-Distance (LD)

Figure 3.7: Experimental setup of 3 scenarios.

Application scenarios

The experiments were conducted in 3 different scenarios: line of sight (LOS), non-line of sight (NLOS) and long distance (LD) range, with the top-view structure graph shown in Fig. 3.7. In the LOS scenario, the room area occupied for the activity experiment is $6m$ in length and $5m$ in width. One line has marked a $5m$ distance on which people walk to and from the front of the transmitter and receiver. In NLOS scenario, all apparatus containing the transmitter and receiver are in one room, and activity is being monitored outside of the room, shown as walking trajectories. The space between devices and humans is separated by a brick wall. In the LD scenario, the implementation is setup in a corridor of $20m$ length. Volunteers were arranged to walk along the trajectory at the end of the corridor, shown in Fig. 3.9.

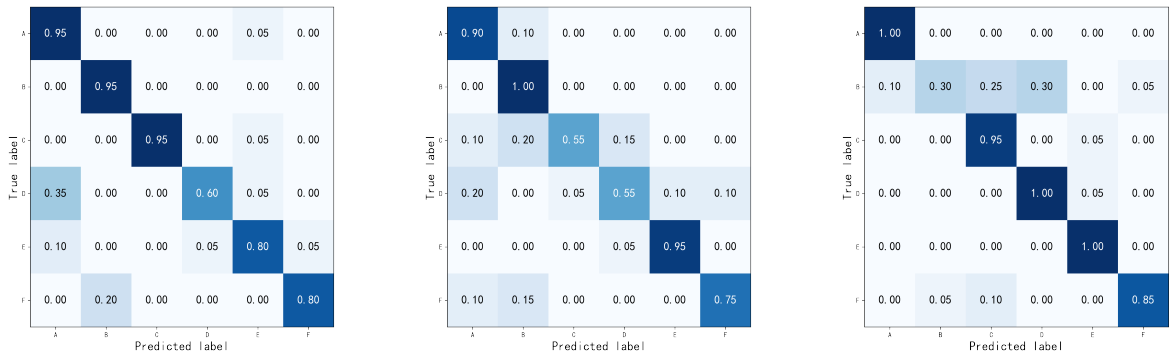

(a) LOS (b) NLOS (c) LD

Figure 3.8: Confusion matrix of gait recognition in 3 scenarios

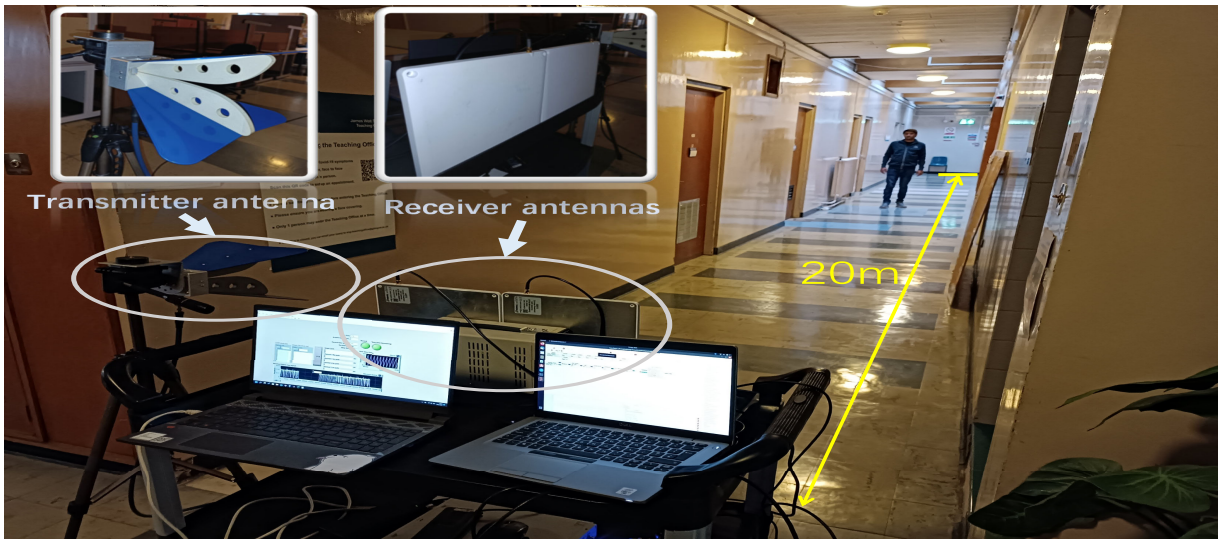

Figure 3.9: Experimental setup in Long distance scenario

Gait profiles

The basic human gait in our experiment contains three phases: rotating, walking and standing. During one data collection, one person was asked to turn back, walk along the trajectory and stand still for 8 seconds. Then, it took another 8 seconds for subjects to walk back to the starting point. The gait signal in each profile lasts for 16 seconds in total. Besides, we downsample the signals to $200Hz$ for speeding up the machine learning algorithm.

We recruited 13 volunteers for data collection of human gait including 4 females and 9 males. In each scenario, we ask 6 subjects to conduct the experiments and data was collected for 20 rounds for each person that provides $16s$ gait data. In total, we have collected 5744 seconds of gait signals for experimental validation.

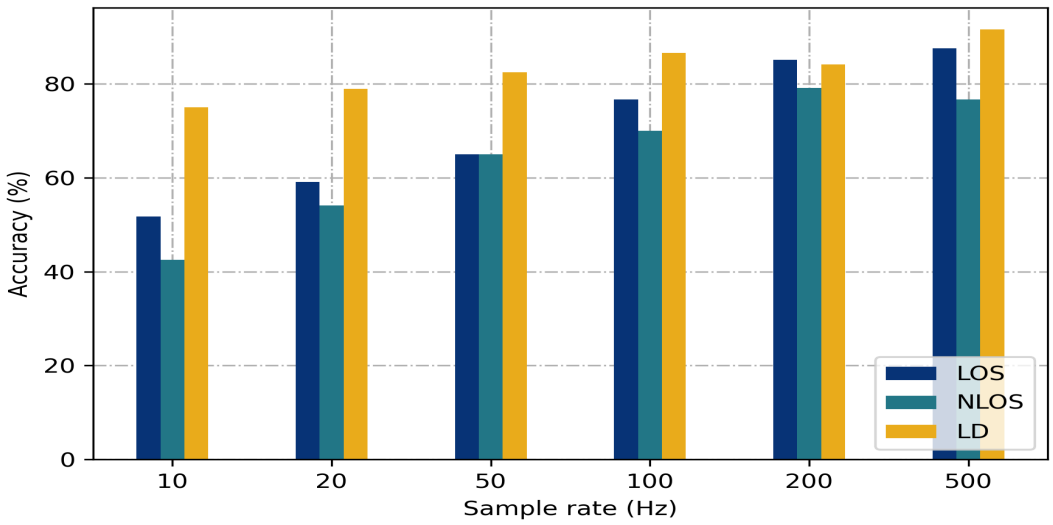

Figure 3.10: Recognition accuracy via sample rate in 3 scenarios

3.1.3 Overall performance and Discussion

The recognition performance of 3 scenarios with confusion matrices is shown in Fig. 3.8. We perform a 5-fold cross-validation on collected data with an overall accuracy of 85.13% in LOS range, 79.13% in NLOS and 84.14% in LD respectively. The average accuracy of 82.8% validates the effectiveness of our system. To study the performance of the LoRa system affected by different factors, we design the comparison tests and analyse the influence of Sample rate, Classification distance algorithm. Meanwhile, we explain the difference in Data collection methods of gait signal between LOS/NLOS and LD scenarios.

Sample Rate

The sample rate of gait profiles is the significant parameter that balance of recognition performance and processing speed. We resample the gait profiles from $10Hz$ sample rate to $500Hz$ to test the performance of the LoRa system. The recognition performance is illustrated in Fig. 3.10, which validates that a higher sample rate preserves more gait information.

Vector distance algorithm

To approve the assumption in Section. 3.1.1, we compared the classification results using the other three distance algorithms with DTW distance, shown in Fig. 3.11. It illustrated that the DTW-based classification method acquires the best performance among the traditional distance estimation algorithms.

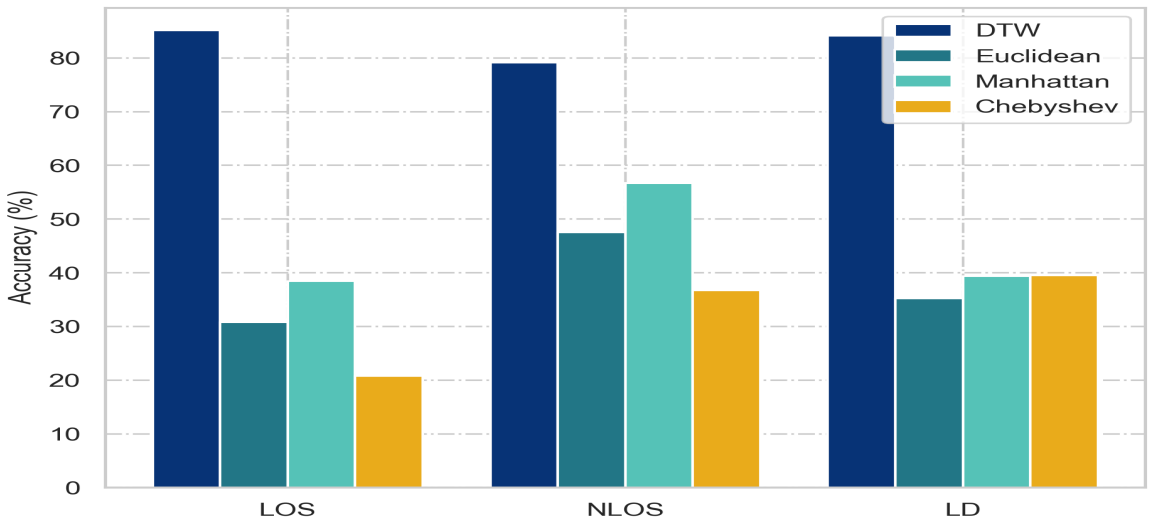

Figure 3.11: Recognition accuracy of distance algorithms in 3 scenarios

Walking directions

In our experiment, we divided the data collection of one profile into two phases, moving forward and back, as shown in Fig. 9 (depicted by blue and red dashes). To effectively evaluate the performance of our system, we separated the profile into three parts: forward, back, and integration.

Data collection methods

In both LOS and NLOS scenarios, we asked volunteers to do free walking in a restricted space. In this case, the users are easy to control their speed without following usual habits. To study the robustness of the gait recognising system, in the LD scenario, the volunteers were asked to walk freely in a given time slot instead of limiting the moving area. From the results, the accuracy under the LD environment approves the popularization potential of the LoRa system.

3.1.4 Summary

This work proposes a LoRa system for human gait recognition under different indoor scenarios including living room, through-wall and corridor. In our system, we firstly analyzed the availability of LoRa sensing, and then propose multiple preprocessing methods to acquire LoRa gait profiles. Then, we adopted a DTW-based machine learning algorithm to recognize user identity and evaluate our system in 3 scenarios, with the identification accuracy of 85.13% in room, 79.13% in through-wall and 84.14% in 20m corridor. Our LoRa system contributes to a gait recognition prototype that can be established in complex indoor environments including through-wall and long-distance corridors.

3.2 LoRa enabled non-invasive robust security in next-generation smart houses

There are many security and surveillance applications in which camera-based or invasive human activity recognition is not permissible due to privacy, insecurity, and discomfort issues. Moreover, vision-based surveillance systems have a few key technical challenges that limit their practicality such as bad illumination, obstacles, and occlusion. In such cases, we require a more reliable system which can work in challenging situations such as in darkness, long-range, through walls or obstacles, a rainy and smoky environment where vision-based systems do not deliver good results. Only high-energy and long-range wireless sensors which can identify targets through obstacles, walls, worst climate or surrounding conditions can serve the purpose. In this work, we propose to use the LoRa transceiver to identify different persons from their walking patterns through bricks and a concrete wall where people other than the target person are moving freely. Moreover, we employed three different deep-learning models to evaluate the efficacy of the proposed system. Our highly accurate 99% results encourage the use of contactless LoRa sensors in many privacy-critical applications such as healthcare, security, and surveillance, where short-range and low-energy signals have limited utilisation.
Different from traditional sensor-based sensing, contactless sensing does not require any sensors but relies on the signal itself for detection. The sensor-free and contact-free nature make contactless sensing appealing in many real-life applications including security and survival in life-saving operations, intrusion detection, indoor and outdoor human activity recognition and vitals monitoring. Diverse contactless sensors such as WiFi [80], long range radio (LoRa) [81], RFID [82], radars [83], ultrasonic and visible light had been deployed for sensing purpose.

The underlying principle of contactless sensing is that wireless signals get reflected from the target and the reflection signals vary with target movements [84]. By carefully analysing the movement-induced signal variations, rich contextual information regarding the target's movements can be obtained. As compared to other contactless sensing technologies such as WiFi, RFID, FMCW radars, and ultrasounds, which have a few meters sensing range, LoRa has a relatively very high range and high energy signal which can easily pass through obstacles and brick walls. This makes it highly suitable for applications where low range, low energy, and high power consumption signals do not work.

In this work, we present a LoRa signal by using a pair of universal software radio peripherals (USRP), one as a transmitter having one antenna and another as a receiver have two antennas to detect people from their walking patterns through a thick brick wall. Human activity include strolling outside the room wall and the resulting information is person detection from their walking patterns. Below sections include experimental setup, data collection, pre-processing of the complex I/Q signal data and walking patterns results for the strolling activities of six different people.

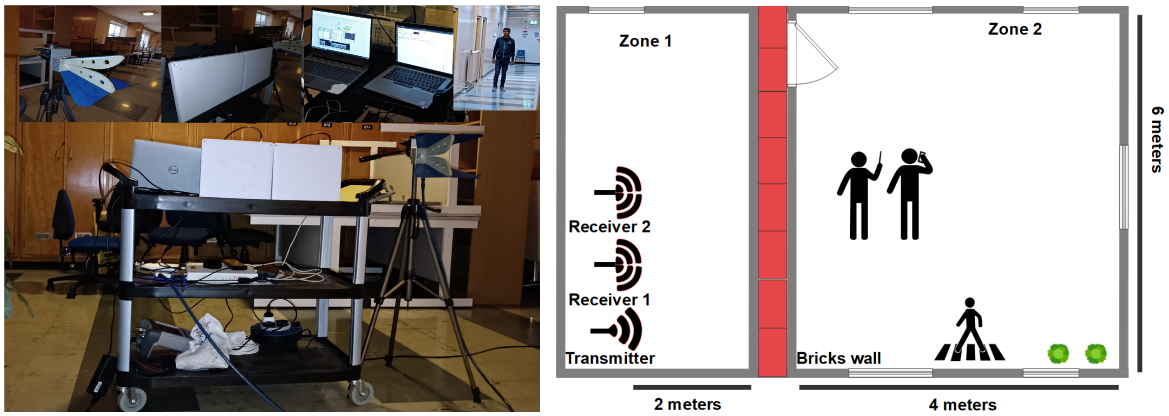

(a) Hardware and Software Setup (b) Experimental Setup

Figure 3.12: Illustration of hardware and software setup (Fig. 3.12a) and experimental setup (Fig. 3.12b) used for data collection.

3.2.1 Methodology

Experimental Setup and Data Collection

Our data collection setup includes two 310 USRPs, where one is used as a transmitter and another as a receiver. Transmitter has one Aaronia Ag vertical polarized antenna and the receiver has two Slimline A5010 circular polarized antennas with 8.5 dB gain as shown in Figure 3.12a. LoRa signal is generated on the transmitter end through USRP simulated using LabVIEW and USRP on receiving end is operated using two receivers' physical layer setup. The transceiver as a module for GNU Radio 3.10 has been used for software defined radio (SDR) implementation of the LoRa transceiver. This module operates correctly even at exceptionally low signal to noise ratio (SNR), which is available as an open source in [131].

All the apparatus USRPs, antennas, laptops and power wires are setup on a wheeled moveable trolly near the outer wall of the room at a two-meter distance away from the separation wall, while activities have performed inside the room away from the separation wall all over in the four meters long and six-meter-wide area floor. Rom has a door near the one end of the separation wall in between the transceiver and the activities performed area.

Data collection setup has been established in a room available in Communication, sensing and imaging (CSI) lab at the James Watt School of Engineering in the University of Glasgow, United Kingdom. Setup is divided into two zones; zone one is outside the room where USRPs, antennas, laptops, and other apparatus are placed, and zone two is inside the room where activities have been performed for data collection, where zone one and zone two are separated by a twelve-inch thick double brick wall. Area details inside and outside the room and activity details are illustrated in Figure 3.12b. The activities include persons strolling other side of the brick wall and resultant information includes the person identification from their walking patterns. Total six people; four males and two females aged in-between 22-30 years old took part

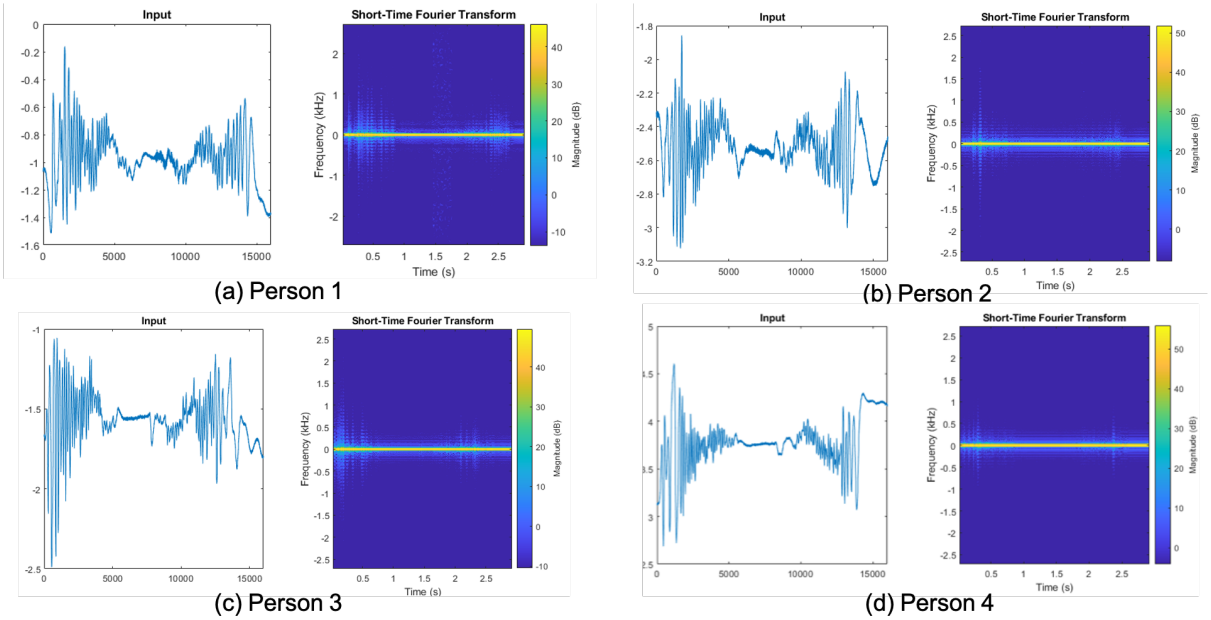

Figure 3.13: Depiction of data variations in the received LoRa signals reflected from individuals' walking patterns in time and frequency domains.

in the data collection activities.

Data Pre-Processing and Machine Learning

The transceiver consists of one separate USRP and antenna to generate LoRa signal as a transmitter and another separate USRP and two antennas as a receiver. Baseband signal is I/Q complex data which provides amplitude and phase information (having same magnitude but different phases) on both individual antennas on the receiver end. Walking information comes from the phase difference of receiving antennas. To get phase differences, as a first step we need conjugated multiplication of two received LoRa signals, and separate the phase and magnitude the second step is to further downsample the data to apply a threshold filter to get precise phase information and the third step is resampling the conjugated LoRa signal. Finally, we compute spectrograms of the preprocessed signals for the training of three different deep learning (DL) architectures. These images were cropped to eliminate colour bars and titles prior to using them for model training and testing. All images have the same dimensions of $224 \times 224 \times 3$.

3.2.2 Results and Discussions

We demonstrate the data variations that are reflected by the individuals' walking movements that were used to identify persons in Figure 3.13. The figures suggest that the collected data contains distinct characteristics in terms of measuring LoRa signal that makes it suitable for training DL models to identify persons in a privacy-aware fashion. Specifically, we have trained and tested three widely used DL models namely VGG16, VGG19, and MobileNet. These models were

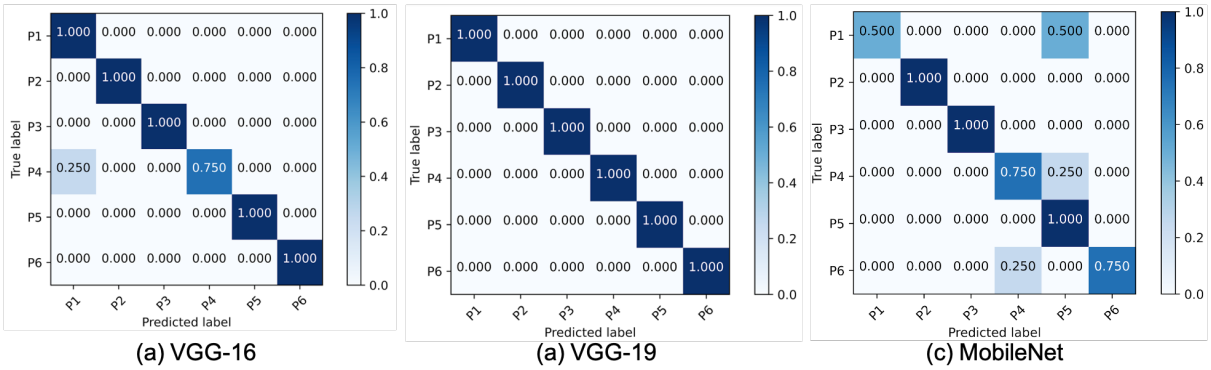

Figure 3.14: Classification performance of three different models in recognising six different persons using proposed LoRa-based contactless sensing.

trained and tested using 80% and 20% of the collected data for training and testing, respectively. Furthermore, to ensure efficient training, we employed 4× data augmentation to increase the size of the training set. The experimental results in terms of confusion matrix are summarized in Figure 3.14. We can see that the VGG19 outperformed VGG16 and MobileNet, while effectively recognising each individual. Moreover, the figure reveals that the performance of the MobileNet is the worst, which can be due to the fact that the architecture of the MobileNet is much smaller than the other two models.

3.2.3 Summary

In this work, we propose to use the LoRa transceiver to identify individuals from their walking patterns. Highly accurate 99% results advocate long-range, low power, low SNR and high energy LoRa capability to be used as a reliable system in many contactless sensing applications in next-generation smart houses, hospitals and public places. In our future work, we plan to optimize our proposed framework and to incorporate more critical activities.

3.3 Room-Level Activity Classification Using Electricity Usage Data

Human activity recognition is challenging without compromising users' privacy and burdening them with wearable devices, cameras, mobile applications, etc. As the smart energy meter usage trend is increasing worldwide, it can be used as a non-invasive activity monitoring methodology without violating users' privacy and requiring an additional installation cost where smart energy meters are already in use. In addition, household energy consumption patterns, including the consumed power, current intensity, and energy usage, are mainly determined by the individual's needs, lifestyle, and time context, which can offer important information about the household's daily activities. Using energy data, users can get information about ongoing activities

in each room of the house under observation. This work uses different machine-learning (ML) algorithms such as Random Forest, Decision Tree, K-Nearest Neighbour, and Support Vector Machines for activity recognition from load classification. The ML model classifies different real-time activities in the same room based on the consumed power estimates. By utilizing an open smart energy sub-meter dataset, activity patterns of household occupants are identified. The load classification analyses, employing the aforementioned ML algorithms, demonstrate an activity recognition accuracy of up to 99%.

Recently, activity monitoring technology has emerged as an efficient method to assist decision-making and reduce the burden on caretakers to detect emergencies concerning elderly people [2, 78]. The current state-of-the-art for activity monitoring typically depends on smartphone applications and internet-of-things (IoT) devices, including cameras, specialized sensors, smart plugs, etc to monitor individual health in real-time [71, 79]. In [70], vision-based activity recognition systems are used to increase detection accuracy. Although the existing works offer accurate detections, they may violate users' privacy. Further, there is a significant cost and burden incurred by installing and distributing these IoT devices. For example, homeowners are reluctant to install cameras in their homes for privacy reasons; other occupants are uncomfortable wearing and charging wearable devices.

In this challenging scenario, the energy consumption-based activity monitoring method has been introduced as a privacy-preserving method. This method avoids the aggravation of purchasing, wearing, and installing various sensors and devices. The only information required for activity detection is energy consumption data from an existent smart energy meter and a smart device that can compute a baseload, compare continuously incoming data with the baseload, and predict activities. Electricity usage data can accurately identify operational devices and their locations in rooms accurately when compared to baseload and device load descriptors. Previous work on activity detection approach based on power disaggregation data, commonly known as non-intrusive load monitoring (NILM), is presented in [76]. Contrary to the existing work, our approach focuses on activity detection utilizing electricity usage data. The proposed work employs energy consumption data as a privacy-preserving methodology compared to vision-based approaches. The following summarizes the contribution of this work.

- Using machine-learning algorithms, we propose an efficient activity-level classification throughout the year based on fine-grained electricity usage data from a sub-metering system.
- We highlight the concept behind using high-resolution electricity usage data to recognize different activities in a day.

With the advancement in IoT, smart homes are introduced to facilitate users by providing several home services such as health care monitoring, privacy, etc. In smart homes, many actuators and sensors are used to control daily life equipment and they are linked together with communica-

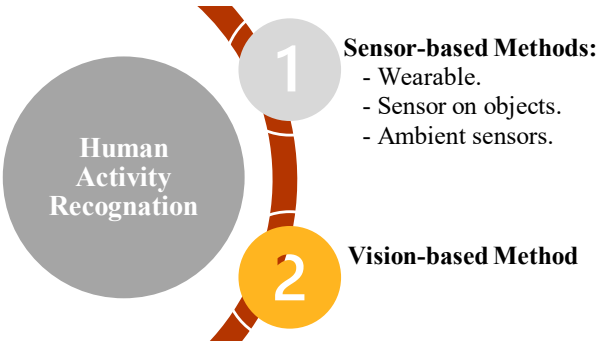

Figure 3.15: Activity recognition methodologies.

tion protocols. Now, human activity recognition techniques are being developed by researchers to monitor and analyze behavior of people using sensors and actuators.

Generally, human activity recognition can be categorized into vision-based and sensor-based methods [132], as shown in Fig. 3.15. The former systems use cameras and computer-based vision techniques; however, younger adults (till age 35) are more concerned with privacy and are not happy with sharing and tracking their activities [133]. Sensor-based systems are further divided into three categories: wearables, sensors on objects, and ambient sensors. The use of sensor-based smart homes is a feasible solution [134]. However, human activity recognition is challenging because everyone has their own way of living a life. Several algorithms are proposed and implemented for human activity recognition in smart homes, including pattern recognition, feature extraction algorithms, etc.

Pattern recognition techniques are further divided into two categories including data-driven and knowledge-driven techniques. In-depth knowledge about the domain is required in a knowledge-driven approach; however, domain experts are needed to make new rules which may replace previous rules. This limitation is subsequently addressed through the implementation of a data-driven approach that incorporates both supervised and unsupervised methods for the purpose of human activity recognition utilizing energy data. These approaches do not require prior knowledge; further, they can handle uncertainties in data such as noise, incomplete data, etc. However, much clear, correctly labeled data and more computational time is required for a data-driven approach [135]. To summarize, the use of deep learning and machine-learning models in a data-driven approach for human activity recognition using energy data is a viable solution to train more complex models and they do not invade people's privacy. In this regard, this work uses the Random Forest, Decision Tree, K-Nearest Neighbor, and Support Vector Machines-based machine-learning algorithms for activity recognition and load classification by considering the privacy of individuals.

3.3.1 The proposed approach

In this section, the approach employed for energy consumption-based activity categorization utilizing machine learning techniques is presented.

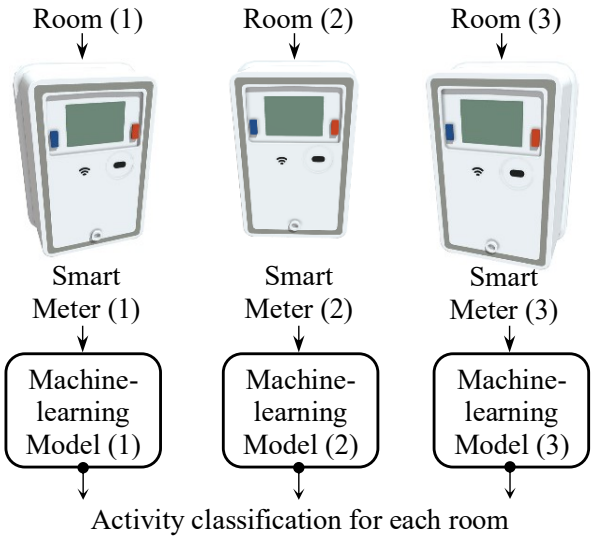

Figure 3.16: System model for the proposed approach.

Activity recognition

In energy consumption-based activity recognition, the amount of energy consumed during a certain period of time during the day is correlated with the activity of the home occupants. By learning the daily consumed energy of a house, known by the baseload, one can predict the type of activity and investigate any anomalies. The type of activity in the house can be discerned by comparing electricity usage data with the baseload, operated load, and location in the house. In this work, we evoked the household electric power consumption data in [136]. This dataset is generated from a sub-metering system that monitors three different rooms in the house and reports the energy consumption in Watt-hour (Wh), as shown in Fig. 3.16. The data has been presented for each day of the year in the form of [*dd/mm/yyyy*] at a specific time [*hh:mm:ss*]. The estimated consumed energy from each room is recorded every minute (sampling rate) for the whole year. Each room has a list of electric devices, each of which has a unique power rate (PR) represented as follows:

- *Room (1)*: The kitchen contents are a dishwasher (PR: $\sim 1200 : 2400\ W$), and an oven (PR: $\sim 2000 : 5000\ W$).
- *Room (2)*: The laundry room contents are a washing machine (PR: $\sim 2000 : 2500\ W$), a tumble dryer (PR: $\sim 2000 : 2500\ W$), a refrigerator (PR: $\sim 300 : 800\ W$), and a light (PR: $\sim 6 : 60\ W$).
- *Room (3)*: The contents are an electric water heater (PR: $\sim 1375 : 4245\ W$), and an air-conditioner (PR: $3500\ W$).

As a proof of concept, we aggregated the energy consumed by each room every minute within a time interval of half an hour for the whole day. Fig. 4.1 presents the aggregated consumed energy for a randomly selected day from each season. It can be seen from Fig. 4.1

that the activities of the house occupants in all rooms are low at the night hours from [23 : 00 : 00] to [06 : 00 : 00]. Contrary to the morning hours, activities are observed in Room (1) "Kitchen" at breakfast and lunch times. Meanwhile, we can observe other activities in Room (2) due to high energy consumption from the tumble dryer and washing machine (e.g., see Fig. 4.1(a) between [14 : 00 : 00] and [16 : 00 : 00]) which can indicate that the residents are doing their laundry.

Furthermore, as can be observed in Fig. 3.17, the behavior of Room (3)'s sub-meter, in all sub-figures (a) to (d), indicates that the air-conditioning unit and/or the water heater were actively used during the afternoon hours and occasionally at night, despite the season.

Machine-learning-based load classification approach

In a two-phase process, we train and test the machine-learning kernel using the energy consumption data related to different activities in each room at different time slots (t). The training and testing phases are further elaborated on in this subsection.

As a first step, we split the energy consumed every half hour of a specific activity (x) into different classes. The adjustable parameters pertaining to the classification scheme are the number of classes and the range of each class. These parameters can be tailored according to the characteristics of the room under consideration, specifically the number of devices (N) and their corresponding energy consumption levels (E_i, where i represents the index of each device within the range 1 to N). For instance, in the context of a room denoted as "room (2)," where a total of $N = 4$ devices are present, the resulting number of classes can be calculated as $2^{N=4}$, yielding a value of 16 distinct classes. The range of each class will be determined by the combination of energy consumption levels exhibited by the different devices within the room. Given the open dataset only provide energy consumption information on a room level and not a device level, we use the following classes, as a proof of concept.

- *Class (1)*: $200\,Wh > x \geq 100\,Wh$.
- *Class (2)*: $300\,Wh > x \geq 200\,Wh$.
- *Class (3)*: $400\,Wh > x \geq 300\,Wh$.
- *Class (4)*: $500\,Wh > x \geq 400\,Wh$.
- *Class (5)*: $600\,Wh > x \geq 500\,Wh$.

Note that, we did not consider very low consumption data ($x < 100\,Whr$) for the entire year, as it indicates no holding activity. For the training purposes of different machine-learning algorithms, 80% of the data in the same form presented in Fig. 3.17 is used for training, while the rest of the data, 20%, is used for testing purposes. The classifier output categorizes each room's daily activities into five classes. In this study, we investigated this approach with different types

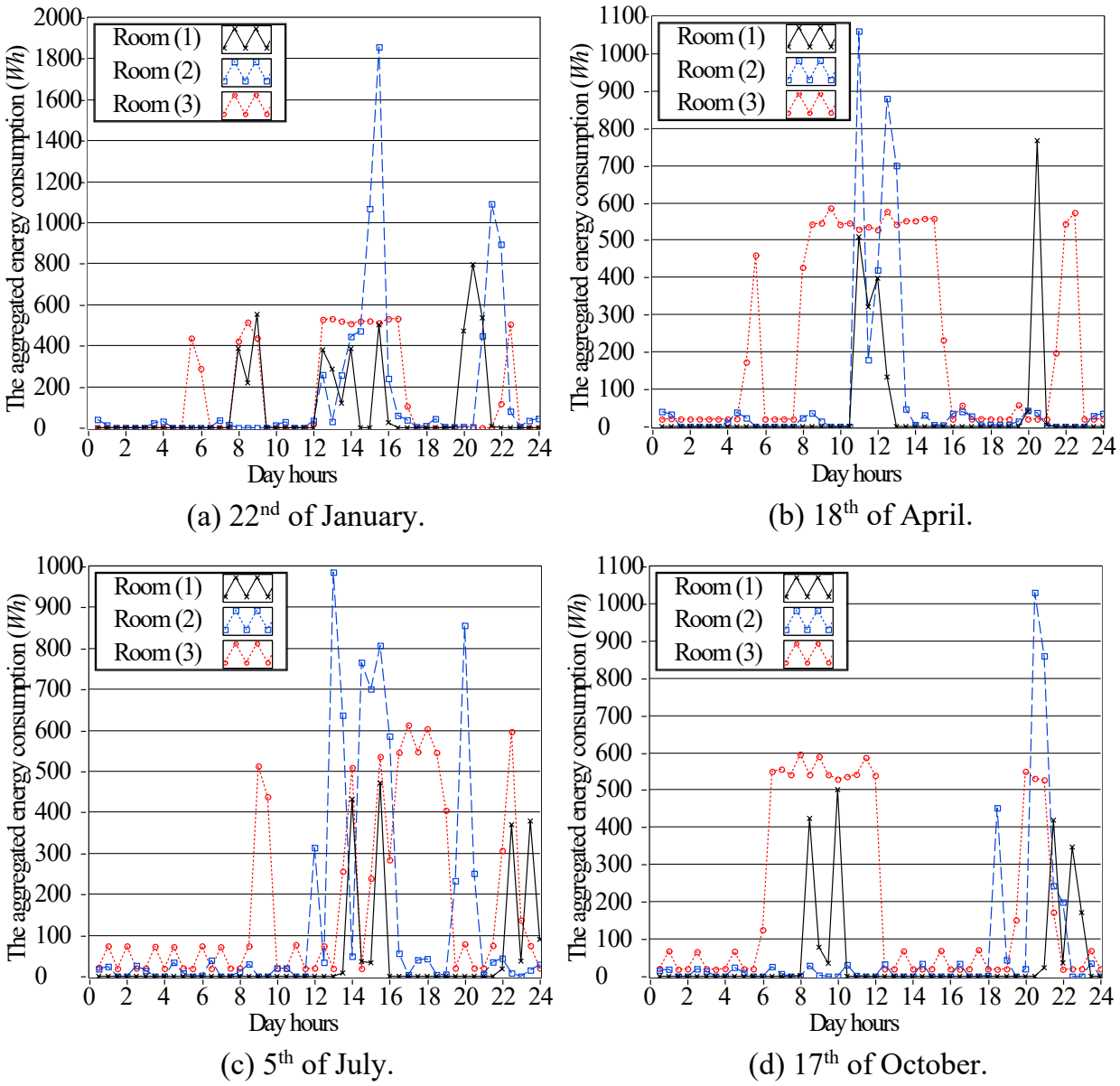

(a) 22nd of January.

(b) 18th of April.

(c) 5th of July.

(d) 17th of October.

Figure 3.17: The energy consumption (Wh) over randomly selected days.

of machine-learning algorithms, including Decision Tree, K-Nearest Neighbour, Random Forest, and Support Vector Machine. The specific configurations used for each algorithm were as follows:

1. *Decision Tree (DT)*: We employed a distribution smoothing factor of 1 and a feature fraction of 1.

2. *K-Nearest Neighbour (KNN)*: For this algorithm, we set the number of neighbors to 20, the distribution smoothing factor to 0.5, and used the KDtree method for determining nearest neighbors.

3. *Random Forest (RF)*: In the Random Forest algorithm, we utilized a feature fraction of 1, a leaf size of 5, and a total of 50 trees. Additionally, we applied a distribution smoothing

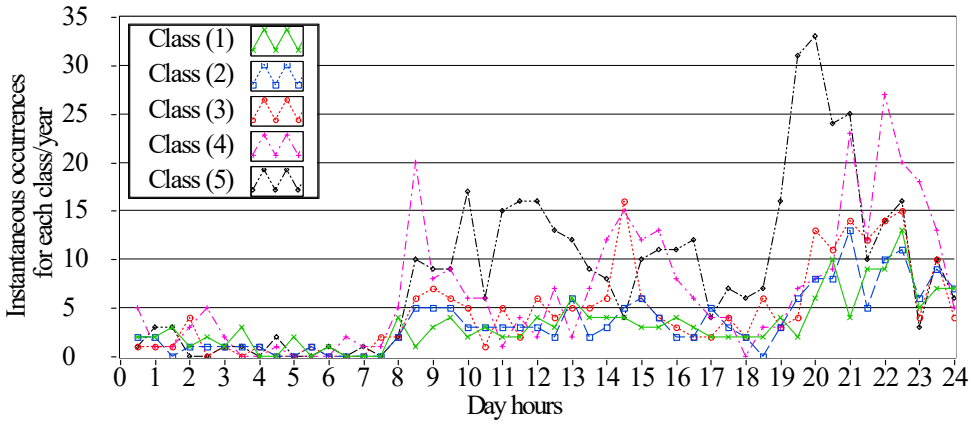

(a) Room (1).

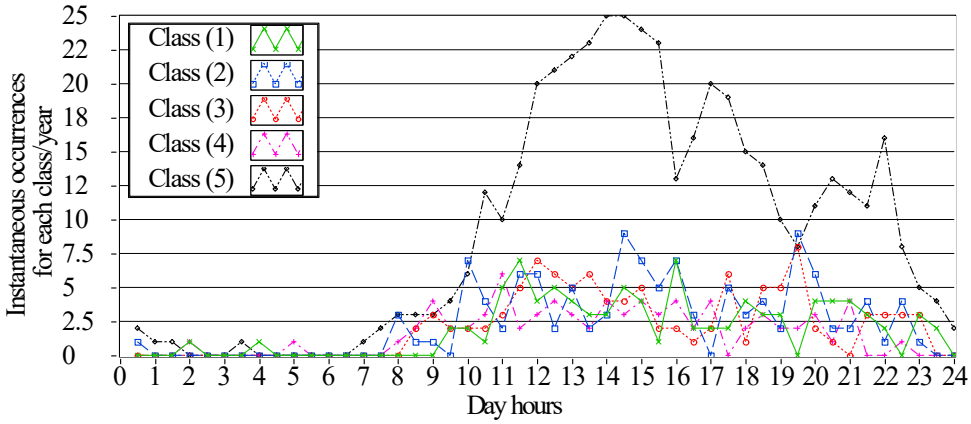

(b) Room (2).

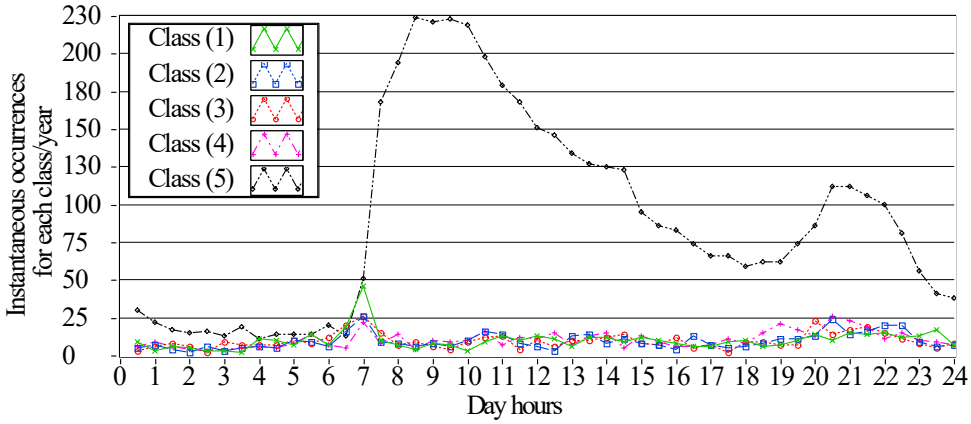

(c) Room (3).

Figure 3.18: Instantaneous occurrences for each class/year.

factor of 0.5.

4. *Support Vector Machine (SVM)*: The SVM algorithm was configured with a radial basis function as the kernel type. We set the Gamma scaling parameter to 0.473, the soft margin parameter to 3, the polynomial degree to 3, the bias parameter to 1, and employed the one versus one strategy for handling multiclass classification.

Table 3.2: The classification report of
SVM-based machine-learning methods

Class No.	Room (1)			
	Precision	Recall	F1-Score	Support
Class (1)	1	0.965	0.982	28
Class (2)	0.975	1	0.987	39
Class (3)	1	1	1	32
Class (4)	1	1	1	54
Class (5)	1	1	1	97
Class No.	Room (2)			
	Precision	Recall	F1-Score	Support
Class (1)	1	1	1	16
Class (2)	0.923	1	0.96	2
Class (3)	1	0.833	0.909	10
Class (4)	0.937	1	0.967	15
Class (5)	1	1	1	74
Class No.	Room (3)			
	Precision	Recall	F1-Score	Support
Class (1)	1	0.981	0.990	106
Class (2)	0.955	1	0.977	86
Class (3)	1	0.941	0.97	97
Class (4)	0.962	0.971	0.967	104
Class (5)	0.997	1	0.998	1030

3.3.2 Results and Discussion

Four machine-learning classification algorithms are applied to the electricity data to recognize daily activities in three rooms. The classification results are presented in Fig. 3.18. In this study, the number of instantaneous occurrences of a specific activity x in the whole year is denoted by $|x|$. As can be seen from Fig. 3.18, $|x|_{Room(1)} \sim 17$ times/year for class (5) at $t = [12:00:00]$, while this value at $t = [19:30:00]$ is about ~ 33 times/year. In other words, we observe high energy consumption activities in Room (1) at this time of the day. Similarly for Room (2) and (3), $|x|_{Room(2)}$ for class (5) is higher than that for other classes at $[22:00:00] > t > [12:00:00]$. In Room (3), $|x|_{Room(3)} \sim 225$ times/year at $t = [09:00:00]$, which means high energy consumption activity in the range of class (5) occurred around 225 times/year with probability of daily occurrence equals $\left(\frac{220}{365} \times 100\right) = 60\%$. Any holding activities out of the range of the probability of occurrence at a certain time slot can be considered anomalies. In Table 3.2, you can see an example of the classification report produced by the SVM-based algorithm. As can be seen, the precision, recall, and F1-score are about 0.99, indicating precise classification. In Table 3.3, the accuracies of classification for the four types of machine-learning algorithms are given. The four types of classifiers give high detection accuracy of about ~ 0.99, proving

Table 3.3: The accuracy of detection of different machine-learning methods for Room 1

Room No.	machine-learning Method			
	DT	KNN	RF	SVM
Room (1)	0.999431	0.999715	0.999431	0.999146
Room (2)	0.998862	0.998862	0.999431	0.998293
Room (3)	0.99687	0.99687	0.998008	0.997439

the practicality of the proposed approach to support efficient activity recognition. As a future work, we can build an additional layer of a machine-learning model that can take different classifications from the rooms' models and classifies the activities in the whole house. However, this is outside the scope of this study, but we are eager to explore this area in the future.

3.3.3 Summary

This work proposes an efficient way to classify activities based on energy consumption data generated from a residential building's sub-metering system. Four types of machine-learning algorithms are used to classify the daily activities of house occupants for each room at different times. Through the machine-learning classification algorithms, which had an accuracy of $\sim$ 99%, associated with information on the appliances monitored by each sub-meter, we were able to identify the number of occurrences of using each room throughout the day and across the whole year. With more fine-grained data, this method can be further exploited to develop systems that can give indications of abnormal activities that can be identified from deviations in the usual consumption patterns, which can potentially be used to predict critical events. In the future, we intend to investigate methods for constructing an additional layer within the proposed machine learning-based method. This layer will enable the classification of various activities for detecting anomalies and the prediction of human activity patterns throughout an entire house by leveraging distinct classifications obtained from individual room models. Moreover, we are committed to addressing data protection and security concerns throughout the implementation of this methodology, prioritizing the preservation of security measures and privacy pertaining to sensitive information.

3.4 Human Activity Recognition from Energy Usage Data

Human activity recognition is challenging without losing a user's privacy and loading a user with invasive devices such as wearables, cameras, and mobile applications. As the smart energy meter usage trend is increasing worldwide, there are no privacy losses and new installation cost issues where smart energy meters already exist. Furthermore, out of several factors, household energy consumption patterns mainly depend on the user's day-to-day needs, lifestyle, and time context, which can provide essential activity information within a house. In this work, we have used an open smart energy meter dataset to recognize the activity patterns of inhabitants living in the house. Active and reactive power, current intensity, and energy usage took towards activity recognition analysis. Energy is used to get information related to ongoing activities, and reactive power is used to obtain information about the types of loads used. The Random Forest, Decision Tree, K-Nearest Neighbour, and Support Vector Machines machine learning algorithms are used for activity recognition and load classification. The activity recognition from load classification has given us highly accurate results from Random Forest and Decision Tree with more than 97% accuracy. The human activity recognition approach from smart energy meter data has usage in many real-world applications, like non-invasive activity monitoring of lonely living adults.

Inspired by the previous LoRa-based sensing work [124–127], we attempt to analyse the feasibility of adopting LoRa sensing in long and narrow environments. Purpose of LoRa system is to push the range of gait recognition to multiple indoor scenarios including a corridor of $20m$ length; LoRa system is shown in Fig. 3.1.

Vision-based gait analysis and human identification systems have been widely proposed in the literature. However, these systems cannot be readily applied in many real-time applications due to involved challenges such as video quality, obstructuion, and serious privacy concerns.

To overcome such issues, the LoRa system that leverages LoRa signals recognise gait in different indoor environments is useful. LoRa sensing work is based on the intuition that the walking pattern of different users can be distinguished by distinct stride size and frequency. The wireless LoRa signal which is interfered by human walking will capture the gait information of subjects. In combination with the long-distance transmission ability of LoRa signal, the system enables a larger sensing range of gait recognition compared to the WiFi-based gait recognition system. The proposed LoRa system has been validated in three different scenarios for gait recognition namely line of sight (LOS), non-line of sight (NLOS), and long-distance, with accuracy of 85.13%, 79.14%, and 84.14%, respectively.

3.4.1 Methodology

Electricity usage data recognize human activities and behavior towards energy utilization while avoiding the hassle of buying, wearing, and installing different sensors and devices. Activity recognition from smart energy meter data needs electricity usage data from a smart energy meter

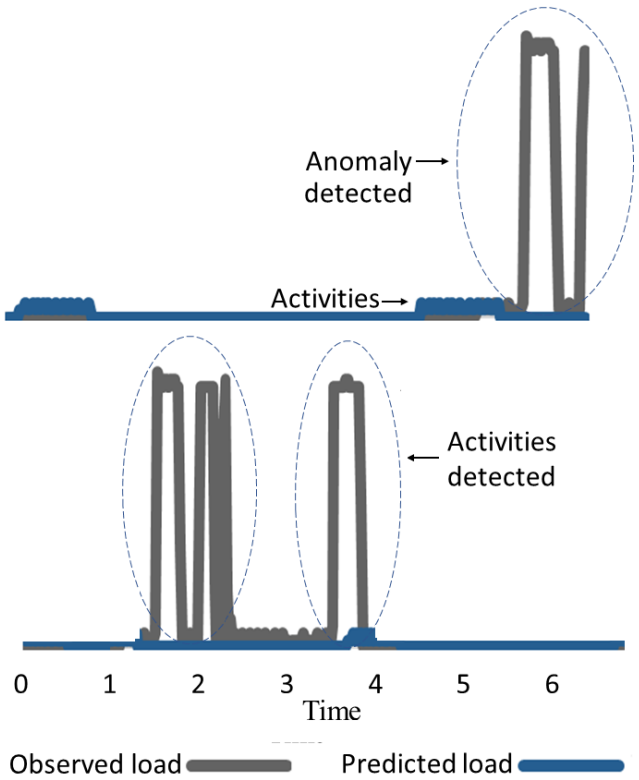

Figure 3.19: Activities and anomalies: Anomalies are not only on the higher side of the load but also on the lower side, e.g. if no load is detected or the load is less than the baseload for a long time.

and an intelligent device that can receive data from the energy meter, calculate a base load, compare newly coming data with the baseload and predict activities, as shown in Figure 3.19. Electricity usage data, when compared with the baseload; operated load, and their location in the house, can be recognized precisely. A separate smart energy meter has been installed in each room to identify specific activities in different rooms. Activities coming from individual room meters can be cross-compared later with activities coming from the main meter.

Activity classification

It is difficult to explicitly model anomalies in Figure 3.19, so it is better to define and monitor normal activities and let the model learn abnormal behavior when anomalies occur over time. One smart energy meter is installed to monitor overall household voltage, current, power, and energy. Each room has its own sub energy meter that monitors all electricity parameters. The household baseload is calculated from the minimum hourly load for one month. If the load at any interval of time goes beyond the baseload, some activity will start, which will remain alive until the load changes. There can be more than one overlapping activities at one interval of time. If the load on the main smart energy meter remains equal to or less than the baseload, then there will be nobody at the house, or if someone is in the house, however, there is no ongoing activity.

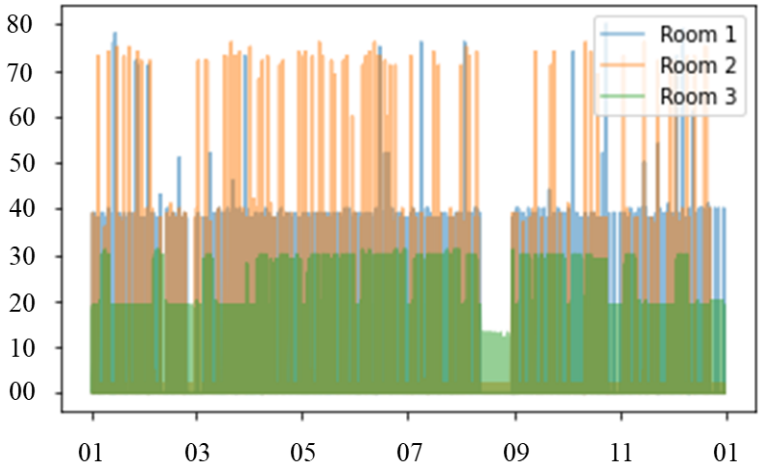

Figure 3.20: Household annual energy consumption in three rooms

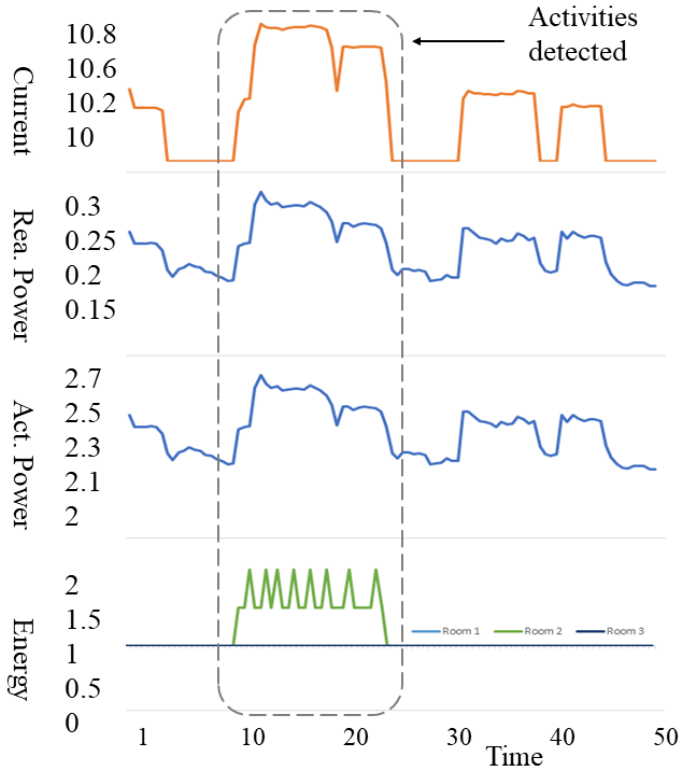

Figure 3.21: Activity detection from current, power and energy consumption.

Apart from regular activities, if either there is no activity happening for the last twenty-four hours or there is not any change in current activity over the previous twenty-four hours, there will be anomaly detection.

Time and load context

Time context has divided into weekdays and weekends. Weekdays are further divided into working days and holidays. Activities and anomalies behavior can vary according to time context. Time context also includes the daytime and nighttime. For example, frequent visits to the bath-

Table 3.4: Data Classes and their Description

S.No	Class	Class Descriptions	No. of Classes	Count
1	Empty	No human subject in the activity area.	1×1	100
1	Sitting	"Sitting" activity at a designated location.	1×2	200
2	Standing	The action of "Standing" activity at the designated location	1×2	200
3	Leaning Forward	The action of "Leaning" activity at the designated location	1×2	200
4	No Activity	The action of "No" activity at the designated location	1×2	200
5	Walking Rx-Tx and Tx-Rx	From USRP X310 Rx to USRP X300 Tx	1×2	200

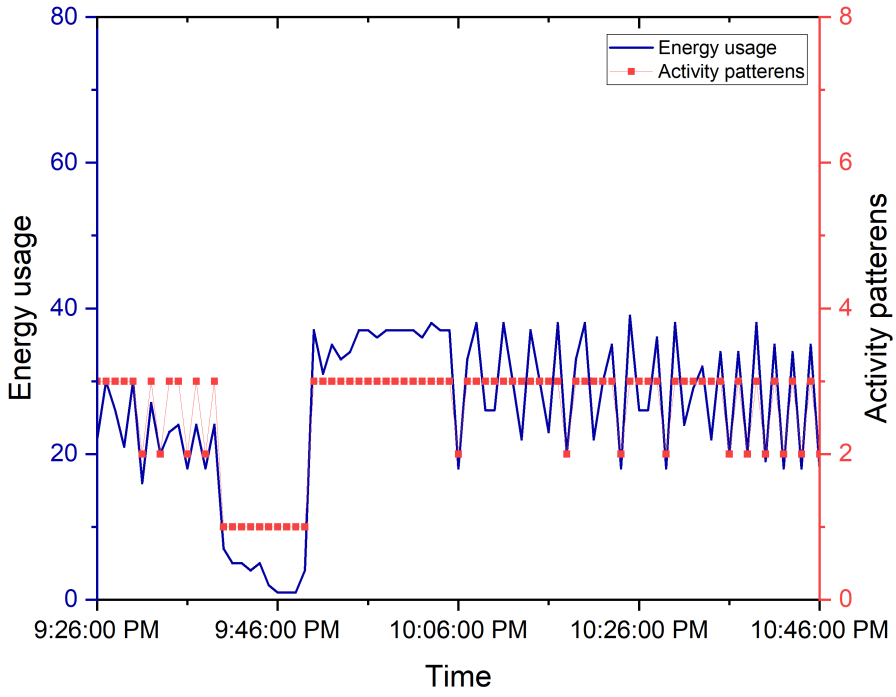

Figure 3.22: Activities during OFF working hours

room during the day can detect may be a user has some stomach, bladder, or glucose level disorder. Similarly, lights on during the night or frequent visits to the bathroom can detect if a user might have some sleeping disorder that can lead to serious health problems.

Electricity components used for activity recognition are active power, reactive power, energy, and current, as shown in Figure 3.21. The main smart energy meter uses power and current to

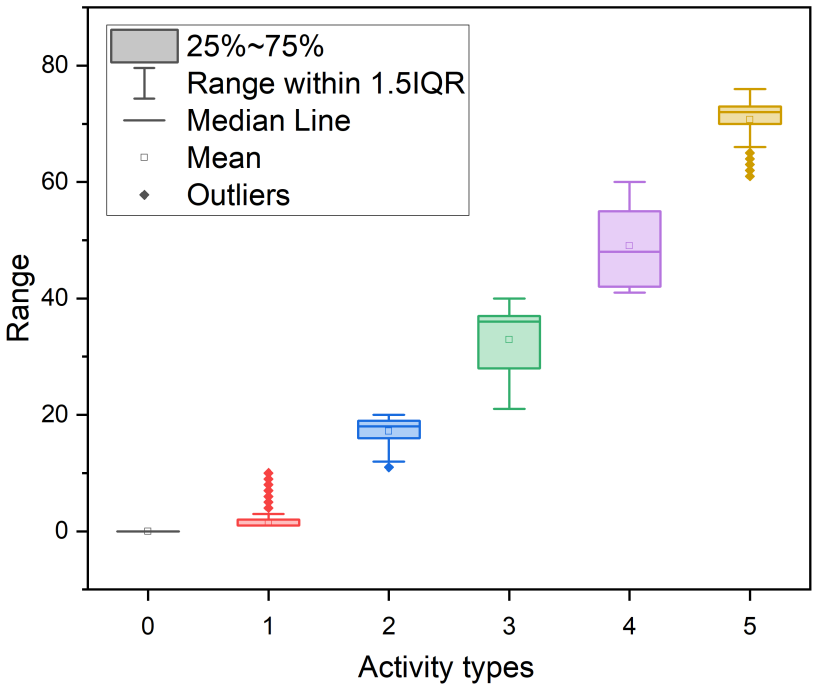

Figure 3.23: Load classification from different energy levels: Some outliers are due to AC load fluctuations, and others are transitions between previous and subsequent classes.

recognize activities. In contrast, energy from submeters is used to determine further which room or house location activity has happened. Both power and current have been used simultaneously from the main energy meter to monitor activities. In contrast, only energy data is used for submeters to check activity recognition and location confirmation. Reactive power provides only information related to the load on which activity is being performed, while energy locates the exact place of activity. Data is collected from one house for two years of duration.

Load classification

There is one main smart energy meter for complete load and three submeters for individual rooms. Data is divided into sub electricity parameters voltage, current, active and reactive power, and energy units. The highest resolution of data is in minutes, and lower resolutions are available in hours, days, months, and years. Energy data (kWh), as shown in Figure 3.20 has been divided into seven classes. The first chunk has zero to 10 kWh, the second 10 to 20 kWh, the third has 20 to 40 kWh, the fourth has 40 to 60 kWh, then 60 to 80 kWh, and finally above 80 kWh as shown in Figure 3.23. Energy usage against baseload in each room has been calculated according to the minimum hourly load for thirty days. Minimum energy usage for three rooms from baseload for thirty days is zero, and max energy usage is 80 kWh as shown in Figure 3.23 Each energy level, e.g., between 20 to 40 kWh, represents an approximate load rating. In

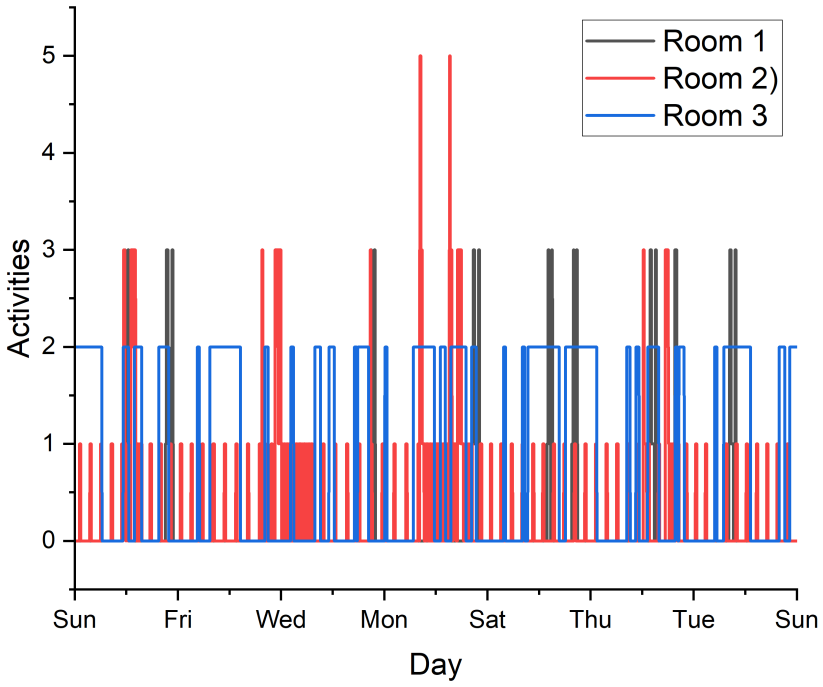

Figure 3.24: Activities patterns during the whole week.

Figure 3.23 energy levels 0-10 kWh represent activity type one, 10-20 kWh represent activity type two, 20-40 kWh represent activity type three, 40-60 kWh represent activity type four, 60-80 kWh represent activity type five, and above 80 kWh represent activity type 6. Whenever a load achieves a certain energy level or one energy level switches to another energy level, an activity will be logged.

Activity Recognition

According to time context, during working weekdays, if the resident is away from home, there should be either no activity or very few activities as most of the load will be OFF. In Figure 3.22 from 9 PM to 11 PM, the resident is inside his home, so there are many different activities. During the daytime, when a resident is out of the house, the activity graph mostly remains either zero or constant between zero and 10 kWh on activity type one. In weekly activity patterns during the nights between Saturday and Monday, activity levels change rapidly while energy consumption is highest during the weekdays, as shown in Figure 3.24. While activity patterns and energy consumption during other weekdays are almost similar during the days and nights, activities and energy consumption are relatively on the higher side during the nights, as shown in Figure 3.22.

Table 3.5: Classification report for Random Forest classifier

Class	Precision	Recall	F1-score	Support
0.0	1.0000	1.0000	1.0000	31964
1.0	0.9998	1.0000	0.9999	37183
2.0	0.9991	0.9994	0.9993	28860
3.0	0.9888	0.9923	0.9906	4175
4.0	0.9910	0.9821	0.9865	2682
5.0	0.9391	0.9391	0.9391	279
6.0	1.0000	0.9622	0.9807	238
Accuracy	-	-	0.9998	105381
Macro avg	0.9882	0.9822	0.9851	105381
Weighted avg	0.9988	0.9988	0.9988	105381

Table 3.6: Classifiers hyperparameter and accuracy for all activity levels.

Classifier	Hyper Parameters	Accuracy
Random Forest	n-estimators=10	0.9990
Decision Tree	max-depth=10, ran state=42	0.9990
K Neighbors	n-neighbors=10	0.9990
Support Vector Classifier	Default	0.9760
Linear Kernel SVC	dim= 6, density= 1.0000	0.9999

3.4.2 Results and Discussion

Four machine learning classification algorithms, such as Random Forest, Decision Tree, K-Nearest Neighbours, and Support Vector Machines, have been applied to the electricity data to recognize daily activities in three rooms. Random Forest Classifier used as the first classifier for 10-estimator. A classification report containing all classes and accuracy is given in Table 3.5. Minimum accuracy is for activity level five, which is 93.91 % due to an unbalanced alternating current load containing high oscillations beyond the estimated activity levels. Accuracy is excellent, around 99% for all other classes containing activity levels besides level five. The confusion matrix in Figure 3.25 contains all data points used to monitor energy and estimated activity levels. Again, for activity level 5, accuracy is minimum while excellent for all other activity levels. A complete comparison of classifiers' details and accuracy is given in Table 3.6. Activity recognition from electricity usage data is efficient in all aspects related to user privacy, system cost, installation complexity, installation time, and non-intrusive and non-invasive solution. Overall accuracy in estimating activity patterns is very high; around 99% accept some activity levels containing high oscillations for AC types of loads. The method is also best to

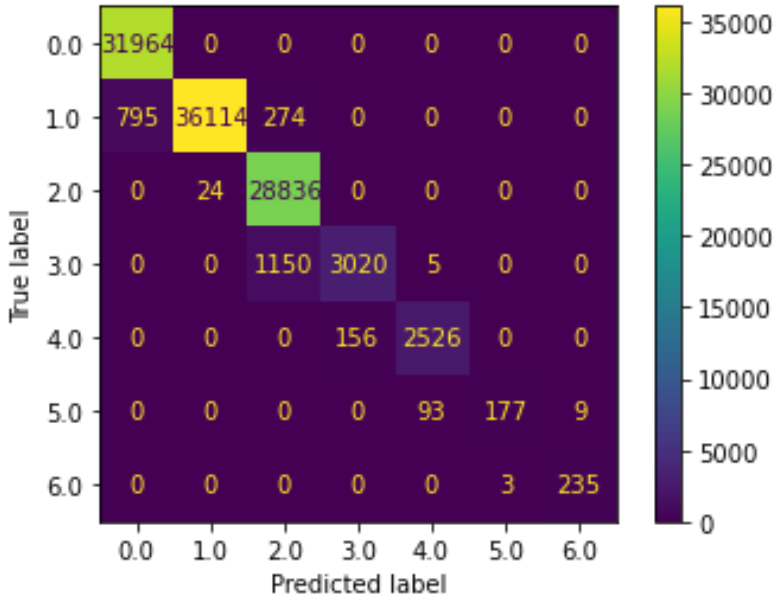

Figure 3.25: Confusion matrix for Random Forest Classifier

predict early symptoms of some of the health-related issues; for example, if activity patterns find frequent visits to the toilet during the night may indicate early signs of diabetes, bladder, or kidney problems. Bedroom lights detected during the night or walking over the rooms late at night can predict early symptoms of depression or some mental health disorder.

Chapter 4

Radar and SDR Signal Driven Human Activity Detection

4.1 Human Activity Recognition from WiFi Signal

Human activity detection in indoor environments is an attractive research field that can assist the elderly and disabled live independently. To detect human activity, various technologies have been proposed, including the use of sensors, cameras, wearables, and contactless radio frequency (RF). With applications in localization, smart homes, retail, gesture recognition, intrusion detection, etc., RF sensing has the potential to become a universal sensing mechanism due to the omnipresent of electromagnetic signals. Recently, there has been a lot of interest in RF sensing's ability to solve the discomfort of wearables and the privacy concerns with cameras using Channel State Information (CSI). This study reports the findings of an experiment to locate activity in an indoor environment utilising Universal Software-Defined Radio Peripherals (USRP) devices. A single subject is observed while performing seven distinct activities. Additional CSI is also collected while the monitored area is empty for further comparison. Machine learning and deep learning techniques are used to classify data more accurately, and convolutional neural network (CNN) has a 97.43% accuracy when it to locating seven distinct activities.

4.1.1 Experimental Setup

The experiment was conducted with ethical approval in a $3.8 \times 5.2 \quad m^2$ room on 5^{th} floor of the James Watt South Building, University of Glasgow. The room is divided into three parts that are spaced one metre apart. The USRP devices were kept at a 45° angle for the transmitter (Tx) and receiver (Rx). Figure 1 depicts seven different activities, including sitting, standing, walking in both the direction of T_x - R_x and R_x - T_x, in two different locations. All seven activities are shown in Figure 4.1 along with CSI amplitude fluctuations. Each colour represents a subcarrier during an activity, with the number of packets on the x-axis and the amplitude of the subcarrier on the y-

axis. Each data sample represents an OFDM transmission of three seconds. As a consequence, a sample of 1200 packets is created. A total of 100 data samples were collected for every activity, i.e., sitting, standing, and walking in both directions. Hence, resulting in a dataset with a total of 700 samples (see Table 3.4).

Preprocessing

It is common for the data to have some missing values after it has been collected and saved in CSV files owing to loss of received packets, hence requiring data cleansing. For data preprocessing and the implementation of ML and DL techniques, we utilize *Scikit*, a widely used data

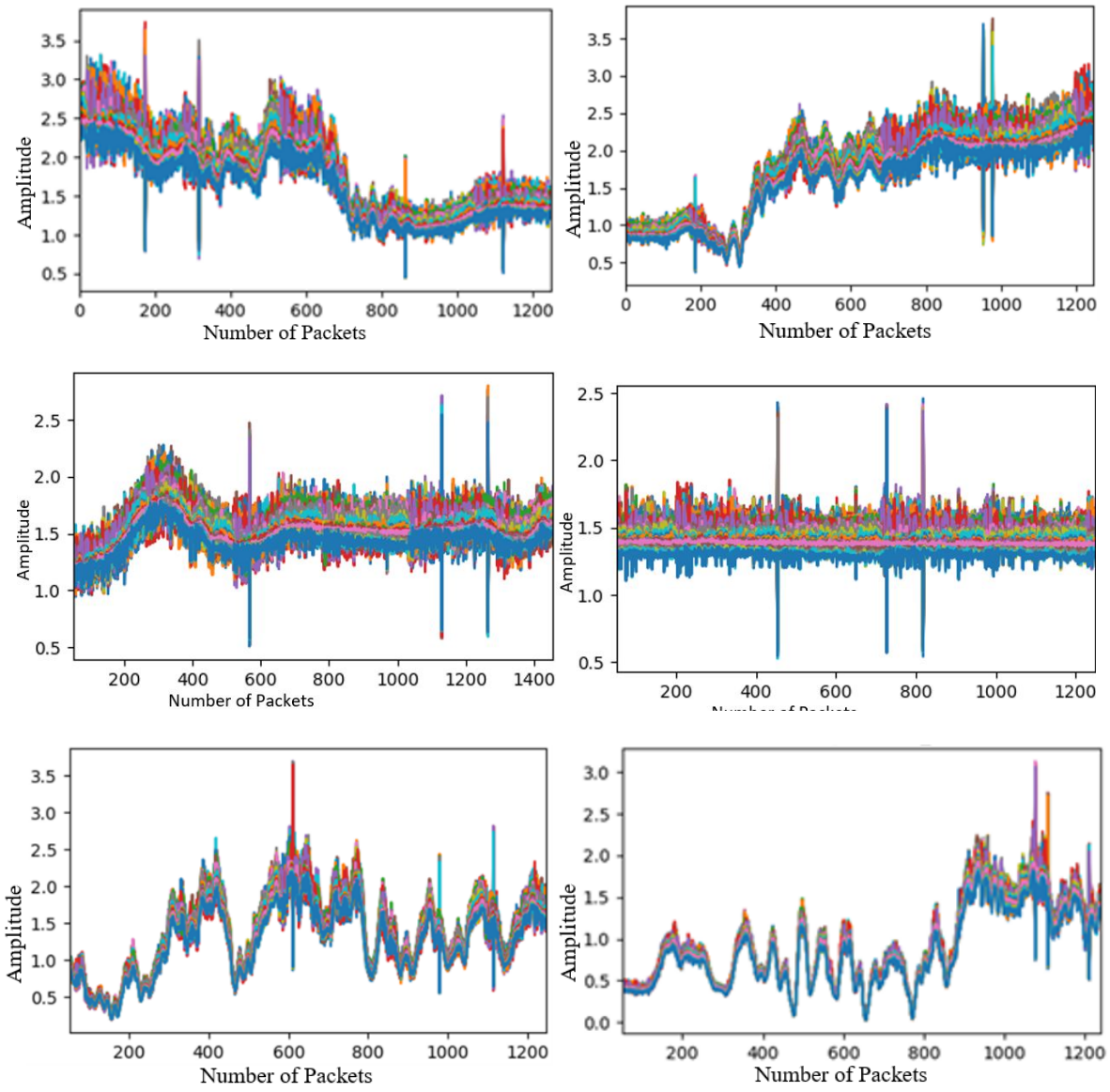

Figure 4.1: CSI wireless data samples of four activities. From Left to Right
(a) Sitting (b) Standing (c) Leaning (d) No Activity (e) Walking from Rx to Tx (f) Walking from Tx to Rx.

analysis toolbox in Python [137]. Additionally, CSV files are interpreted using Pandas, a python library. SciKit [138] is used to analyse Python data frames created by the conversion of .txt files to CSV files. Labels are added into the first column of the dataframes. Not a number (NaN) values are included in the dataset obtained by merging the dataframes from each sample due to inconsistency in data length. These NaN values are changed to the average of each row using SciKit's *SimpleImputer* built-in function. Remember that the overall pattern of the data is unaffected by this kind of data cleansing. The three ML algorithms (RF, SVM, and KNN) and DL algorithms (ANN, CNN and RNN) are used to process this data once it had been normalized.

Machine Learning and Deep Learning Algorithms

The proposed wireless sensing-enabled indoor human activity monitoring system is evaluated using three ML and DL algorithms.The assessment criterion used in this experiment is the precision of accurately recognising different human activities. The accuracy was evaluated using *RepeatedStratifiedKFold* cross validation. Repeated k-fold cross-validation provides a way to improve the estimated performance of a ML model. This involves simply repeating the cross-validation procedure multiple times and reporting the mean result across all folds from all runs. For example, 10-fold cross-validation was repeated five times, 50 different held-out sets would be used to estimate model efficacy.

Deep learning neural networks used to supports this multi-label classification problems that can be easily defined and evaluated using the Keras deep learning library. We have used the *make-multilabel-classification()* function in the scikit-learn library with the popular *ReLU, Softmax* activation function in the hidden layer. The hidden layer has 200 nodes that were chosen after some trial and error. We have fit the model using the Adam version of stochastic gradient descent and the hyper parameters are shown in Table 4.1.

4.1.2 Result and Discussion

The results of the ML and DL are shown in Table 4.1. These results show the relationship between locating and identifying activity at two separate locations in the monitoring area. The CNN algorithm has the highest accuracy score of all the algorithms when compared to the results in the combined data experiments i.e. Location 1 and Location 2. The DL (CNN and ANN) algorithms are able to attain accuracy score of 97.43% and 92.30% respectively. Similarly ML (SVM and RF) algorithms have accuracy scores 91.11% and 90.72% respectively on combined (Location-1 and Location-2) dataset. On the other side, KNN and ANN achieved lowest accuracy which are 88.56% and 90% respectively. The comparison graph on combined (Location-1 and Location-2) dataset is shown in Figure 4.2. These results indicated that algorithms are better at discriminating between locations when they are separated from one another by a greater distance. The fact that CSI fluctuations increase with distance from the transmitter most proba-

Table 4.1: Hyper-parameters of Machine Learning and Deep Learning algorithms

S.No	Algorithms	Hyper Parameters
1	Random Forest	RepeatedStratifiedKFold (n-splits : 10, n-repeats :3, random-state : 1), max-features: log2, n-estimators: 1000
2	Support Vector Machine	RepeatedStratifiedKFold (n-splits : 10, n-repeats :3, random-state : 1), C: 50, gamma: scale, kernel: rbf
4	K-Nearest Neighbor	RepeatedStratifiedKFold (n-splits : 10, n-repeats :3, random-state : 1), metric : euclidean, n-neighbors : 1, weights : uniform
5	Artificial Neural Networks	units=4, hidden-layer-activation='relu', kernel-inetiaizer:'uniform', optimizer='adam', batch-size=32, epochs = 200, connected-layer-activation:'softmax'
6	Convolutional Neural Networks	units=4, hidden-layer-activation='relu', kernel-inetiaizer:'uniform', optimizer='adam',layer:4, kernel-size:6, batch-size=28, epochs = 250, connected-layer-activation:'softmax', filter:(128,64,32,4)
7	Recurrent Neural Networks	Layer:5, Dense: horizon, dropout:0.2, activation-function: 'tanh', optimizer:(lr:0.01, momentum:0.9)

bly explains this. As locations are closely connected to one another, the difference between CSI fluctuations becomes less. Despite this, the algorithms, particularly the CNN algorithm followed by RNN have proved to be very accurate.

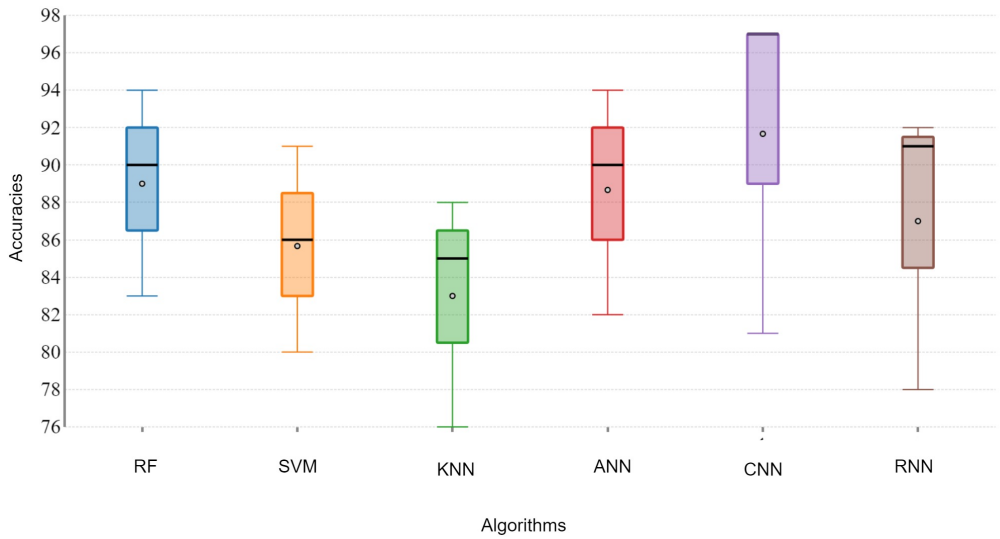

Figure 4.2: Comparison of ML and DL Algorithms on combined dataset from Location-1 and Location-2

4.2 Contactless Sleep Quality Monitoring Exploiting Radar Signal

Sleep quality monitoring is vital for managing health risks associated with sleep disorders. Traditional methods, such as polysomnography, are invasive and can disrupt natural sleep patterns. This section presents a novel, contactless approach to sleep monitoring using ultra-wideband (UWB) radar, providing a non-intrusive solution that detects key indicators of abnormal sleep, including periodic limb movements, frequent body position changes, and prolonged static position. Exploiting deep neural networks, specifically the VGG16 model, our method achieves 98% accuracy in classifying sleep quality features, shows its robustness for reliable analysis. The radar's high sensitivity to body movement enables monitoring without the need for wearable sensors, making it a practical alternative for clinical and home applications to a scalable, accurate and comfortable sleep monitoring.

Recent studies show that between 10 and 40% of the global population experience sleep disturbances linked to an increased risk of conditions such as cognitive problems, depression, and cardiovascular disease [136, 139, 140]. In clinical settings, sleep quality monitoring methods, such as polysomnography (PSG), portable devices, and cameras, face significant limitations despite their widespread use [141]. PSG, the gold standard in clinical sleep analysis, requires that numerous sensors be attached to the patient, leading to discomfort and possible disruption of natural sleep patterns [141]. Similarly, wearable devices, while less invasive, can cause discomfort and produce inaccurate results due to inconsistent wear habits [142]. These challenges highlight the need for a convenient, contactless solution that can provide accurate, real-time sleep data without disturbing the user's natural sleep environment [142]. Radar-based sleep quality monitoring has potential as a promising alternative that overcomes the limitations of traditional contact-based methods [143–145]. Radar offers a contactless approach that detects even subtle body movements with high sensitivity while preserving patient comfort [146]. This non-invasive approach is beneficial for capturing detailed sleep data including normal and abnormal sleeping patterns without the need for sensors directly applied on the body [146]. Further, radar-based solutions allow for continuous monitoring over extended periods, which is essential for long-term sleep assessment and for detecting irregular patterns that may indicate underlying health conditions [147].

Feature extraction from radar-based sleep data is critical for interpreting sleep quality and automating data analysis analysis [148]. Important features, such as periodic movement of the limbs, frequent changes in the lying position of the body, and prolonged periods of static sleep, provide insight into sleeping behaviour and potential sleep disturbances. Integrating these features with deep neural networks, such as convolutional models, enhances the classification and analysis of sleep-related disorders. The combination of feature extraction and the deep learning model allows more accurate and efficient analysis, allowing healthcare providers to assess sleep

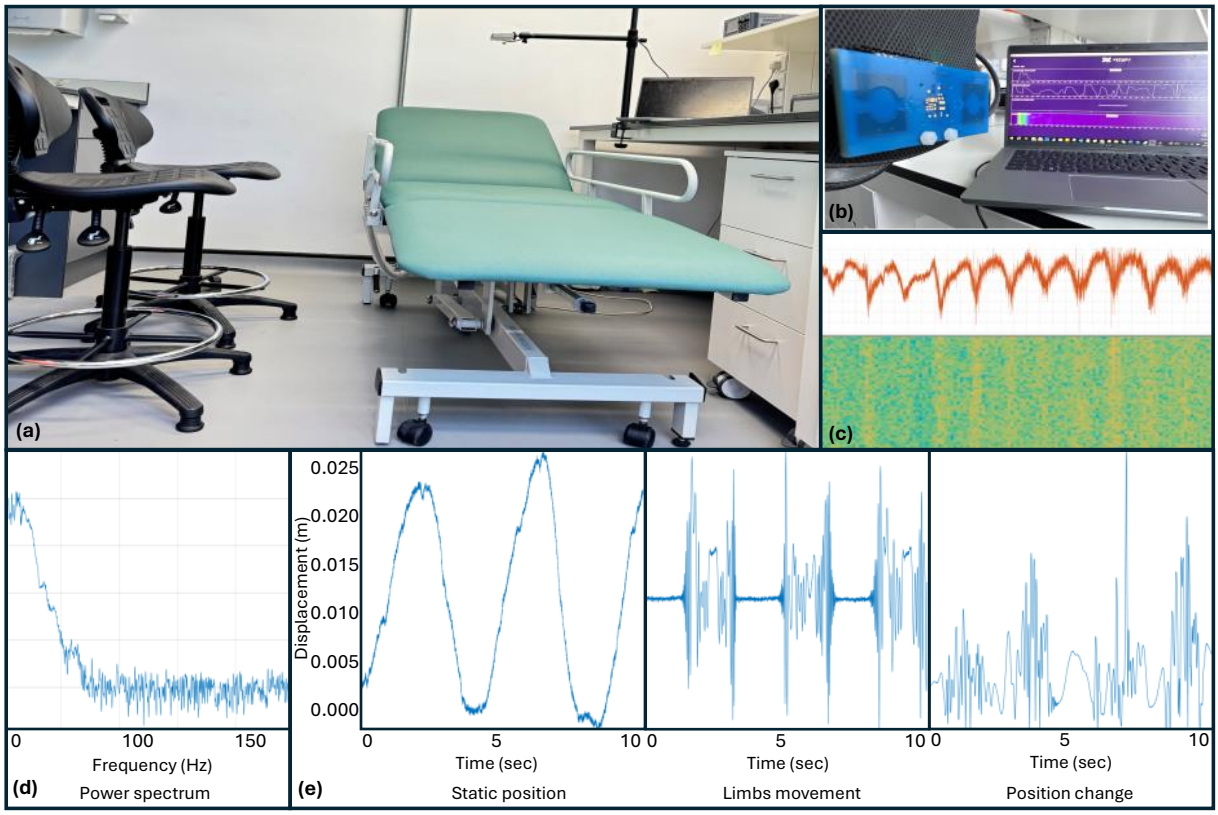

Figure 4.3: Figure 1(a) illustrates the experimental setup, while Figure 1(b) presents the study used the following hardware. Figure 1(c) displays the raw data captured by the radar, and Figure 1(d) includes the power spectral density. Finally, Figure 1(e) shows the various sleep features extracted from the processed radar data.

quality without manual intervention and with higher precision [85].

In this section, we used an ultrawideband (UWB) radar to non-invasively extract abnormal sleep related features such as periodic limb movements, frequent body position changes, and prolonged static sleep periods. To automate the feature classification analysis, we applied a deep learning classification model to predict abnormal sleeping patterns among normal sleep orders with high accuracy. We made the following contributions for the first time to the best of our knowledge:

1. Contactless sleep monitoring using UWB radar and feature extraction, focusing on periodic limb movements, body position changes, and static sleep periods.
2. Achieving 98% classification accuracy in sleep quality analysis with the VGG16 deep learning algorithm, demonstrating the robustness and precision of the model.
3. Provide a scalable framework for nonintrusive sleep monitoring that simplifies long-term data collection and analysis for potential healthcare applications.

4.2.1 Methodology

Experimental Setup and Data Collection

The experimental setup, as illustrated in Figs. 4.3(a) and 4.3(b), comprises an adjustable hospital bed, an UWB radar system, and a Dell Latitude 5421 laptop, forming an integrated system for contactless sleep monitoring. The core sensor employed is the XeThru X4 radar system-on-chip (SoC) developed by NOVELDA, a high-resolution UWB radar capable of operating within a frequency range from 7.29 to 8.75 GHz, placing it within the C and X bands, provided in TABLE 4.2. The radar is configured to operate at a fixed frequency of 7.29 GHz, with a maximum detection range of up to 9.6 meters, ensuring sufficient coverage for monitoring patients in various bed positions. The transmitter emits a power output of 6.3 dBm, facilitating effective signal transmission for detecting movements within its operational range. With a maximum bandwidth of up to 1.5 GHz, the radar provides high resolution data capture, which is essential for accurately detecting sleep-related movements and subtle positional shifts. This wide bandwidth and precise centre frequency make the XeThru X4 particularly effective for capturing abrupt motion without the need for direct contact with the patient.

This combination of non-invasive approach, radar range, frequency, and power enable the UWB radar to serve as a robust tool for monitoring sleep dynamics and movement with high precision in clinical or home environments, making it an ideal component in continuous, real-time sleep analysis application. The data collection system included a Dell Latitude 5421 laptop, which controlled and powered the hardware throughout the experimental sessions. The laptop, equipped with an 11th Gen Intel® Core™ i7-11850H processor (featuring a 24 MB cache, 8 cores, 16 threads, and a peak frequency of 4.80 GHz), as well as 16.0 GB of RAM, provided sufficient processing capacity for managing and recording the radar data. Powered by a 37.5 W laptop power supply ensured stable operation of the system, even during extended periods of data acquisition. For optimal sensing arrangement, the radar was positioned on a side table 1.5 meters from the subject lying on the bed. This setup placed the radar at an unobstructed position facing the subject, allowing for precise capture of movements and positional changes. The careful alignment and distance ensured that the radar could operate effectively within its

Table 4.2: Parameters configuration of radar software and hardware.

Parameter	**Value**
Platform	Xetru radar X4MO3
Instrumental range	9.6 metres
Target's distance from radar	1.5 m
Operating frequency	7.29GHz
Transmitter power	6.3dBm
Activity duration	10 seconds
Collected samples in each class	15

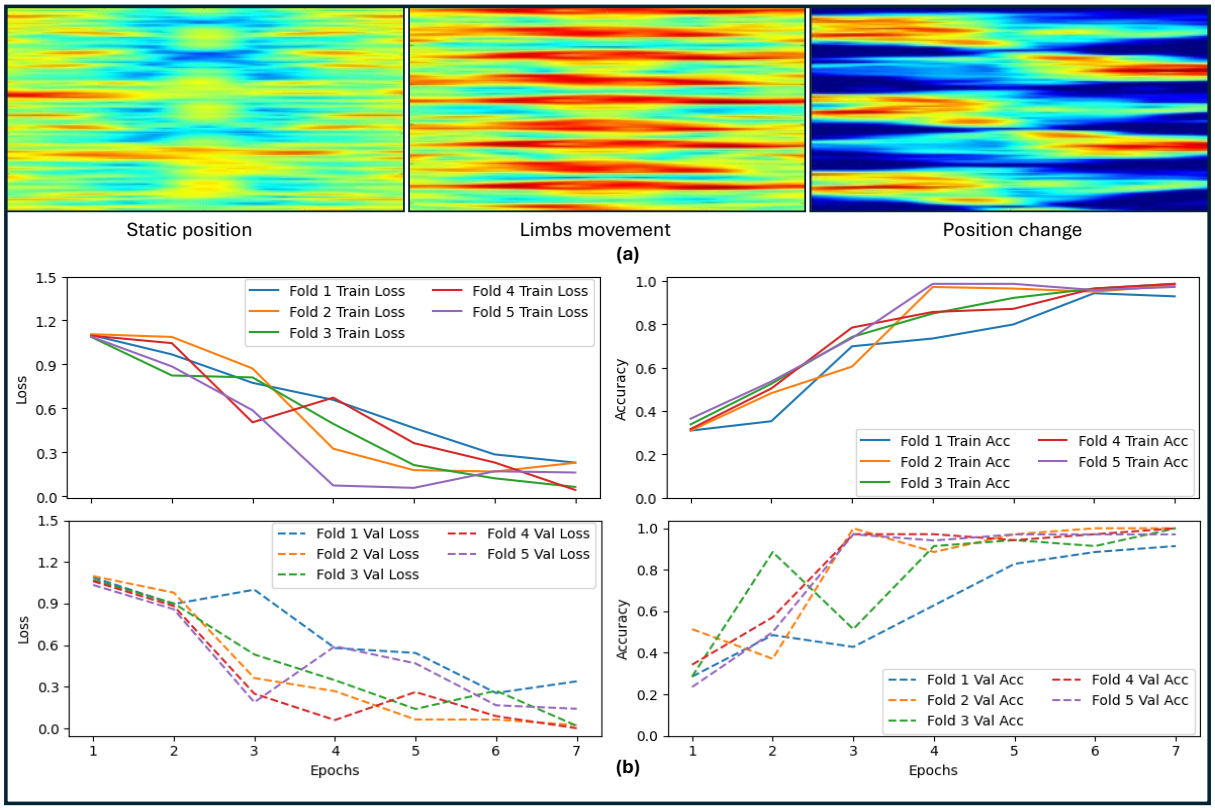

Figure 4.4: Figure 2(a) presents spectrograms corresponding to different sleeping patterns, including static positions, limb movements, and position changes. Figure 2(b) illustrates the training loss, training accuracy, validation loss, and validation accuracy from k-fold cross-validation test for 5 folds over 20 epochs.

range and resolution specifications, thereby maximising data accuracy and reliability during sleep monitoring.

Features Extraction

The radar system generated a DAT data file containing raw radar readings, captured with a sampling frequency of 500 Hz, providing one frame per second. To optimize data management and processing, these data files were segmented into five-minute, one-minute, and 30-second chunks. This segmentation approach helped mitigate the challenges associated with storing, managing, and analysing large volume of continuous data, as extended unbroken data streams can complicate efficient event extraction. In total, six adult male and female participants were involved in the data collection, each repeating a consistent set of sleep activities 30 times. This protocol resulted in the collection of 180 data files, which were subsequently processed for feature extraction. The raw radar data consisted of in-phase (I) and quadrature (Q) components, represented in complex form, as shown in Fig. 4.3(c). The data was carefully examined for missing values and extreme outliers that fell outside the optimal sensing range, as these could negatively impact the analysis. To focus on relevant signal content, frequency bands were applied to the data, as

Table 4.3: Parameter settings for VGG16 Model.

Parameters	VGG16
Initial learning rate	0.0001
Mini-batch size	16
Learning algorithm	Adam
Loss function	Cross entropy
Maximum epochs	20
Iteration per epoch	25

shown in Fig. 4.3(d), all sleep-related activities were found to be contained within an upper frequency band of 100 Hz. From this refined data, key features of sleep activities were identified, including static positions, limb movements, and position changes, illustrated in Fig. 4.3(e). To further analyse the radar signal, a short-time Fourier transform (STFT) was applied, producing spectrograms that captured radar doppler shifts corresponding to participant movements during sleep. This frequency-time analysis facilitated the observation of movement dynamics over time, enhancing the ability to extract meaningful sleep activity features from the radar data.

4.2.2 Results and Discussion

The spectrograms generated from the radar data shows distinct patterns related to different types of sleep-related movements, such as static positions, limb movements, and position changes, as illustrated in Fig. 4.4(a). For classifying these movements, a pre-trained VGG16 model was selected due to its effectiveness in handling spectrograms. The model's parameters are provided in TABLE 4.3. To prepare the data for training, the spectrogram dataset was split into training and testing sets, with 80% of the data allocated for training and 20% for testing. During the training phase, 80% of the spectrogram data was fed into the VGG16 model, and a 5-fold cross-validation test was conducted, as shown in Fig. 4.4(b). This approach utilized a value of k equal to 5 and was executed over 20 epochs, with each epoch containing 25 iterations. The 5-fold cross-validation yielded high training and validation accuracies, ranging from 92% to 99%, and exhibited minimal loss values between 0.4 and 0.05. Detailed metrics such as precision, recall, F1-score, and overall accuracy are presented in TABLE 4.3. Additionally, Fig. 4.5 contains a confusion matrix displaying actual versus predicted labels, providing accuracy details for each classified feature. The VGG16 model achieved excellent overall classification accuracy of 98%, meeting the accuracy criteria of clinical healthcare standards for sleep monitoring applications. Further, the accuracy demonstrates the model's suitability for reliably distinguishing between different sleep movements based on radar driven data patterns.

Table 4.4: Classification report for three classes and accuracy metrics.

Class	Precision	Recall	F1-Score	Support
Class 1: Static position	1.00	1.00	1.00	48
Class 2: Limbs movement	0.95	1.00	0.97	48
Class 3: Position change	1.00	0.94	0.97	48
Accuracy			0.98	72
Macro Avg	0.98	0.98	0.98	72
Weighted Avg	0.98	0.98	0.98	72

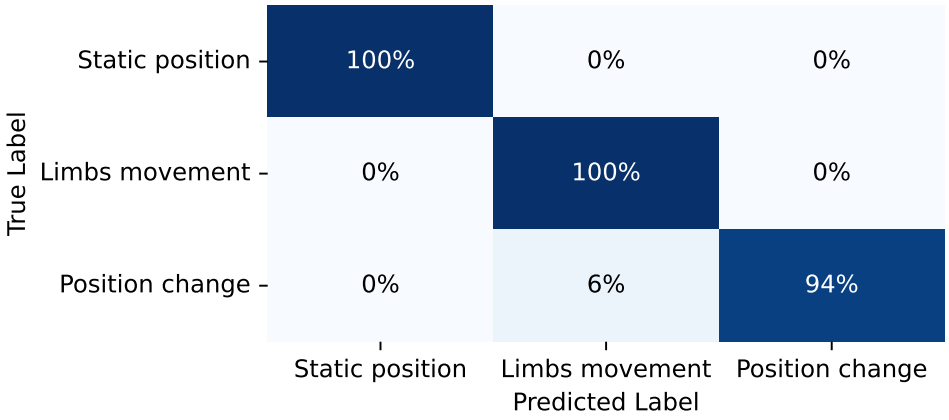

Figure 4.5: Confusion matrix illustrates true and predicted labels for three classes.

4.2.3 Summary

In conclusion, this section introduces a non-invasive approach for sleep quality monitoring using ultra-wideband (UWB) radar technology to detect key sleep-related features, such as periodic limb movements, frequent body position changes, and extended static sleep periods. By integrating UWB radar with a deep learning classification model, we achieved a high accuracy of 98% in distinguishing between normal and abnormal sleep patterns, restructuring the analysis process and eliminating the need for physical contact with the subject. This framework offers a scalable and reliable solution for accurate, comfortable sleep monitoring, underscoring the potential of UWB radar paired with deep learning model to advance non-intrusive sleep quality assessment. This simple approach makes it suitable for both clinical and at-home applications, where continuous, precise, and user-friendly sleep monitoring is essential.

4.3 Contactless Privacy-Preserving Speaker Recognition Exploiting Radar Signal

Speaker recognition (SR) from speech can help determine the environmental context in multi-talker conversational scenarios to enable the design of context-aware multi-modal hearing as-

sistive technology. In this work, we argue that the use of wireless sensors such as radars can offer many benefits over conventional audio and visual sensors, such as not being afflicted by privacy and environmental issues, e.g., improper lighting, environmental noise, and potential security concerns of audio and video channels. Radar is relatively less explored and has many advantages over other contactless approaches, such as being more compact compared to RFID and having a better range and resolution than ultrasound and microwave sensors. To this end, we propose the use of ultrawideband radar coupled with a deep learning model for SR from silent speech to enable the design of future context-aware multimodal hearing assistive technology. We collected a dataset from five individuals with origins in Europe, Asia, and the United Kingdom. We obtained an average performance of approximately 82% in recognising an unknown person from a set of known people. This demonstrates that the radar has good potential to be used for privacy-preserving SR in multi-talker environments where audio-visual and other contactless techniques have limited capabilities.

4.3.1 Introduction

Speaker recognition is the process of identifying or verifying the identity of an individual based on their voice [86]. It has a wide range of applications including security, authentication, and access control. Traditional SR systems rely on audio signals captured by microphones, which can be affected by background noise, distance, and some environmental factors [87, 88]. SR using audio-visual signals, which involves combining information from both audio and visual cues to identify or verify the speaker's identity, has gained increasing attention in recent years [89, 90]. While SR using audio-visual signals has the potential to improve the accuracy and reliability of SR systems [91–93], it is important to consider the limitations of this technology [94]. These limitations include lighting conditions, environmental noise, occlusions, facial expressions, privacy concerns, equipment costs, and algorithmic bias. By understanding these limitations, researchers and practitioners can develop more effective and reliable SR systems [95–97]. In recent years, ultra-wideband (UWB) radar technology has emerged as a promising alternative to traditional microphone-based SR systems. UWB radar technology is capable of detecting and tracking human movements and can provide information about the individual's vocal tract and speech characteristics, which can be used to identify or verify the speaker's identity. UWB radar technology has several advantages over traditional microphone-based systems. One of the main advantages is its ability to operate in noisy environments, as it is not affected by background noise. It can also penetrate through walls and other obstacles, making it suitable for use in surveillance and security applications. Another advantage of UWB radar is its ability to detect small movements and vibrations, such as those caused by the human vocal tract during speech. Overall, non-invasive radar-based SR technology offers a number of advantages over traditional invasive methods of SR. It is non-invasive, accurate, contactless, versatile, cost-effective, portable, and capable of providing real-time results, making it an attractive option

Table 4.5: Summery of contactless sensors used for corpus detection and speaker recognition other than audio-visual techniques.

Reference	Year	Sensing technology	Language	Corpus size	Speakers diversity	Speaker/words recognition	Accuracy
[98]	2022	FMCW radar	European Portuguese words	13	Four speakers	words	84.50% (average)
[99]	2022	SFCW radar	German words	40	Five male speakers 28 to 36 years old	words	76.50%
[100]	2022	SFCW radar	Forty German words and digits zero to nine	50	Two individual speakers	Words	94.02% (average)
[101]	2016	Impulse radio ultra-wideband radar	English	5	Five Korean speakers	Words	85%
[102]	2021	RFID	N/A	0	Fifty dynamic and static users	Person	95.05% (average)
[103]	2018	Microwave	German	25	Two male native German speakers	Words	89% (average)

for a wide range of applications. In this work, we proposed a modality to adopt UWB radar for human identification. Total of five speakers from Europe, China, Pakistan, and the United Kingdom volunteered to take a data set consisting of fourteen different words commonly used in emergency conditions and five English vowels as given in Table 4.5. To the best of our knowledge, this is the first contribution of this kind to recognise a speaker among other known speakers or recognise an unknown person from other known speakers from their speaking styles and facial features detected by radar. In the summary, there are two main contributions of our work:

1. We adopt a contactless method of human identification using UWB signal. The work frequency band of UWB is allowed from 3 GHz to 10 GHz, less distorted by the 2.4 GHz broad Wi-Fi system and other wireless signals.

2. We collected a multimodal human speech dataset including vowels and words by using RF, audio and video signals, from radar and kinect v2 sensor.

UWB radar technology uses short pulses of electromagnetic waves with a very wide frequency spectrum to detect different changes in objects. The pulses are typically in the range of a few nanoseconds to a few microseconds and are transmitted from an antenna [104–106]. The pulses reflect off objects and are received by a receiver antenna. The time delay between the transmitted and received pulses is used to calculate the distance to the object, while the amplitude and phase of the received pulse provide information about the object's properties, such as lips and vocal tract movements, shape of face and speech characteristics. While exploring silent speech interfaces based on frequency-modulated continuous-wave (FMCW) radar in [98], the author recognized 13 words spoken by four different speakers of Portuguese origin with 84.5% average accuracy. Another step frequency modulated continuous wave (SFCW) radar used for silent speech recognition, total of forty German words including nouns, adjectives, verbs, and digits spoken by five male native German speakers aged between 28 and 36 years old. Results accuracy for word recognition is 76.50% and 68.18% obtained using the headset and the tape, respectively [99]. While recognizing forty German words and zero to nine German digits from two persons

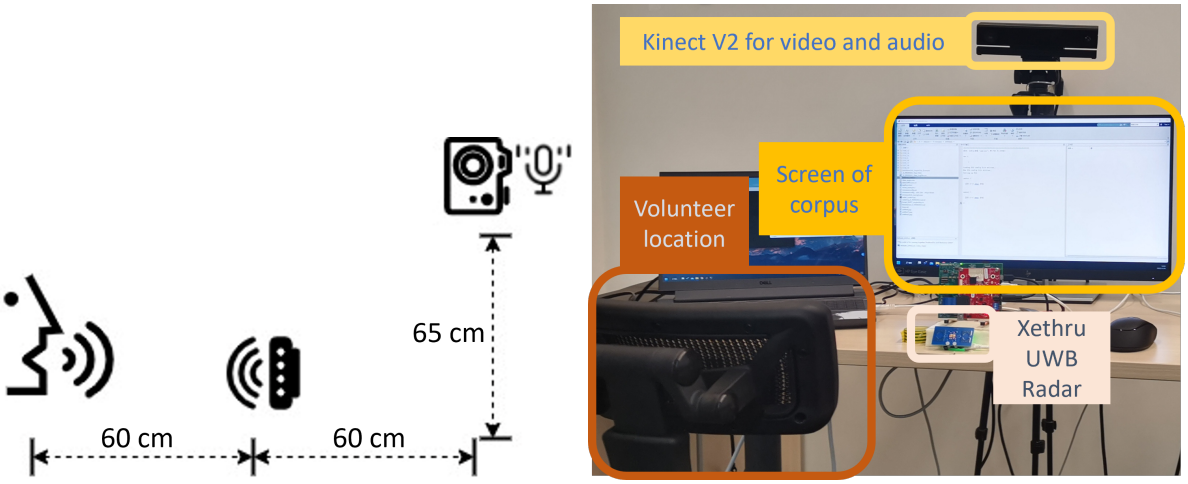

Figure 4.6: Multimodal experimental setup used for data collection.

with the help of SFCW radar, author obtained recognition accuracies of 99.17% and 88.87% for the speaker-dependent multi-session and inter-session accuracy respectively (average accuracy 94.02%) [100]. RFID tags have been used for the identification of people for static and dynamic users [102], author collected walking and body information for identification purposes. Other studies includes microwave sensors [103] and Radars [107, 108], details provided in Table 4.5.

4.3.2 Methodology

Data Collection

In this section, we discuss our data collection strategy and the setup in which data was collected. We start by first describing our experimental setup.

Experimental Setup

This study involves five volunteers from various countries, including Europe, China, Pakistan, and the United Kingdom. Due to the volunteers' distinct accents and body sizes, an adjustable table was implemented to ensure a consistent distance between the speaker's head and the sensors. The dataset collected from the volunteers includes Xethru UWB radar signal for lip motion and audio signal, with the setup shown in Figure 4.6. In this work we are using only RF signal from radar, audio-visual details from Kinect 2 sensor is for ground truth and future data usage for further results.

Data Collection Strategy

To make the data collection process simple, we design a system that can generate the sound of "speaking" and "stop" with timestamps. At the same time, all the other sensors including

Kinect and Xethru radar will be activated for recording. While the sensors were running, the volunteer can read the vowels and words shown on the screen. We manually selected five vowels and fourteen words for reading on a computer screen. All volunteers were informed of the potential risks of the experiment and signed a consent form. The details of data collection are referred to in [149]. No privacy-related information was collected in our dataset and appropriate anonymization was applied to ensure the confidentiality of the participant's data.

Data Preprocessing

The UWB radar we used is based on impulse modulation. The response of radar signal is completely dependent on impulse delay from transmitting to receiving back, which can be represented as the Eq. 4.1

$$s(\tau,t) = \sum_{i=1}^{N} a_i(\tau,t) e^{-j2\pi \frac{d(t)+d_i(\tau)}{\lambda}} \tag{4.1}$$

where the τ and t represent impulse indication in fast-time range and time in frame range, N is the index of the impulse; $a_i(\tau,t)$ represents the complex attenuation factor of the related t slot and i^{th} impulse; λ represents the wavelength of the UWB signal with centre frequency in C or X-Band. The transmitters bandwidth is up to 1.5 GHz, while frames frequency is seventeen frames per second. After the data collection, we first extract the IQ radar signal from binary file and reshape it to the frame which contains fast-time and slow-time dimensions. The frames are identical to the range-time response image because the fast-time domain represents the indicator of time of flight (ToF), which can be calculated to distances. Then, we adopted the moving target indication of frames in sequence to filter the static object out. Then, we calculated the STFT results in the fast-time dimension which is close to the sensing range, and add them together. The spectrograms can be viewed in Figure 4.7.

Machine Learning-based Data Analytics

We formulated the problem of SR as a classical image classification problem. The objective is to learn a latent function $f : x \rightarrow y$ to map x to y, where x and y represent the input spectrogram and its corresponding label, respectively. We leveraged a widely used convolutional neural network architecture known as VGG16 for learning f. Since this model is proposed for 1000 classes, we removed its output layer and stacked a convolutional layer on top of it, having a depth of 32 and a kernel size of 3×3. We then added a max pooling layer that applies a pooling operation with

Table 4.6: List of Corpus used by five different participants.

Type	**Corpus**	**Participants**
Word	Order, Assist, Help, Ambulance, Bleed, Fall, Shock, Medical, Sanitize, Doctor, Rescue, Emergency, Heart, Break.	User 1-5
Vowel	A,E,I,O,U	User 1-5

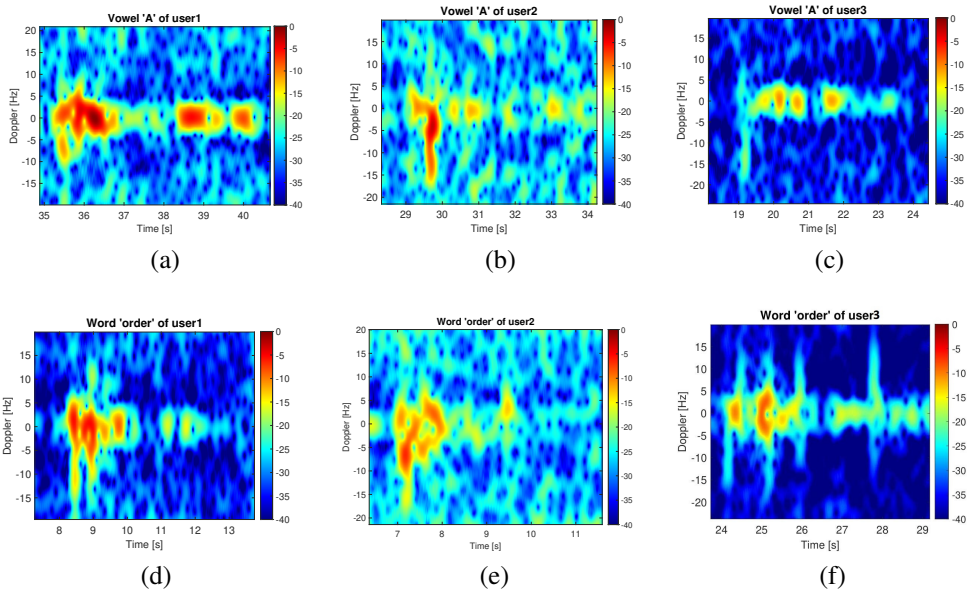

Figure 4.7: The spectrograms generated from UWB radar datasets for corpus from five different users.

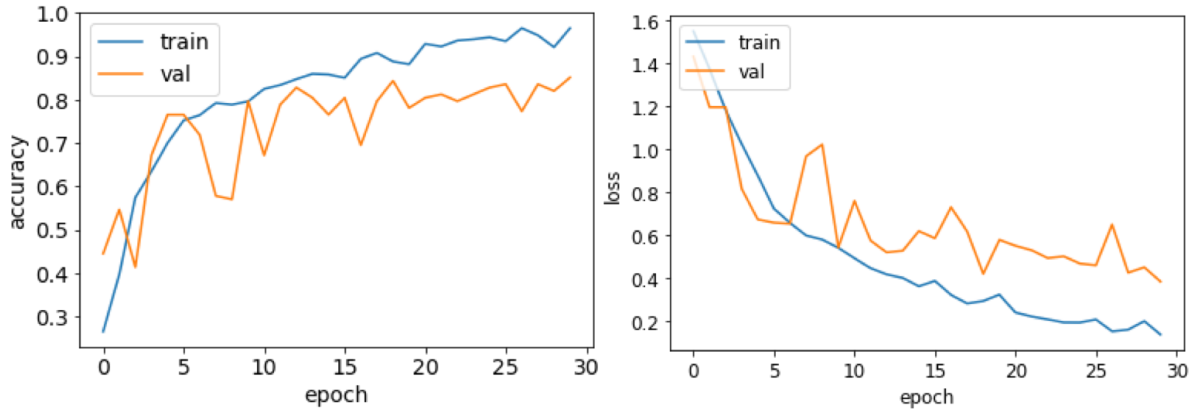

Figure 4.8: Depiction of model training in terms of accuracy and loss over increasing epochs.

a kernel size of 2×2. After that, we added three fully connected layers having 128, 64, and 32 units, respectively. Finally, we used softmax to get the probability vector of size 1×5. We used pre-training with ImageNet weights that allow the model to extract relevant features from the input spectrograms.

4.3.3 Results and Discussions

Data Description

We have data collected from five different persons having native languages from Europe, China, Pakistan, and the United Kingdom. We asked the speakers to speak five English vowels and fourteen different words (a summary is presented in Table 4.5). To ensure a fair comparison and

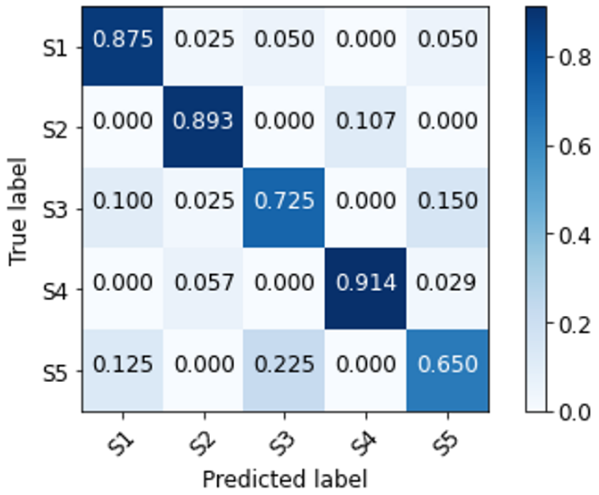

Figure 4.9: Confusion matrix for speaker recognition using our proposed method.

to avoid data bias, we have collected an equal number of samples for each participant. However, note that the resulting signals for each of the speakers vary in terms of time duration (due to demographic variations).

4.3.4 Model Training Setup

We partitioned the collected data into training and testing sets using a split of 80% and 20%, respectively. Furthermore, to ensure an efficient training, we applied 3x data augmentation by using widely used techniques such as shear, horizontal flip, and zooming. We then trained the DL models using training data and evaluated their performance using test data. All images were resized to the same size (i.e., 224×224) prior to training and testing. Since our data size is small, we used pre-training (with ImageNet weights) and fine-tuned the models using our training data. All models were trained using a batch size of 64 and a learning rate of $1e^{-3}$.

Results for Speaker Recognition

The performance curves depicting the model training in terms of accuracy and loss for both training and validation (test) data is shown in Figure 4.8. It is evident from the figure that the underlying model was able to learn latent features from silent speech signal to recognise the speaker. Also, we can see from the figure that the model tends to show an overfitting behaviour (that highlights that the training samples need to be increased for more robust training). We note that the focus of this work is to demonstrate the feasibility of using non-speech signals to perform SR. The confusion matrix that illustrates the SR performance of the trained model is shown in Figure 4.9. The figure reveals that the model provided superior performance for "speaker 4" while it provided the worst performance for "speaker 5". The performance of the model for "speaker 1" and speaker 2" is almost similar and for "speaker 3", the model provided

Table 4.7: Comparison of speaker-wise recognition performance in terms of precision, recall, and f1-score. Legend: S: Speaker; P: Precision; R: Recall; and F1: F1-Score.

S	**P**	**R**	**F1**
S1	0.80	0.88	0.83
S2	0.86	0.89	0.88
S3	0.72	0.72	0.73
S4	0.91	0.91	0.91
S5	0.74	0.65	0.69

comparatively lower performance than speaker "1", "2", and "4" but is considerably higher than "speaker 5". A summary and comparison of speaker-wise recognition performance in terms of different performance metrics, including precision, recall, and F1-score is presented in Table 4.7. The table also supports the analysis from Figure 4.9.

4.3.5 Summary

In this work, we present the feasibility of using data collected through radar to perform speaker recognition. Specifically, we collected a dataset from five different persons speaking different native languages and asked them to speak five English vowels and fourteen different words. We then analyzed the collected dataset using a convolutional neural network (CNN) that provided an overall average performance of more than 82%. While we got a maximum performance of more than 91% for a single speaker ("speaker 4"). Our results demonstrate that the radar possesses great potential to be used for the speaker recognition task that offers a number of advantages over conventional audio-visual signals, including preserving the privacy of users. In our future work, we plan to improve the performance of the developed system along with increasing the size of the dataset. Also, we plan to visualize internal embeddings of underlying deep neural networks to see if the learned features are distinguishable in the embedding space. In addition, we plan to use explainability techniques like class activation maps to see if the model is learning distinct features for each class or not.

Chapter 5

Contactless Horizon of Human Breathing and Pulse Variability

5.1 Contactless Respiration Variability Detection and Accuracy Test Using UWB Radar

This work investigates the potential of radar technology for precise and non-intrusive detection of respiration rate variability. UWB radar, with its ultra-short pulses and extensive bandwidth, offers significant advantages in capturing subtle chest wall movements associated with respiration. It possesses the unique ability to penetrate clothing and physical barriers, making it an excellent candidate for remote physiological monitoring. This ultra-wideband radar system ensures the extraction of accurate respiration waveforms, and deep learning models, including VGG16, Inception V3, and ResNet50, are employed to evaluate respiration rate variability. Remarkably, VGG16 attains outstanding accuracy in results. This study advances the field of radar-based respiration monitoring, emphasizing the importance of robust signal processing and deep learning techniques. It showcases the potential of UWB radar for non-contact respiration monitoring, with applications spanning healthcare and in-home environments, promising to revolutionize the assessment of well-being and health.

5.1.1 Introduction

Contactless respiration rate detection is a critical aspect of healthcare and well-being assessment, offering valuable insights into an individual's physiological state. Traditionally, respiration rate measurements have relied on contact-based methods, such as chest straps and piezoelectric sensors [150]. While these methods have demonstrated accuracy, they are often intrusive, uncomfortable, and may disrupt the natural breathing pattern. In response to these limitations, there is a growing interest in non-contact methods for respiration rate monitoring, utilizing advanced technologies like radar and machine learning [151]. In this context, radar technology has emerged as

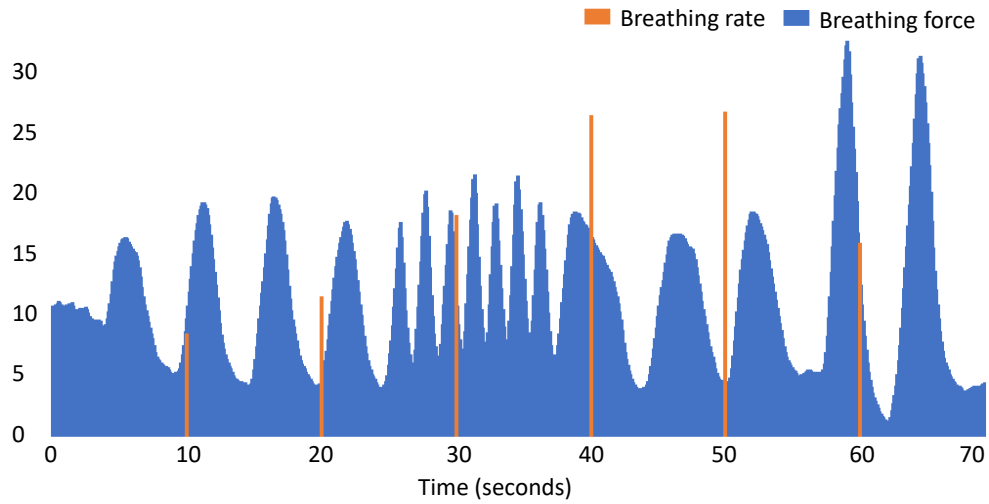

Figure 5.1: Respiration rate variability test for one minute at every ten seconds interval.

a promising candidate, offering the ability to remotely and accurately measure respiration rates without the need for physical contact.

This work presents an investigation into the utilization of Ultra-Wideband (UWB) radar technology for the detection of respiration rate variability (Fig. 5.1), focusing on its potential to provide reliable and unobtrusive monitoring. UWB radar, characterized by its ultra-short pulses and broad bandwidth, offers several advantages for respiration rate monitoring. It provides high resolution in both time and frequency domains, making it capable of capturing subtle chest wall movements associated with respiration. Moreover, UWB radar is well-suited for non-contact applications, as it can penetrate clothing and even through-wall structures, making it a versatile tool for remote physiological monitoring [152].

While UWB radar technology holds significant promise, its effective utilization for respiration rate variability detection relies not only on its hardware capabilities but also on the development of robust signal processing and machine learning techniques. These techniques must accurately extract and analyze the respiration-induced signal from radar data, mitigate environmental interference, and provide real-time and precise respiration rate estimations. Moreover, understanding the limitations and challenges associated with UWB radar-based respiration monitoring is essential for its successful application in healthcare, patient monitoring, and even in-home settings [85]. To the best of our knowledge, we made following significant contributions to this work:

1. We make use of UWB radar system for adults' respiration rate variability detection for the first time.

2. We applied three deep learning models for respiration rate variabilities detection and got maximum accuracy so far with 100% results for VGG16, 93.3% for ResNet50 and 86.6% for Inception V3.

Table 5.1: Summary of papers that used radar technology for respiration rate detection in recent years.

Reference	Year	Sensing technology	Radar Frequency	Human Vitals	Accuracy (%)	Respiration variability
Hernandez et al. [153]	2022	Doppler radar	70 MHz to 6 GHz	Respiration rate detection	NA	No.
Widiyasari et al. [154]	2022	FMCW radar	60 GHz	Respiration rate detection	NA	No.
Siddiqui et al. [155]	2022	UWB radar	8.748 GHz	Respiration rate detection	93	No.
Song et al. [156]	2023	FMCW radar	77 GHz	Respiration rate detection	NA	No.
Han et al. [157]	2022	UWB radar	6.3–8 GHz	Respiration rate detection	95.02	No.
Ebrahim et al. [158]	2023	CW radar	875 MHz	Respiration rate detection	NA	No.
This work	2023	UWB radar	7.29 or 8.748 GHz	Respiration rate detection	100	Yes.

5.1.2 Related Work

The exploitation of radar technology for respiration rate detection has gained significant interest in recent years, with various radar types and methodologies were explored. We review several relevant papers that focus on radar-based respiration rate monitoring while conferring radar type used for respiration rate detection, radar frequency, respiration rate accuracy, if paper discussed respiration rate variability, error in respiration rate, number of subjects used for respiration rate detection and highlighted some limitations from following papers given in Table 5.1. Hernandez et al. [153] developed a method for respiration rate detection by using Doppler radar and Empirical Modal Decomposition. While their work primarily employed Doppler radar, the radar frequency varies from 70 MHz to 6 GHz while respiration rate accuracy was not explicitly mentioned in the paper. The authors discussed the incorporation of radar data into their respiration rate estimation process. A potential limitation of their methodology is the lack of specificity regarding radar parameters and the absence of a detailed discussion on error in respiration rate estimation. Widiyasari et al. [154] introduced contactless respiratory rate monitoring using 60 GHz Frequency-Modulated Continuous Wave (FMCW) radar.

Siddiqui et al. [155] focused on respiration-based chronic obstructive pulmonary disease (COPD) detection by using 8.748 GHz UWB radar combined with machine learning techniques. The paper lack of discussion on the generalizability of their model to different subjects in different environments, which could affect the accuracy of COPD detection. Song et al. [156] introduced non-contact human respiratory rate measurement based on the fusion of video and 77 GHz FMCW radar information. A limitation of their work is the complexity of the fusion process, which might introduce additional sources of error, and the sensitivity of video-based techniques to lighting conditions. Han et al. [157] proposed real-time contactless respiration monitoring

from 6.3 to 8 GHz UWB radar along image processing method. This method needs for clear line-of-sight between the radar sensor and the subject, which could limit its applicability in certain scenarios. Ebrahim et al. [158] developed a low-frequency portable continuous wave radar system for vital signs monitoring. Radar frequency is 875 MHz, it highlighted the use of continuous wave radar for vital signs monitoring, including respiration rate. A limitation of their work might be the lower resolution and penetration capabilities associated with low-frequency radar, which could affect its accuracy in certain situations.

Most of the work demonstrate the growing interest in radar-based respiration rate monitoring, employing various radar types and methodologies [159]. However, the specific radar type, frequency and respiration rate accuracy vary across these studies. Limitations include the lack of detail in radar specifications and potential challenges related to environmental factors and data fusion techniques [136, 145, 160, 161].

5.1.3 Methodology

Experimental Setup and Data Collection

Our data collection setup, as seen in Fig. 5.2, includes XeThru X4, a low-power 7.29 to 8.748 GHz NOVELDA ultra wideband radar system on chip (SoC) with center frequency in C or X-Band. The transmitters bandwidth is up to 1.5 GHz. This UWB radar can detects human vitals by detecting all major and minor movements inside human body.

Radar is attached on a tripod stand for ease of different positions. A micro USB cable connect radar with laptop for radar parameters adjustment and data transfer from radar board to laptop

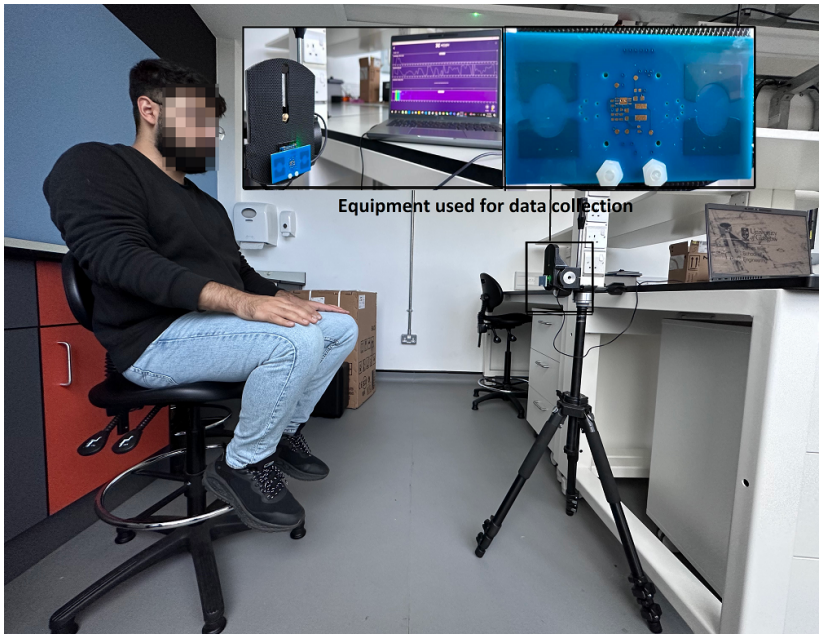

Figure 5.2: Experimental setup and data collection environment.

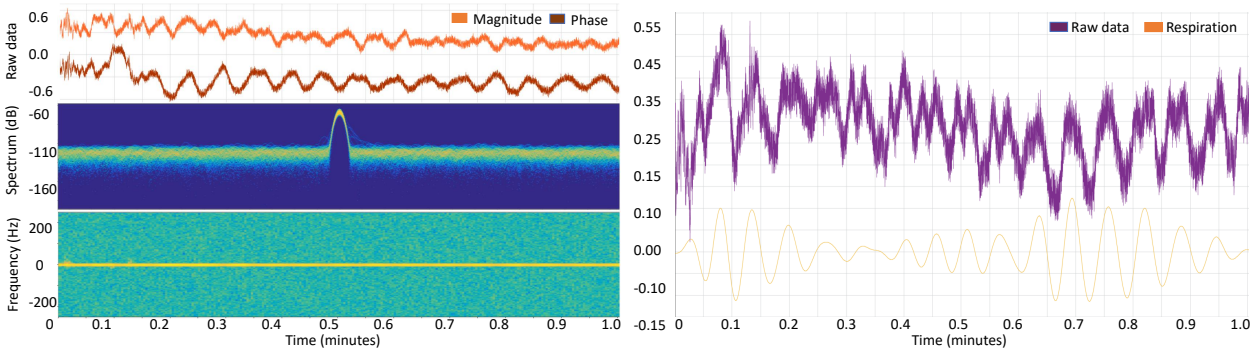

(a) Radar-based processed I/Q data including magnitude and phase.

(b) Phase data and filtered processed data for respiration rate.

Figure 5.3: Magnitude and phase extracted from raw data in Fig. 5.3a, and filtered phase data for respiration rate in Fig. 5.3b.

as given in Fig. 5.2. There are two frequency ranges 7.29 GHz and 8.748 GHZ while maximum bandwidth is 1.5 GHz for data collection parameters adjustment. We used high frequency band 8.748 GHz and Radar data type baseband signal (BB) while detection zone has set to 1.5 meter along the radar line of sight. We located data collection setup in communication sensing and imaging (CSI) lab on level six, James Watt School of Engineering in University of Glasgow. Experiment environment setup selected considering other people flow in the room kept normal so experimental setup comparable to healthcare canters where healthcare staff kept around the subject and radar reading does not change with others nearby influence outside the detection zone.

Data Pre-Processing and Deep Learning

In this section we present a comprehensive data collection and preprocessing details for the evaluation of respiration rate variability using UWB radar data. The radar data is acquired through a USB micro cable and initially received in the form of .DAT files, representing complex In-phase/Quadrature (I/Q) data as given in Fig. 5.3a. The data processing workflow encompasses several key steps to ensure the extraction of accurate and meaningful respiration waveforms as shown in Fig. 5.3b.

First, the raw radar data is organized into discrete frames, with a frame rate of 17 frames per second. This step is essential for segmenting the continuous data stream into manageable units for further analysis. Subsequently, the complex I/Q data is separated into its phase and magnitude components. This separation enables the isolation of amplitude and phase information, facilitating more in-depth analysis, can be seen in Fig. 5.3a. To conduct respiration rate variability testing, a total of 90 samples were collected, categorized into three distinct respiration rate categories: slow, normal, and fast. Each sample has a fixed duration of 30 seconds, ensuring consistency in the dataset. These categories represent different respiration patterns, allowing for

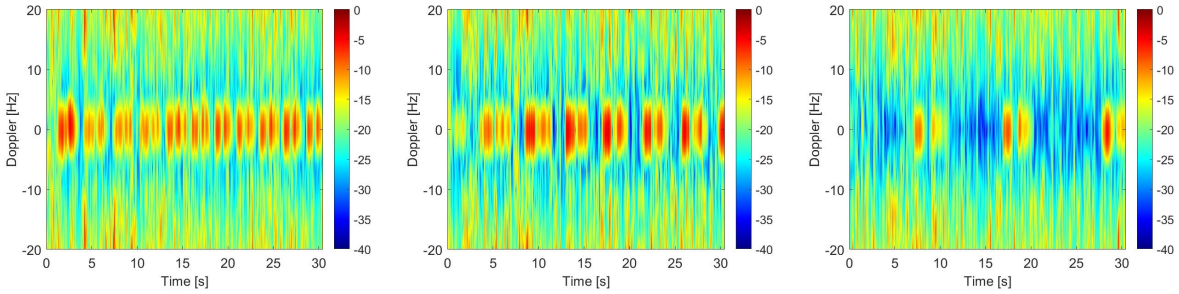

(a) Fast Breathing (b) Normal Breathing (c) Slow Breathing

Figure 5.4: Spectrogram for: (a) Fast breathing; (b) Normal breathing; (c) Slow breathing.

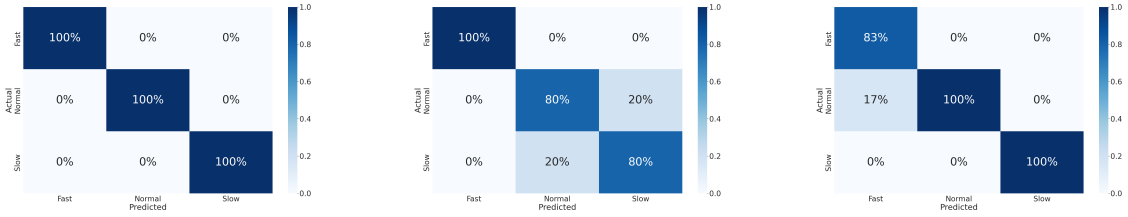

(a) vgg16 (b) Inception V3 (c) ResNet50

Figure 5.5: Confusion matrix for VGG16 in Fig. 5.5a, for Inception V3 in Fig. 5.5b and for ResNet50 is shown in Fig. 5.5c.

comprehensive analysis of variability.

The preprocessing also incorporates a low-pass filter to eliminate high-frequency noise from the data. This step is critical for improving data quality by retaining the essential low-frequency respiration components while removing unwanted noise. A thorough data quality check was conducted to ensure the reliability of the dataset. The examination revealed that there were no missing values or data repetitions in any of the 90 data files, underscoring the reliability of the collected data. To get frequency characteristics of the radar dataset, both first and second-order Fast Fourier Transforms (FFTs) were applied. FFT is a powerful tool for transforming time-domain data into the frequency domain, enabling the identification of relevant frequency components associated with respiration. Following data preprocessing (Fig. 5.3) and the generation of spectrograms (Fig. 5.4), the dataset was split into 80% for training and 20% for testing to ensure robust model assessment. The spectrograms were then taken as an input for the deep learning pre-trained models such as VGG16, Inception V3, and ResNet50. The detailed parameters configurations for each model were meticulously given in Table 5.2.

5.1.4 Results and Discussions

Experiments were conducted using a test and train-split methodology, where 80% of the data served as training data, and the remaining 20% served as testing data. Pretrained models, namely

Table 5.2: Parameter settings used for deep learning models.

DL Model	Parameters	Settings
VGG16	L-Rate	0.0001
	B-Size	32
	L-Algo	Adam
	L-Fntn	Cross-entropy
	Max-Epochs	50
	IPE	30
	Layers	16
Inception V3	L-Rate	0.0001
	B-Size	32
	L-Algo	Adam
	L-Fntn	Cross-entropy
	Max-Epochs	50
	IPE	30
	Layers	48
ResNet50	L-Rate	0.0001
	B-Size	32
	L-Algo	Adam
	L-Fntn	Cross-entropy
	Max-Epochs	50
	IPE	60
	Layers	50

VGG16, Inception V3, and ResNet50, were trained for 50 epochs. The optimizer used was Adamax, with a learning rate set to 0.001. The outcomes of the experiments are given in Fig. 5.5a, 5.5b, and 5.5c.

For VGG16, as depicted in Fig. 5.5a, all classes achieve perfect 100% accuracy.

In the case of Inception V3, represented in Fig. 5.5b, the Fast class attains 100% classification accuracy, while Normal and Slow exhibit 80% classification accuracy due to their 20% similarity with each other.

With ResNet50, illustrated in Fig. 5.5c, all classes are accurately classified, with the exception of Fast due to its 17% similarity with Normal.

Table 5.3 displays the overall accuracy, precision, recall, and F1-score for the considered DL models. The table clearly indicates that VGG16 outperforms Inception V3 and ResNet50, achieving a remarkable overall test accuracy of 100%.

5.1.5 Summary

Our work has demonstrated the efficacy of Ultra-Wideband radar, operating within the C/X-Band frequency range with a substantial 1.5 GHz bandwidth. This radar system, equipped to detect human respiration variability through intricate chest micro movements. Our experimental

Table 5.3: Evaluation of resulting metrics, encompassing accuracy, recall, precision, and F1-score, conducted for various Deep Learning models for respiration rate variability testing.

DL Models	Precision	Recall	F1-Score	Accuracy (%)
VGG16	1.00	1.00	1.00	100
Inception V3	0.87	0.87	0.87	86.6
ResNet50	0.94	0.93	0.93	93.3

environment accurately mirrors healthcare scenarios, ensuring data reliability by mitigating external influences. The preprocessing technique, encompassing frame division, filtering, and frequency analysis, have successfully extracted refined respiration waveforms from radar datasets. Deep learning models, including VGG16, Inception V3, and ResNet50, has significantly increased the scope of our analysis, offering insights into respiration rate variability. This research is poised to contribute to the advancement of non-invasive healthcare monitoring, providing a reliable methodology for assessing respiration rate variability tests in clinical settings.

5.2 Impact of Breathing Rate Variability on Heart Rate Estimation via Radar

This work explores the influence of breathing rate variability on heart rate estimation through UWB radar sensing. The study leverages a low-power ultra-wideband radar system operating in the 7.29 to 8.748 GHz range with a 1.5 GHz bandwidth. Through meticulous data pre-processing and various deep learning models, the study classifies respiration rates into slow, normal, and fast categories. The results showcase the effectiveness of models such as MobileNet, ResNet50, and VGG19, achieving an impressive overall test accuracy of 93.3%. This research contributes to advancing the application of radar technology in the precise detection of vital signs, offering potential implications for non-invasive health monitoring.

5.2.1 Introduction and Related Work

The exploitation of radar technology for respiration rate detection has gained significant interest in recent years, with various radar types and methodologies were explored [85, 145, 150]. We review several relevant papers that focus on radar-based respiration rate monitoring while conferring radar type used for respiration rate detection, radar frequency, respiration rate accuracy, if the paper discussed respiration rate variability, error in respiration rate, number of subjects used for respiration rate detection, and highlighted some limitations from the following papers [136, 147, 158, 160, 162, 163] given in Table 5.4. This work explores the intricate relationship between breathing rate variability and heart rate estimation using Ultra-Wideband

References	Year	Sensing Technology	Radar Frequency	Human Vitals	Long Term Monitoring	Accuracy(%)
Li et al. [162]	2009	Doppler Radar	10GHz	Heart rate and Respiration rate	No	NA
farooq et al. [147]	2010	UWB Radar	3.1 GHz to 10.6 GHz	Heart rate and Respiration rate	No	NA
Alizadeh et al. [160]	2019	FMCW Radar	77 GHz	Heart rate and Respiration rate	No	80-94
Wang et al. [163]	2015	FMCW Radar	80 GHz	Heart rate and Respiration rate	Yes	87.2-91.08
Ebrahim et al. [158]	2023	CW	sub GHz to 12 GHz	Heart rate and Respiration rate	No	NA
This work	2023	UWB Radar	7.29 GHz	Heart rate and Respiration rate	Yes	94

Table 5.4: Summary of recent and past papers utilizing radar technology for vital signs detection.

radar sensing. Through meticulous data pre-processing and deployment of diverse deep learning models, the research aims to classify respiration rates into slow, normal, and fast categories and observe its impact on non-invasive heart rate detection. This research significantly advances the application of radar technology for precise human vital signs detection, facilitating contactless sensing in non-invasive healthcare monitoring.

5.2.2 Methodology

Experimental Setup and Data Collection

The data collection setup includes a low-power NOVELDA ultra-wideband radar system operating in the 7.29 to 8.748 GHz range. With a 1.5 GHz bandwidth, it detects human vitals by sensing both major and minor movements within the body. The radar, mounted on a tripod, connects to a laptop for parameter adjustment and data transfer via a micro-USB cable. Distance between radar and target is set 1.5 meter along the radar line of sight. While doing the experiment considering healthcare setup in view, the setup considers normal room traffic, ensuring radar readings remain unaffected by other people outside the detection zone.

Data Pre-Processing and Deep Learning

This section describes in details data pre-processing steps for evaluating respiration rate variability using UWB radar dataset Fig. 5.6. Raw data comes from radar in .DAT files, then organized into 17 frames per second. The complex I/Q data undergoes separation into phase and magnitude components, allowing for detailed amplitude and phase analysis. For heart rate monitoring during breathing tests, datasets categorized into slow, normal, and fast respiration rates Fig. 5.4, each lasting 500 seconds, ensure dataset consistency.

A low-pass filter is applied to eliminate high-frequency noise, enhancing data quality. A thorough quality check confirms data reliability, with no missing values or data repetitions in all data files. Frequency characteristics are obtained using Fast Fourier Transforms, and the dataset is split into 80% for training and 20% for testing. Spectrograms (Fig. 5.4) serve as input for a deep learning pre-trained model, with detailed parameter configurations provided in a table for each model.

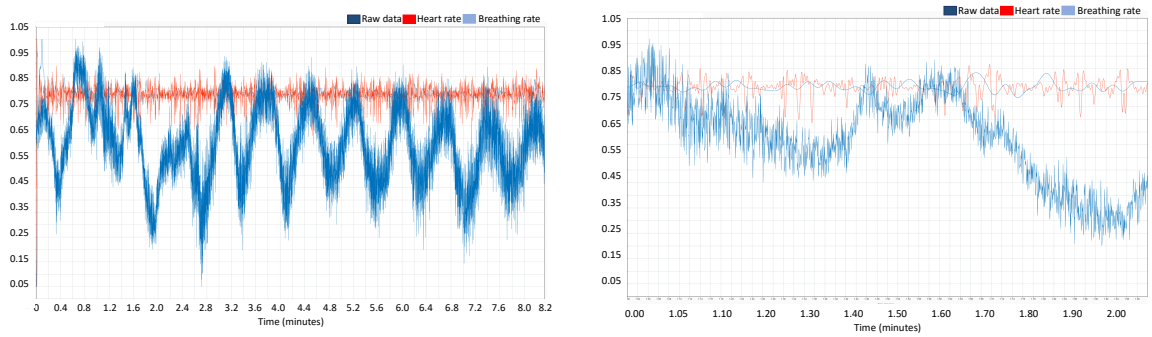

(a) Raw data, heart rate, and breathing rate wave forms.

(b) Heart rate on normal breathing.

Figure 5.6: Filtered raw data, heart rate and breathing rate waveforms. Relevant spectrograms for heart rate on slow breathing in Fig. 5.4c, normal breathing in Fig. 5.4b and for fast breathing is shown in Fig. 5.4a.

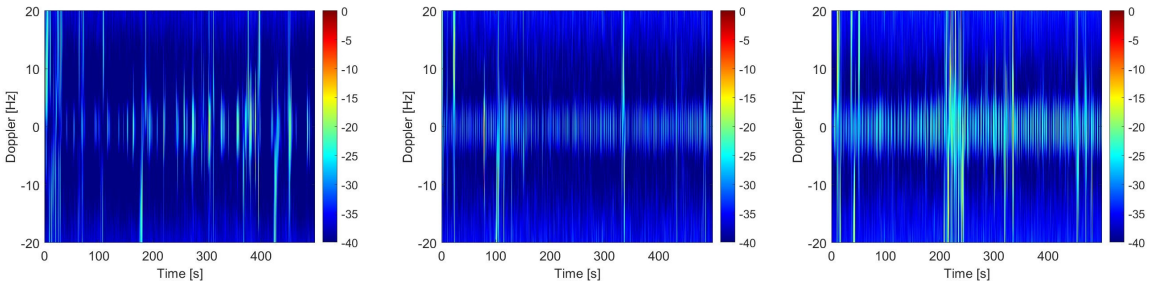

(a) Slow Breathing

(b) Normal Breathing

(c) Fast Breathing

Figure 5.7: Spectrogram for slow breathing is in Fig. 5.4c, for normal breathing is in Fig. 5.4b and for fast breathing is shown in Fig. 5.4a.

Performance Matrix

The performance evaluation of deep learning models in classifying three sub-groups (Fast, Normal, and Slow), as well as the combined dataset, is based on several common classification metrics, including weighted average accuracy, precision, recall, and F1-score.

5.2.3 Results and Discussions

The experiments followed a train-test split approach, where 80% of the data was designated for training purposes, while the remaining 20% was reserved for testing. Multiple deep learning models, such as InceptionV3, VGG16, MobileNet, ResNet50, VGG19, and EfficientNet, were applied to the UWB radar datasets. The outcomes of these experiments are detailed in Table 5.5. Using InceptionV3, Slow is correctly classified as 100% different forms of respiration, except for Fast and Normal. Fast exhibits a 25% similarity with Normal and a 13% similarity with Slow. Likewise, Normal bears a 25% resemblance to Slow. For VGG16, Slow is classified at 100%, except for Fast and Normal. Fast exhibits a 29% similarity with Normal, while Normal shares a

Table 5.5: Results from different deep learning models for classification of respiration rate including true positive rate, false positive rate, average-precision (p), average-recall (r), averaage-f1-score (f) and percentage accuracy (a).

DL Models		Classes			P	R	F	A
		Fast	Normal	Slow				
InceptionV3	**TPR**	62.0	75.0	100	0.79	0.73	0.73	73.3
	FPR	38.0	25.0	0.0				
VGG16	**TPR**	71.0	75.0	100	0.82	0.80	0.80	80.0
	FPR	29.0	25.0	0.0				
MobileNet	**TPR**	83.0	100	100	0.94	0.93	0.93	93.3
	FPR	17.0	0.0	0.0				
ResNet50	**TPR**	83.0	100	100	0.94	0.93	0.93	93.3
	FPR	17.0	0.0	0.0				
VGG19	**TPR**	100	83.0	100	0.94	0.93	0.93	93.3
	FPR	0.0	17.0	0.0				
EfficientNet	**TPR**	71.0	100	100	0.90	0.87	0.86	86.6
	FPR	29.0	0.0	0.0				

25% similarity with Slow. In the case of MobileNet and ResNet50, all the classes are correctly classified except for Fast, which has a 17% similarity with Normal. Using VGG19 Fast and Slow are accurately classified around 100% except Normal has 17% resemblance with Slow. In the case of EfficientNet, Normal and Slow are accurately classified with 100% accuracy, except for Fast, which has a 29% resemblance to Normal. Table 5.5 displays the overall accuracy, precision, recall, and F1-score of the DL models being evaluated. The table reveals that, in the combined data set, MobileNet, ResNet50 and VGG19 outperform other algorithms, achieving an impressive overall test precision of 93. 3% in terms of average precision, average recall, average F1 score and accuracy.

5.2.4 Summary

This work investigates the impact of breathing rate variability on heart rate estimation using UWB radar sensing. Employing a low-power ultra-wideband radar system with a 1.5 GHz bandwidth, the study classifies respiration rates into slow, normal and fast categories, exploring their influence on heart rate. Results highlight the effectiveness of models like MobileNet, ResNet50, and VGG19, achieving an impressive overall test accuracy of 93.3%. This research advances the application of radar technology in the precise detection of vital signs, with potential implications for non-invasive health monitoring.

Chapter 6

NextGen Heart Sounds Listening Without Touch: Contactless Stethoscope

6.1 Contactless Heart Sound detection using Advanced Signal Processing Exploiting Radar Signals

Contactless vital signs detection has the potential to advance healthcare by offering precise and convenient patient monitoring. This groundbreaking approach not only streamlines the monitoring process, but also allows continuous, real-time assessment of vital signs, allowing early detection of anomalies and prompt intervention. This work presents a novel framework for contactless vital signs detection using continuous-wave (CW) radar and advanced signal processing techniques. We achieved unprecedented precision in capturing 1,261 samples for radar based heart sound waveforms compared to the ground truth ECG signal. Further, our heart sounds method yields highly accurate human heart pulse readings, surpassing previous benchmarks with a mean absolute percentage error (MAPE) of 0.0129 and mean absolute error (MAE) below one (0.8712). In addition, we derived heart rates from the heart sound waveforms and compare them with conventional radar-derived heart rates and ground truth ECG signal. Through analysis, we identified regions where conventional radar based methods exhibit limitations. Our approach demonstrates minimal errors and superior accuracy across all heart rate states, which can potentially set new standards for noninvasive vital sign monitoring.

6.2 Introduction

Contactless vital signs detection has potential to advance healthcare by offering precise and convenient patient monitoring. This groundbreaking approach transforms the monitoring process by enabling seamless, contactless tracking of vital signs. It facilitates continuous, real-time assessment, enhancing the ability to detect abnormalities early and intervene promptly. It has immense

potential in remote patient monitoring, empowering individuals to proactively manage their health from the comfort of their homes. As this technology continues to evolve [147, 164, 165], it promises to improve healthcare delivery, improve patient diagnostics, and ultimately redefine the standard of care in modern practice.

Conventionally, pulse rate (PR) typically has been measured at the pulse points in the body, such as the wrist or neck, reflects the number of times the heart beats per minute, providing essential information about cardiac function and blood circulation [166–168]. Heart rate (HR), often assessed by auscultation with a stethoscope or by using specialised equipment such as electrocardiography (ECG), offers a more comprehensive understanding of cardiac rhythm and electrical activity [167–170]. The breathing rate, observed by counting the number of breaths taken per minute, indicates respiratory efficiency and can help identify respiratory distress or abnormalities [85, 171]. Although these techniques are effective, they typically require physical contact with the patient, which can be uncomfortable or impractical in certain scenarios [158, 172]. Therefore, the development of contactless monitoring methods for pulse, heart, and respiratory rates presents an exciting opportunity to improve patient comfort and streamline healthcare delivery.

Contactless monitoring approaches represent a transformative shift in healthcare technology, offering innovative solutions that provide physiological data efficiently and conveniently. These approaches use various technologies such as infrared sensors, radar systems, and camera-based devices to capture and analyse physiological parameters remotely [145]. Infrared sensor enables temperature measurement by detecting infrared radiation emitted by the body's surface [173]. Camera-based techniques can analyse video footage to estimate vital signs based on subtle changes in skin colour, chest movements, or pulse wave patterns [174]. Radar-based systems can track tiny movements of the body, allowing an accurate assessment of pulse rate and respiratory rate without any physical sensors attached to the patient [175]. By eliminating the need for physical contact, contactless monitoring approaches not only enhance patient comfort but also offer potential advantages in infection control, remote patient monitoring, and healthcare accessibility.

As compared to the other contactless sensing techniques, radar stands out as a dominant technique, characterized by its better performance and robust results [136]. Using electromagnetic waves, the radar system excels at capturing complicated physiological movements, penetrates through clothing and environmental obstructions, and ensures reliable monitoring in various clinical settings [176, 177]. Through advanced signal processing, radar can accurately extract vital signs information such as pulse rate, respiratory rate, and heart sounds. Its ability to capture even the smallest movements of the chest or fluctuations in heartbeat frequency sets radar as a pivotal tool in healthcare applications [178], allowing clinicians to access comprehensive physiological data remotely and in real time, thus improving diagnostic precision, clinical decision making, and patient care outcomes. In radars, lower end microwave frequency ranges can

penetrate clothing and non-metallic materials while being reflected by the human body. This allows radar systems to capture data through barriers, providing non-intrusive monitoring without requiring direct contact with the skin [179]. This range interacts safely with biological tissues in ways that are conducive to monitoring vital signs [180]. They are less absorbed by tissues compared to higher frequencies like millimetre waves, reducing potential heating effects and ensuring safety during prolonged monitoring periods in clinical settings. The radar frequency in the range is often regulated and allocated for medical and scientific applications, ensuring compliance with international safety standards [181], and minimising interference with other wireless devices.

Gold standard vital signs monitoring methods, particularly ECG, remain the cornerstone of accurate measurement of cardiac activity and serve as a reliable reference for evaluating the performance of contactless monitoring systems. Comparisons with ECG provide information on the precision and sensitivity of contactless system, facilitating their integration into clinical practice. However, the widespread adoption of contactless radar systems in clinical settings requires rigorous validation against gold standard methods to ensure precision and reliability [182].

While [183] and [184] proposed radar-based systems for contactless vital signs monitoring, utilizing Doppler and MIMO radar respectively, they lacked detailed accuracy assessment and comparison with ground truth measurements. Similarly, reviews by [156] and [185] discussed radar technologies for vital sign monitoring but lacked specific experimental data. In contrast, [186] explored radar-based cardiac motion analysis, yet lacked detailed accuracy assessments. Meanwhile, [187] provided insights into radar-based vital sign detection methods but lacked experimental data. Reviews by [188], [189], and [190] addressed radar applications, but not traditional vital sign monitoring. These gaps highlight the need for more focused research in radar-based vital sign monitoring [191–195]. Overall, while these papers provide insights from various radar technologies and their potential for vital sign monitoring, many lack specific experimental data, accuracy metrics, and proper comparisons including all heart rate states with some gold standard ground truth, as tabulated in TABLE 6.1. There's a need for more practical studies with detailed methodologies and evaluations to assess the accuracy and reliability of radar-based vital signs monitoring systems in real-world applications.

In this work, we used a 24 GHz continuous-wave (CW) radar to derive contactless heart sounds, pulse, and heart rate. We used the subscripts "CON" and "HS" to denote the radar-derived heart rate (HR) and pulse rate (PR) from conventional (CON) methods and heart sounds (HS), respectively. Additionally, we employed the subscript "ECG" to indicate the gold standard ECG signal-derived pulse rate and heart rate as the ground truth. In the first step, we measure and monitor pulse rate $(\mathrm{PR}_{\mathrm{CON}})$ of multiple male and female adult participants by using radar signal and convert them to heart rate $(\mathrm{HR}_{\mathrm{CON}})$, compare them with a three-lead ECG ground truth $(\mathrm{PR}_{\mathrm{ECG}}, \mathrm{HR}_{\mathrm{ECG}})$, and measure the accuracy of the system through performance metrics

as illustrated in flowchart (Fig. 6.3). Second step, we find heart sounds from the same radar data and convert it into pulse (PR_{HS}) and find heart rate (HR_{HS}). We again compared the HR_{HS} with the HR_{ECG} and measured the precision through performance metrics. In the third step, we compared the accuracy of the whole system with the accuracy of the two subsystems measured in the first and second step, the whole process is illustrated in Fig. 6.1 and flowchart in Fig. 6.3. Finally, we collected data from male and female adult participants and applied machine learning classification techniques to see overall accuracy of the whole system. Through rigorous validation of measured heart rate from different techniques against ECG, we aim to demonstrate the reliability and accuracy of the contactless vital signs monitoring system, paving the way for their integration into clinical practice and healthcare. We made the following contributions for the first of time to the best of our knowledge:

1. We pioneered the development of a cutting-edge contactless framework using continuous-wave radar and advanced signal processing techniques to meticulously capture heart sounds waveforms, achieving unprecedented precision compared to the gold standard ECG ground truth.

2. Our approach yielded highly precise human heart pulse readings derived from the heart sounds waveform, surpassing all previous accuracy benchmarks with an exceptional mean absolute percentage error (MAPE) of 0.0129 and mean absolute error (MAE) of less than one (0.8712) as listed in TABLE 6.1.

3. Furthermore, we were the first to compare heart rates derived from our state-of-the-art radar-based heart sound waveforms with those generated from conventional radar-based method and to further compare both contactless heart rate methods against the gold standard ECG ground truth.

4. We categorized pulse and heart rate data from both the state-of-the-art heart sounds and conventional radar methods into resting, anxiety, and transition states, dissecting them into six distinct error categories. Through rigorous analysis, we pinpoint areas within heart rate states where conventional contactless radar methods faltered in precise measurement.

5. Our results demonstrated the superior performance of our state-of-the-art heart sounds method across all heart rate states, boasting minimal errors and unparalleled accuracy compared to existing state-of-the-art methods. Additionally, we identified specific regions where pulse and heart rate measurements from conventional radar methods exhibited inaccuracies.

The overall structure of the work is shown in Fig. 6.1 and 6.3. We already have covered an overview of conventional and contactless vital signs monitoring approaches in the Introduction section 7.1.1. We reviewed some of the most relevant recent work related to the use of

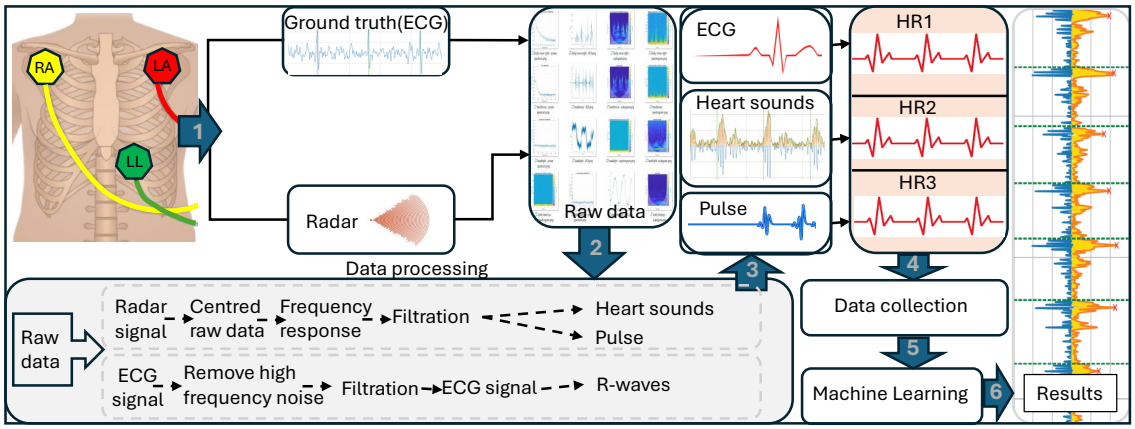

Figure 6.1: Overview of the schematic illustrating the workflow from raw data obtained from continuous-wave radar and electrocardiogram (ECG) signals, leading to the extraction of heart sounds, pulse signals from radar, and R waves from ECG. Subsequently, all three signals are processed to derive heart rates (HR1, HR2 and HR3), leading to subsequent stages of large data collection for analysis, machine learning, and performance metric analysis of results.

radar in contactless vital signs monitoring, tabulated in TABLE 6.1. The experimental and data collection setup has been described in section 6.3 and 6.4, respectively. Raw ECG data, data preprocessing, and extraction of vital signs from ECG data have been given in detail in section 6.3 and illustrated in Figs. 6.1, 6.5 and 6.4. Raw radar data, data preprocessing, heart sounds detection, pulse extraction, and heart rate calculation are detailed in Section 6.4 and illustrated in Figs. 6.6, 6.7 and 6.8, respectively.

Table 6.1: Accuracy comparison of heart rate vs heart sound estimation under noisy conditions

References	Human Vitals	Sensing Technology	Heart sounds	Ground truth	Accuracy(%)
Wu et al. [183]	ECG and respiration	mmWave Radar	No	ECG	Not given
Song et al. [156]	Respiratory rate measurement	FMCW Radar	No	No	Not mentioned explicitly
Liu et al. [185]	Heart rate, respiratory rate	FMCW mm-Wave Radar	No	No	Not mentioned explicitly
Brulc et al. [186]	Cardiac signature detection	FMCW Radar	No	ECG	Not given
Pan et al. [187]	Vital sign detection	UWB Radar	No	ECG	93
Pervez et al. [188]	Infant apnea detection	K-Band Biomedical Radar	No	No	96
Wang et al. [189]	Vital sign monitoring	mmWave Radar	No	No	Not given
Hur et al. [190]	Heart rate variability	MIMO FMCW Radar	No	ECG	97
Islam et al. [196]	Heartbeat	CW Radar	No	ECG	95.27
Sardanah et al. [197]	Cardiorespiratory monitoring	mmWave Radar	No	ECG	96
This work	**Heart sounds, pulse, and heart rate**	**CW Radar**	**Yes**	**ECG**	**98.7601 (MAE: 0.8712)**

6.3 Vital Signs Extraction from ECG Data

6.3.1 Experimental Setup

In traditional healthcare environments, where vital tests are conducted involving healthcare staff and patients, it is crucial to consider potential interference when setting up experiments. This includes recognising that time-of-flight signals can reflect off moving objects such as healthcare

staff, relatives, caregivers, and chaperones, in addition to the intended target, the patient. Moreover, modern vitals data collection machines are portable and facilitate recordings in a wide variety of environments, including hospitals, surgeries, ambulances, sports facilities, and patients' homes. The challenge is to ensure that high-quality and consistent recording techniques are maintained regardless of the clinical scenario. Data collection not performed to appropriate standards can result in incorrect diagnoses and inappropriate treatments. Considering the actual healthcare environment, the experimental setup was arranged in a room where people other than the target person could move around freely. Although we can record radar signals for vitals detection from an individual in various poses such as sitting, walking, or lying down, however, combining ECG with other monitoring methods, such as echocardiography or radar-based heart rate monitoring, requires the patient to be in a lying position to ensure that all measurements are taken under similar conditions, thereby improving data correlation. The experimental setup illustrated in Fig. 6.2 consisted of an adjustable bed, a radar system, a set of ECG electrodes, and a Latitude 5421 laptop. The laptop, equipped with an 11th Gen Intel® Core™ i7-11850H processor (24 MB Cache, 8 cores, 16 threads, 2.50 GHz to 4.80 GHz), 16.0 GB RAM, and a 37.5 W power supply, was used to power up and control the hardware during the experiments. We used Sykno 24 GHz continuous-wave radar and ECG set as illustrated in Fig. 6.2. The radar was positioned one meter away from the target person in a normal room environment. This setup allowed for the precise collection and analysis of radar and ECG data. Data collection involved six participants, comprising both males and females. For each participant, data was recorded in three different time segments: 20 seconds, 1 minute, and 5 minutes. In total, 50 data files were collected and subsequently used for classification and error analysis. The experiments for the study were approved ethically by the Research Ethics Committee (approval nos.: 300200232, 300190109) of the University of Glasgow.

6.3.2 ECG Raw Data

In three electrode ECG setup, one electrode serves as a common electrode for both ADC channels and the RA, LA and LL electrodes indicate the right arm, left arm, and left leg, respectively, as given in Fig. 6.1. For reducing noise due to unexpected movements in electrodes connecting wires, and for best signal quality, RA, the yellow electrode placed within the frame of rib cage, right under the clavicle near shoulder. LA, the red electrode is placed below the left clavicle, which is at the same level as the red electrode, and LL, the green electrode is located on the left side, under the pectoral muscles, lower edge of the left rib cage, as shown in Fig. 6.1. Data from the ADC channels stored in a csv file keeping same sampling rate and same time stamp as in the radar raw data case, sampling frequency (f) is 1 kHz. However, in later sections, we will see that the ECG and radar data have synchronised time stamp, since the radar data is the result of mechanical activities happening inside the body, but the ECG data are the result of electrical activities in the heart, so the radar data lag in a few milliseconds as compared to the

Figure 6.2: A set of figures illustrating the experimental setup for data collection, including an adjustable medical standard bed, radar, USB connecting cable for radar, a set of ECG electrodes, and a laptop. (a) The overall experimental setup. (b) A subject lying under the radar with ECG electrodes connected via hanging wires (electrode setup on the body shown in Fig. 1). (c) Back and side views of the radar, the radar's USB connecting cable, and the ECG electrodes.

ECG electrode data. This is quite obvious, as there is a small difference in both the ECG and the transmission time of the radar signal. The raw ECG data power spectrum is shown in Fig. 6.4.

6.3.3 Pulse Extraction

ECG data power spectrum, as shown in Fig. 6.4, contains 50 Hz supply noise [198], then its second and third harmonics at 100 Hz and 150 Hz respectively. We designed an infinite impulse response (IIR) notch filter to remove these frequency components and then designed a second-order Butterworth bandpass filter with a cutoff high-frequency pass band greater than 3 Hz and a low-frequency pass band less than the 40 Hz range [199] for the refined ECG waveform, as shown in Fig. 6.5.

R wave peak detection: The R wave represents the depolarisation of the ventricles of the heart and is the most prominent feature of the ECG signal for pulse detection [199], which further leads to heart rate calculations. Peak detection involves finding local maxima in the signal that exceeds a certain minimum threshold. Peaks corresponding to R waves are typically the highest peaks in the ECG signal, as shown in Fig. 6.5.

R wave intervals: After identifying the R wave peaks, the R wave intervals (RR intervals) are calculated. The RR interval represents the time between successive R wave peaks and is a fundamental measure in heart rate calculations. Mathematically, the RR interval are the time difference between consecutive R wave peaks. If R peaks are detected at the sample points $R_1, R_2, R_3, \ldots, R_n$, then the RR interval is calculated $RR_i = R_{i+1} - R_i$, where RR_i represents the i^{th} RR interval.

6.4 Vital Signs Extraction from Radar Data

6.4.1 Radar Raw Data

I vs Q Data

We utilized a 24 GHz continuous-wave radar with an ADC data rate of one thousand samples per second. Consequently, the sampling frequency (f) is 1 kHz, and the wavelength (λ) is calculated as $3 \times 10^8 \div 24 \times 10^9$. Initially, the baseband signal was extracted from the radar and converted to millivolts (mV). This conversion process involves applying a scaling factor to relate the digital values to voltage units. The in-phase (I) and quadrature (Q) components of "V," as seen in the blue waveform in Fig. 6.6b, initially do not align with the origin (0,0). To rectify this, we

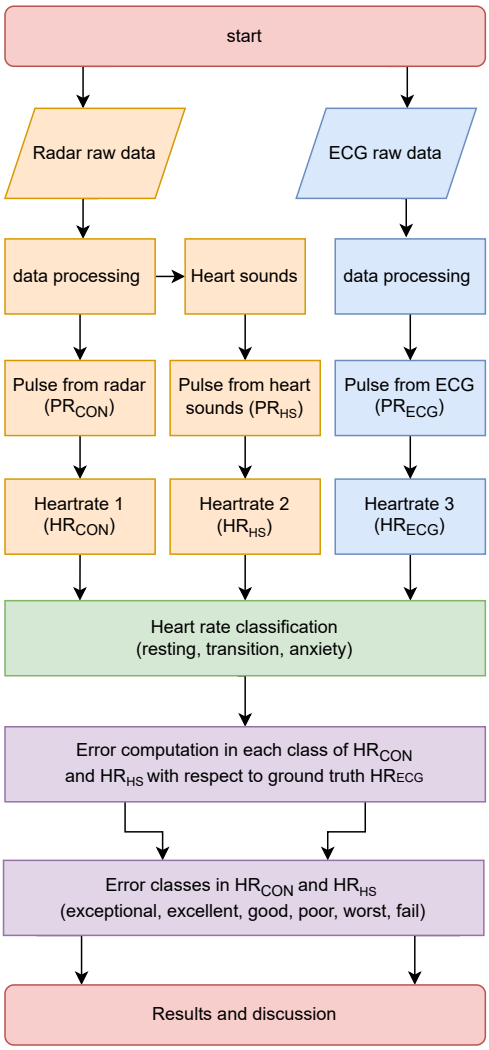

Figure 6.3: Flowchart illustrating the complete process employed for analyzing radar and ECG signals. The radar data is divided into human pulse and heart sounds, leading to heart rates, while the heart rate extracted from ECG data is used as the ground truth. Errors are computed and further classified in all heart rate classes, and a performance matrix is presented in the results section.

computed the offsets in both the I and Q components. Using a scaling factor of ten points for offset estimation, we subtracted these offsets from the raw data, resulting in centred data around the origin. The balanced data are coloured orange on the graph of I vs. Q in Fig. 6.6b.

IQ vs Time

The length of the signal is determined by the number of data points and the sampling rate in the raw data, which is then converted into a time series. The variation of the raw voltage in millivolts (mV) in the I and Q components with respect to time (seconds) is depicted in Fig. 6.7a. Additionally, the raw displacement in millimeters (mm) from the baseband signal over time is shown in Fig. 6.7b. These figures illustrate the radar's sensitivity in capturing minute movements occurring within the stationary human body, such as chest vibrations and mechanical motions resulting from the opening and closing of the heart atrium.

Raw Displacement vs Time

The chest displacement resulting from respiration typically follows a rhythmic pattern that corresponds to the breathing cycle. In addition, the beating heart generates minor vibrations. When the heart valves open and close, they emit sound waves that propagate through the chest cavity. These vibrations can also be transmitted through the chest wall and detected by the radar, as depicted in Fig. 6.7b. Vibrations attributed to heart sounds are typically more periodic and synchronous with the cardiac cycle. Although both respiration and heart sounds can induce chest vibrations, they exhibit distinct characteristics. The displacement (d) illustrated in Fig. 6.7b has been formulated and plotted by using the following equations 6.1 and 6.2:

$$d = \arctan2\left(\frac{Q_c}{I_c}\right) \cdot \frac{\lambda}{4\pi f} \tag{6.1}$$

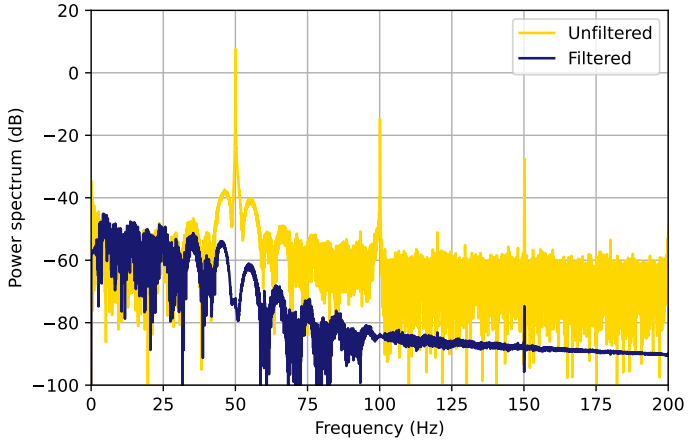

Figure 6.4: The raw data encompasses random noise, noise stemming from leads, and 50 Hz power supply noise, including its 2nd and 3rd harmonics. The resultant filtered power spectrum is depicted in blue here, with the processed ECG waveform illustrated in Fig. 6.5.

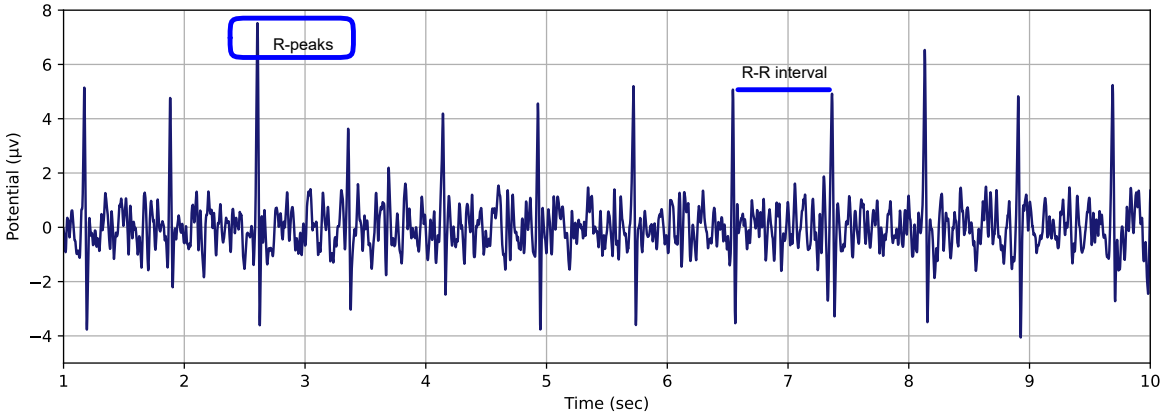

Figure 6.5: ECG waveform after filtration and preprocessing presenting the enhanced clarity and accuracy of the signal. The raw data and the power spectrum corresponding to this refined waveform are depicted in Fig. 6.4, providing complementary information on the preprocessing and spectral analysis procedures.

where,

$$\lambda = \frac{3 \times 10^8}{24 \times 10^9} \text{m} \tag{6.2}$$

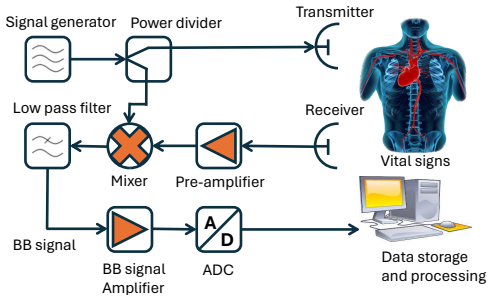

(a)

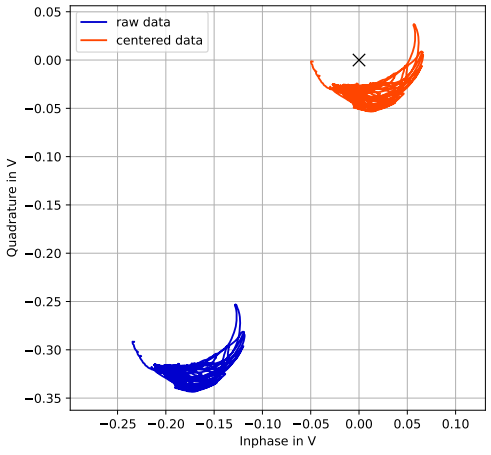

(b)

Figure 6.6: Raw data collection setup by using continuous-wave radar is in Fig. 6.6a, and raw centred data quadrature vs in-phase ilustrated is in Fig. 6.6b.

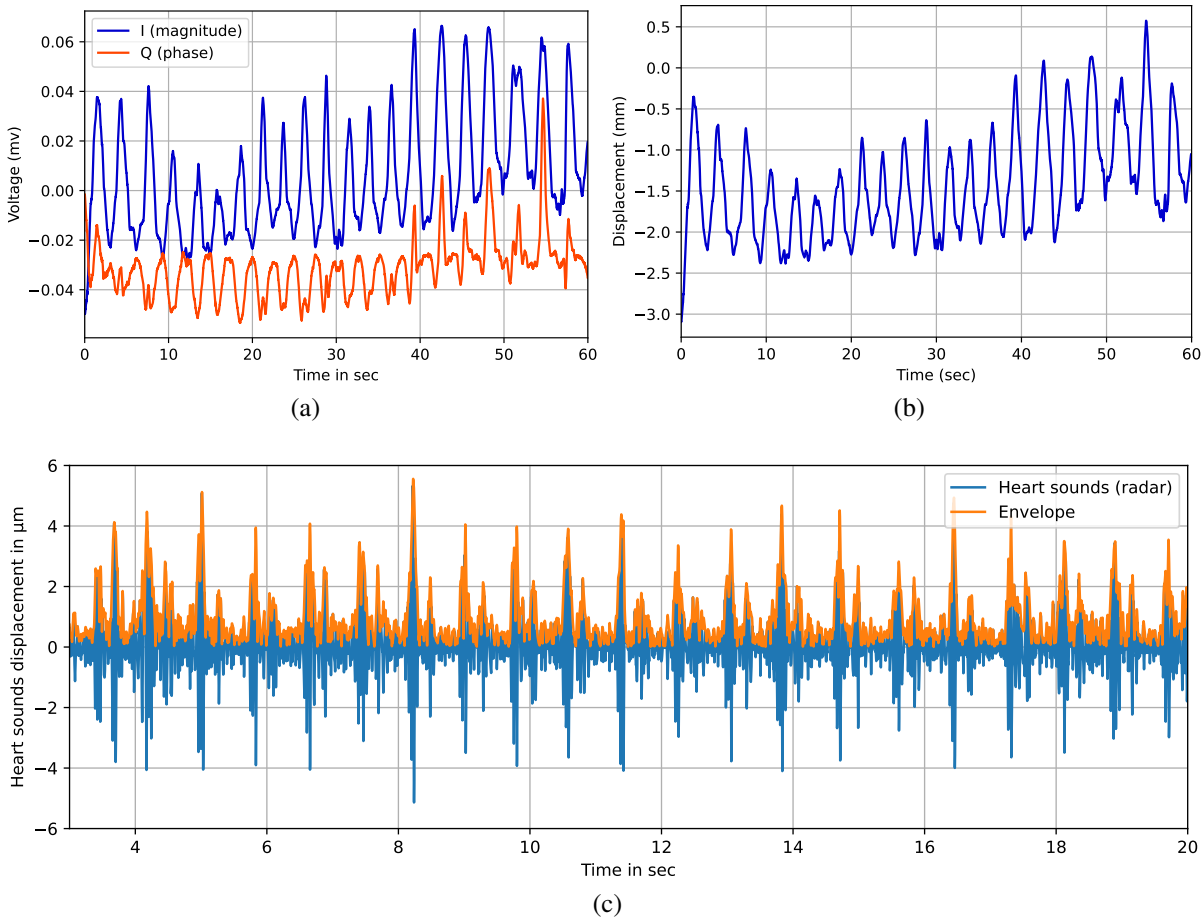

Figure 6.7: In-phase and quadrature data, presented in millivolt units over time, are depicted in Fig. 6.7a, while slow-time displacement versus time is shown in Fig. 6.7b. The basic heart sound waveform is illustrated in blue, with its absolute envelope highlighting prominent peaks depicted in orange in Fig. 6.7c.

Q_C represents the quadrature component of the centered data in V, while I_C corresponds to the in-phase component of the centered data in V. The frequency f is equal to 1 kHz.

6.4.2 Data Pre-processing

Filter radar data

Both the in-phase and quadrature components of radar data contain vital signs and heart sounds information in their entirety. In our initial step, we meticulously process the data for pulse detection, followed by their conversion to heart rate values. This conversion enables a direct comparison with the ground truth ECG signal, facilitating an efficient evaluation of the reliability and accuracy of the system. Since adult pulse signals typically fall within the frequency range 0.5 to 10 Hz, a cutoff frequency of 10 Hz is selected to effectively encompass the pulse signal bandwidth. The filter order is then determined using formula 6.3, taking into account the desired cut-off frequency and the necessary stopband attenuation, ensuring optimal performance

in capturing pulse signals [200].

$$n = \frac{\log\left(\frac{\sqrt{10^{0.1A_{\max}}-1}}{\sqrt{10^{0.1A_{\min}}-1}}\right)}{2\cdot\log(\omega_c)} \tag{6.3}$$

where n is filter order, $A_{\max}$ is maximum allowable passband ripples in dB, $A_{\min}$ is minimum stopband attenuation in dB, and ω_c is normalized cutoff frequency. The implementation of the Butterworth filter is carried out using digital signal processing techniques. Subsequently, in the second phase, radar data is processed to plot heart sounds and filter out the pulse signal from heart sounds for heart rate calculation. This approach facilitates accurate heart rate computation for subsequent comparison with the ECG ground truth. Similar to pulse detection, designing a Butterworth filter for heart sounds detection involves careful consideration of design parameters. Given the frequency range of heart sounds 20 to 200 Hz [201], a cutoff frequency of 200 Hz is selected to effectively capture the relevant signal components. The filter order is determined using the formula 6.3, ensuring sufficient stopband attenuation. Implementation of the Butterworth filter for heart sounds detection follows same signal processing as outlined for pulse detection, ensuring accurate detection of heart sounds. After applying the filter to the radar data to isolate heart sounds and eliminate pulse signals, the process of obtaining the pulse waveform involves following process. First, the filtered data is analysed to identify characteristic features associated with each heart sound, such as peak amplitudes and intervals between peaks, Fig. 6.8(b). Subsequently, these features are used to determine the time intervals between successive heart beats, from which the pulse waveform is plotted. This calculation typically involves taking the reciprocal of the average time interval between heart beats, which gives the heart rate in beats per minute (BPM).

Peaks and Time Duration Between Peaks: We detect peaks in the signal $x(t)$ corresponding to each heartbeat. Data points $P = \{p_1, p_2, \ldots, p_n\}$ denote the set of time instances in which peaks are detected. The pulse is calculated as the reciprocal of the average time interval $\frac{1}{\overline{\Delta t}}$ between successive peaks, where $\overline{\Delta t}$ is the average time interval between successive peaks, calculated as:

$$\overline{\Delta t} = \frac{1}{n-1}\sum_{i=1}^{n-1}(p_{i+1} - p_i) \tag{6.4}$$

6.4.3 Heart Rate Formulation

Heart Rate From Heart Sounds

Initially, we generate a plot of heart sounds from the filtered radar data and envelope the heart sound curve to facilitate the identification of peaks in the magnitude of heart sounds, along with determining the time duration between consecutive peaks. The heart sound curve and its envelope are depicted in Fig. 6.7c. The peaks and durations between consecutive peaks are illustrated in Fig. 6.8(b) and Fig. 6.8(c), respectively. A noticeable observation is the slight

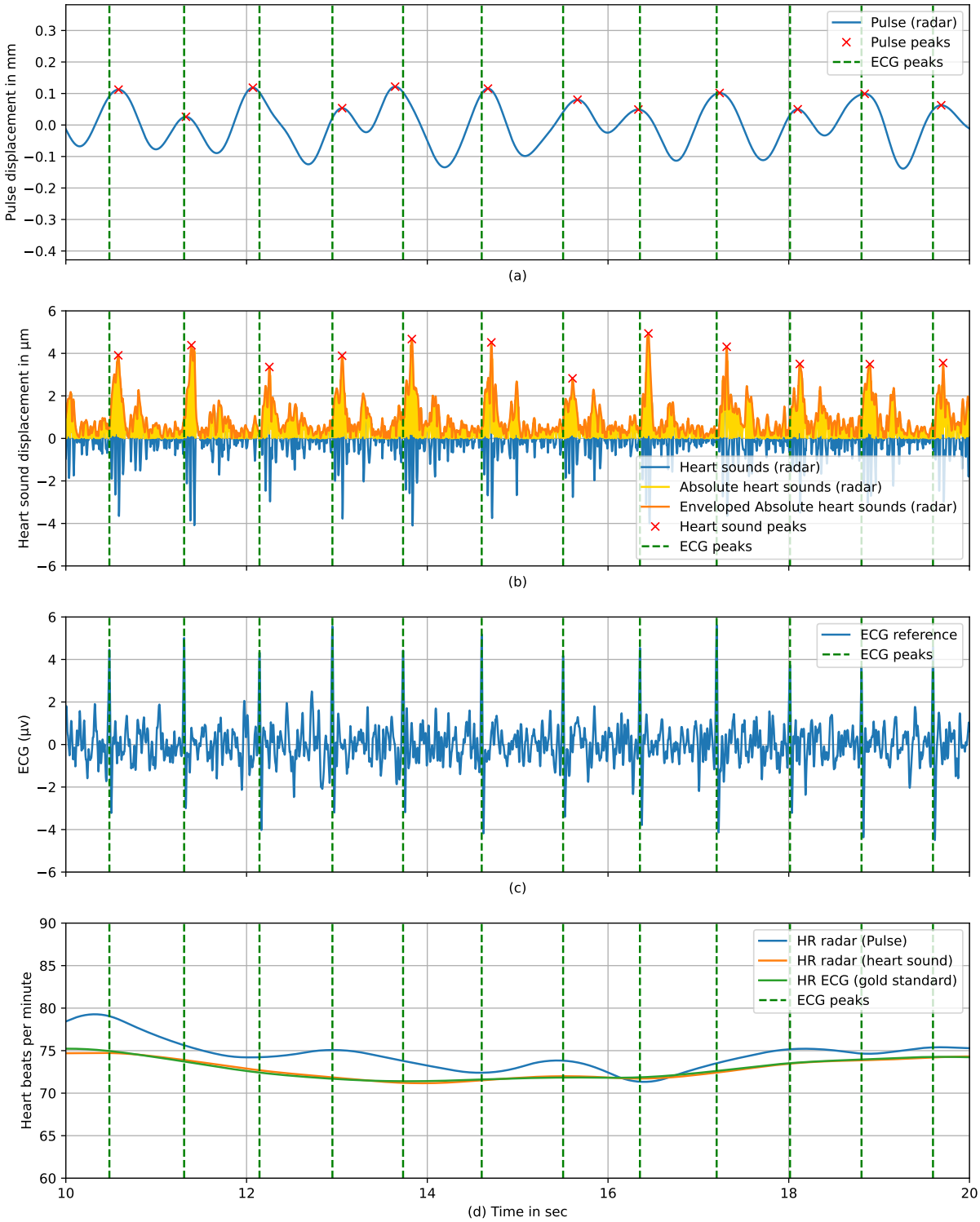

Figure 6.8: This figure illustrates heart sounds waveform and resulting pulse rate waveforms from radar processed data in comparison with gold standard ECG data. The dotted lines have been generated from ECG R-wave peaks to compare pulse wave form generated from radar heart sounds and direct direct radar data. Upper yellow part in figure (b) under the peaks is in the result of heart sounds wave envelope which has been taken for upper half part of the magnitude.

Table 6.2: Summary statistics of the whole dataset used for heart rate framework performance evaluation.

Statistics	PR_{CON}	PR_{HS}	PR_{ECG}	PR_{HS} error	PR_{CON} error
Count	1,261	1,261	1,261	1,261	1,261
Mean	65.47	72.05	72.04	0.94	14.93
Std	12.69	18.50	18.43	0.96	17.96
Min	32	57	58	0	0
25%	57	62	62	0	3
50%	63	64	64	1	8
75%	71	68	68	1	17
Max	119	120	120	3	83

time shift between the peaks of the ECG ground truth and the radar heart sound peaks. This discrepancy is typical because the ECG signal is derived from the electrical activity of the heart, which precedes the mechanical activity responsible for the generation of heart sounds. Despite this time shift, the number of peaks remains consistent between the contactless radar data and the ECG ground truth signal, ensuring the accuracy of the heart rate calculation. The heart rate is calculated as the reciprocal of the average time interval between successive peaks, multiplied by 60 to convert to beats per minute:

$$\mathrm{HR} = \frac{60}{\bar{\Delta}t}\ \mathrm{BPM} \tag{6.5}$$

Heart Rate From Radar Data

In addition to measuring heart rate from the heart sounds from radar data, we also directly measure heart rate from the filtered radar data. This direct measurement entails calculating peaks from the filtered radar data and determining the time duration between consecutive peaks within the filtered radar data, as shown in Fig. 6.8(a).

6.5 Results and Discussions

The ECG serves as the gold standard reference for pulse and heart rate measurements due to its inclusion of R-peaks, which correspond to pulse spikes. In Fig. 6.8(c), R-peaks are marked with dotted lines, which also repeated in each sub figure of Fig. 6.8, providing a reference for ground truth pulse occurrences. In Fig. 6.8(b), the largest peaks marked with red crosses represent the first heart sound (S1). Similar to R-peaks in the ECG waveform, pulses occur at every S1 peak indicated by the red cross. It is observed that pulse occurrence points in heart sounds lag behind when compared with pulse occurrence points in ECG R-waves. However, the number of peaks and the lag time interval remain the same, ensuring consistency in the pulse rate and

Table 6.3: Accuracy classes and corresponding absolute error.

Accuracy	Classes	Absolute Error(AE)	HR_{HS}	HR_{CON}
(97-100)%	Exceptional	AE = 0	✓	✓
	Excellent	[1 - 2]	✓	✓
	Good	(2 - 3]	✓	✓
(80-97)%	Poor	(3 - 10]	×	✓
	Worst	(10 - 20]	×	✓
	Fail	AE > 20	×	✓

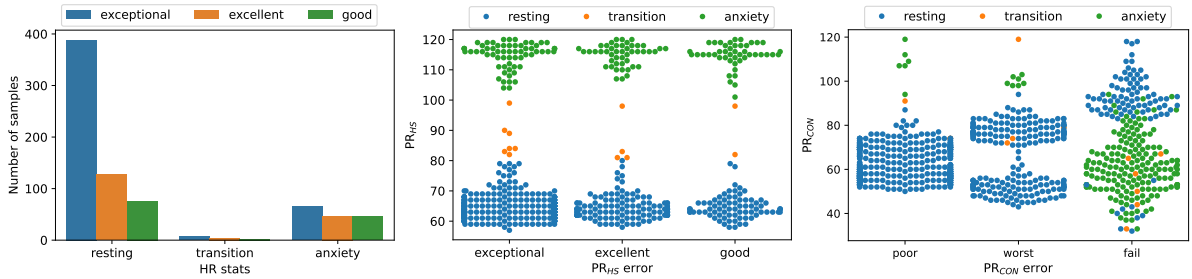

(a) (b) (c)

Figure 6.9: In Fig. 6.9a, the majority of the data points correspond to the resting state, with a smaller portion indicating the anxiety state, and the least amount representing the transition state. Pulse rate cut-off points for each state under heart sound (HS) data are displayed in Fig. 6.9b, while direct radar pulse rate data along with its classes and cut-off points are presented in Fig. 6.9c. Error state for each class and its two bonds has also been illustrated in all figures.

heart rate calculations. Fig. 6.8(a) displays a pulse waveform generated directly from the filtered radar data, where pulse points occur at each peak in the pulse waveform. As a statistical observation, the number of spikes in Fig. 6.8(a) matches the number of S1 heart sound peaks and R-peaks in the ground truth ECG given in Fig. 6.8(b) and 6.8(c), respectively. Heart rate was calculated from each waveform given in Fig. 6.8(a), 6.8(b), and 6.8(c) using the formula provided in equation 6.5 and plotted in Fig. 6.8(d). It is evident that the heart rate displayed on the Y-axis in Fig. 6.8(d) closely aligns with the ECG ground truth compared to the heart rate calculated from the pulse plotted directly from the filtered radar data in the blue waveform. For our conclusive performance evaluation, we gathered 50 datasets in three distinct time intervals: 30, 60, and 300 seconds. To conduct a thorough analysis, we systematically assessed three subsets of data independently to discern trends in short-term and long-term monitoring. Subsequently, we pooled all datasets, totalling 1,261 samples, to gauge the comprehensive efficacy of the prescribed framework. The collective dataset is presented in Fig. 6.9a, with corresponding statistics provided in TABLE 6.2. The summary statistics of the dataset in the TABLE 6.2 include the total data count, mean, standard deviation, minimum, maximum, and the lower and upper percentiles (25th and 75th percentiles, respectively). Furthermore, the 50th percentile is equivalent to the median. Heart rate variation is primarily divided into two states: resting (60-80

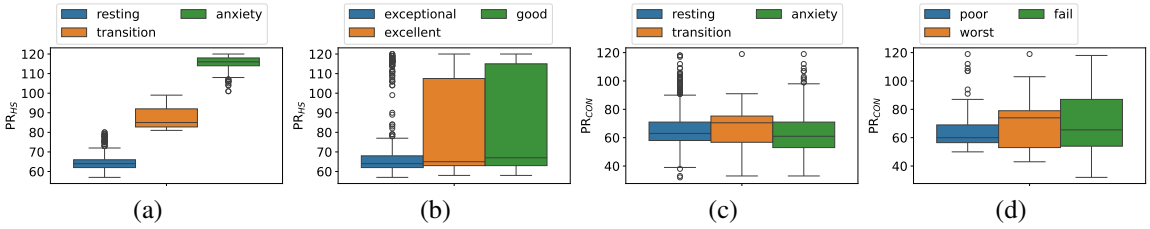

Figure 6.10: Fig. 6.10a illustrates the box plot for heart rate classes derived from heart sounds data, while Fig. 6.10b displays the error class distribution under heart sounds data. In Fig. 6.10c, the heart rate data obtained directly from radar pulses is depicted, along with its corresponding error classes illustrated in Fig. 6.10d.

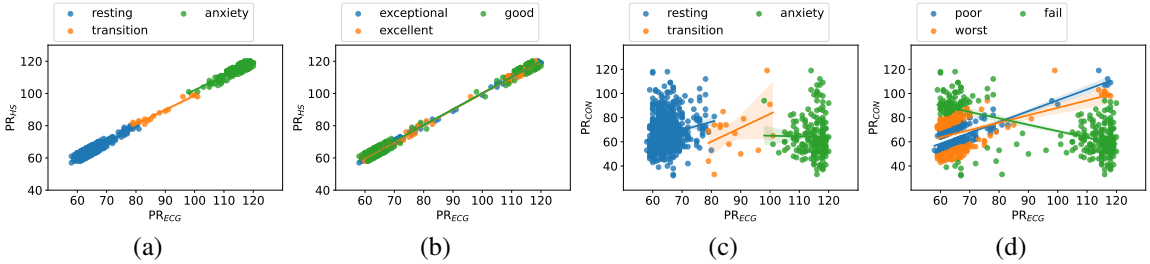

Figure 6.11: The correlation between heart rate derived from heart sounds data and the gold standard heart rate obtained from ECG, categorized by each heart rate class, is depicted in Fig. 6.11a. Similarly, the correlation with reference to each error state is illustrated in Fig. 6.11b. Fig. 6.11c shows the correlation between the heart rate obtained directly from radar pulses and the gold standard heart rate calculated from the ECG, classified by each heart rate class. Consequently, Fig. 6.11d displays the correlation with reference to each class in the error state. We see a strong correlation in heart rate derrived from heart sounds data.

bpm) and anxiety (100-130 bpm) [202, 203]. To account for changes from resting to anxiety, we introduced a transition state (80-100 bpm) [203]. These states naturally occurred during data collection and were identified during data analysis for error computation. Heart rate was finally categorized into three groups: resting, transition, and anxiety. The range and quantity of data within each class are depicted in Figs. 6.9b and 6.9c. TABLE 6.3 shows how we divided the accuracy ranges into two groups: 80-97% and 97-100%. Each group is further divided into three classes. For the 97-100% group, we named the classes "exceptional," "excellent," and "good." For the 80-97% group, the classes are named "poor," "worst," and "fail." Furthermore, we assigned an absolute error range to each accuracy class and analysed which error class range lies in contactless HR_{HS} and HR_{CON}. Data within each heart rate and error range class are illustrated in Figs. 6.9b and 6.9c. The absolute error ranges for resting, transition, and anxiety states in radar heart rate derived from heart sounds, and radar pulse rate concerning ECG ground truth, are presented via box and whisker plots in Figs. 6.10a and 6.10b. The open circles outside the whiskers, representing data points below the minimum and above the maximum, appear when data density is very high near the mean, and a few points exhibit high variance. These outliers

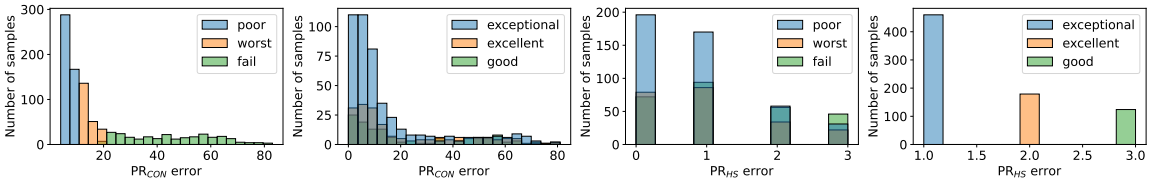

Figure 6.12: In Figs. 6.12a and 6.12b, the total error count and error range cutoffs, both lower and upper bounds, are provided for each error class derived from direct radar pulse and heart sounds data, respectively. In contrast, in Figs. 6.12c and 6.12d, the total error count for the heart rate derived from the heart sounds data, classified by each class, is presented. Furthermore, Figs. 6.12a and 6.12d depict separate errors observed within each class, while the correlation between errors across both heart rate classes is illustrated in Figs. 6.12b and 6.12c. Again, we see that most of the data in Fig. 6.12d have zero error, while Fig. 6.12a has many fail cases. On the other side, Fig. 6.12b has some exceptional cases where error is zero but in Fig. 6.12c there are no worst or fail cases at all.

are displayed as open circles beyond the whiskers For radar heart rate derived from heart sounds, the interquartile range is notably short, and data density is concentrated near the mean, resulting in negligible variance across all heart rate states. The density of data around the mean, particularly within a very short range, is visualised in Figs. 6.11a and 6.11b. On the other hand, heart rate derived directly from the radar pulse exhibits significantly larger variance, with a considerable amount of data lying outside the whiskers of the box plots. The whiskers themselves are notably elongated compared to the previous scenario, as depicted in Figs. 6.10c and 6.10d.

Additionally, in Figs. 6.11c and 6.11d, the density of data appears to be widely dispersed from the central line, and the lines themselves exhibit a piecewise nature. This observation suggests that there is a weak correlation between the ground truth ECG and the heart rate derived from the radar pulse. In contrast, the data presented in Figs. 6.11a and 6.11b demonstrate a strong correlation with the ECG ground truth, characterized by very small covariance. The correlation between all accuracy classes in both radar-based HR_{HS} and HR_{CON} is illustrated in Fig. 6.12. In Figs. 6.12c and 6.12d, it is noticeable that more than 50% of the data exhibits zero absolute error, with the majority of the remaining data falling within the 1-2 absolute error range. However, only a small fraction of the data is within the absolute error range of 2-3. In contrast, for HR_{CON} shown in Figs. 6.12a and 6.12b, the absolute error is notably higher, with a significant portion of the data having absolute errors exceeding 20%, indicating instances where the model fails to provide accurate heart rate predictions. The final performance metrics for each class and overall data are provided in TABLE 6.4. The mean absolute error for HR_{HS} is 0.8712, with a mean absolute percentage error of only 0.0129. In contrast, for HR_{CON}, the mean absolute error is 16.6991, with a mean absolute percentage error of 0.2027.

Table 6.4: Overall performance for each use case and all classes. Abbreviations used in the table header contain the following details. MAE: mean absolute error, MAPE: mean absolute percentage error, RMSE: root mean square error, MSE: mean square error, HS: heart sounds, PR: direct pulse rate from radar.

Heart rate	MAE-HS	MAPE-HS	RMSE-HS	MSE-HS	MAE-PR	MAPE-PR	RMSE-PR	MSE-PR
Resting	0.8250	0.0129	1.2242	1.4986	8.4976	0.1322	11.7275	137.5345
Transition	1.3125	0.0152	0.0152	2.5625	21.3125	0.2417	25.7354	662.3125
Anxiety	1.5798	0.0138	1.8836	3.5479	50.5851	0.4401	53.1840	2828.5426
30 sec overall	0.7688	0.0110	1.1330	1.2814	15.7143	0.1941	20.5704	423.1264
60 sec overall	1.1707	0.0174	1.5338	2.3525	19.7067	0.2297	26.5682	705.9110
300 sec overall	1.2208	0.0141	1.5820	2.5092	17.6135	0.2045	23.3052	543.2215
Whole data	0.8712	0.0129	1.2399	1.5356	16.6991	0.2027	22.0287	485.2636

6.6 Summary

Accuracy of the heart rate (HR_{HS}) derived from the heart sounds is markedly improved, demonstrating a much higher correlation with the heart rate (HR_{ECG}) derived from the ground truth ECG signal. This improved accuracy is attributed to the the substantial improvement in the signal processing that we have introduced in our approach, and distinctiveness and reliability of the first heart sound peaks (S1) that represent cardiac activity. The S1 heart sound, associated with the closure of the mitral and tricuspid valves during ventricular contraction, serves as a robust indicator of each cardiac cycle. It is clear and evident pattern, which enables precise identification of pulse occurrences, thereby minimizing discrepancies in heart rate calculations. Consequently, leveraging the S1 heart sound peaks for heart rate estimation yields results that closely mirror the ground truth provided by the ECG waveform. This emphasise the significance of utilizing comprehensive cardiac signals, such as heart sounds, in enhancing the accuracy and reliability of cardiovascular monitoring systems. As such, incorporating S1 heart sound peaks into heart rate determination approach holds promise for advancing noninvasive cardiac assessment techniques and improving patient care outcomes.

Chapter 7

Pushing The Limits of Contactless Biomarkers Sensing Exploiting Joint Human-Activity and Vital-Signs Monitoring

7.1 Contactless Sleep Quality Monitoring for Autistic Behaviour Detection

Sleep posture recognition is crucial in various scenarios, including sleep healthcare, bedridden patient care, chronic disease diagnosis, and early autism detection. The existing methods for sleep recognition have drawbacks, including privacy concerns, problems with poor lighting, line of sight blockage, difficulties in training with longer video sequences, computational complexities, and disruptions to daily routines. To address concerns about user privacy, contactless sensing methods are preferred over computer vision methods for sleep posture recognition. This study introduces a novel contactless and privacy-preserving sleep pattern recognition system that utilise ultra wideband (UWB) radar combined with Deep Learning (DL) techniques to classify normal and abnormal sleep patterns and help to identify sleep Autism. Specifically, the study focuses on nine common sleep patterns: Body Left, Body Right, Feet Move, Hand Move, Head Left, Head Right, Static Head Left, Static Head Right, and Static Head Up. The recorded data is obtained in the form of micro-doppler radar signals, and DL models such as VGG16, VGG19, MobileNet, and SqueezeNet are employed to extract relevant features. High classification accuracy is achieved by combining the entire dataset. On the combined radar dataset, the VGG16 model achieves a classification accuracy of 84.6%.

7.1.1 Introduction

Austism Spectrum Disorder (ASD) encompasses a diverse range of conditions affecting at least 1% of the global population [204]. It is characterized by challenges in social interaction, repetitive behaviors, and difficulties in verbal and nonverbal communication. Individuals with ASD exhibit varying cognitive and intellectual abilities, necessitating different levels of support in their daily lives [205]. Additionally, ASD often co-occurs with other disorders, with sleep disruption being a prominent concern among both children [206–208] and youth [209–211] with ASD. This issue affects approximately 40-80% of individuals with ASD, compared to 10-40% of those without ASD [212, 213]. Research indicates that poor sleep quality can adversely affect brain maturation [214], biological energy transfer [215], memory consolidation [216], and neurobehavioral functioning [217]. Individuals with ASD face further complexities related to sleep disturbances [218, 219]. Studies have shown that individuals with severe forms of autism often experience more frequent and persistent disruptions in their sleep-wake cycles compared to those with milder forms of ASD [219]. Further, research suggests that children who sleep fewer hours per night tend to exhibit lower verbal skills, adaptive functioning, socialization, and communication skills [220].

Sleeping disorders of ASD are mostly detected with a camera-based system. Cameras are the technology that holds a significant potential for recognition of activities. However, the real event camera datasets limit the number of approaches in many applications. To overcome this challenge, researchers have investigated the use of near-infrared and depth cameras [221]. With a near-infrared camera, motion analysis and computing statistics at the source to evaluate sleep quality among individuals severely affected by autism spectrum disorder have been conducted. The experimental dataset comprises movement patterns that facilitate the exploration of correlations between sleep quality and associated behaviors in ASD like self-injury, aggression, and disruptive conduct [222]. This [223] presents the idea of wearable sensors to monitor sleep tracking at home. The sleep aid system monitors multiple physiological signals and delivers customized auditory stimulation to promote faster sleep onset. Overall, it offers an effective solution for improving sleep onset, tracking, and social acceptance [224]. Existing camera-based and wearable-based technologies face significant challenges such as privacy concerns [136, 177], inadequate lighting, obstructed line of sight, training difficulties with extended video sequence data, computational complexities, and disruption to daily routines caused by wearable devices.

On the contrary, radio frequency (RF) head movement sensors offer promise as next-generation technologies. By utilizing RF sensing in conjunction with machine learning (ML) and deep learning (DL) techniques to recognize sleep pattern motions, provide highly accurate cues and benefiting various applications. However, UWB radar-based systems [145, 225] offer a more privacy-friendly solution as they operate without capturing visual images [226], offer more flexibility in placement and may be easier to maintain over time due to their reduced sensitivity to environmental factors, can operate effectively in various conditions, including darkness and

through obstacles [227]. UWB radar-based systems [147] typically offer wider coverage and can detect movement through walls [85] and other obstacles, making them suitable for monitoring larger areas [136,228]. TagSleep3D utilizes an RFID tag array under the bedsheet to create body imprints, which are analyzed by a deep learning model for precise posture recognition. Evaluation with 43 users demonstrates TagSleep3D's effectiveness in recognizing skeleton joints with low errors [229]. PosMonitor monitor angle purification and respiratory feature extraction. Experimental results demonstrate PosMonitor's high accuracy (98%) in identifying six common sleep postures, highlighting its reliability across diverse conditions [230].
Limited literature is available on RF sensing-based sleep movement detection, emphasizing the necessity to create a comprehensive dataset encompassing diverse subjects across various age and gender groups. This study aims to differentiate between different sleep patterns using spectrogram data obtained through a UWB radar. This research also examines nine types of spectrogram data, including Body Left, Body Right, Feet Move, Hand Move, Head Left, Head Right, Static Head Left, Static Head Right, and Static Head Up. The collected data is represented in spectrogram values, and various deep learning models, such as VGG16, VGG19, MobileNet, and SqueezeNet, are utilized for classification. The main contributions of the work are summarized as follows:

- We have proposed a unique RF sensing-based sleep pattern recognition monitoring system that integrates deep learning algorithms for accurate sleep recognition, applicable for various applications such as healthcare and mental health.
- We introduced a contactless sleep pattern recognition system design to automatically identify autism based on sleep patterns.
- We have collected a data set comprising 1620 samples representing nine different types of sleep patterns captured at a distance of 1 metre from the target. The data samples were collected using radar sensors. To ensure diversity, data were gathered from six participants (two males and four females) aged between 20 and 40 years.
- For the radar dataset, VGG16, VGG19, GoogleNet, and SqueezeNet algorithms were applied to a combined dataset of six subjects. VGG16 outperformed other algorithms, achieving an accuracy of 84.6%.

The remaining sections of the work are structured as follows: section Methodolgy presents details on the experimental setup, data processing, fine-tuned deep learning, and performance metrics. The ection Results and Discussion provides an analysis of the classification results obtained from various deep learning models. Finally, the section Conclusion summarizes the work and suggests potential avenues for future research.

Table 7.1: Parameters configuration of radar software and hardware.

Parameter	Value
Platform	Xetru radar X4MO3
Instrumental range	9.6 metres
Target's distance from radar	1.5 m
Operating frequency	7.29GHz
Transmitter power	6.3dBm
Activity duration	10 seconds
Collected samples in each class	15

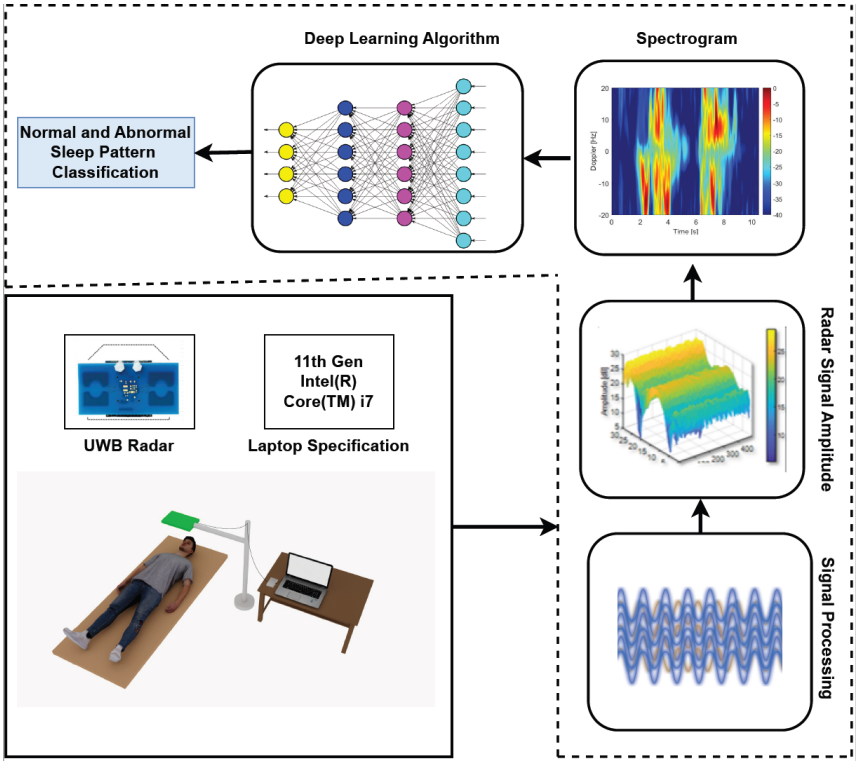

Figure 7.1: The Overall flow diagram of proposed Sleep Pattern Recognition system.

7.1.2 Methodology

Experimental Setup and Data Collection

The hardware setup for radar-based sleep monitoring is given in Tabel 7.1. Utilizing the Xethru X4M03, an ultra-wideband radar sensor was placed on the top of a stand. This sensor has built-in transmitter antennas (Tx) and receiver antennas (Rx), offering a maximum detection range of 9.6 metres. The settings of the radar key parameters are outlined in Table 7.1. During the sleep pattern experiments, the subject was placed one metre away from the radar in a normal lying position, with minimal movements during sleep. Each activity interval was set to 10 seconds, during which data for a single sleep pattern from a single subject was collected. All methods followed the guidelines and regulations of the Research Ethics Committee and all subjects gave

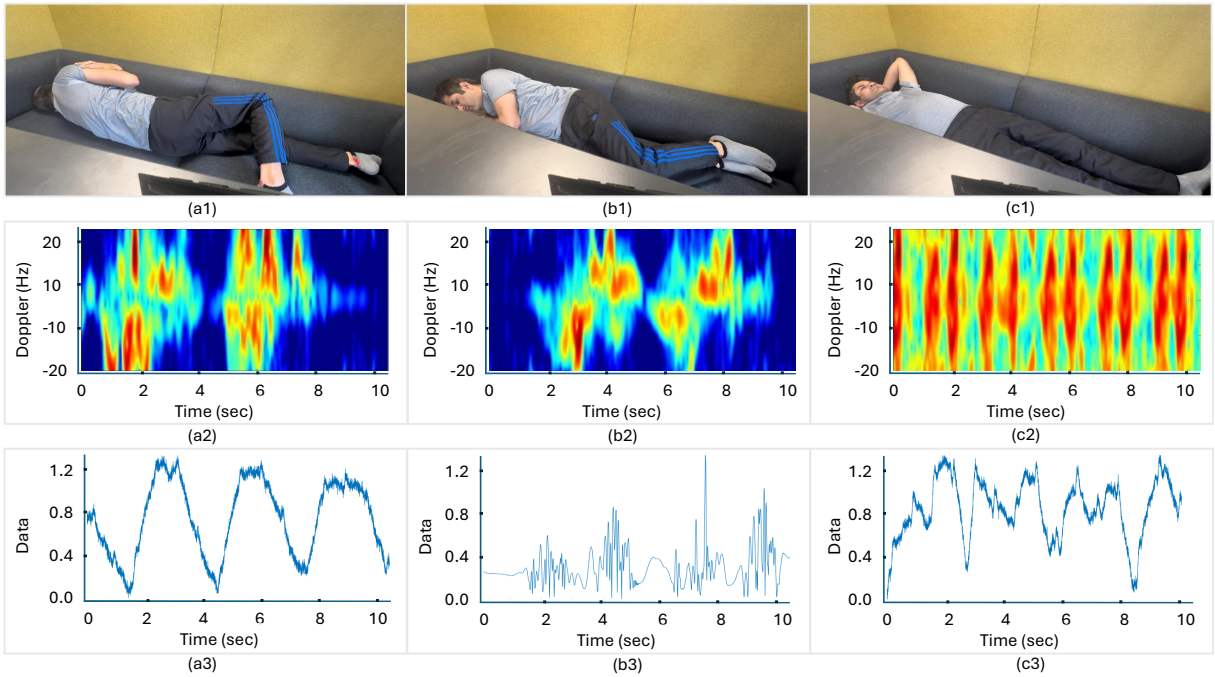

Figure 7.2: Illustration of sleeping pattern recognition for specific body movements. Subfigures (a1, b1, c1) show visual images, (a2, b2, c2) show corresponding spectrograms, and (a3, b3, c3) present Region of Interest (ROI) plots. Each column (a, b, c) represents the same activity across modalities: (a) body turning left, (b) body turning right, and (c) feet movement.

Table 7.2: An overview of the data collected, number of subjects and the activities performed.

Classes	**Experimental Dataset**						
	Subject (S1)	**Subject (S2)**	**Subject (S3)**	**Subject (S4)**	**Subject (S5)**	**Subject (S6)**	**Total**
Body Left	30	30	30	30	30	30	180
Body Right	30	30	30	30	30	30	180
Feet Move	30	30	30	30	30	30	180
Hand Move	30	30	30	30	30	30	180
Head Left	30	30	30	30	30	30	180
Head Right	30	30	30	30	30	30	180
Static Head Left	30	30	30	30	30	30	180
Static Head Right	30	30	30	30	30	30	180
Static Head Up	30	30	30	30	30	30	180
Total	270	270	270	270	270	270	**1620**

their written informed consent before data collection. Each subject provided informed consent, authorised by the University of Glasgow institutional review board. The RF signal was transmitted and received from the radar within this duration. The experiments carried out involved the collection of nine sleep patterns: Body Left, Body Right, Feet Move, Hand Move, Head Left, Head Right, Static Head Left, Static Head Right, and Static Head Up. These patterns were collected with subjects in normal sleeping positions. An illustration of the movements of the sleep patterns of all classes, their corresponding spectrogram, and visualisation is provided in the form of an ROI plot shown in Figure 7.2, 7.3, and 7.4 (each subject shown in Figure 7.2 provided their informed consent to publish their images, Figure 7.3 provided their informed

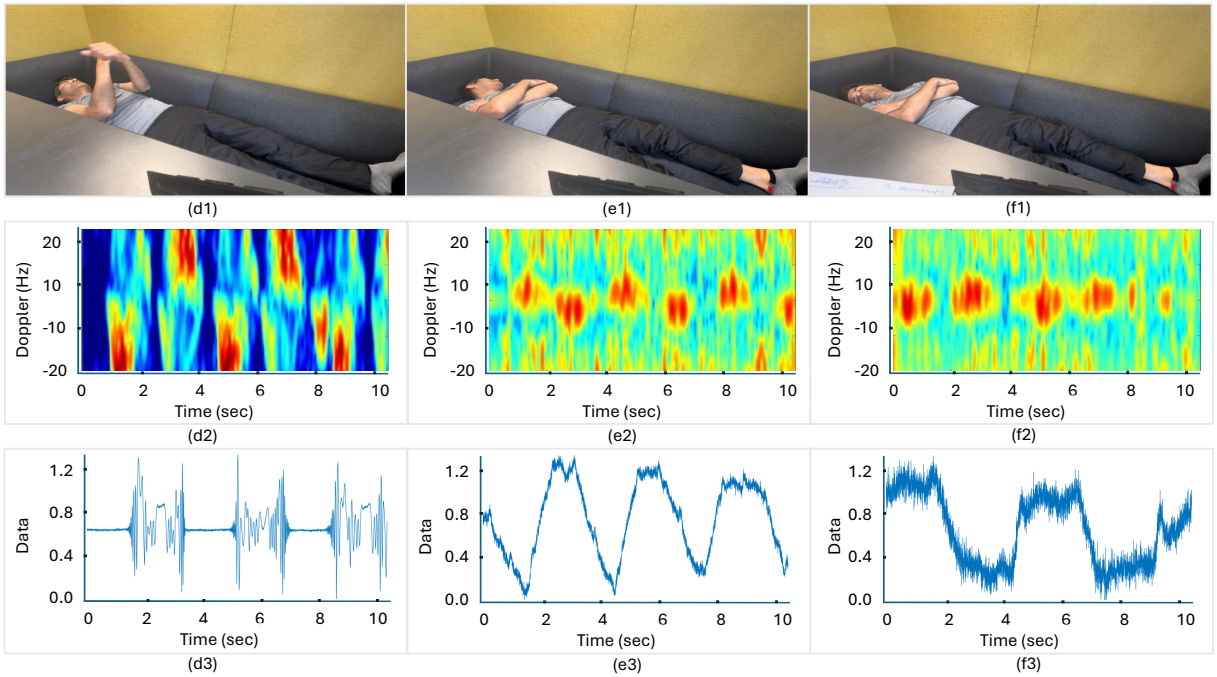

Figure 7.3: Visualization of sleeping pattern recognition involving upper body and head movements. Subfigures (d1, e1, f1) display visual images, (d2, e2, f2) provide corresponding spectrograms, and (d3, e3, f3) illustrate ROI plots. Each set of plots corresponds to a specific activity: (d) hand movement, (e) head turning left, and (f) head turning right.

consent to publish their images and Figure 7.4 provided their informed consent to publish their images, authorised by the institutional review board of the University of Glasgow). In Figure 7.2, we presented body left position in Figure 7.2(a1,a2,a3), body right position in Figure 7.2(b1,b2,b3), and movement of feet in Figure 7.2(c1,c2,c3). All Figures 7.2(a), 7.2(b), and 7.2(c) contains three sub figures in each column, actual subject picture, spectrogram, and ROI graph respectively. Similarly, in Figure 7.3, we presented hand movement in Figure 7.3(a), head left movement in Figure 7.3(b), and head right movement in Figure 7.3(c). All Figures 7.3(a), 7.3(b), and 7.3(c) contains three sub figures in each column, actual subject picture, spectrogram, and ROI graph respectively. Further, in Figure 7.4, we presented body static position with head on left side in Figure 7.4(a), body static position with head on right side in Figure 7.4(b), and body static position with head upward in Figure 7.4(c). All Figures 7.4(a), 7.4(b), and 7.4(c) contains three sub figures in each column, actual subject picture, spectrogram, and ROI graph respectively. A total of six participants, comprising two males and four females were involved in the data collection process for the experiment. This addition aims to enhance the practicality and diversity of the dataset. In total, 1620 data samples were collected in all experiments for nine classes shown in Table 7.2. Each participant repeated each sleep activity 30 times with the radar. Ethical approval for these experiments was obtained from the University of Glasgow Research Ethics Committee (approval no.: 300200232, 300190109). The UWB radar-based system setup for sleep pattern data collection and processing is illustrated in Figure 7.1. The details of all

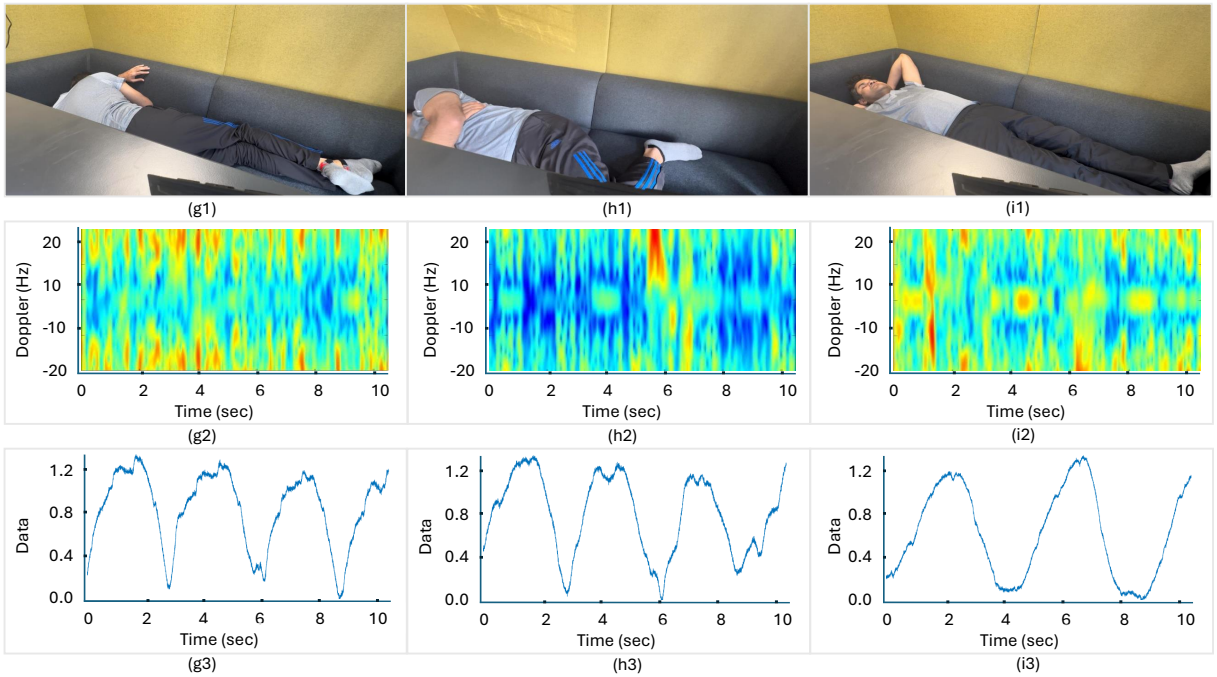

Figure 7.4: Representation of sleeping pattern recognition for static head positions. Subfigures (g1, h1, i1) show visual images, (g2, h2, i2) present corresponding spectrograms, and (g3, h3, i3) contain ROI plots. Each group represents a different static head posture: (g) head facing left, (h) head facing right, and (i) head facing upward.

components presented in Figure 7.1 are discussed later in this section. The features utilised for radar analysis were obtained from the short-time Fourier transform (STFT) of the radar signal, providing spectrograms of radar doppler shifts due to sleep movements. Analysis of the spectrograms revealed different patterns that correspond to different movements in sleep. To classify sleep movements, pre-trained VGG models were utilized due to their better performance on abstract images like spectrograms.

Data Pre-Processing and Deep Learning

In the initial phase, the radar chip underwent configuration via the XEP interface with x4 software. Data were recorded from the radar at 500 samples per frame per second. A loop was used to read the data file and store the data into an array, which was then mapped into a complex range-time matrix. Subsequently, a moving target indication (MTI) filter was applied to obtain the doppler range map. Following that, MTI mode of operation was used along Butterworth 4^{th} order filter to generate the spectrograms using the parameters window length, overlap percentage, and fast Fourier transform (FFT) padding factor. Specifically, a window length of 128 samples and a padding factor of 16 were used. Additionally, a range profile was established by initially converting each chirp to an FFT. Subsequently, a second order FFT was conducted on a defined number of consecutive chirps for a given range bin. Furthermore, STFT was used to refine the features used for spectrograms, unlike Fourier transform, STFT offers both temporal

and frequency information [231]. This was accomplished by segmenting the data and using Fourier transform on each segment. Altering the window length inversely affected both the temporal and frequency resolutions. The level of doppler detail in radar data is determined by the hardware sampling capability. The greatest unambiguous doppler frequency in RADAR is $F_d, max = \frac{1}{2}t_r$, where t_r represents the chirp time. In this paper, we explore sleep pattern recognition at a distance $D(t)$ from a specified location such as the body. $V(t)$ represents the point of target movement in front of the RADAR, and T_s represents the transmitted signal:

$$T_s(t) = A\cos(2\pi ft). \tag{7.1}$$

The received signal is denoted by $R_s(t)$:

$$R_s(t) = \acute{A}\cos(2\pi f(t - \frac{2D(t)}{c})), \tag{7.2}$$

where A is the reflection coefficient, and c is the speed of light. The reflected signal can be expressed as $R_s(t)$, where the signal reflected off the target points at an angle θ to the direction of RADAR:

$$R_s(t) = \acute{A}\cos(2\pi f(1 + \frac{2v(t)}{c})(t - \frac{4\pi D(\theta)}{c})). \tag{7.3}$$

The Doppler shift corresponding to it can be written as:

$$f_d = f\frac{2v(t)}{c}. \tag{7.4}$$

The returned signal becomes a composite of several moving elements such as the head, hand, legs, and body. Each component moves at its own speed and acceleration. If we consider i to be the various moving components of the body, we can write the received signal as:

$$R_s(t) = \sum_{i}^{N} A_i\cos(2\pi f(1 + \frac{2vi(t)}{c})(t - \frac{4\pi D_i(0)}{c})). \tag{7.5}$$

The Doppler shift is the result of a complex interaction of numerous Doppler shifts induced by different body parts. Detection of sleep patterns in a reliable fashion clearly depends upon the characteristics of the Doppler signatures. After obtaining the spectrograms of various sleep pattern files from the participants, a dataset was constructed. As indicated in the high-level signal flow diagram in Figure 7.1, the dataset consisted of two key modules: (i) System Training and (ii) System Testing. The proposed pre-trained DL classification algorithms were implemented on a spectrogram to recognize the sleep pattern dataset.

Classification via Deep Models

The spectrograms generated in the previous step are fed into DL models for classification purposes. For this purpose, four different pre-trained models, namely VGG16, VGG19, GoogLeNet, and SqueezeNet, are considered. Our classification framework to differentiate in sleep patterns is mainly based on fine-tuning pre-trained models where multiple state-of-the-art CNN architectures pre-trained on ImageNet [232] are fine-tuned on the spectrogram images generated from the radar data. In fine-tuning the pre-trained models, we modify the top layers of the models to classify the collected data into nine considered classes, namely Body Left, Body Right, Feet Move, Hand Move, Head Left, Head Right, Static Head Left, Static Head Right, and Static Head Up. In the following subsections, we provide a detailed description of the CNN architectures used in this work.

GoogLeNet Model

GoogLeNet [233] is one of the state-of-the-art and commonly used CNN architecture for different image classification tasks [234].The architecture is composed of 22 layers including convolutional, pooling layers, inception modules, and a fully connected layer. The inception module is made up of 6 convolutional layers and a pooling layer. The module consists of patches or filters of sizes 1×1, 3×3 and 5×5. These filters of different sizes help to obtain different patterns of the input image. The feature maps obtained from various filters are concatenated at the output of each module. Furthermore, 1×1 convolutions are performed prior to convolutions by large filters. The use of 1×1 convolution filter decreases the number of parameters required by GoogLeNet [1, 235].The hyper-parameter settings of GoogleNet are shown in Table 7.3.

SqueezeNet Model

Our second pre-trained model is based on SqueezeNet architecture [236], which is composed of 18 layers. This architecture has shown comparable results with fifty times fewer parameters, which makes it a preferable choice for applications with fewer data and low computational resources. Squeezenet adapts to three major strategies. The first strategy reduces the 3×3 filters to 1×1 filters given in the squeeze layer. The second strategy uses expand layer in which 1×1 and 3×3 filters are fed with less input parameters from the squeeze layer. The third strategy downsamples late (having smaller stride values), so that the last layer has larger activation maps which results in better accuracy [1, 235].The parameter settings of SqueezeNet are shown in Table 7.3.

VGG16 Model

Another pre-trained model is based on VGG16 architecture [237], which is composed of 16 layers. This architecture contains a total of 138 million parameters, which used a 3x3 filter size with a stride 1 and always use the same padding and max-pooling layer of a 2x2 filter with stride

Table 7.3: Parameter settings for the selected Models [1].

Parameters	VGG16	VGG19	GoogleNet	SqueezeNet
Initial learning rate	0.0001	0.0001	0.0001	0.0001
Mini-batch size	16	16	128	128
Learning algorithm	Adam	Adam	Adam	Adam
Loss function	Cross entropy	Cross entropy	Cross entropy	Cross entropy
Maximum epochs	100	100	100	100
Iteration per epoch	46	46	500	500

2. The arrangement of the layers in this architecture is as follows convolutional layers, ReLU layers, and max pool layers. ReLU is more computationally efficient because it results in faster learning and it also decreases the likelihood of vanishing gradient problems. The end of the model has 3 fully connected layers followed by a softmax for output [1, 235]. The parameter settings of VGG16 are shown in Table 7.3.

VGG19 Model

The data was passed through a different layer which consists of 3×3 filters with five stages of convolutional layers, five pooling layers, and three fully connected layers to get image information. The convolution kernel depth has been increased from 64 to 512 of the VGG16 network for better image feature vector extraction. Every stage of convolutional layers was followed by pooling layers which have the size and step size of 2×2 [1, 235]. The parameter settings of VGG19 are shown in Table 7.3.

Performance Matrix

The performance of deep learning (DL) models in classifying nine sub-sleep patterns on the combined dataset is assessed using weighted average accuracy, precision, recall, and F1-score. The F1-score, a widely used classification metric, is computed using equation (7.8). Precision and recall, calculated through equations (7.6) and (7.7), respectively, are combined in the F1-score calculation. Equation (7.9) is employed to determine the average accuracy, a measure used to evaluate the performance of DL models.

$$\text{Precision} = \frac{\sum(TP)}{\sum(TP+FP)} \tag{7.6}$$

$$\text{Recall} = \frac{\sum(TP)}{\sum(TP+FN)} \tag{7.7}$$

$$\text{F1-Score} = 2\frac{(Precision.Recall)}{(Precision+Recall)} \tag{7.8}$$

Table 7.4: The evaluation of the DL models on the sleep patterns dataset involved measuring weighted average recall, weighted average precision, weighted average F1-score, accuracy, and determining a 95% confidence interval.

DL Models	Precision	Recall	F1-Score	Accurcay (%)	95% CI
VGG16	0.84	0.86	0.85	84.6	0.82-0.85
VGG19	0.77	0.82	0.78	77.2	0.75-0.79
GoogleNet	0.82	0.83	0.81	82.1	0.80-0.84
SqueezeNet	0.79	0.81	0.81	79.0	0.77-0.81

$$\text{Accuracy} = \frac{\sum(TP+TN)}{\sum(TP+FP+TN+FN)} \tag{7.9}$$

7.1.3 Results and Discussions

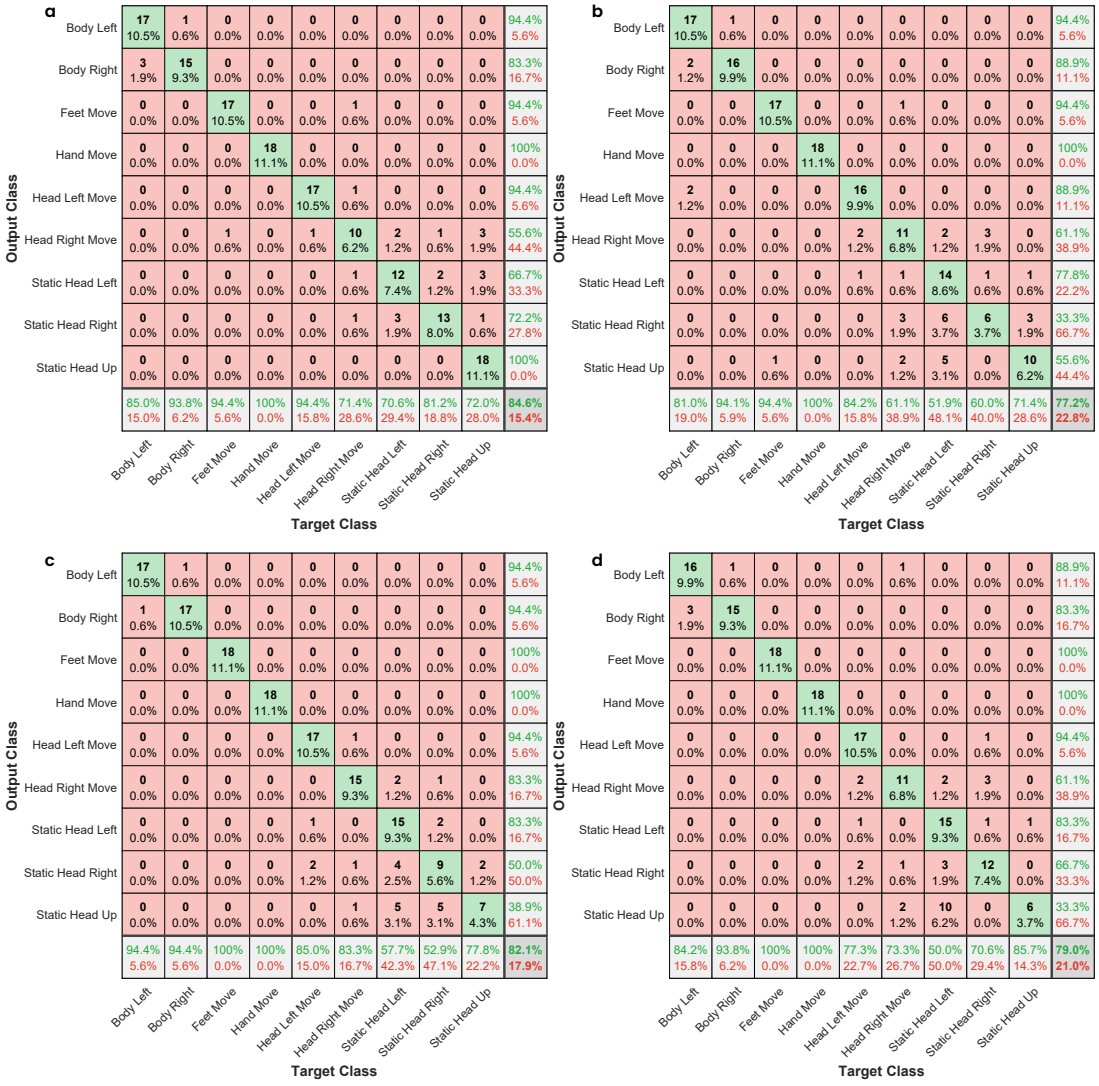

Figure 7.5: The Confusion Matrices of all the models of Normal and Abnormal sleep monitoring patterns. (a) VGG16. (b) VGG19. (c) GoogleNet. (d) SqueezeNet.

This research describes the experiment involving the analysis of sleep patterns using radar-based technology and deep learning models such as VGG16, VGG19, MobileNet, and SqueezeNet. The experiment involves collecting and analyzing data on normal and abnormal sleep patterns from various datasets related to body movements during sleep, such as "Body Left, Body Right, Feet Move, Hand Move, Head Left, Head Right, Static Head Left, Static Head Right, and Static Head Up," across different genders. The parameter settings for the deep learning models are provided in Table 7.3. The models were fine-tuned on the dataset, and the training and testing sets remained fixed throughout the studies, with 80% of the data used for training and 20% for testing. The outcomes of the experiment are presented in terms of precision, recall, F1-score, accuracy, and interval, which aid in the decision-making and comparisons. Moreover, the performance of all proposed models on the collected datasets is illustrated through a confusion matrix in Figure 7.5, showcasing the models' effectiveness. In summary, the results suggest improved outcomes for both combined and individual datasets across all models.

In the VGG16 algorithm, the combined dataset includes males and females. We achieved a high classification accuracy of 84.6%, along with precision, recall, and F1-score, as well as an accurate interval, as depicted in Figure 7.5(a) and Table 7.4. All classes are correctly classified except for "Head Right Move" and "Static Head Left." The "Head Right Move" exhibits similarities of 0.6%, 1.2%, and 1.9% with "Feet Move", "Static Head Left," and "Static Head Up" respectively. Similarly, "Static Head Left" shows similarities of 1.2%, 0.6%, and 1.9% with "Static Head Right", "Head Right Move", and "Static Head Up" respectively.

Similarly, VGG19 performs well on the combined dataset with 77.2% accuracy, precision, recall, F1-score, and valid interval, as shown in Figure 7.5(b) and Table 7.4. All classes are correctly classified except for "Static Head Right" and "Static Head Up." "Static Head Right" has been misclassified with "Head Right Move," "Static Head Left," and "Static Head Up" at ratios of 1.9%, 3.7%, and 1.9% respectively. "Static Head Up" exhibits similarities with "Feet Move," "Head Right Move," and "Static Head Left" at rates of 0.6%, 1.2%, and 3.1% respectively.

Using GoogleNet, the combined dataset includes males and females. We achieved a high classification accuracy of 82.1%, along with precision, recall, F1-score, and accurate interval, as shown in Figure 7.5(c) and Table 7.4. All classes are correctly classified except for "Static Head Right" and "Static Head Up." "Static Head Right" exhibits similarities with "Head Left Move, Head Right Move, Static Head Left, and Static Head Up" at ratios of 1.2%, 0.6%, 2.5%, and 1.2% respectively. Similarly, "Static Head Up" has similarities with "Head Right Move, Static Head Left, and Static Head Right" at ratios of 0.6%, 3.1%, and 3.1% respectively.

In the case of the SqueezeNet algorithm, we achieved a high classification accuracy of 79.0%, along with precision, recall, F1-score, and interval, as depicted in Figure 7.5(d) and Table 7.4. Except for "Static Head Up" all classes are correctly classified because it has similarity with "Head Right Move" and "Static Head Left." "Head Right Move" exhibits similarities with "Head Left Move, Static Head Left, Static Head Right" at rates of 1.2%, 1.2%, and 1.9% re-

spectively. Similarly, "Static Head Up" shows similarities with "Head Right Move, Static Head Left" at rates of 1.2% and 6.2% respectively.

7.1.4 Summary

This work introduces a contactless and privacy-preserving framework for sleep pattern recognition, specifically focusing on normal and abnormal sleep patterns to identify early autism spectrum disorder. The diverse dataset comprises micro-doppler signals collected from various users and is input into deep learning models. The dataset includes nine classes: Body Left, Body Right, Feet Move, Hand Move, Head Left, Head Right, Static Head Left, Static Head Right, and Static Head Up. The experiment involved six participants, two male and four female, aged from 20 to 40 years. Micro-doppler radar datasets are processed using various deep learning models, including VGG16, VGG19, MobileNet, and SqueezeNet. Sleep movements were predominantly classified correctly, achieving around 100% accuracy rate. Among the tested models, the VGG16 algorithm performed the best, achieving an overall accuracy of 84.6% for all nine classes. Moving forward, the long-term objective is to improve accuracy, enlarge dataset with more sleeping patterns and more diverse range of age groups, such as children and the elderly.

7.2 Contactless Sleep Quality and Vital Signs Monitoring for Autism Spectrum Disorder Detection

Recent studies reveal that over 70 million people worldwide are estimated to live with autism spectrum disorder (ASD) and sleep disturbances that affect up to 80% of individuals with ASD [238]. ASD and sleep disturbances are intricately linked to cardiovascular health, a critical factor in ensuring healthier lives for individuals with autism [136, 239]. Sleep monitoring poses significant challenges due to the reliance on conventional methods, such as polysomnography (PSG) and wearable devices, which often disrupt natural sleep patterns and require intrusive setups in specialised sleep labs [240]. PSG is considered the gold standard, but involves complex connection, electrode placement, and overnight monitoring in clinical environments, leading to discomfort for patients and potentially compromising the results [147, 241]. Wearable devices, while more portable, can cause discomfort due to direct skin contact, and may compromise accurate data due to improper placement and body movements due to discomfort [242]. These issues were identified when monitoring individuals with ASD, who may experience significant sensitivity to touch or environmental changes, further complicating the use of conventional tools for sleep analysis.

ASD monitoring also faces significant issues due to its reliance on subjective observations, questionnaires, and behavioural assessments, which can lead to variability and bias in diagnosis and tracking [144]. The heterogeneity of ASD symptoms, particularly in communication and

Table 7.5: Comparison of existing monitoring methods; highlighting the limitations of previous work and contributions of this work.

Study	Technology Used	Monitoring Parameters	Contactless	Focus on ASD	Limitations
[239]	Polysomnography (PSG)	Sleep quality, respiration, movements	No	No	Intrusive, clinical setup required
[243]	Wearable sensors	Heart rate, respiration, movement	No	Partial	User compliance required, discomfort
[244]	Infrared camera	Sleep postures, body movements	Yes	No	Limited accuracy in low-light conditions
[245]	Doppler radar	Respiration, sleep postures	Yes	NO	Limited focus on ASD-related metrics
[240]	ML on EEG data	Sleep patterns, ASD-related abnormalities	No	Yes	Requires electrode placement, intrusive setup
Our Work	UWB Radar	Sleep postures, movements, respiration disorders	Yes	Yes	non-invasive monitoring

behaviour, often requires highly skilled professionals and multiple sessions to ensure accurate evaluation. Additionally, many adults with ASD struggle to stand prolonged assessments, reducing the effectiveness of conventional monitoring techniques. Similarly, vital signs monitoring presents its own set of challenges, as traditional methods, such as electrocardiograms, respiration belts, or pulse oximeters, often involve direct physical contact and repetitive measurements. This can be uncomfortable or difficult for individuals with ASD, making consistent and reliable monitoring difficult, particularly in long-term scenarios.

Radar offers transformative advantages for monitoring sleep quality, vital signs, and ASD-related behaviour, overcoming the limitations of traditional methods. Radar-based sensing is completely contactless, allowing it to monitor physiological parameters such as respiration disorder and sleep patterns without the need for physical contact and wearable devices [85, 145]. This non-invasive approach is particularly beneficial for individuals with ASD, as it eliminates the discomfort and sensory challenges associated with conventional methods. Moreover, continuous wave ultrawide band (UWB) radar can operate seamlessly in real-world environments, such as homes and clinical setups, providing continuous and accurate data without disrupting patients comfort and daily routines. In addition to comfort, radar-based sensing provides objective and reliable data, reducing the variability associated with subjective assessments. By integrating advanced signal processing and machine learning, radar systems can analyse physiological and behavioural patterns linked to ASD, enabling earlier detection and better intervention strategies. Furthermore, the ability of radar to monitor multiple parameters simultaneously, such as sleep quality, cardiovascular health, and respiratory functions, provides a detailed view of an individual's wellbeing, improving the understanding of the interconnections between ASD, sleep disorders, and vital signs. Ultimately, radar-based contactless sensing has the potential to transform ASD monitoring, offering a scalable, accurate, and user-friendly solution to improve the quality of life for individuals with autism and their families.

In this paper, we used an UWB radar to simultaneously monitor critical parameters related to sleep and respiration, including sleeping postures, body movements during sleep, and respiratory disorders during periods of movement. By capturing and analysing these metrics, we identified the significant role that irregular sleep quality and respiration disorders play in early detection of ASD. This groundbreaking contactless sensing approach provides an understanding of the interconnected physiological and behavioural patterns associated with ASD, highlighting the potential of radar as a noninvasive tool for early diagnosis and continuous monitoring in

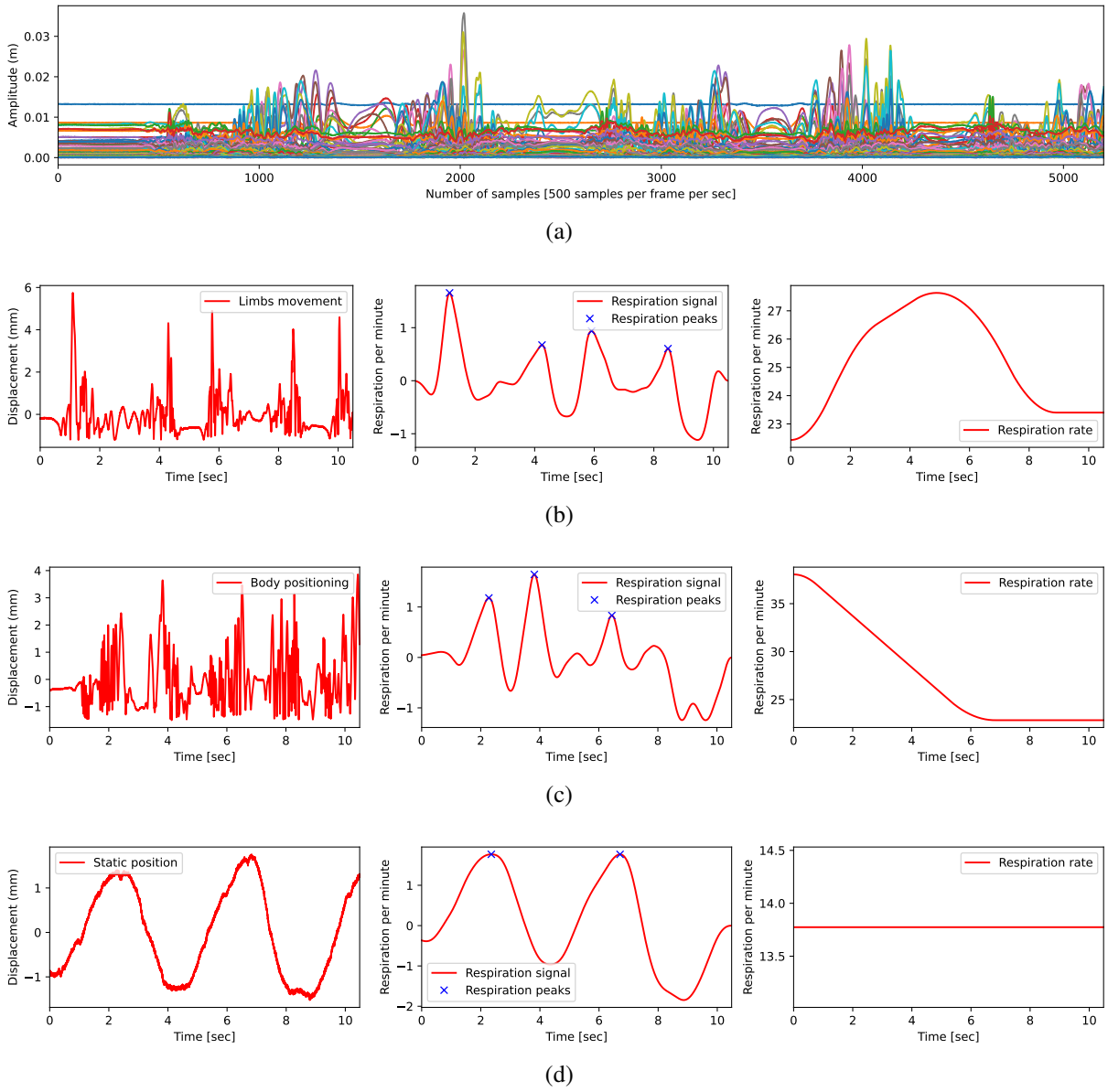

Figure 7.6: Figure (a) illustrates the raw radar data, including samples and amplitude. Figure (b) is divided into three subfigures: the first describes limb movement signals during sleep, the second shows the respiration signal, and the third represents the respiration rate. Similarly, Figures (c) and (d) display body positioning and static sleep positions, respectively, in the first subfigure, followed by the respiration signal and respiration rate in the second and third subfigures.

real-world environments. We made following novel contributions for the first time as per best of our knowledge:

1. Developed a contactless UWB radar-based system to simultaneously monitor sleep postures, body movements, and respiratory disorders during sleep.

2. Identified irregular sleep quality and respiration disorders as potential biomarkers for early detection of ASD.

3. Demonstrated the feasibility of integrating sleep and vital sign analysis using radar for non-invasive real-time ASD monitoring.

The structure of this paper is organized as follows: Section 3.2 provides an overview of the challenges in sleep and vital signs monitoring, tabulated in TABLE 7.5, particularly in the context of ASD, and highlights the motivation and significance of UWB radar for contactless sensing. Section 7.2.1 details the experimental design and data acquisition process in Subsection 7.2.1, including the setup of the UWB radar system and the protocols followed for data collection, while Subsection 7.2.1 focuses on the techniques used for feature extraction from the radar signals to derive meaningful physiological and behavioural benchmarks. Section 7.2.2 presents the key findings of the study, including the analysis of sleeping postures, body movements, and respiratory patterns, and discusses their implications for early ASD detection. Section 7.2.3 summarizes the contributions and insights gained from the study, emphasizing the potential of UWB radar for ASD monitoring and outlining directions for future.

7.2.1 Methodology

Experimental Setup and Data Collection

The experimental setup, shown in Fig. 2, consists of an adjustable hospital bed, a UWB radar system, and a Dell Latitude 5421 laptop, collectively forming a contactless sleep monitoring system. The core sensor used is the XeThru X4 radar system-on-chip (SoC) developed by NOVELDA. This high-resolution UWB radar operates within the 7.29 to 8.75 GHz frequency range, covering the C and X bands. Configured to a fixed frequency of 7.29 GHz, the radar offers a maximum detection range of 9.6 meters, enabling comprehensive monitoring of patients in various bed positions. With a transmitter power output of 6.3 dBm, the system ensures reliable signal transmission for detecting body movements within its range. The radar has a maximum bandwidth of 1.5 GHz, enabling high-resolution data acquisition that is vital for accurately identifying sleep-related movements, positional changes and respiration signal.

Features Extraction

Data collection involved six adult male and female participants, each performing a consistent set of sleep-related activities 30 times. This process resulted in a total of 180 data files, which were then prepared for feature extraction. The radar system generates DAT files containing raw radar data with sampling frequency 0.5 kHz, and 500 samples per frame per second. To simplify data handling and analysis, data files were segmented into smaller chunks of five minutes, one minute, and 30 seconds. This segmentation reduced the complexity of managing and processing continuous large-scale data, as uninterrupted data streams can complicate efficient event extraction. The raw radar data included in-phase (I) and quadrature (Q) components in complex form, as shown in Fig. 7.6a. The dataset checked for missing values and outliers beyond the radar's optimal sensing range to ensure the reliability of the analysis. Frequency filtering was applied to isolate relevant signal content, with all sleep-related activities identified within an

upper frequency limit of 100 Hz. From the refined dataset, key sleep activity features, such as static positions, position changes, and limbs movement were extracted, as illustrated in Figs. 7.6b, 7.6c, and 7.6d. To further analyse the radar signals for body posture and movement detection, a short-time Fourier transform (STFT) was applied, generating spectrograms, illustrated in Fig. 7.7, that revealed Doppler shifts caused by participant movements during sleep. This frequency-time analysis provided perceptions into the dynamics of movement over time, enabling the extraction of features related to sleep activities from the radar data.

To extract the respiration signal and respiration rate from the radar data, the raw radar readings, consisting of in-phase and quadrature components, were first processed to isolate quadrature signal corresponding to chest movements caused by breathing. A bandpass filter was applied then to the radar data to filter out the frequency range of human respiration, which lies between 0.1 Hz and 0.5 Hz for adults. The filtered data was then analysed to identify periodic variations corresponding to the inhalation and exhalation cycle. By applying Fourier transform techniques, the dominant frequency components within the respiration band were extracted, representing the respiration rate. Additionally, phase analysis of the I/Q radar signals was used to enhance the accuracy of the respiration rate estimation by capturing complex chest movements. This approach allowed for reliable and non-contact monitoring of respiratory patterns, even during body movements or shifts in sleeping posture.

7.2.2 Results and Discussions

Variations in the respiration signal and sleep-related features are closely associated with ASD, as individuals with ASD often exhibit complex physiological and behavioural patterns during sleep. Irregularities in respiration, such as abnormal breathing rates, disrupted respiratory cycles, or apnea-like events, are commonly reported among individuals with ASD and may contribute to poor sleep quality. These disruptions in respiration are indicative of autonomic dysfunction, which is often linked to ASD. Variations in the respiration signal reflect stress-related arousals, fragmented sleep, or irregular sleep phases, all of which are frequently observed in individuals with ASD. In addition to respiration, sleep-related features such as sleep posture, frequency of body movements, and transitions between regular and irregular sleep states also provide critical insights into ASD-associated sleep disturbances. For example, frequent positional changes or restless movements during sleep may signal underlying discomfort or extreme sensory sensitivities, both of which are prevalent in individuals with ASD. Similarly, prolonged periods of static posture or irregular transitions between sleep stages could indicate an inability to maintain restful sleep, which is an indicator of sleep issues in ASD. By analysing these features alongside variations in the respiration signal, a more complete understanding of the corelation between sleep disturbances and ASD can be achieved, potentially enabling earlier detection and intervention strategies. The spectrograms generated from the processed radar data were used as input to a pretrained VGG16 model to classify breathing and sleep pattern features for identify-

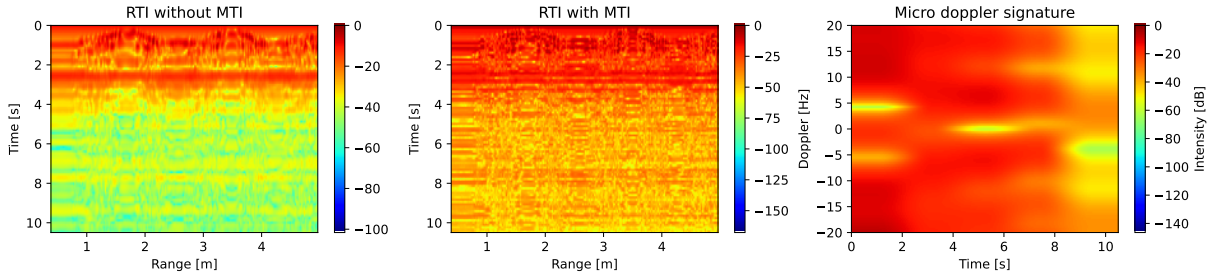

Figure 7.7: This figure is divided into three subfigures: the first subfigure shows the range-time intensity (RTI) plot over the UWB radar range, the second subfigure presents RTI data processed using a moving target indication (MTI), which enhances the visual representation of signal strength across range and time by filtering out stationary clutter to highlight moving targets. The third subfigure illustrates motion captured through micro-Doppler signatures over time.

Table 7.6: Classification report summarizing the results for VGG16.

Class	Precision	Recall	F1-Score
Class 1: Static position	1.00	1.00	1.00
Class 2: Limbs movement	0.95	1.00	0.97
Class 3: Position change	1.00	0.94	0.97
Overall accuracy			98.0%

ing Autism Spectrum Disorder. The VGG16 model was trained with an initial learning rate of 0.0001 using the Adam optimization algorithm. A mini-batch size of 16 was used, with cross-entropy as the loss function to evaluate classification performance. Training was conducted for a maximum of 20 epochs, with 25 iterations per epoch. The classification results, including the accuracy of individual classes and an overall classification accuracy of 98%, are summarized in TABLE 7.6.

7.2.3 Summary

This work demonstrated the potential of an ultra-wideband radar-based system for contactless monitoring of sleep-related features and respiration patterns, with a specific focus on autism spectrum disorder (ASD). By analysing variations in respiration signals, sleep postures, and body movements, we identified key physiological and behavioural markers associated with ASD. The proposed system offers a non-invasive, efficient, and scalable approach to identify sleep disturbances and autonomic dysfunctions commonly observed in individuals with ASD. This work lays the foundation for future research making use of radar technology for early detection and management of ASD-related sleep and health challenges for scalable implementation in next generation homes and healthcare centres setup.

7.3 Contactless Snores Apnea Detection During Sleep by Exploiting Radar Signal

Obstructive sleep apnea (OSA) is a widespread sleep disorder affecting a minimum 4% and up to 30% of adults globally with significant health risks, such as cardiovascular diseases and cognitive impairment. Current diagnostic methods, such as polysomnography, load patients with multiple sensors, require special laboratories, and are uncomfortable for long-term monitoring. In this paper, we present a radar-based contactless system to monitor respiratory disorder patterns to detect fatal sleep problems. Using a 24 GHz continuous-wave radar, we extracted respiratory displacement waveforms and respiration rates, validated them against a ground-truth and achieved high accuracy. Following this, we applied signal processing techniques to extract key respiratory events such as apnea, hypopnea, and snores. These features were used to train a multiclass k-nearest neighbours (KNN) classification model. The model demonstrated excellent performance for the detection of apnea, hypopnea, and snores. We achieved a validation accuracy of 99.79% for respiratory displacement waveforms and 99.99% for respiration rates against the ground truth. Multiclass classification model achieved over 99% accuracy in detecting apnea, hypopnea, and snore events. The results indicate that radar-based system can be used effectively in clinical and home settings to monitor respiratory health and detect abnormal events in real time.

The earliest known description of a person suffering from obstructive sleep apnea (OSA) occurs in The Posthumous Papers of the Pickwick Club by the novelist Charles Dickens, published in 1836 [246]. Dickens describes "Joe," an excessively sleepy, obese boy who snored loudly and possibly had right-sided heart failure [246–248]. Guilleminault, who was a French physician, formally described OSA in 1976 to emphasise the occurrence of this condition in non-obese patients [249]. OSA is a condition in which a person stops breathing or experiences severely reduced airflow during sleep, leading to episodes of breathlessness [250]. Although not all snorers have apnea, the two conditions are often correlated. As snoring increases, the possibility of sleep apnea increases [251]. A person with apnea observes pauses in breathing between snores, these are episodes of apnea, which can occur hundreds of times each night [252]. During sleep, individuals with OSA experience partial, complete, or multiple obstructions of the airway [253], known as hypopneas, apnea, and mixed apnea (when both apnea and hypopnea occur together) [253–255]. Additional symptoms may include loud snoring, gasping, or choking [256]. The American Academy of Sleep Medicine (AASM) estimates that OSA is a common sleep disorder affecting at least 2% to 4% of all adults [257].

According to AASM, apnea is a period during which a person stops breathing or almost stops for at least 10 seconds and airflow is reduced by at least 90% [258, 259]. Although there is no airflow, the person's muscles continue to attempt to breathe. Apnea can be classified as obstructive, central, or mixed [260]. In obstructive apnea, the muscles continue to try to breathe,

whereas in central apnea, no effort is made [261]. In mixed apnea, the muscles initially do not exert any effort to breathe, but try again toward the end of the episode [260–262]. AASM also explains that hypopnea is a period of time when airflow is partially blocked, leading to shallow breathing. During hypopnea, airflow decreases by at least 30% and can last for at least 10 seconds or more [263]. Hypopnea can cause a decrease in oxygen saturation less than 3% or may cause the person to wake up from sleep [262, 263].

Hypopnea is typically categorized as obstructive, central, or mixed. During an obstructive hypopnea, breathing is partially obstructed and reduced due to a narrowed airway [264]. These hypopneas are often accompanied by snoring, caused by the vibration of tissue [265]. The sleeper continues to make an effort to breathe, which may result in abnormal abdominal movements, such as moving the abdomen inward while inhaling [263]. In contrast, during a central hypopnea, the brain fails to send the signal to breathe, leading to reduced effort by the sleeper [266]. Since the differences in brain signalling and breathing effort can be difficult to detect, a hypopnea is generally considered a central event when there are no signs of airway narrowing, such as snoring [267]. Apnea and hypopnea are often related, and individuals with hypopnea are likely to develop apnea. Doctors can diagnose sleep apnea-hypopnea disorder by measuring the apnea-hypopnea index (AHI) [268] during a sleep study. The AHI represents the number of apnea and hypopnea episodes that occur per hour of sleep, with a higher AHI indicating more severe sleep apnea. A normal AHI is less than 5 events per hour [268], while a severe AHI is more than 30 events per hour [268–270].

PSG is the gold standard test for diagnosing OSA. It is an overnight sleep test conducted in a specialized sleep laboratory where physiological parameters including brain activity, eye movements, muscle activity, heart rate, oxygen levels, airflow, and respiratory effort are monitored by using electroencephalogram, electrooculogram, electromyogram, electrocardiogram, pulse oximetry, airflow monitor, and respiratory effort belt, respectively. Despite the diagnostic accuracy of PSG, patients face several challenges that limit the widespread use of PSG. The cost of PSG testing is high due to specialized equipment and trained operators, making it difficult to access in resource-limited environment. Sleep tests are often available in specific laboratories, leading to long waiting times and delay in diagnoses. Patient comfort is another issue, as the lab environment and the need to sleep with many sensors can disturb sleep and result in possibly inaccurate results. While PSG remains the gold standard test for diagnosing OSA, its limitations in multiple sensors complexity, test cost, lab accessibility, and patient comfort require the need for alternative approaches, such as contactless sensing.

Radar-based systems offer a promising solution for mitigating the challenges associated with invasive monitoring techniques in OSA [85]. These systems can track tiny movements of the body, allowing for an accurate assessment of respiration rates without requiring any physical sensors to be attached to the patient [145]. By eliminating the need for physical contact, radar-based monitoring not only enhances patient comfort but also provides potential benefits in infection

control, remote patient monitoring, and overall healthcare accessibility [136]. Exploiting electromagnetic waves, radar systems detect complex physiological movements, penetrating through clothing and environmental obstructions, and ensure reliable monitoring in various clinical settings. Their ability to detect even the smallest chest movements or sensitive fluctuations in heartbeat frequency, positions radar technology as an essential tool in healthcare applications, particularly in the context of OSA. Radar systems enable healthcare staff to remotely access physiological data in real time, hence improving diagnostic accuracy, clinical decision making, and patient care convenience.

In radar-based systems, lower-end microwave frequencies, up to 30 GHz, can penetrate clothing and non-metallic materials while being reflected by the human body [147]. This potential allows radar systems to collect data through obstructions, providing monitoring without the need for direct physical contact. These frequencies interact safely and absorb a smaller amount in body tissues compared to the higher millimetre wave frequencies, thus reduce potential heating effects and ensure safety during continuous monitoring in clinical settings [242]. The continuous-wave (CW) radar frequency in the lower microwave range is particularly allocated for healthcare applications, ensuring compliance with international safety standards and minimising interference with other communication devices. This makes radar-based monitoring a safe, noninvasive approach for managing and diagnosing OSA. It offers significant advantages compared to the PSG such as avoid skin mounting, no privacy concerns, portable device, cost effective, remote monitoring, convenient clinical settings, and patient comfort [144, 177].

Table 7.7 summarizes recent and past studies that utilized radar technology to monitor obstructive sleep apnea. We examined the type of radar used, the specific parameters monitored (e.g., apnea, hypopnea, snores, and respiration rate), the number of subjects involved, the type of ground truth data applied, and the reported overall accuracy. Our review reveals that many studies either did not use a ground truth signal or relied on pre-existing patient data, such as the PSG or AHI index, instead of employing real-time ground truth data for direct comparison with radar signals. Additionally, most papers lacked complete validation procedures before deploying the radar system to monitor patient conditions. In this paper, we used a 24 GHz continuous-wave radar to derive contactless respiration displacement signal, respiration rate, apnea, hypopnea, normal breathing, and snores. In the first step, we measure and monitor respiration displacement ($\mathrm{RD_{radar}}$) waveform and respiration rate ($\mathrm{RR_{radar}}$) by using radar signal and compared it with ground truth respiration displacement ($\mathrm{RD_{sensor}}$) waveform and respiration rate ($\mathrm{RR_{sensor}}$). We use machine learning (ML) regression algorithms to derive performance matrices to assess noninvasive radar system accuracy in comparison with gold standard ground truth signal. The performance test we performed in this step is to make sure that our data collection setup and radar system algorithms should be highly accurate in order to collect next phase volunteers sleep monitoring dataset. In a second step, we collect data from volunteers in a sleeping state and apply algorithms we developed in the first step. In the third step, we identify regions in

Table 7.7: Detailed summary of recent and past research papers making use of radar technology for apnea-hypopnea detection, offering insights into methodologies, key findings and gaps in research for further evaluation, and advancements in the field.

References	Radar Used	Monitored Parameters	Number of Patients	Ground truth	Accuracy
[271]	24 GHz and 2.4 GHz radars	Sleep apnea and RR	10	PSG	92%
[272]	Radar technology	Sleep apnea	14	None	N/A
[273]	60 GHz FMCW radar	Apnea hypopnea events	44	None	0.784 and 0.857
[274]	UWB radar	Abnormal breathing events	92	AHI index	0.93
[275]	Two Doppler radars	Apnea hypopnea events.	31	None	90%
[276]	24 GHz radar	Apnea	141	PSG	Multiple
[277]	UWB radar	Apnea hypopnea index	67	None	N/A
[278]	Two doppler radars	Apnea hypopnea	31	SAHS	90%
This work	24 GHz CW Radar	Apnea, hypopnea, and snores	10	Gold standard	99% (MAE: 0.2865 and 0.1486)

the respiration displacement waveforms where apnea, hypopnea, snores, and normal respiration occur. We used machine learning regression algorithms to identify these regions. Finally, we derive performance matrices again to assess the accuracy of the whole system towards OSA monitoring. Through rigorous validation of measured respiration displacement, respiration rate, apnea, hypopnea, and snores from radar against ground truth signal, our aim is to demonstrate the reliability and accuracy of the contactless vital signs monitoring system, paving the way for their integration into clinical practice and healthcare systems. We made the following contributions for the first time to the best of our knowledge. 1. This paper introduces an advanced signal

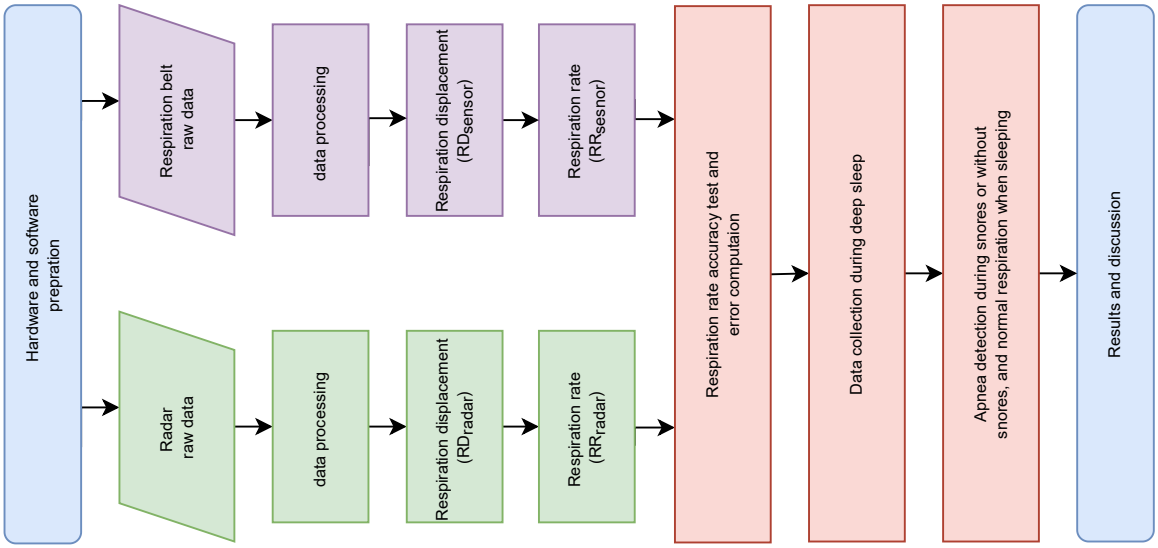

Figure 7.8: Figure 1 outlines the step-by-step process of the study, describing the derivation of respiratory chest displacement and respiration data from both radar and ground truth sources. Initially, rigorous hardware validation was conducted to ensure system accuracy before measuring the desired parameters. Following validation, advanced signal processing techniques were used to identify apnea, hypopnea, and snore events. Finally, classification methods were applied to evaluate the system's automated detection and response capabilities for apnea, hypopnea, and snore events.

processing pipeline to accurately extract key features from the respiratory displacement waveform, enabling precise differentiation between apnea, hypopnea, snoring, and normal breathing

events.
2. The radar-based system detects and classifies apnea and hypopnea events with 99% accuracy, offering a reliable, non-invasive solution for diagnosing respiratory sleep disorders.
3. The system accurately detects snoring events and triggers an alarm if snoring persists for 10 or more seconds, prompting users to change positions and preventing prolonged disturbances in sleep.
4. The proposed radar and signal processing approach is rigorously validated against the gold standard, achieving 99.7% accuracy in measuring respiratory displacement and 99.9% accuracy in breathing rate, demonstrating clinical-grade precision.
5. The research introduced a simple, yet effective classifier to achieve high accuracy in classifying respiratory events with minimal computational resources, supporting real-time remote health monitoring applications. We used the subscripts "radar" and "sensor" to denote the respiration displacement (RD_{radar}) and the respiration rate (RR_{radar}) derived from the radar from contactless methods and ground-truth-derived respiration displacement (RD_{sensor}) and respiration rate (RR_{sensor}), respectively.
The general structure of the paper is shown in Figure 7.8. We have covered an overview of conventional and contactless OSA monitoring approaches in the Introduction section. We reviewed some of the most relevant recent work related to the use of radar in contactless OSA monitoring, described in the Introduction section, and tabulated in TABLE 7.7. The experimental and data collection setup has been described in Methods sections 7.3.1 and 7.3.1. Raw ground truth respiration data, data preprocessing, and extraction of respiration displacement and respiration rate from respiration belt have been given in detail in Methods sections 7.3.1 and 7.3.1, and illustrated in Figure 7.10. Raw radar data, data preprocessing and extraction of respiration displacement, respiration rate, apnea, hypopnea, and snores data are detailed in Method sections 7.3.1, 7.3.1, 7.3.1,7.3.1 and 7.3.1, and illustrated in Figures 7.11 and 7.12.

7.3.1 Methods

Experimental Setup

The electromagnetic waves emitting from radar antennas can absorb or reflect from any obstacle coming in radar line of sight. Traditional healthcare and ambulatory settings involve both healthcare staff and patients. The waves from radar, for example, can reflect not only from the intended patient but also from other moving bodies like healthcare staff and caregivers. Modern portable vital sign monitoring systems can further complicate when it is used in diverse environments, including hospitals, clinics, ambulances, sports facilities, and even patients' homes. It's important to consider potential interference during data collection from patients. The most important is to ensure consistent data collection technique that maintain data quality regardless of the clinical scenario. Data collection not performed to appropriate standards can result in

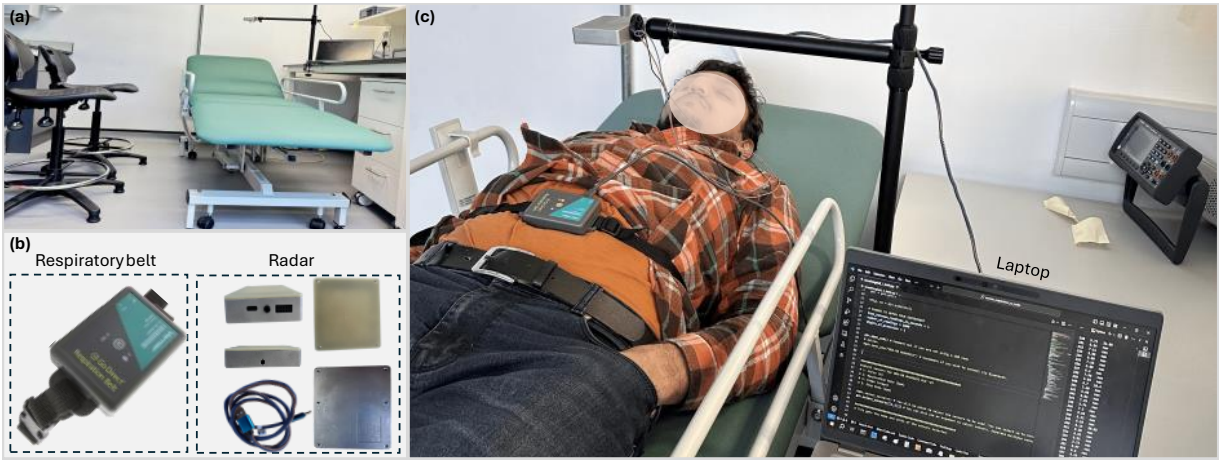

Figure 7.9: Figure 5 illustrates the experimental setup and data collection setup: (a) the room environment containing a medical-grade bed, radar frame, and attendant chairs; (b) the respiratory sensing belt used as the ground truth for respiratory displacement signals and respiration rate, alongside the radar device and its power cable; and (c) an actual participant under observation besides a laptop used for data collection and data storing.

incorrect diagnoses and unnecessary treatments.

Considering the diversity of the healthcare scenarios, the experimental setup was arranged in a room where people other than the target person could move around freely. Although we can record radar data for respiratory signal from an individual in various poses such as sitting, walking, or lying down, however, combining respiration belt for ground truth dataset, and patient comfort require the person in a lying position. Lying position also ensure that measurements are taken under similar conditions, thereby improving data correlation between radar and ground truth.

The experimental setup illustrated in Figure 7.9 consist of an adjustable hospital bed, a radar system, a set of respiration belt, and a Latitude 5421 laptop. The laptop, equipped with an 11th Gen Intel® Core™ i7-11850H processor (24 MB Cache, 8 cores, 16 threads, 4.80 GHz, 16.0 GB RAM), and a 37.5 W power supply was used to power up and control the hardware during the data collection. We used Skyno 24 GHz continuous-wave radar and a Vernier Go Direct® respiration belt as illustrated in Figure 7.9. The radar was positioned one meter away from the target person in a normal room condition. This setup allowed us for the precise collection and analysis of radar and respiration belt dataset.

The experiments for the study were approved ethically by the Research Ethics Committee (approval nos.: 300200232, 300190109) of the University of Glasgow.

Data Collection

Data collection involved ten adult volunteers, comprising both males and females. For each participant, data was recorded in three different time segments: 20 seconds, 1 minute, and 5 minutes. In total, 1,200 samples in 60 data files were collected and subsequently used for clas-

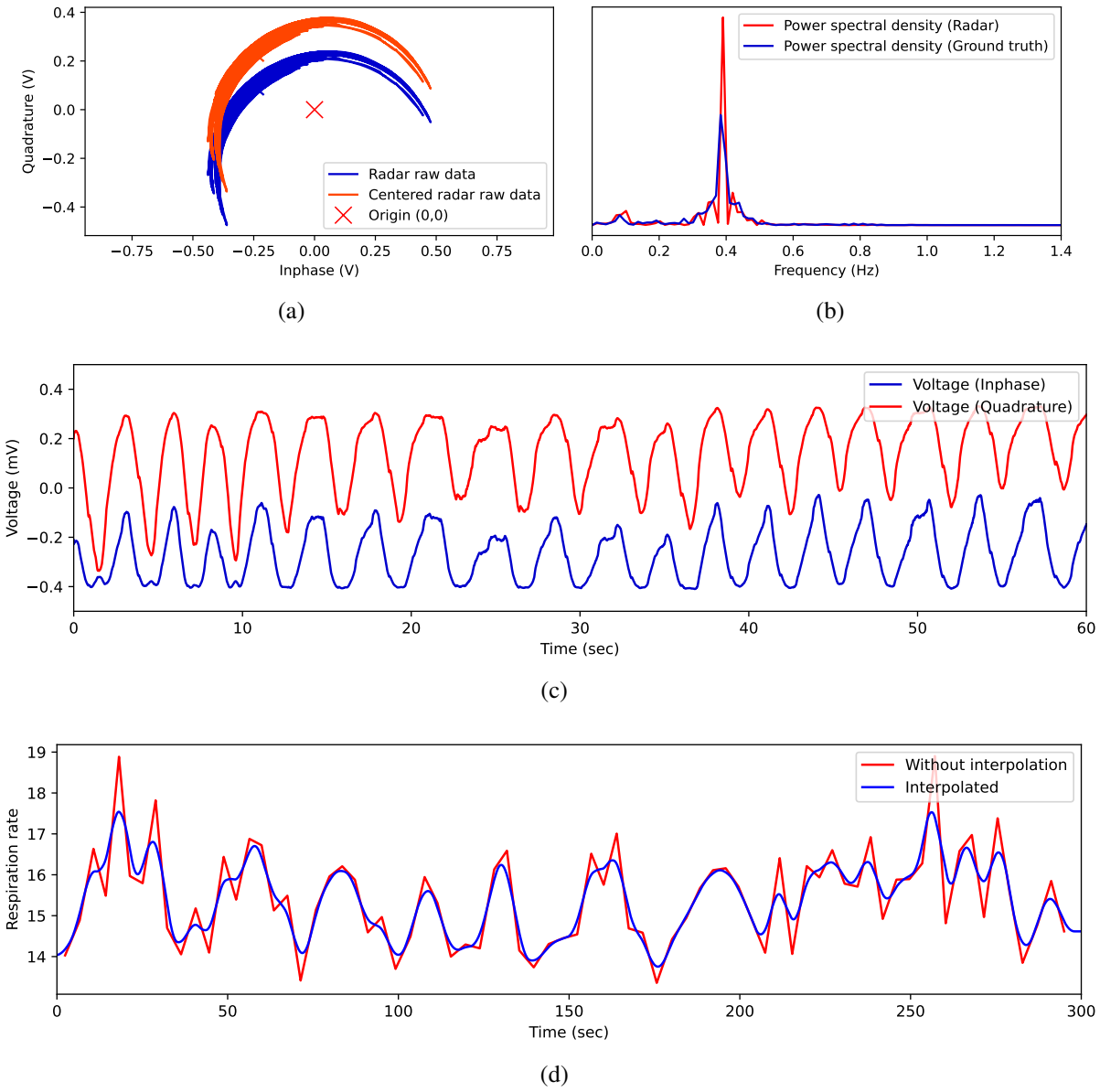

Figure 7.10: Figure 6(a) presents the in-phase and quadrature raw data alongside the centered raw data on origin. Figure 6(b) displays the in-phase and quadrature data in millivolt units over time. Figure 6(c) compares the interpolated respiration signal with the respiration signal without interpolation.

sification and error analysis. The overall structure and flow of the data from radar and ground truth respiration belt is shown in flowchart Figure 7.8. It includes radar and respiration belt raw dataset collection simultaneously on the same time axis. Further, raw data illustration, data processing, respiration signal extraction and comparison with the ground truth signal is given in the following Sections.

Respiration Extraction from Radar Data

We used a 24 GHz CW radar for contactless respiration signal detection, operating with an ADC data rate of 1,000 samples per second, sampling frequency (f_s) 1 kHz, and wavelength (λ) calculated as $3 \times 10^8 \div 24 \times 10^9$. The radar raw data is initially captured in the form of in-phase and quadrature components. As shown in Figure 7.10a, this raw data is not centred at the origin. To correct for this, we calculated the minimum, maximum, and mean values of the raw data and then offset it to align with the origin (0,0). Both the original and adjusted data points are shown in Figure 7.10a, with the (0,0) position marked by a red cross symbol. Since the radar raw data is in complex IQ components form, we reshaped these into a voltage signal by using a scaling factor depending on data. The length of the recorded signal depends on the number of data points and the sampling rate, which we then converted into a time series. Figure 7.10c shows the radar IQ data components in millivolts (mV) and the signal length in time (sec).
We converted the raw IQ data in terms of V; however, chest displacement due to respiration typically follows a rhythmic pattern that corresponds to the breathing cycle, while the heart generates smaller and more periodic vibrations. These heart-induced vibrations are synchronous with the cardiac cycle and can be detected by the radar as they travel through the chest cavities and the wall. Although both respiration and heart produce chest vibrations, they have different characteristics, which is crucial to accurately identify respiratory patterns. Additionally, the radar's ability to capture subtle movements, such as chest vibrations and minor mechanical motions from the heart's atrium during the opening and closing of valves, shows potential for OSA detection. We also converted the IQ voltage signal into a respiration displacement signal (d_{radar}) to represent vibrations in terms of distance parameters.

$$d_{radar} = \tan^{-1}\left(\frac{Q_c}{I_c} \cdot \frac{3 \times 10^8}{24 \times 10^9 \times 4\pi f_s}\right) m \tag{7.10}$$

In equation 7.10, Q_c represents the quadrature component of the centerd data in V, while I_c corresponds to the inphase component of the centred data in V. The frequency f_s is equal to 1 kHz and $3 \times 10^8 \div 24 \times 10^9$ represent the radar wave length λ measured in metres (m).

Respiration Extraction from Ground Truth

The Go Direct® respiration belt measures respiration signals by detecting chest and abdominal expansions and contractions when a person breathes. The belt has built-in force sensors that monitor these movements and convert them into electrical signals that represent the breathing pattern. Belt transfer data through a universal serial bus which can be captured either by using a USB cable or by connecting through low-energy bluetooth (BLE) connection with laptop. To synchronise the belt data with the radar, we prefer to collect data by cable to avoid latency and synchronisation issues. We capture electrical signals, analyse the frequency and amplitude and convert them into respiration displacement signal (RD_{sensor}) similar to the radar dataset. This

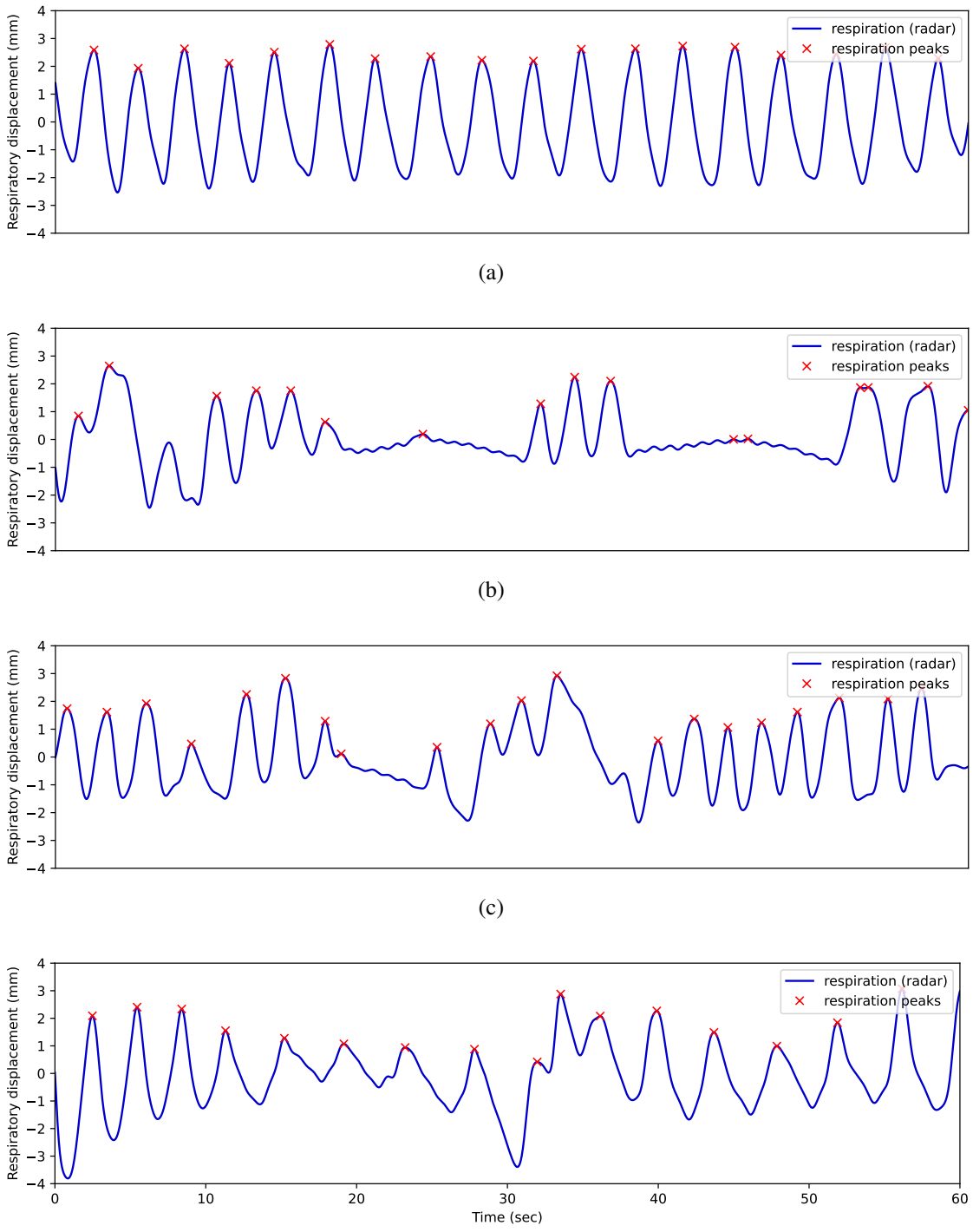

Figure 7.11: Figure 7 illustrates different respiratory events: normal respiration, apnea, hypopnea, and snores. Figure 7(a) shows the pattern of normal respiration. Figure 7(b) demonstrates an apnea event characterized by the absence of respiration activity for at least 10 seconds. Figure 7(c) shows a hypopnea event, featuring a combination of shallow breathing or absence of breathing for a minimum of 10 seconds. Figure 7(d) represents snoring events, identified by variations in frequency and amplitude. These respiratory events keep up repeating according to participant sleeping health.

data provides a continuous, real-time measurement of respiration activity, which makes it useful for monitoring breathing patterns in various clinical settings in a healthcare environment.

Comparison Between Radar and Ground Truth

As the respiration activity is more prominent than the tiny vibrations due to the heart, the peaks shown in radar respiration signal in Figure 7.10c represent the tidal force, while the power spectral density of the radar and the respiration belt signal is illustrated in Figure 7.10b.

$$\begin{aligned} \mathrm{f_{Nyq}} &= \frac{\mathrm{f_s}}{2} = \frac{1,000}{2} = 500\,\mathrm{Hz} \\ \text{Lower cutoff frequency bond: } \mathrm{f_L} &= 0.1\,\mathrm{Hz} \\ \text{Upper cutoff frequency bond: } \mathrm{f_H} &= 0.5\,\mathrm{Hz} \end{aligned} \tag{7.11}$$

We derived a 2^{nd} order Butterworth low pass filter to remove unnecessary components in $\mathrm{d_{radar}}$ and to obtain a refined respiration displacement waveform $\mathrm{RD_{radar}}$. The radar sampling frequency $\mathrm{f_s}$, the Nyquist frequency $\mathrm{f_{Nyq}}$, the lower and upper cutoff frequency bonds $\mathrm{f_L}$, and $\mathrm{f_H}$ respectively given in Equation 7.11. The lower cutoff angular frequency (ω_L), upper cutoff angular frequency (ω_H), and central angular frequency for the bandpass filter (ω_C) are calculated in Equation 7.12. The total number of peaks in one minute and time interval between consecutive peaks are use to extract respiration rate ($\mathrm{RR_{radar}}$) per minute.

$$\begin{aligned} \omega_L &= 2\pi \mathrm{f_L} = 2\pi \times 0.1 \approx 0.628\,\text{rad/sec} \\ \omega_H &= 2\pi \mathrm{f_H} = 2\pi \times 0.5 \approx 3.14\,\text{rad/sec} \\ \omega_c &= \sqrt{\omega_L \cdot \omega_H} = \sqrt{0.628 \times 3.14} \approx 1.4\,\text{rad/s} \end{aligned} \tag{7.12}$$

$$\mathrm{n} = \frac{\log\left(\frac{\sqrt{10^{0.1\mathrm{A_{max}}}-1}}{\sqrt{10^{0.1\mathrm{A_{min}}}-1}}\right)}{2 \cdot \log(\omega_c)} \tag{7.13}$$

$$\begin{aligned} \mathrm{A_{min}} &= 20\log_{10}(\omega_c) \approx 3\,\mathrm{dB} \\ \mathrm{A_{max}} &= -10\log_{10}\left(1+\left(\frac{\omega_s}{\omega_c}\right)^{2n}\right) \\ &= -10\log_{10}\left(1+\left(\frac{4}{1.4}\right)^{2\times 2}\right) \\ &= -10\log_{10}\left(1+(2.857)^4\right) \\ &= -10\log_{10}(1+665.6) \\ &= -10\log_{10}(666.6) \\ &\approx -28.24\,\mathrm{dB} \end{aligned} \tag{7.14}$$

where n is filter order, A_{max} is maximum allowable passband ripples in dB, A_{min} is minimum stopband attenuation in dB, and ω_c is normalized cutoff frequency given in Equations 7.13 and 7.14. Let's the stopband frequency $\omega_s = 4$ rad/sec, the cutoff frequency $\omega_c = 1.4$ rad/sec, and the filter order is 2, then A_{min} and A_{max} is derived in Equation 7.14.

$$y(t) = \text{Butterworth filter}(x(t)) \tag{7.15}$$

We identified the peaks (P) at any time (t) of the filtered waveform $y(t)$ using a height threshold h, to find the breathing cycles. The time between two consecutive peaks is represented by Δt and the subsequent respiration rate is given in Equations 7.16, 7.17 and 7.18.

$$\begin{aligned} P(t_i) = \{\, t_i \,|\, & y(t_i) > h \;\&\; \\ & y(t_i) > y(t_{i-1}) \;\&\; \\ & y(t_i) < y(t_{i+1}) \,\} \end{aligned} \tag{7.16}$$

In Equation 7.16, the parameter h refers to the minimum height required for a peak to be detected. In this context, the height h sets a threshold value, which means that only the peaks in the signal that have a value greater than or equal to h will be considered valid peaks. For example, in Equation 7.16, the numerical value of $h = 0.5$ indicates that the algorithm will only detect peaks with an amplitude greater than or equal to 0.5 mm.

$$\Delta t_i = t_{i+1} - t_i \tag{7.17}$$

$$R_i = \frac{60}{\Delta t_i} \tag{7.18}$$

Interpolation is required to estimate unknown values that fall between known data points (t_i, R_i) and (t_{i+1}, R_{i+1}). In the case of linear interpolation, we use two known points (t_i, R_i) and (t_{i+1}, R_{i+1}) to linearly estimate a value $R(t)$ for some t where $t_i \leq t \leq t_{i+1}$. We start with the general interpolation formula for the respiration rate $R(t)$ given in Equation 7.19 based on known data points (t_i, R_i) and (t_{i+1}, R_{i+1}). To estimate the value of $R(t)$ for some time t between t_i and t_{i+1}, we use linear interpolation.

$$R(t) = \text{interp}(t, \{t_i\}, \{R_i\}) \tag{7.19}$$

We have two known points, (t_i, R_i) and (t_{i+1}, R_{i+1}). These points correspond to the time and respiration rate at two consecutive peaks in the respiration signal. The normalised difference in time between t and t_i is given in Equation 7.20.

$$\frac{(t - t_i)}{(t_{i+1} - t_i)} \tag{7.20}$$

This fraction indicates how far t is between t_i and t_{i+1}, and it ranges from 0 (when $t = t_i$) to 1 (when $t = t_{i+1}$). The difference in the respiration rate between the two points is $(R_{i+1} - R_i)$. This is the change in the respiration rate between t_i and t_{i+1}. Using the normalised time difference and the change in respiration rate, we estimate $R(t)$ as given in Equation 7.21.

$$R(t) = R_i + \frac{(t - t_i)}{(t_{i+1} - t_i)} \times (R_{i+1} - R_i) \tag{7.21}$$

This formula gives the respiration rate at any time t between t_i and t_{i+1} by linearly interpolating between the known values R_i and R_{i+1}. This interpolation is valid for $t_i \leq t \leq t_{i+1}$. Outside this range, we would need to use different pairs of consecutive points for interpolation. Thus, the complete formula for the interpolated respiration rate is given in Equation 7.22.

$$\begin{aligned} R(t) = & R_i + \frac{(t - t_i)}{(t_{i+1} - t_i)} \times (R_{i+1} - R_i), \\ & \text{for} \, t_i \leq t \leq t_{i+1} \end{aligned} \tag{7.22}$$

In this process we extract the breathing rate from the respiration displacement waveform. We first applied a Butterworth second order filter to remove noise and unnecessary components, refining the respiration waveform for further analysis. Next, we identified the peaks in the filtered waveform using the function given in Equation 7.16, which detected the breath cycles by finding local maxima where the displacement exceeded a set threshold, given in Figs. 7.12(a), 7.12(b), and 7.12(c). We then calculated the time intervals between consecutive peaks using Equation 7.17 to determine the time differences between breaths. In addition, the respiration rate was calculated applying the formula given in Equation 7.18, converting the time differences into breaths per minute. Finally, we interpolated the respiration rate over the entire time series using Equation 7.22, providing a continuous estimation of the respiration rate throughout the recording period. The difference between the interpolated and without interpolated waveform is given in Figure 7.10d and the comparison between the respiration rate of the belt and the radar is given in Figure 7.12(d).

Normal respiration

In Figure 7.11a, normal breathing shows a consistent magnitude for respiration displacement waveform that indicate a normal airflow during the breathing cycle. The time period difference between successive breathing peaks has relatively small variations, reflecting a stable breathing cycle. Inhalation is represented by positive peaks in the waveform, while exhalation is represented by negative peaks. This results in a regular pattern without significant variations. The regularity of the sleeping respiration pattern closely resembles the relaxed respiration during awaking state, and the respiration rate remains nearly constant, with only minimal variations. These consistent features are necessary to distinguish normal respiration from abnormal events

such as apnea or hypopnea, where significant deviations from these patterns are observed, shown in the following sub-figures in Figure 7.11.

Apnea and Hypopnea Events

According to the AASM, apnea is defined as a period during which breathing nearly stops for at least 10 seconds, with airflow reduced by at least 90%. Although minimal airflow persists, the individual's muscles continue making efforts to breathe. Compared to the normal breathing patterns shown in Figure 7.11a, Figure 7.11b illustrates a respiration drop that begins with a shallow breathing, followed by almost no inhalation for more than 10 seconds. Despite ongoing muscular efforts to breathe, the force is insufficient to complete the breathing cycle. A small breathing attempt follows the first apnea event, which is then followed by a second apnea episode. This repetitive pattern continues until a hypopnea event or snoring occurs, changing the breathing cycle.

The AASM also explains that hypopnea is a period during which air flow is partially blocked, leading to shallow breathing. During a hypopnea event, airflow decreases by at least 30% and can last a minimum of 10 seconds. Hypopnea can cause a decrease in blood oxygen levels less than 3% or can disturb sleep by awakening the person. In Figure 7.11c, a normal breathing pattern is observed initially, followed by a period of shallow breathing lasting more than 10 seconds. After an attempt to breathe with an increase in breathing force, the breathing pattern gradually returns to normal. The Figure 7.11c also shows a brief pause in inhalation, which lasts less than 10 seconds, followed by shallow breathing, marking this event as hypopnea. Hypopnea events occur repeatedly, often mixed with episodes of apnea-hypopnea and snoring.

Mix Apnea-Hypopnea and Snores

Compared to the normal, apnea, and hypopnea events shown in Figures. 7.11a, 7.11b, and 7.11c respectively, Figure 7.11d shows a longer inhalation lasting over 10 seconds, followed by an exhalation of around 10 seconds, with higher repeating inhalation and exhalation amplitudes afterwards during snoring. In this case, although respiration does not drop to zero for more than 10 seconds, shallow breathing is observed in the first 25 seconds as shown in Figure 7.11d, indicating a hypopnea event. Following this, there is a strong breathing snore for the next 25 seconds, followed by another shallow breathing episode, marking another hypopnea event. For this individual, snoring and hypopnea events are observed to occur repeatedly over a considerable time period.

Features Extraction for Events Identification

In the context of events identification algorithm for machine learning, identifiable respiratory patterns are important for accurate classification. First, the absence of breathing for at least 10

seconds is classified as an apnea event. Second, shallow breathing that persists for 10 seconds is identified as hypopnea. A combination of shallow breathing and no breathing is classified as an apnea-hypopnea event. Lastly, shallow breathing accompanied by a higher amplitude breathing force during snoring is noted as a snoring event. These distinct patterns help machine learning differentiate between normal breathing and abnormal respiratory events such as episodes of apnea, hypopnea, mix (apnea-hypopnea), and snoring. Besides, following alerts will generate in the events of apnea, hypopnea, and snores:

1. If three consecutive events of apnea or hypopnea occur, an alarm will be activated.
2. If the snore continues for up to 10 seconds, the alarm will trigger.

7.3.2 Results

System Validation (Radar Vs Ground Truth)

We compared radar-based respiratory displacement with respiration belt-based displacement, as shown in Figures. 7.12(a), 7.12(b), and 7.12(c). Additionally, we compared the respiration rates derived from the radar to those obtained from the respiration belt, presented in Figure 7.12(d). To further assess the accuracy and reliability of our system against the gold standard, we computed mean absolute error (MAE), mean absolute percentage error (MAPE), mean square error (MSE), and root mean square error (RMSE). The maximum MAE recorded was 0.2865 for respiratory displacement and 0.1486 for respiration rate. We also observed a MAPE of 0.2071% for respiratory displacement and 0.0063% for respiration rate, resulting in an accuracy of 99.79% and 99.99% for respiration displacement and respiration rate, respectively. Rest of the results for MSE and RMSE are provided in Table 7.8.

Overall Accuracy

To identify apnea, hypopnea, and snore events, we categorized the respiration displacement peaks, inter-peak displacement differences, and inter-peak time intervals, as shown in Figure 7.13a. Additionally, we marked the peak displacements to calculate average displacements from the zero position, which allowed us to classify average peak intervals between apnea, hypop-

Table 7.8: We used mean absolute error (MAE), mean absolute percentage error (MAPE), mean square error (MSE), and rote mean square error (RMSE) to validate accuracy and reliability of our system against gold standard respiration belt.

Error	Displacement	Respiration rate
MAE	0.2865	0.1486
MAPE	0.2071	0.0063
RMSE	0.3439	0.2111
MSE	0.1183	0.0446

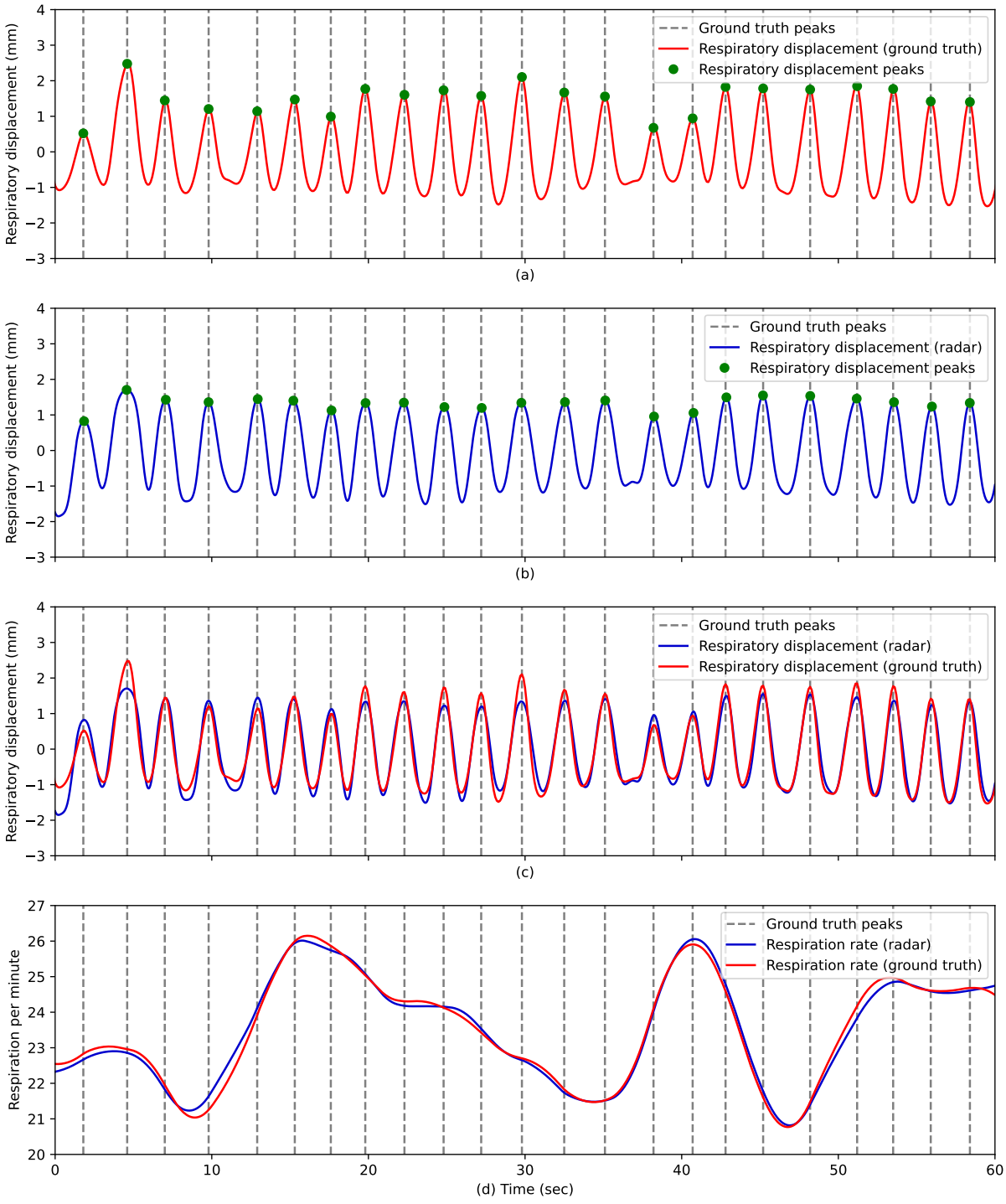

Figure 7.12: Figure 2 presents a comparison between the contactless radar signal and the ground truth from the respiration belt. Figure 2(a) shows the ground truth respiration signal from the belt, with detected peaks indicated by grey dotted lines for reference, which are carried over to Figures 2(b), 2(c), and 2(d). Figure 2(b) illustrates the respiratory signal obtained from the radar, while Figure 2(c) compares the radar respiratory signal with the belt-derived ground truth signal for direct comparison. Finally, Figure 2(d) illustrates the refined radar respiratory signal alongside the ground truth.

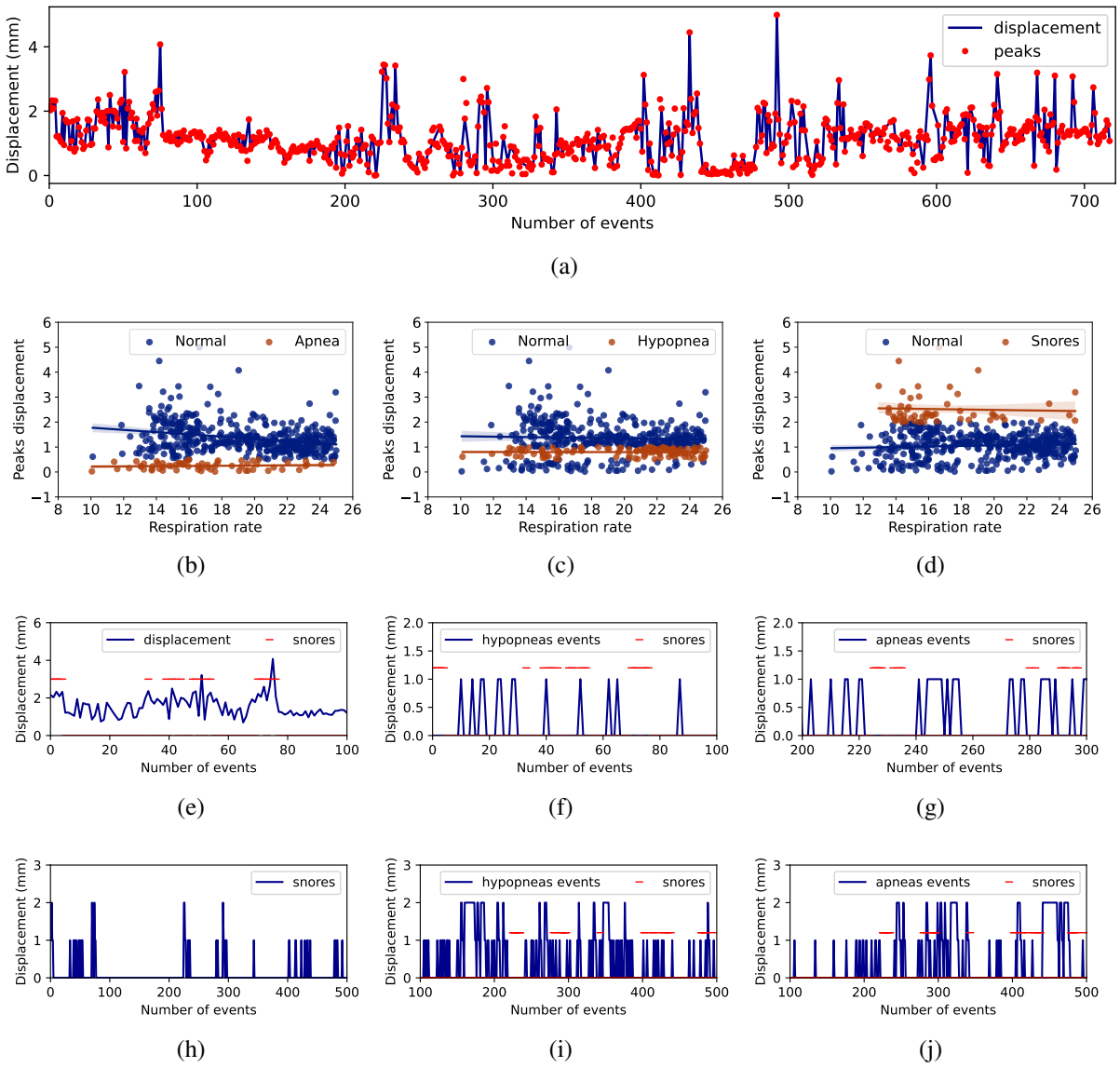

Figure 7.13: Figure 3 illustrates the process for identifying apnea, hypopnea, and snore events. Figure 3(a) categorizes respiration displacement peaks, inter-peak displacement differences, and inter-peak time intervals. Figures 3(b), 3(c), and 3(d) show peak displacements and classify average intervals and peaks to events apnea, hypopnea and snores, respectively. Figure 3(e) plots inter-peak displacement differences and inter time interval differences to differentiate hypopnea, apnea, and snore events, with further illustrations of apnea and hypopnea events in 3(f) and 3(g), respectively. An alert is triggered for events apnea, hypopnea and snores exceeding ten seconds, marked above the first peaks in Figures 3(h), 3(i), and 3(j).

nea, and snore events, as demonstrated in Figs. 7.13b, 7.13c, and 7.13d. In Figure 7.13e, we plotted inter-peak displacement differences to further distinguish hypopnea and apnea events, including snores, as shown in Figs. 7.13f and 7.13g. Furthermore, we triggered an alert when any hypopnea, apnea, or snore event exceeded ten seconds, which is indicated by markers above the first peaks in Figs. 7.13h, 7.13i, and 7.13j. The primary purpose of the trigger is twofold: first, to detect if an event has lasted over 10 seconds for counting the total number of events;

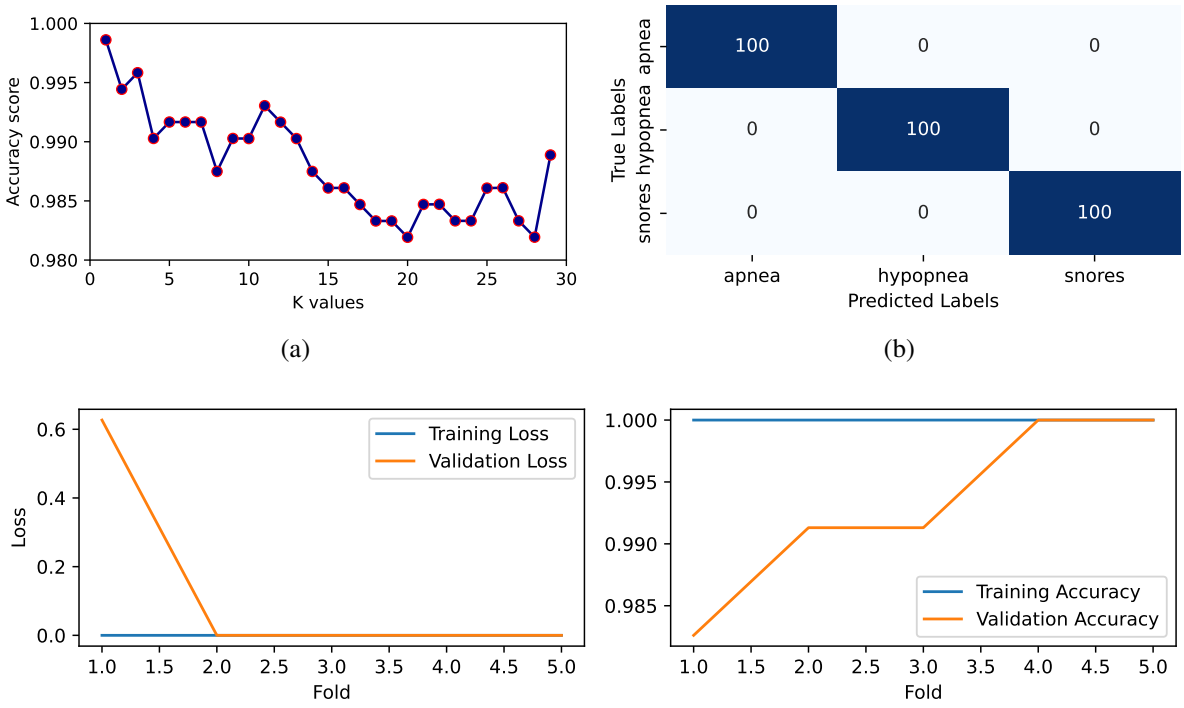

Figure 7.14: Figure 4 presents the evaluation of the k-nearest neighbours classification model. Figure 4(a) illustrates the selection of the optimal k value from 1 to 30, showing the accuracy corresponding to each value. Figure 4(b) displays the confusion matrix for the three classes: apnea, hypopnea, and snores. Figure 4(c) demonstrates the results of the k-fold cross-validation for the first five folds, presenting training and validation performance.

second, in real-time scenarios, it can activate an alarm to awaken the individual or encourage a change in sleeping position to restore normal breathing. From the 718 recorded events across ten subjects, we identified 59 apnea events (8%), 44 hypopnea events (6%), and the remaining 86% were normal respiration events. Apnea, hypopnea, and snore events often overlapped with normal respiration. After successfully identifying and distinguishing different respiratory events

Table 7.9: We used mean absolute error (MAE), mean absolute percentage error (MAPE), mean square error (MSE), and rote mean square error (RMSE) to validate accuracy and reliability of our system against gold standard respiration belt.

Class	Precision	Recall	F1-Score	Support
Class 0: Apnea	1.00	1.00	1.00	48
Class 1: Hypopnea	1.00	1.00	1.00	18
Class 2: Snores	1.00	1.00	1.00	6
Accuracy			1.00	72
Macro Avg	1.00	1.00	1.00	72
Weighted Avg	1.00	1.00	1.00	72

using signal processing approach shown in Figure 7.13, we developed a multiclass k-nearest neighbours (KNN) classification model to evaluate overall classification accuracy. Initially, we determined the optimal value of k for the KNN algorithm, which ranged between 1 and 3 for our dataset, shown in Figure 7.14a. For our model, we selected k=3. We divided the data into 80% for training and 20% for testing and applied five-fold cross validation on the training data to ensure model validation. The training accuracy, training loss, validation accuracy, and validation loss for each fold are presented in Figure 7.14c. After training, we tested the model with the remaining 20% of unseen data, and the test accuracy and error metrics are provided in Table 7.8. The signal processing we conducted to clearly identify signal components related to apnea, hypopnea, and snores, enable the KNN model that achieved over 99% accuracy with minimal computational time and resources outlined in the experimental setup. The final accuracy metrics, including precision, recall, F1-score, and overall accuracy for each class (hypopnea, apnea, and snores), are listed in Table 7.9. The resultant confusion matrix is shown in Figure 7.14b. The purpose of implementing a simple KNN machine learning algorithm was to show that multiclass classification could be achieved with ease and deliver excellent results across all classes. In our analysis, we focused on extracting key features such as apnea, hypopnea, and snores from respiratory peak intervals and inter-time intervals of respiratory displacement peaks. For model selection, we chose k-nearest neighbours due to its simplicity and minimal computational requirements, making it ideal for real-time applications with limited resources. To compare the performance, we initially experimented with logistic regression, which yielded an overall accuracy of 76%. However, given its relatively lower performance, logistic regression was not considered further. To optimize the KNN model, we performed a grid search with k ranging from 1 to 30 and utilized the standard scaler from the Scikit-learn library for feature scaling. This process led to the selection of k=3 as the optimal value for our classification model ensuring best accuracy.

7.3.3 Summary

Radar-based sleep apnea detection offers a non-contact and potentially more comfortable alternative to traditional methods. In this study, we addressed the growing need for non-invasive, contactless monitoring of respiratory patterns, particularly for respiration related obstructive sleep apnea (OSA). Given the high prevalence of OSA and its fatal impact on health, radar-based contactless monitoring offers significant advantages over traditional methods such as polysomnography, which can be uncomfortable and disruptive to sleep. Radar systems enable continuous, long-term monitoring without physical contact, making them ideal for early detection and management of sleep-related breathing disorders.

Our approach followed a systematic process, starting with the validation of our radar based contactless model against the gold standard respiratory belts. We successfully demonstrated the model's ability to accurately measure both respiratory displacement waveforms and respiration

rates. The results of this comparison were highly accurate, with 99.7% accuracy for respiratory displacement and 99.9% accuracy for respiration rate, as shown in Table 7.8 and Figure 7.11. This validation not only proved the reliability of our radar-based system but also highlight its potential for clinical applications in monitoring sleep-related disorders.

Following this validation, we used signal processing techniques to extract key respiratory features such as apnea, hypopnea, and snores from the respiratory displacement waveforms. These features were key in identifying abnormal breathing patterns, and the extracted events are provided in Figure 7.13. Finally, we implemented a multiclass classification model using the k-nearest neighbours (KNN) algorithm to classify these events. By tuning the model to the optimal k value, we achieved excellent classification results, with accuracy exceeding 99%. This high level of accuracy, combined with the minimal computational resources required by KNN, demonstrates the effectiveness of our approach for real-time, contactless detection of OSA.

The clinical impact of this contactless monitoring system is significant, offering a non-invasive alternative to traditional polysomnography (PSG) which load the patients with sensors and not accurate due to intrusive nature in several cases. This contactless technology enhances patient comfort, highly precise, and ensures reliability comparable to invasive clinical methods. This approach supports early detection and long-term monitoring of OSA in both home and clinical settings, potentially reduce undiagnosed cases and improving both patient and clinical outcomes. Additionally, the ability to trigger alerts for prolonged apnea or snoring events allows for timely intervention, reducing health risks associated with untreated sleep disorders. The system's minimal computational requirements and ease of deployment further support its integration into telemedicine and remote healthcare frameworks, making advanced sleep monitoring more accessible and scalable.

In conclusion, our radar-based system offers a highly accurate, non-invasive method for respiratory health monitoring, which could be transformative in the management of OSA and related disorders. The successful validation of the system against the ground truth and the implementation of an efficient classification algorithm shows the robustness of our approach and its potential for broader use in clinical and home settings.

Chapter 8

Epilogue

8.1 Conclusions

This thesis presents an in-depth investigation of contactless sensing technologies for human activity detection, vital signs monitoring, heart sounds detection, and sleep pattern recognition using advanced RF and radar-based systems. Through multiple novel approaches, the research demonstrates the feasibility and effectiveness of these technologies in diverse real-world applications, including smart homes, healthcare environments, and public spaces. The proposed LoRa based systems for walking patterns recognition and through wall sensing highlight the potential of LoRa technology in identifying individuals based on their walking patterns, achieving high accuracy across different indoor and outdoor settings. Similarly, the use of energy consumption data for human activity classification offers an efficient, machine-learning-driven approach to behavioural monitoring in residential spaces, with implications for anomaly detection and predictive analytics. The thesis further explores the feasibility of radar-based speaker recognition, demonstrating promising results in distinguishing individuals while preserving privacy. Additionally, sleep pattern recognition through micro doppler radar signals presents a non-invasive method for detecting sleep abnormalities, particularly in early autism spectrum disorder diagnosis. This work establishes the foundation for future improvements in dataset expansion and model optimization. Vital signs monitoring is another key focus of this research, with the application of ultra-wideband and continuous wave radar systems to detect respiration variability and heart rate. The results illustrate the effectiveness of deep learning models in extracting meaningful physiological markers, advancing non-invasive health monitoring capabilities. The study also emphasises the significance of heart sound analysis for accurate heart rate estimation, reinforcing the reliability of cardiac signal processing techniques in medical applications. Overall, this research underscores the transformative potential of RF and radar-based sensing technologies in modern healthcare and smart living environments. While the findings contribute significantly to the field. Future research should address challenges related to environmental constraints, data security, and system scalability. By refining algorithms, incorporating advanced

machine learning techniques, and expanding datasets, these innovations can further enhance the accuracy, efficiency, and applicability of contactless monitoring solutions. This thesis paves the way for the next generation of non-invasive sensing technologies, offering practical solutions for improved health and well-being.

8.2 Future Directions in Contactless Human Activity Recognition

Despite significant advancements in contactless human activity recognition, several areas remain open for exploration and improvement. Future research should focus on developing more robust and adaptable models that can perform accurately in different environments, including outdoor and dynamic settings. Enhancing system resilience to environmental factors such as occlusions, multi-user scenarios, and varying human factors will further increase the practicality of these systems. The integration of multimodal sensing approaches, which combine RF, radar, infrared, and vision-based techniques, holds promise for improving recognition accuracy and reliability. In addition, leveraging advanced deep learning models, particularly self-supervised and federated learning techniques, can enable personalised and efficient activity recognition without compromising user privacy. Another critical direction involves the miniaturisation and optimisation of hardware to facilitate real-time processing with minimal energy consumption. Developing energy-efficient, low-cost sensing devices will make contactless activity recognition more accessible for widespread adoption in smart homes, healthcare monitoring, and security applications. Furthermore, ensuring data security and privacy remains a pressing challenge. Future research should explore privacy-preserving techniques, such as differential privacy and homomorphic encryption, to enable secure data processing while maintaining user confidentiality. Finally, expanding data sets with diverse demographics, activity types, and real-world scenarios will improve the generalisability and robustness of the model. Incorporating explainability and interpretability techniques will also enhance trust in AI-driven recognition systems, making them more transparent and understandable to end users. By addressing these challenges and opportunities, future advancements in contactless human activity recognition will significantly impact the healthcare, smart living, and security domains, paving the way for more intelligent and user-friendly environments.

8.3 Future Directions in Contactless Human Vitals Detection

Contactless human vital signs has made significant progress, but several areas require further research to improve its reliability, robustness, and applicability. Future efforts should focus on advancing signal processing techniques and developing advanced machine learning models to

improve the accuracy of vital sign monitoring in diverse healthcare environment. One promising direction is the integration of multi-modal sensing techniques, combining radar, RF, thermal imaging, and optical sensors to enhance detection accuracy and resilience against environmental interferences. The fusion of data from multiple modalities can help mitigate issues such as signal noise, occlusions, and motion artifacts, resulting in more reliable health monitoring systems. Another critical aspect is improving real time processing and power efficiency. Future research should explore lightweight and energy efficient algorithms that can run on edge devices with minimal computational overhead. This will enable seamless deployment in wearable devices, smart home systems, and clinical settings without compromising performance. Personalized healthcare solutions represent an important frontier for contactless vital signs monitoring. Developing adaptive algorithms that account for individual physiological variations will enhance the accuracy of health assessments. Additionally, incorporating AI-driven predictive analytics can enable early detection of health anomalies, facilitating timely medical interventions. Ensuring data security and patient privacy is also important. Future studies should investigate privacy preserving techniques such as secure data encryption, federated learning, and anonymization methods to protect sensitive health information while enabling efficient remote monitoring. Furthermore, expanding the dataset diversity to include a broader range of demographics, health conditions, and environmental scenarios will enhance the generalisability of developed models. Panel studies involving real-world clinical trials will be instrumental in validating the reliability and practicality of these technologies for widespread adoption. By addressing these future research directions, contactless vital signs detection can evolve into a more accurate, scalable, and privacy-preserving solution for healthcare applications, ultimately improving patient outcomes and quality of life.

8.4 Future Directions in Contactless Heart Sounds Detection

Contactless heart sound detection is an emerging area with immense potential for advancing non-invasive cardiac monitoring. Future research should focus on improving the accuracy and robustness of heart sound acquisition and processing techniques to enhance diagnostic capabilities. One key area is the development of advanced signal processing and machine learning algorithms that can effectively filter noise, distinguish between different heart sound components, and accurately extract critical cardiovascular features. Additionally, integrating multi-modal sensing approaches, such as combining radar with thermal or optical sensors, could improve heart sound detection and analysis. Another crucial direction involves real-time monitoring and edge computing solutions. Future research should explore lightweight and efficient models that can be deployed on wearable or portable devices for continuous, real time heart sound monitoring in home and clinical settings. Privacy and data security considerations must also be addressed. Future studies should investigate methods to ensure secure and encrypted transmis-

sion of sensitive cardiac data, while also exploring privacy-preserving AI techniques to process heart sounds without compromising user confidentiality. Expanding datasets to include diverse populations, various health conditions, and real-world environmental settings will be essential for improving model generalisation and clinical applicability. Panel studies involving extensive clinical validation will further establish the credibility of contactless heart sound detection systems for widespread adoption in healthcare. By advancing these research directions, contactless heart sound detection has the potential to revolutionize cardiac health monitoring, providing a non-invasive, efficient, and accessible solution for early disease detection and personalised healthcare.

Bibliography

[1] M. Hameed, M. Shah, U. Khalil, H. Khan, Z. Rehman, and H. Iftikhar. Energy efficient mechanisms and techniques for internet of things (iot). *IEEE Communications Surveys & Tutorials*, 25:490–515, 2023.

[2] Gyubaek Kim and Sanghyun Park. Activity detection from electricity consumption and communication usage data for monitoring lonely deaths. *Sensors*, 21(9):3016, 2021.

[3] Anastasia Lewis. Housing An Ageing Population: A Reading List, house of commons library united kingdom parliament, 2021.

[4] D. Clark. Number of people living alone in the United Kingdom, 2022.

[5] Janet Wesson, George Mujuru, and Lester Cowley. Health and activity monitoring using smart devices to support the self-management of health behavior. In *International Conference on Intelligent Human Systems Integration*, pages 395–401. Springer, 2021.

[6] Maiya Hori, Tatsuro Harada, and Rin-ichiro Taniguchi. Anomaly detection for an elderly person watching system using multiple power consumption models. In *ICPRAM*, pages 669–675, 2017.

[7] Md Atiqur Rahman Ahad, Paula Lago, and Sozo Inoue. *Human activity recognition challenge*. Springer, 2021.

[8] Ankur Sial, Amarjeet Singh, and Aniket Mahanti. Detecting anomalous energy consumption using contextual analysis of smart meter data. *Wireless Networks*, 27(6):4275–4292, 2021.

[9] Shane A Lowe and Gearóid ÓLaighin. Monitoring human health behaviour in one's living environment: a technological review. *Medical engineering & physics*, 36(2):147–168, 2014.

[10] Min Chen, Yujun Ma, Jeungeun Song, Chin-Feng Lai, and Bin Hu. Smart clothing: Connecting human with clouds and big data for sustainable health monitoring. *Mobile Networks and Applications*, 21(5):825–845, 2016.

[11] Robert Steele, Amanda Lo, Chris Secombe, and Yuk Kuen Wong. Elderly persons' perception and acceptance of using wireless sensor networks to assist healthcare. *International journal of medical informatics*, 78(12):788–801, 2009.

[12] Samih Eisa and Adriano Moreira. A behaviour monitoring system (bms) for ambient assisted living. *Sensors*, 17(9):1946, 2017.

[13] Honghai Liu, Zhaojie Ju, Xiaofei Ji, Chee Seng Chan, and Mehdi Khoury. *Human motion sensing and recognition*. Springer, 2017.

[14] Fadel Adib and Dina Katabi. See through walls with wifi! In *Proceedings of the ACM SIGCOMM 2013 conference on SIGCOMM*, pages 75–86, 2013.

[15] Ju Wang, Jie Xiong, Hongbo Jiang, Kyle Jamieson, Xiaojiang Chen, Dingyi Fang, and Chen Wang. Low human-effort, device-free localization with fine-grained subcarrier information. *IEEE Transactions on Mobile Computing*, 17(11):2550–2563, 2018.

[16] Fusang Zhang, Zhaoxin Chang, Kai Niu, Jie Xiong, Beihong Jin, Qin Lv, and Daqing Zhang. Exploring lora for long-range through-wall sensing. *Proceedings of the ACM on Interactive, Mobile, Wearable and Ubiquitous Technologies*, 4(2):1–27, 2020.

[17] Fadel Adib, Zachary Kabelac, Dina Katabi, and Rob Miller. Witrack: motion tracking via radio reflections off the body. In *Proc. of NSDI*, 2014.

[18] Alain Olivier, Guillermo Bielsa, Irene Tejado, Michele Zorzi, Joerg Widmer, and Paolo Casari. Lightweight indoor localization for 60-ghz millimeter wave systems. In *2016 13th Annual IEEE International Conference on Sensing, Communication, and Networking (SECON)*, pages 1–9. IEEE, 2016.

[19] Te-Yu Jason Kao and Jenshan Lin. Vital sign detection using 60-ghz doppler radar system. In *2013 IEEE International Wireless Symposium (IWS)*, pages 1–4. IEEE, 2013.

[20] Swaroop Venkatesh, Christopher R Anderson, Natalia V Rivera, and R Michael Buehrer. Implementation and analysis of respiration-rate estimation using impulse-based uwb. In *MILCOM 2005-2005 IEEE Military Communications Conference*, pages 3314–3320. IEEE, 2005.

[21] Anran Wang and Shyamnath Gollakota. Millisonic: Pushing the limits of acoustic motion tracking. In *Proceedings of the 2019 CHI Conference on Human Factors in Computing Systems*, pages 1–11, 2019.

[22] Tianben Wang, Daqing Zhang, Yuanqing Zheng, Tao Gu, Xingshe Zhou, and Bernadette Dorizzi. C-fmcw based contactless respiration detection using acoustic signal. *Proceed-*

ings of the ACM on Interactive, Mobile, Wearable and Ubiquitous Technologies, 1(4):1–20, 2018.

[23] Ju Wang, Jie Xiong, Hongbo Jiang, Xiaojiang Chen, and Dingyi Fang. D-watch: Embracing" bad" multipaths for device-free localization with cots rfid devices. In *Proceedings of the 12th International on Conference on emerging Networking EXperiments and Technologies*, pages 253–266, 2016.

[24] Yanwen Wang and Yuanqing Zheng. Tagbreathe: Monitor breathing with commodity rfid systems. *IEEE Transactions on Mobile Computing*, 19(4):969–981, 2019.

[25] Tianxing Li, Qiang Liu, and Xia Zhou. Practical human sensing in the light. In *Proceedings of the 14th Annual International Conference on Mobile Systems, Applications, and Services*, pages 71–84, 2016.

[26] Tianxing Li, Chuankai An, Zhao Tian, Andrew T Campbell, and Xia Zhou. Human sensing using visible light communication. In *Proceedings of the 21st Annual International Conference on Mobile Computing and Networking*, pages 331–344, 2015.

[27] Muhammad Usman, James Rains, Tie Jun Cui, Muhammad Zakir Khan, Muhammad Ali Imran, Qammer H Abbasi, et al. Intelligent wireless walls for contactless in-home monitoring. *Light: Science & Applications*, 11(1):1–13, 2022.

[28] Wenda Li, Bo Tan, and Robert Piechocki. Passive radar for opportunistic monitoring in e-health applications. *IEEE journal of translational engineering in health and medicine*, 6:1–10, 2018.

[29] Yao Ge, Ahmad Taha, S.A Shah, Kia Dashtipour, Shuyuan Zhu, Jonathan M. Cooper, Qammer Abbasi, and Muhammad Imran. Contactless wifi sensing and monitoring for future healthcare - emerging trends, challenges and opportunities. *IEEE Reviews in Biomedical Engineering*, pages 1–1, 2022.

[30] Wei Wang, Alex X Liu, and Muhammad Shahzad. Gait recognition using wifi signals. In *Proceedings of the 2016 ACM International Joint Conference on Pervasive and Ubiquitous Computing*, pages 363–373, 2016.

[31] Yi Zhang, Yue Zheng, Guidong Zhang, Kun Qian, Chen Qian, and Zheng Yang. Gaitid: robust wi-fi based gait recognition. In *International Conference on Wireless Algorithms, Systems, and Applications*, pages 730–742. Springer, 2020.

[32] Youwei Zeng, Dan Wu, Jie Xiong, Enze Yi, Ruiyang Gao, and Daqing Zhang. Farsense: Pushing the range limit of wifi-based respiration sensing with csi ratio of two antennas. *Proc. ACM Interact. Mob. Wearable Ubiquitous Technol.*, 3(3), sep 2019.

[33] Fadel Adib, Hongzi Mao, Zachary Kabelac, Dina Katabi, and Robert C Miller. Smart homes that monitor breathing and heart rate. In *Proceedings of the 33rd annual ACM conference on human factors in computing systems*, pages 837–846, 2015.

[34] Juha Petäjäjärvi, Konstantin Mikhaylov, Rumana Yasmin, Matti Hämäläinen, and Jari Iinatti. Evaluation of lora lpwan technology for indoor remote health and wellbeing monitoring. *International Journal of Wireless Information Networks*, 24(2):153–165, 2017.

[35] Christopher A Miles. Through-the-wall surveillance: a new technology for saving lives. *National Institute of Justice Journal*, 258:20–25, 2007.

[36] Teodor Tomic, Korbinian Schmid, Philipp Lutz, Andreas Domel, Michael Kassecker, Elmar Mair, Iris Lynne Grixa, Felix Ruess, Michael Suppa, and Darius Burschka. Toward a fully autonomous uav: Research platform for indoor and outdoor urban search and rescue. *IEEE robotics & automation magazine*, 19(3):46–56, 2012.

[37] Shengjie Li, Zhaopeng Liu, Yue Zhang, Xiaopeng Niu, Leye Wang, and Daqing Zhang. A real-time and robust intrusion detection system with commodity wi-fi. In *Adjunct Proceedings of the 2019 ACM International Joint Conference on Pervasive and Ubiquitous Computing and Proceedings of the 2019 ACM International Symposium on Wearable Computers*, pages 316–319, 2019.

[38] Qifan Pu, Sidhant Gupta, Shyamnath Gollakota, and Shwetak Patel. Whole-home gesture recognition using wireless signals. In *Proceedings of the 19th annual international conference on Mobile computing & networking*, pages 27–38, 2013.

[39] Fadel Adib, Zachary Kabelac, and Dina Katabi. {Multi-Person} localization via {RF} body reflections. In *12th USENIX Symposium on Networked Systems Design and Implementation (NSDI 15)*, pages 279–292, 2015.

[40] Kamran Ali, Alex X Liu, Wei Wang, and Muhammad Shahzad. Recognizing keystrokes using wifi devices. *IEEE Journal on Selected Areas in Communications*, 35(5):1175–1190, 2017.

[41] Peter Jones and Daphne Comfort. localising the sustainable development goals. *Town and Country Planning*, pages 132–136, 2019.

[42] David E Bloom, David Canning, and Alyssa Lubet. Global population aging: Facts, challenges, solutions & perspectives. *Daedalus*, 144(2):80–92, 2015.

[43] Kaare Christensen, Gabriele Doblhammer, Roland Rau, and James W Vaupel. Ageing populations: the challenges ahead. *The lancet*, 374(9696):1196–1208, 2009.

[44] Eduardo Teixeira, Hélder Fonseca, Florêncio Diniz-Sousa, Lucas Veras, Giorjines Boppre, José Oliveira, Diogo Pinto, Alberto Jorge Alves, Ana Barbosa, Romeu Mendes, et al. Wearable devices for physical activity and healthcare monitoring in elderly people: A critical review. *Geriatrics*, 6(2):38, 2021.

[45] William Taylor, Kia Dashtipour, Syed Aziz Shah, Amir Hussain, Qammer H Abbasi, and Muhammad A Imran. Radar sensing for activity classification in elderly people exploiting micro-doppler signatures using machine learning. *Sensors*, 21(11):3881, 2021.

[46] William Taylor, Syed Aziz Shah, Kia Dashtipour, Adnan Zahid, Qammer H Abbasi, and Muhammad Ali Imran. An intelligent non-invasive real-time human activity recognition system for next-generation healthcare. *Sensors*, 20(9):2653, 2020.

[47] Yang Zhao, Gangliang Zhao, Prabhu Janakaraj, Lynn Derose, Austars Schnore, and Sm Hasan. Non-cooperative personnel tracking with cross modality learning in 5g-enabled warehouse application. In *2021 IEEE 4th 5G World Forum (5GWF)*, pages 194–199. IEEE, 2021.

[48] Fang-Jing Wu and Gurkan Solmaz. We hear your activities through wi-fi signals. In *2016 IEEE 3rd World Forum on Internet of Things (WF-IoT)*, pages 251–256. IEEE, 2016.

[49] Zheng Yang, Zimu Zhou, and Yunhao Liu. From rssi to csi: Indoor localization via channel response. *ACM Computing Surveys (CSUR)*, 46(2):1–32, 2013.

[50] Samarth Mathur, Anand Sankar, Prajwal Prasan, and Bob Iannucci. Energy analysis of lorawan technology for traffic sensing applications. In *Proceedings of the Intelligent Transportation Society of America (ITS) World Congress, Montréal, QC, Canada*, volume 29, 2017.

[51] Philipp Sommer, Yannick Maret, and Dacfey Dzung. Low-power wide-area networks for industrial sensing applications. In *2018 IEEE International Conference on Industrial Internet (ICII)*, pages 23–32. IEEE, 2018.

[52] Kai-Hsiang Ke, Qi-Wen Liang, Guan-Jie Zeng, Jun-Han Lin, and Huang-Chen Lee. A lora wireless mesh networking module for campus-scale monitoring: demo abstract. In *Proceedings of the 16th ACM/IEEE International Conference on Information Processing in Sensor Networks*, pages 259–260, 2017.

[53] Sujuan Liu, Chuyu Xia, and Zhenzhen Zhao. A low-power real-time air quality monitoring system using lpwan based on lora. In *2016 13th IEEE International Conference on Solid-State and Integrated Circuit Technology (ICSICT)*, pages 379–381. IEEE, 2016.

[54] Thomas Ameloot, Patrick Van Torre, and Hendrik Rogier. Lora indoor performance: an office environment case study. In *2018 International Applied Computational Electromagnetics Society Symposium-China (ACES)*, pages 1–2. IEEE, 2018.

[55] Vamsi Talla, Mehrdad Hessar, Bryce Kellogg, Ali Najafi, Joshua R Smith, and Shyamnath Gollakota. Lora backscatter: Enabling the vision of ubiquitous connectivity. *Proceedings of the ACM on interactive, mobile, wearable and ubiquitous technologies*, 1(3):1–24, 2017.

[56] Tahera Hossain, Yusuke Doi, Tahia Tazin, Md Atiqur Rahman Ahad, and Sozo Inoue. Study of lorawan technology for activity recognition. In *Proceedings of the 2018 ACM International Joint Conference and 2018 International Symposium on Pervasive and Ubiquitous Computing and Wearable Computers*, pages 1449–1453, 2018.

[57] Tahera Hossain, Md Atiqur Rahman Ahad, Tahia Tazin, and Sozo Inoue. Activity recognition by using lorawan sensor. In *Proceedings of the 2018 ACM International Joint Conference and 2018 International Symposium on Pervasive and Ubiquitous Computing and Wearable Computers*, pages 58–61, 2018.

[58] Bashima Islam, Md Tamzeed Islam, and Shahriar Nirjon. Feasibility of lora for indoor localization. *Appl. Sci*, 2017:8565550, 2017.

[59] Rajalakshmi Nandakumar, Vikram Iyer, and Shyamnath Gollakota. 3d localization for sub-centimeter sized devices. In *Proceedings of the 16th ACM Conference on Embedded Networked Sensor Systems*, pages 108–119, 2018.

[60] Mingmin Zhao, Shichao Yue, Dina Katabi, Tommi S Jaakkola, and Matt T Bianchi. Learning sleep stages from radio signals: A conditional adversarial architecture. In *International Conference on Machine Learning*, pages 4100–4109. PMLR, 2017.

[61] M Nowogrodzki, DD Mawhinney, and HF Milgazo. Non-invasive microwave instruments for the measurement of respiration and heart rates. *NAECON 1984*, pages 958–960, 1984.

[62] Zhicheng Yang, Parth H Pathak, Yunze Zeng, Xixi Liran, and Prasant Mohapatra. Monitoring vital signs using millimeter wave. In *Proceedings of the 17th ACM international symposium on mobile ad hoc networking and computing*, pages 211–220, 2016.

[63] Neal Patwari, Lara Brewer, Quinn Tate, Ossi Kaltiokallio, and Maurizio Bocca. Breathfinding: A wireless network that monitors and locates breathing in a home. *IEEE Journal of Selected Topics in Signal Processing*, 8(1):30–42, 2013.

[64] Kai Niu, Fusang Zhang, Zhaoxin Chang, and Daqing Zhang. A fresnel diffraction model based human respiration detection system using cots wi-fi devices. In *Proceedings of the*

2018 ACM International Joint Conference and 2018 International Symposium on Pervasive and Ubiquitous Computing and Wearable Computers, pages 416–419, 2018.

[65] Rajalakshmi Nandakumar, Bryce Kellogg, and Shyamnath Gollakota. Wi-fi gesture recognition on existing devices. *arXiv preprint arXiv:1411.5394*, 2014.

[66] Xiang Li, Shengjie Li, Daqing Zhang, Jie Xiong, Yasha Wang, and Hong Mei. Dynamic-music: accurate device-free indoor localization. In *Proceedings of the 2016 ACM international joint conference on pervasive and ubiquitous computing*, pages 196–207, 2016.

[67] Youwei Zeng, Dan Wu, Ruiyang Gao, Tao Gu, and Daqing Zhang. Fullbreathe: Full human respiration detection exploiting complementarity of csi phase and amplitude of wifi signals. *Proceedings of the ACM on Interactive, Mobile, Wearable and Ubiquitous Technologies*, 2(3):1–19, 2018.

[68] Xiang Li, Daqing Zhang, Qin Lv, Jie Xiong, Shengjie Li, Yue Zhang, and Hong Mei. Indotrack: Device-free indoor human tracking with commodity wi-fi. *Proceedings of the ACM on Interactive, Mobile, Wearable and Ubiquitous Technologies*, 1(3):1–22, 2017.

[69] Jochen Meyer, Daniel Epstein, Parisa Eslambolchilar, Judy Kay, and Lie Ming Tang. A short workshop on next steps towards long term self tracking. In *Extended Abstracts of the 2018 CHI Conference on Human Factors in Computing Systems*, pages 1–8, 2018.

[70] Chengyou Li and Tao Hua. Human action recognition based on template matching. *Procedia Engineering*, 15:2824–2830, 2011.

[71] Seon-Woo Lee and Kenji Mase. Activity and location recognition using wearable sensors. *IEEE pervasive computing*, 1(3):24–32, 2002.

[72] Liming Chen, Chris D Nugent, and Hui Wang. A knowledge-driven approach to activity recognition in smart homes. *IEEE Transactions on Knowledge and Data Engineering*, 24(6):961–974, 2011.

[73] Xinpeng Zhang, Takekazu Kato, and Takashi Matsuyama. Learning a context-aware personal model of appliance usage patterns in smart home. In *2014 IEEE Innovative Smart Grid Technologies-Asia (ISGT ASIA)*, pages 73–78. IEEE, 2014.

[74] Kotaro Ishizu, Teruhiro Mizumoto, Hirozumi Yamaguchi, and Teruo Higashino. Home activity pattern estimation using aggregated electricity consumption data. *Sens. Mater*, 33:69–88, 2021.

[75] Lina Stankovic, Vladimir Stankovic, Jing Liao, and Clevo Wilson. Measuring the energy intensity of domestic activities from smart meter data. *Applied Energy*, 183:1565–1580, 2016.

[76] George William Hart. Nonintrusive appliance load monitoring. *Proceedings of the IEEE*, 80(12):1870–1891, 1992.

[77] Seunghyun Choi, Changgyun Kim, Yong-Shin Kang, and Sekyoung Youm. Human behavioral pattern analysis-based anomaly detection system in residential space. *The Journal of Supercomputing*, 77(8):9248–9265, 2021.

[78] Nicola Camp, Martin Lewis, Kirsty Hunter, Julie Johnston, Massimiliano Zecca, Alessandro Di Nuovo, and Daniele Magistro. Technology used to recognize activities of daily living in community-dwelling older adults. *International Journal of Environmental Research and Public Health*, 18(1):163, 2021.

[79] Aitor Almeida, Rubén Mulero, Piercosimo Rametta, Vladimir Urošević, Marina Andrić, and Luigi Patrono. A critical analysis of an iot—aware aal system for elderly monitoring. *Future Generation Computer Systems*, 97:598–619, 2019.

[80] Jin Zhang, Zhuangzhuang Chen, Chengwen Luo, Bo Wei, Salil S Kanhere, and Jianqiang Li. Metaganfi: Cross-domain unseen individual identification using wifi signals. *Proceedings of the ACM on Interactive, Mobile, Wearable and Ubiquitous Technologies*, 6(3):1–21, 2022.

[81] Leixin Shi, Hongji Xu, Wei Ji, Beibei Zhang, Xiaojie Sun, and Juan Li. Real-time human activity recognition system based on capsule and lora. *IEEE Sensors Journal*, 21(1):667–677, 2020.

[82] Xuanke He, Jiang Zhu, Wenjing Su, and Manos M Tentzeris. Rfid based non-contact human activity detection exploiting cross polarization. *IEEE Access*, 8:46585–46595, 2020.

[83] Chengxi Yu, Zhezhuang Xu, Kun Yan, Ying-Ren Chien, Shih-Hau Fang, and Hsiao-Chun Wu. Noninvasive human activity recognition using millimeter-wave radar. *IEEE Systems Journal*, 16(2):3036–3047, 2022.

[84] Ashish Mishra and Changzhi Li. A low power 5.8-ghz ism-band intermodulation radar system for target motion discrimination. *IEEE Sensors Journal*, 19(20):9206–9214, 2019.

[85] Muhammad Farooq, Adnan Qayyum, Yao Ge, Muhammad Zakir Khan, Ahmad Taha, Muhammad Ali Imran, Qammer H Abbasi, and Hasan Tahir Abbas. Lora-based privacy-aware and contactless surveillance in next-generation smart homes. In *2023 IEEE International Symposium on Antennas and Propagation and USNC-URSI Radio Science Meeting (USNC-URSI)*, pages 1751–1752. IEEE, 2023.

[86] Marcus Faundez-Zanuy, S McLaughlin, Arianna Esposito, Amir Hussain, Jean Schoentgen, Gernot Kubin, W Bastiaan Kleijn, and Petros Maragos. Nonlinear speech processing: overview and applications. *Control and intelligent systems*, 30(1):1–10, 2002.

[87] Sadaoki Furui. An overview of speaker recognition technology. *Automatic Speech and Speaker Recognition: Advanced Topics*, pages 31–56, 1996.

[88] Muaz Niazi and Amir Hussain. Agent-based computing from multi-agent systems to agent-based models: a visual survey. *Scientometrics*, 89(2):479–499, 2011.

[89] Hira Hameed, Muhammad Usman, Ahsen Tahir, Amir Hussain, Hasan Abbas, Tie Jun Cui, Muhammad Ali Imran, and Qammer H Abbasi. Pushing the limits of remote rf sensing by reading lips under the face mask. *Nature Communications*, 13(1):5168, 2022.

[90] Leandro A Passos, João Paulo Papa, Javier Del Ser, Amir Hussain, and Ahsan Adeel. Multimodal audio-visual information fusion using canonical-correlated graph neural network for energy-efficient speech enhancement. *Information Fusion*, 90:1–11, 2023.

[91] Soujanya Poria, Erik Cambria, Rajiv Bajpai, and Amir Hussain. A review of affective computing: From unimodal analysis to multimodal fusion. *Information fusion*, 37:98–125, 2017.

[92] Kia Dashtipour, Soujanya Poria, Amir Hussain, Erik Cambria, Ahmad YA Hawalah, Alexander Gelbukh, and Qiang Zhou. Multilingual sentiment analysis: state of the art and independent comparison of techniques. *Cognitive computation*, 8:757–771, 2016.

[93] Soujanya Poria, Erik Cambria, Newton Howard, Guang-Bin Huang, and Amir Hussain. Fusing audio, visual and textual clues for sentiment analysis from multimodal content. *Neurocomputing*, 174:50–59, 2016.

[94] Hendrik Laux, Ahmed Hallawa, Julio Cesar Sevarolli Assis, Anke Schmeink, Lukas Martin, and Arne Peine. Two-stage visual speech recognition for intensive care patients. *Scientific Reports*, 13(1):928, 2023.

[95] Dmitry Ryumin, Denis Ivanko, and Elena Ryumina. Audio-visual speech and gesture recognition by sensors of mobile devices. *Sensors*, 23(4):2284, 2023.

[96] Homayoon Beigi and Homayoon Beigi. *Speaker recognition*. Springer, 2011.

[97] Douglas A Reynolds. An overview of automatic speaker recognition technology. In *2002 IEEE international conference on acoustics, speech, and signal processing*, volume 4, pages IV–4072. IEEE, 2002.

[98] David Ferreira, Samuel Silva, Francisco Curado, and António Teixeira. Exploring silent speech interfaces based on frequency-modulated continuous-wave radar. *Sensors*, 22(2):649, 2022.

[99] Pouriya Amini Digehsara, Joao Vıtor Possamai de Menezes, Christoph Wagner, Michael Bärhold, Petr Schaffer, Dirk Plettemeier, and Peter Birkholz. A user-friendly headset for radar-based silent speech recognition. *Proc. Interspeech 2022*, pages 4835–4839, 2022.

[100] Christoph Wagner, Petr Schaffer, Pouriya Amini Digehsara, Michael Bärhold, Dirk Plettemeier, and Peter Birkholz. Silent speech command word recognition using stepped frequency continuous wave radar. *Scientific Reports*, 12(1):4192, 2022.

[101] Young Hoon Shin and Jiwon Seo. Towards contactless silent speech recognition based on detection of active and visible articulators using ir-uwb radar. *Sensors*, 16(11):1812, 2016.

[102] Chao Feng, Jie Xiong, Liqiong Chang, Fuwei Wang, Ju Wang, and Dingyi Fang. Rf-identity: Non-intrusive person identification based on commodity rfid devices. *Proceedings of the ACM on Interactive, Mobile, Wearable and Ubiquitous Technologies*, 5(1):1–23, 2021.

[103] Peter Birkholz, Simon Stone, Klaus Wolf, and Dirk Plettemeier. Non-invasive silent phoneme recognition using microwave signals. *IEEE/ACM Transactions on Audio, Speech, and Language Processing*, 26(12):2404–2411, 2018.

[104] James D Taylor. *Introduction to ultra-wideband radar systems*. CRC press, 2020.

[105] Chia-Hung Chang and Wei-Hsien Chen. Vital-sign processing receiver with clutter elimination using servo feedback loop for uwb pulse radar system. *IEEE Transactions on Very Large Scale Integration (VLSI) Systems*, 28(1):292–296, 2019.

[106] Yazhou Wang, Quanhua Liu, and Aly E Fathy. Cw and pulse–doppler radar processing based on fpga for human sensing applications. *IEEE Transactions on Geoscience and Remote Sensing*, 51(5):3097–3107, 2012.

[107] Edward L Campbell, Judith Dineley, Pauline Conde, Faith Matcham, Femke Lamers, Sara Siddi, Laura Docio-Fernandez, Carmen Garcia-Mateo, Nicholas Cummins, et al. Detecting the severity of major depressive disorder from speech: A novel hard-training methodology. *arXiv preprint arXiv:2206.01542*, 2022.

[108] JF Holzrichter, GC Burnett, LC Ng, and WA Lea. Speech articulator measurements using low power em-wave sensors. *The Journal of the Acoustical Society of America*, 103(1):622–625, 1998.

[109] Anjie Zhu, Xiaokang Qi, Tenglong Fan, Zhitao Gu, Qinyi Lv, Dexin Ye, Jiangtao Huangfu, Yongzhi Sun, Weiqiang Zhu, and Lixin Ran. Indoor localization for passive moving objects based on a redundant simo radar sensor. *IEEE Journal on Emerging and Selected Topics in Circuits and Systems*, 8(2):271–279, 2018.

[110] Saad Iqbal, Usman Iqbal, Syed Ali Hassan, and Sajid Saleem. Indoor motion classification using passive rf sensing incorporating deep learning. In *2018 IEEE 87th Vehicular Technology Conference (VTC Spring)*, pages 1–5. IEEE, 2018.

[111] Md Nafiul Alam Nipu, Souvik Talukder, Md Saiful Islam, and Amitabha Chakrabarty. Human identification using wifi signal. In *2018 Joint 7th International Conference on Informatics, Electronics & Vision (ICIEV) and 2018 2nd International Conference on Imaging, Vision & Pattern Recognition (icIVPR)*, pages 300–304. IEEE, 2018.

[112] Christine Dewi and Rung-Ching Chen. Human activity recognition based on evolution of features selection and random forest. In *2019 IEEE international conference on systems, man and cybernetics (SMC)*, pages 2496–2501. IEEE, 2019.

[113] Yongsen Ma, Gang Zhou, and Shuangquan Wang. Wifi sensing with channel state information: A survey. *ACM Computing Surveys (CSUR)*, 52(3):1–36, 2019.

[114] Wei Wang, Alex X Liu, Muhammad Shahzad, Kang Ling, and Sanglu Lu. Device-free human activity recognition using commercial wifi devices. *IEEE Journal on Selected Areas in Communications*, 35(5):1118–1131, 2017.

[115] Jianyang Ding and Yong Wang. Wifi csi-based human activity recognition using deep recurrent neural network. *IEEE Access*, 7:174257–174269, 2019.

[116] Lei Zhang, Cong Wang, Maode Ma, and Daqing Zhang. Widigr: Direction-independent gait recognition system using commercial wi-fi devices. *IEEE Internet of Things Journal*, 7(2):1178–1191, 2020.

[117] Dazhuo Wang, Jianfei Yang, Wei Cui, Lihua Xie, and Sumei Sun. Caution: A robust wifi-based human authentication system via few-shot open-set recognition. *IEEE Internet of Things Journal*, 9(18):17323–17333, 2022.

[118] Zhenyuan Zhang, Zengshan Tian, and Mu Zhou. Latern: Dynamic continuous hand gesture recognition using fmcw radar sensor. *IEEE Sensors Journal*, 18(8):3278–3289, 2018.

[119] Haobo Li, Julien Le Kernec, Ajay Mehul, Sevgi Zubeyde Gurbuz, and Francesco Fioranelli. Distributed radar information fusion for gait recognition and fall detection. In *2020 IEEE Radar Conference (RadarConf20)*, pages 1–6. IEEE, 2020.

[120] Asangi Jayatilaka and Damith C Ranasinghe. Real-time fluid intake gesture recognition based on batteryless uhf rfid technology. *Pervasive and Mobile Computing*, 34:146–156, 2017.

[121] Lily Lee and W Eric L Grimson. Gait analysis for recognition and classification. In *Proceedings of Fifth IEEE International Conference on Automatic Face Gesture Recognition*, pages 155–162. IEEE, 2002.

[122] Changsheng Wan, Li Wang, and Vir V Phoha. A survey on gait recognition. *ACM Computing Surveys (CSUR)*, 51(5):1–35, 2018.

[123] Chuanwei Ding, Li Zhang, Chen Gu, Lei Bai, Zhicheng Liao, Hong Hong, Yusheng Li, and Xiaohua Zhu. Non-contact human motion recognition based on uwb radar. *IEEE Journal on Emerging and Selected Topics in Circuits and Systems*, 8(2):306–315, 2018.

[124] Binbin Xie, Yuqing Yin, and Jie Xiong. Pushing the limits of long range wireless sensing with lora. *Proceedings of the ACM on Interactive, Mobile, Wearable and Ubiquitous Technologies*, 5(3):1–21, 2021.

[125] Binbin Xie and Jie Xiong. Combating interference for long range lora sensing. In *Proceedings of the 18th Conference on Embedded Networked Sensor Systems*, pages 69–81, 2020.

[126] Fusang Zhang, Zhaoxin Chang, Jie Xiong, and Daqing Zhang. Exploring lora for sensing. *GetMobile: Mobile Computing and Communications*, 25(2):33–37, 2021.

[127] Fusang Zhang, Zhaoxin Chang, Jie Xiong, Rong Zheng, Junqi Ma, Kai Niu, Beihong Jin, and Daqing Zhang. Unlocking the beamforming potential of lora for long-range multi-target respiration sensing. *Proceedings of the ACM on Interactive, Mobile, Wearable and Ubiquitous Technologies*, 5(2):1–25, 2021.

[128] Youwei Zeng, Dan Wu, Ruiyang Gao, Tao Gu, and Daqing Zhang. Fullbreathe: Full human respiration detection exploiting complementarity of csi phase and amplitude of wifi signals. *Proc. ACM Interact. Mob. Wearable Ubiquitous Technol.*, 2(3), sep 2018.

[129] Kun Qian, Chenshu Wu, Yi Zhang, Guidong Zhang, Zheng Yang, and Yunhao Liu. Widar2. 0: Passive human tracking with a single wi-fi link. In *Proceedings of the 16th Annual International Conference on Mobile Systems, Applications, and Services*, pages 350–361, 2018.

[130] Amaia Abanda, Usue Mori, and Jose A Lozano. A review on distance based time series classification. *Data Mining and Knowledge Discovery*, 33(2):378–412, 2019.

[131] Joachim Tapparel, Orion Afisiadis, Paul Mayoraz, Alexios Balatsoukas-Stimming, and Andreas Burg. An open-source lora physical layer prototype on gnu radio. In *2020 IEEE 21st International Workshop on Signal Processing Advances in Wireless Communications (SPAWC)*, pages 1–5. IEEE, 2020.

[132] L Minh Dang, Kyungbok Min, Hanxiang Wang, Md Jalil Piran, Cheol Hee Lee, and Hyeonjoon Moon. Sensor-based and vision-based human activity recognition: A comprehensive survey. *Pattern Recognition*, 108:107561, 2020.

[133] Deepika Singh, Ismini Psychoula, Johannes Kropf, Sten Hanke, and Andreas Holzinger. Users' perceptions and attitudes towards smart home technologies. In *Smart Homes and Health Telematics, Designing a Better Future: Urban Assisted Living: 16th International Conference, ICOST 2018, Singapore, Singapore, July 10-12, 2018, Proceedings 16*, pages 203–214. Springer, 2018.

[134] Zawar Hussain, Michael Sheng, and Wei Emma Zhang. Different approaches for human activity recognition: A survey. *arXiv preprint arXiv:1906.05074*, 2019.

[135] Damien Bouchabou, Sao Mai Nguyen, Christophe Lohr, Benoit LeDuc, and Ioannis Kanellos. A survey of human activity recognition in smart homes based on iot sensors algorithms: Taxonomies, challenges, and opportunities with deep learning. *Sensors*, 21(18):6037, 2021.

[136] Muhammad Farooq, Mahmoud A Shawky, Aisha Fatima, Ahsen Tahir, Muhammad Z Khan, Hasan T Abbas, Muhammad Imran, Qammer H Abbasi, and Ahmad Taha. Room-level activity classification from contextual electricity usage data in a residential home. In *2023 International Telecommunications Conference (ITC-Egypt)*, pages 96–100. IEEE, 2023.

[137] Jiangang Hao and Tin Kam Ho. Machine learning made easy: a review of scikit-learn package in python programming language. *Journal of Educational and Behavioral Statistics*, 44(3):348–361, 2019.

[138] Shuyu Shi, Stephan Sigg, Lin Chen, and Yusheng Ji. Accurate location tracking from csi-based passive device-free probabilistic fingerprinting. *IEEE Transactions on Vehicular Technology*, 67(6):5217–5230, 2018.

[139] Julita Gmitrzuk, Maciej Karasiński, Zuzanna Malinka, Katarzyna Wiśniewska, Anna Jachymek, Martyna Opatowska, Joanna Jakubiec, and Tomasz Kucharski. Effects of sleep and insomnia on cardiovascular disease-literature review. *Quality in Sport*, 17:53050–53050, 2024.

[140] Marieclaire Overton, Johan Skoog, Erika J Laukka, Timothy Hadarsson Bodin, Alexander Darin Mattsson, Linnea Sjöberg, Scott M Hofer, Lena Johansson, Jenni Kulmala, Miia Kivipelto, et al. Sleep disturbances and change in multiple cognitive domains among older adults: a multicenter study of five nordic cohorts. *Sleep*, 47(3):zsad244, 2024.

[141] Carlijn J de Gans, P Burger, ES Van den Ende, J Hermanides, PWB Nanayakkara, RJBJ Gemke, F Rutters, and DJ Stenvers. Sleep assessment using eeg-based wearables–a systematic review. *Sleep Medicine Reviews*, page 101951, 2024.

[142] Vera Birrer, Mohamed Elgendi, Olivier Lambercy, and Carlo Menon. Evaluating reliability in wearable devices for sleep staging. *npj Digital Medicine*, 7(1):74, 2024.

[143] Xiulong Liu, Wei Jiang, Sheng Chen, Xin Xie, Hankai Liu, Qixuan Cai, Xinyu Tong, Tuo Shi, and Wenyu Qu. Posmonitor: Fine-grained sleep posture recognition with mmwave radar. *IEEE Internet of Things Journal*, 2023.

[144] Muhammad Farooq, Hira Hameed, Prisila Ishabakaki, Syed Aziz Shah, Ahmad Taha, Muhammad Imran, Qammer H Abbasi, and Hassan Tahir Abbas. Breathing rate variability impact on heart rate estimation through radar sensing. In *2024 IEEE International Symposium on Antennas and Propagation and INC/USNC-URSI Radio Science Meeting (AP-S/INC-USNC-URSI)*, pages 2799–2800. IEEE, 2024.

[145] Muhammad Farooq, Yao Ge, Adnan Qayyum, Chong Tang, Amir Hussain, Muhammad Ali Imran, Ahmad Taha, Qammer H Abbasi, and Hasan Tahir Abbas. Privacy-preserving speaker recognition using radars for context estimation in future multi-modal hearing assistive technologies. In *2023 IEEE International Radar Conference (RADAR)*, pages 1–5. IEEE, 2023.

[146] Syed Doha Uddin, Md Shafkat Hossain, Shekh MM Islam, and Victor Lubecke. Heart rate variability-based obstructive sleep apnea events classification using microwave doppler radar. *IEEE Journal of Electromagnetics, RF and Microwaves in Medicine and Biology*, 7(4):416–424, 2023.

[147] Muhammad Farooq, Hira Hameed, Ahmad Taha, Muhammad Imran, Qammer H Abbasi, and Hassan Tahir Abbas. Contactless respiration variability detection and accuracy test using uwb radar. In *2024 18th European Conference on Antennas and Propagation (EuCAP)*, pages 1–4. IEEE, 2024.

[148] Sha Huan, Limei Wu, Man Zhang, Zhaoyue Wang, and Chao Yang. Radar human activity recognition with an attention-based deep learning network. *Sensors*, 23(6):3185, 2023.

[149] Yao Ge, Chong Tang, Haobo Li, Zikang Zhang, Wenda Li, Kevin Chetty, Daniele Faccio, Qammer H. Abbasi, and Muhammad Imran. A large-scale multimodal dataset of human speech recognition, 2023.

[150] Ameen Bin Obadi, Ping Jack Soh, Omar Aldayel, Muataz Hameed Al-Doori, Marco Mercuri, and Dominique Schreurs. A survey on vital signs detection using radar techniques and processing with fpga implementation. *IEEE Circuits and Systems Magazine*, 21(1):41–74, 2021.

[151] Anuradha Singh, Saeed Ur Rehman, Sira Yongchareon, and Peter Han Joo Chong. Multi-resident non-contact vital sign monitoring using radar: A review. *IEEE Sensors Journal*, 21(4):4061–4084, 2020.

[152] Mamady Kebe, Rida Gadhafi, Baker Mohammad, Mihai Sanduleanu, Hani Saleh, and Mahmoud Al-Qutayri. Human vital signs detection methods and potential using radars: A review. *Sensors*, 20(5):1454, 2020.

[153] Miguel Hernandez-Aguila, Jose-Luis Olvera-Cervantes, Aldo-Eleazar Perez-Ramos, and Alonso Corona-Chavez. Methodology for the determination of human respiration rate by using doppler radar and empirical modal decomposition. *Scientific Reports*, 12(1):8675, 2022.

[154] Diyah Widiyasari, Nur Ahmadi, Trio Adiono, Ayu Purwarianti, Ariana Tulus Purnomo, and Ding-Bing Lin. Contactless respiratory rate monitoring using fmcw radar. In *2022 International Symposium on Electronics and Smart Devices (ISESD)*, pages 1–6. IEEE, 2022.

[155] Hafeez Ur Rehman Siddiqui, Adil Ali Saleem, Imran Bashir, Kainat Zafar, Furqan Rustam, Isabel de la Torre Diez, Sandra Dudley, and Imran Ashraf. Respiration-based copd detection using uwb radar incorporation with machine learning. *Electronics*, 11(18):2875, 2022.

[156] Rencheng Song, Cong Ren, Juan Cheng, Chang Li, and Xuezhi Yang. Non-contact human respiratory rate measurement based on two-level fusions of video and fmcw radar information. *Measurement*, page 113604, 2023.

[157] Weiqiao Han, Shaozhang Dai, and Mehmet Rasit Yuce. Real-time contactless respiration monitoring from a radar sensor using image processing method. *IEEE Sensors Journal*, 22(19):19020–19029, 2022.

[158] Malikeh P Ebrahim, Neil Tom, Jean-Michel Redoute, and Mehmet R Yuce. A low-frequency portable continuous wave radar system for vital signs monitoring. *IEEE Sensors Journal*, 2023.

[159] Yong Wang, Wen Wang, Mu Zhou, Aihu Ren, and Zengshan Tian. Remote monitoring of human vital signs based on 77-ghz mm-wave fmcw radar. *Sensors*, 20(10):2999, 2020.

[160] Mostafa Alizadeh, George Shaker, João Carlos Martins De Almeida, Plinio Pelegrini Morita, and Safeddin Safavi-Naeini. Remote monitoring of human vital signs using mm-wave fmcw radar. *IEEE Access*, 7:54958–54968, 2019.

[161] Jian Liu, Hongbo Liu, Yingying Chen, Yan Wang, and Chen Wang. Wireless sensing for human activity: A survey. *IEEE Communications Surveys & Tutorials*, 22(3):1629–1645, 2019.

[162] Changzhi Li, Julie Cummings, Jeffrey Lam, Eric Graves, and Wenhsing Wu. Radar remote monitoring of vital signs. *IEEE Microwave magazine*, 10(1):47–56, 2009.

[163] Siying Wang, Antje Pohl, Timo Jaeschke, Michael Czaplik, Marcus Köny, Steffen Leonhardt, and Nils Pohl. A novel ultra-wideband 80 ghz fmcw radar system for contactless monitoring of vital signs. In *2015 37th Annual International Conference of the IEEE Engineering in Medicine and Biology Society (EMBC)*, pages 4978–4981, 2015.

[164] Christian A Schroth, Christian Eckrich, Ibrahim Kakouche, Stefan Fabian, Oskar von Stryk, Abdelhak M Zoubir, and Michael Muma. Emergency response person localization and vital sign estimation using a semi-autonomous robot mounted sfcw radar. *IEEE Transactions on Biomedical Engineering*, 2024.

[165] Magdalena Liebetruth, Kai Kehe, Dirk Steinritz, and Stefan Sammito. Systematic literature review regarding heart rate and respiratory rate measurement by means of radar technology. *Sensors*, 24(3):1003, 2024.

[166] PJ Arnott, GW Pfeiffer, and ME Tavel. Spectral analysis of heart sounds: relationships between some physical characteristics and frequency spectra of first and second heart sounds in normals and hypertensives. *Journal of biomedical engineering*, 6(2):121–128, 1984.

[167] Grzegorz Redlarski, Dawid Gradolewski, and Aleksander Palkowski. A system for heart sounds classification. *PloS one*, 9(11):e112673, 2014.

[168] Mimma Nardelli, Gaetano Valenza, Alberto Greco, Antonio Lanata, and Enzo Pasquale Scilingo. Recognizing emotions induced by affective sounds through heart rate variability. *IEEE Transactions on Affective Computing*, 6(4):385–394, 2015.

[169] Amit Krishna Dwivedi, Syed Anas Imtiaz, and Esther Rodriguez-Villegas. Algorithms for automatic analysis and classification of heart sounds–a systematic review. *IEEE Access*, 7:8316–8345, 2018.

[170] Omid Ettehadi, Lee Jones, and Kate Hartman. Heart waves: A heart rate feedback system using water sounds. In *Proceedings of the fourteenth international conference on tangible, embedded, and embodied interaction*, pages 527–532, 2020.

[171] Zhi Li, Tian Jin, Yongpeng Dai, and Yongping Song. Motion-robust contactless heartbeat sensing using 4d imaging radar. *IEEE Transactions on Instrumentation and Measurement*, 2023.

[172] Shahzad Ahmed and Sung Ho Cho. Machine learning for healthcare radars: Recent progresses in human vital sign measurement and activity recognition. *IEEE Communications Surveys & Tutorials*, 2023.

[173] Yu Rong, Isabella Lenz, and Daniel W Bliss. Non-contact cardiac parameters estimation using radar acoustics for healthcare iot. *IEEE Internet of Things Journal*, 2023.

[174] Zekun Chen, Yunxue Liu, Chenhong Sui, Min Zhou, and Yuqing Song. A novel scheme for suppression of human motion effects in non-contact heart rate detection. *IEEE Access*, 2023.

[175] Yingxiao Wu, Haocheng Ni, Changlin Mao, Jianping Han, and Wenyao Xu. Non-intrusive human vital sign detection using mmwave sensing technologies: A review. *ACM Transactions on Sensor Networks*, 20(1):1–36, 2023.

[176] Yonathan Eder and Yonina C Eldar. Sparsity-based multi-person non-contact vital signs monitoring via fmcw radar. *IEEE journal of biomedical and health informatics*, 2023.

[177] Yao Ge, Wenda Li, Muhammad Farooq, Adnan Qayyum, Jingyan Wang, Zikang Chen, Jonathan Cooper, Muhammad Ali Imran, and Qammer H Abbasi. Logait: Lora sensing system of human gait recognition using dynamic time wraping. *IEEE Sensors Journal*, 2023.

[178] Moushumi Tazen, Naoto Sasaoka, and Yoshiharu Okamoto. Non-contact heart rate measurement based on adaptive notch filter and elimination of respiration harmonics. *IEEE Access*, 2023.

[179] Min Zhou, Yunxue Liu, Shie Wu, Chengyou Wang, Zekun Chen, and Hongfei Li. A novel scheme of high-precision heart rate detection with a mm-wave fmcw radar. *IEEE Access*, 2023.

[180] Jiachen Li, Shisheng Guo, Guolong Cui, Xuefeng Zhou, Luyuan Shi, Lingjiang Kong, and Xiaobo Yang. Multidomain separation for human vital signs detection with fmcw radar in interference environment. *IEEE Transactions on Microwave Theory and Techniques*, 2023.

[181] Panagiota Kontou, Souheil Ben Smida, and Dimitris E Anagnostou. Contactless respiration monitoring using wi-fi and artificial neural network detection method. *IEEE Journal of Biomedical and Health Informatics*, 2023.

[182] Christoph Will, Kilin Shi, Sven Schellenberger, Tobias Steigleder, Fabian Michler, Jonas Fuchs, Robert Weigel, Christoph Ostgathe, and Alexander Koelpin. Radar-based heart sound detection. *Scientific reports*, 8(1):11551, 2018.

[183] Yingxiao Wu, Haocheng Ni, Changlin Mao, and Jianping Han. Contactless reconstruction of ECG and respiration signals with mmwave radar based on rssrnet. *IEEE Sensors Journal*, 2023.

[184] Andrei Boiko, Natividad Martínez Madrid, and Ralf Seepold. Contactless technologies, sensors, and systems for cardiac and respiratory measurement during sleep: A systematic review. *Sensors*, 23(11):5038, 2023.

[185] Luyao Liu, Jie Zhang, Ying Qu, Sen Zhang, and Wendong Xiao. mmrh: Noncontact vital sign detection with an fmcw mm-wave radar. *IEEE Sensors Journal*, 23(8):8856–8866, 2023.

[186] Mélanie Brulc, Thibaut Deleruyelle, Alain Loussert, Pierre Laurent, Rémi Grisot, and Jean-Paul Caruana. Cardiac signature detection and study using contactless technology: Millimeter wave fmcw radar. *IEEE Open Journal of Instrumentation and Measurement*, 2023.

[187] Tianze Pan, Yuanyue Guo, Weiwei Guo, and Chengcheng Kang. Detection of vital sign based on uwb radar by a time domain coherent accumulation method. *IEEE Sensors Journal*, 2023.

[188] Kawish Pervez, Waqas Aman, M Mahboob Ur Rahman, M Wasim Nawaz, and Qammer H Abbasi. Hand-breathe: Non-contact monitoring of breathing abnormalities from hand palm. *IEEE Sensors Journal*, 2023.

[189] Yingqi Wang, Zhongqin Wang, J Andrew Zhang, Haimin Zhang, and Min Xu. Vital sign monitoring in dynamic environment via mmwave radar and camera fusion. *IEEE Transactions on Mobile Computing*, 2023.

[190] Min Hur, Kawon Han, and Songcheol Hong. Multiple human heart rate variability detection using mimo fmcw radar with differential beam techniques. *IEEE Transactions on Radar Systems*, 1:698–706, 2023.

[191] Baoxian Yu, Yue Hou, Zhiqiang Pang, and Han Zhang. Contactless sensing-aided respiration signal acquisition using improved empirical wavelet transform for rhythm detection. *IEEE Journal of Biomedical and Health Informatics*, 2023.

[192] Sri Venkata Surya Teja Jonnalagadda, Durga Prasad Mishra, and Santanu Kumar Behera. Chipless rf identification sensors for vital signs monitoring: A comprehensive review. *IEEE Microwave Magazine*, 24(11):53–70, 2023.

[193] Pei Wang, Xujun Ma, Rong Zheng, Luan Chen, Xiaolin Zhang, Djamal Zeghlache, and Daqing Zhang. Slprof: Improving the temporal coverage and robustness of rf-based vital sign monitoring during sleep. *IEEE Transactions on Mobile Computing*, 2023.

[194] Li Wen, Shuqin Dong, Yi Wang, Changzhan Gu, Zheng Tang, Zhiwei Liu, Yanfeng Wang, and Junfa Mao. Noncontact infant apnea detection for hypoxia prevention with a k-band biomedical radar. *IEEE Transactions on Biomedical Engineering*, 2023.

[195] Bin Huang, Shen Hu, Zimeng Liu, Chun-Liang Lin, Junfeng Su, Changchen Zhao, Li Wang, and Wenjin Wang. Challenges and prospects of visual contactless physiological monitoring in clinical study. *NPJ Digital Medicine*, 6(1):231, 2023.

[196] Sourav Kumar Pramanik and Shekh Md Mahmudul Islam. Through the wall human heart beat detection using single channel cw radar. *Frontiers in Physiology*, 15:1344221, 2024.

[197] Serene Abu-Sardanah, Ali Gharamohammadi, Omar M Ramahi, and George Shaker. A wearable mm-wave radar platform for cardiorespiratory monitoring. *IEEE Sensors Letters*, 2023.

[198] Sunny WS Wan and Hung T Nguyen. 50 hz interference and noise in ecg recordings—a review. *Aust. Phys. Eng. Sci. Med*, 17:108, 1994.

[199] Danilo Ricciardi, Ilaria Cavallari, Antonio Creta, Giacomo Di Giovanni, Vito Calabrese, Natale Di Belardino, Simona Mega, Iginio Colaiori, Laura Ragni, Claudio Proscia, et al. Impact of the high-frequency cutoff of bandpass filtering on ecg quality and clinical interpretation: A comparison between 40áhz and 150áhz cutoff in a surgical preoperative adult outpatient population. *Journal of electrocardiology*, 49(5):691–695, 2016.

[200] Stefan Niewiadomski. *Filter handbook: a practical design guide*. Newnes, 2013.

[201] Howard Austerlitz. *Data acquisition techniques using PCs*. Academic press, 2002.

[202] Silvia Raquel Soares Ouakinin. Anxiety as a risk factor for cardiovascular diseases. *Frontiers in psychiatry*, 7:25, 2016.

[203] John A Chalmers, Daniel S Quintana, Maree J-Anne Abbott, and Andrew H Kemp. Anxiety disorders are associated with reduced heart rate variability: a meta-analysis. *Frontiers in psychiatry*, 5:80, 2014.

[204] M. Maenner. Prevalence and characteristics of autism spectrum disorder among children aged 8 years — autism and developmental disabilities monitoring network, 11 sites, united states, 2018. *Morbidity and Mortality Weekly Report Surveillance Summaries*, 70:1–16, 2021.

[205] S. Baron-Cohen. Autism: the empathizing–systemizing (e-s) theory, 11 sites, united states, 2018. *Annals of the New York Academy of Sciences*, 1156:68–80, 2009.

[206] O. Veatch, A. Maxwell-Horn, and B. Malow. Sleep in autism spectrum disorders. *Current Sleep Medicine Reports*, 1:131–140, 2015.

[207] J. Mindell and L. Meltzer. Behavioural sleep disorders in children and adolescents. *Annals Academy of Medicine Singapore*, 37:722–728, 2008.

[208] C. Alfano and A. Gamble. The role of sleep in childhood psychiatric disorders. *Child & Youth Care Forum*, 38:327–340, 2009.

[209] Amparo Díaz-Román, Junhua Zhang, Richard Delorme, Anita Beggiato, and Samuele Cortese. Sleep in youth with autism spectrum disorders: systematic review and meta-analysis of subjective and objective studies. *BMJ Ment Health*, 21(4):146–154, 2018.

[210] E. Hoşoğlu, Ö. Akça, A. Bilgiç, and M. Tuzcu. Evaluation of sleep problems and related factors in children newly diagnosed with autism spectrum disorder. *International Journal Of Developmental Disabilities*, pages 1–15, 2024.

[211] R. Budagzad-Jacobson, R. Musicaro, C. Marin, W. Silverman, and E. Lebowitz. Family accommodation in anxious irritable and anxious non-irritable youth. *Behavior Therapy*, 2024.

[212] H. Allik, J. Larsson, and H. Smedje. Sleep patterns in school-age children with asperger syndrome or high-functioning autism: a follow-up study. *Journal Of Autism And Developmental Disorders*, 38:1625–1633, 2008.

[213] T. Anders, A. Iosif, A. Schwichtenberg, K. Tang, and B. Goodlin-Jones. Six-month sleep–wake organization and stability in preschool-age children with autism, developmental delay, and typical development. *Behavioral Sleep Medicine*, 9:92–106, 2011.

[214] R. Dahl and D. Lewin. Pathways to adolescent health sleep regulation and behavior. *Journal Of Adolescent Health*, 31:175–184, 2002.

[215] E. Luby, C. Frohman, J. Grisell, J. Lenzo, and J. Gottlieb. Sleep deprivation: effects on behavior, thinking, motor performance, and biological energy transfer systems. *Psychosomatic Medicine*, 22:182–192, 1960.

[216] L. Graves, A. Pack, and T. Abel. Sleep and memory: a molecular perspective. *Trends In Neurosciences*, 24:237–243, 2001.

[217] A. Sadeh. Consequences of sleep loss or sleep disruption in children. *Sleep Medicine Clinics*, 2:513–520, 2007.

[218] A. Richdale and M. Prior. The sleep/wake rhythm in children with autism. *European Child & Adolescent Psychiatry*, 4:175–186, 1995.

[219] A. Lambert, S. Tessier, A. Rochette, P. Scherzer, L. Mottron, and R. Godbout. Poor sleep affects daytime functioning in typically developing and autistic children not complaining of sleep problems: A questionnaire-based and polysomnographic study. *Research In Autism Spectrum Disorders*, 23:94–106, 2016.

[220] M. Taylor, M. Zawadzki, R. Mirza, and J. Murphy. A neural network model for predicting sleep stages using a combination of polysomnographic and actigraphic data. *IEEE Transactions On Neural Networks And Learning Systems*, 23:1422–1432, 2012.

[221] M. Plou, J. Fernández, E. Luque, S. González, A. Hervás, and A. Danet. Two innovative hybrid indexes for quantifying the spatiotemporal association between pm10 and no2 in children with autism spectrum disorder in spain: global analysis and spatiotemporal heterogeneity analysis. *Sustainable Cities And Society*, 102:104135, 2024.

[222] N. Kiarashi, H. Seitz, Y. Balagurunathan, R. Ha, L. Wilke, K. Gallagher, J. Elmore, M. Duong, I. Bedrosian, H. Rahbar, et al. Quantitative features and radiomic models from low-dose breast ct for breast cancer risk assessment and density categorization. *Radiology*, 307:e231501, 2024.

[223] A. Nguyen, G. Pogoncheff, B. Dong, N. Bui, H. Truong, N. Pham, L. Nguyen, H. Nguyen-Huu, K. Bui-Diem, Q. Vu-Tran-Thien, et al. A comprehensive study on the efficacy of a wearable sleep aid device featuring closed-loop real-time acoustic stimulation. *Scientific Reports*, 13:17515, 2023.

[224] S. Kwon, H. Kim, and W. Yeo. Recent advances in wearable sensors and portable electronics for sleep monitoring. *iScience*, 24, 2021.

[225] Muhammad Zakir Khan, Muhammad Farooq, Ahmad Taha, Adnan Qayyum, Fehaid Alqahtani, Adnan Nadeem Al Hassan, Kamran Arshad, Khaled Assaleh, Shuja Ansari, Muhammad Usman, et al. Indoor localization technologies for activity-assisted living: Opportunities, challenges, and future directions. *Advances in Computers*, pages 59–98, 2024.

[226] W. Hong, H. Lu, and X. Zhao. A survey on the structure of deep convolutional neural networks. *Journal Of Parallel And Distributed Computing*, 113:104–127, 2018.

[227] S. Hong, Z. Wang, L. Zhang, Y. Zhao, Q. Yang, Y. Feng, J. Li, and Y. Liu. Developing tessa: A comprehensive, multi-modal system for sleep staging utilizing wearable sensor technology and machine learning techniques. *IEEE Transactions On Neural Systems And Rehabilitation Engineering*, 27:174–184, 2019.

[228] L. Ren, H. Deng, C. Chen, L. Huang, Y. Guo, X. Wang, Z. Cao, X. Zhu, and X. Xu. Transdermal electrical nerve stimulation (tens) as a treatment modality for sleep disorders: A comprehensive review. *IEEE Access*, 5:11075–11088, 2017.

[229] C. Liu, Z. Dong, L. Huang, W. Yan, X. Wang, D. Fang, and X. Chen. Tagsleep3d: Rf-based 3d sleep posture skeleton recognition. *Proceedings Of The ACM On Interactive, Mobile, Wearable And Ubiquitous Technologies*, 7:1–28, 2024.

[230] X. Liu, W. Jiang, S. Chen, X. Xie, H. Liu, Q. Cai, X. Tong, T. Shi, and W. Qu. Posmonitor: Fine-grained sleep posture recognition with mmwave radar. *IEEE Internet Of Things Journal*, 11:11175–11189, 2024.

[231] T. Fairchild, R. Cooper, M. Curtin, S. Banks, J. Davis, and L. Booker. Through the looking glass: Exploring sleep disorders in asd using wearables and smartphones. *Computer Communications*, 47:17–26, 2014.

[232] J. Deng, W. Dong, R. Socher, L. Li, K. Li, and F. Li. Imagenet: A large-scale hierarchical image database. *IEEE Conference On Computer Vision And Pattern Recognition*, 2009:248–255, 2009.

[233] C. Szegedy, W. Liu, Y. Jia, P. Sermanet, S. Reed, D. Anguelov, D. Erhan, V. Vanhoucke, and A. Rabinovich. Going deeper with convolutions. *IEEE Conference On Computer Vision And Pattern Recognition*, pages 1–9, 2015.

[234] A. Ahmad, K. Abdullah, N. Saad, S. Razak, M. Ismail, and M. Farouk. Deep learning and big data analytics for intelligent sleep disorder recognition. *IEEE Access*, 7:101378–101390, 2019.

[235] M. Hameed, M. Shah, U. Khalil, H. Khan, Z. Rehman, and H. Iftikhar. Pushing the limits of cellular networks for iot connectivity: Challenges, opportunities, and future directions. *IEEE Communications Magazine*, 60:26–32, 2022.

[236] F. Iandola, S. Han, M. Moskewicz, K. Ashraf, W. Dally, and K. Keutzer. Squeezenet: Alexnet-level accuracy with 50x fewer parameters and<0.5mb model size. *arXiv preprint arXiv:1602.07360*, 2016.

[237] R. Krishnaswamy, R. Pooja, and G. Kumar. Disease prediction using machine learning over big data using mapreduce framework. *Journal Of Big Data*, 7:1–20, 2020.

[238] Shalu Shukla. Autism spectrum disorder: Clinical and genetic aspects. *Current Drug Therapy*, 2024.

[239] Kianoosh Kazemi, Arash Abiri, Yongxiao Zhou, Amir Rahmani, Rami N Khayat, Pasi Liljeberg, and Michelle Khine. Improved sleep stage predictions by deep learning of photoplethysmogram and respiration patterns. *Computers in Biology and Medicine*, 179:108679, 2024.

[240] Neha Prerna Tigga, Shruti Garg, Nishant Goyal, Justin Raj, and Basudeb Das. Brain-region specific autism prediction from electroencephalogram signals using graph convolution neural network. *Technology and Health Care*, 33(1):77–101, 2025.

[241] Carmen Berenguer, Inmaculada Baixauli, Soledad Gómez, María de El Puig Andrés, and Simona De Stasio. Exploring the impact of augmented reality in children and adolescents with autism spectrum disorder: A systematic review. *International Journal of Environmental Research and Public Health*, 17(17):6143, 2020.

[242] Muhammad Farooq, Syed Aziz Shah, Dingchang Zheng, Ahmad Taha, Muhammad Imran, Qammer H. Abbasi, and Hasan Tahir Abbas. Contactless heart sound detection using advanced signal processing exploiting radar signals. *IEEE Journal of Biomedical and Health Informatics*, pages 1–12, 2024.

[243] Rajan Jha, Pratik Mishra, and Santosh Kumar. Advancements in optical fiber-based wearable sensors for smart health monitoring. *Biosensors and Bioelectronics*, page 116232, 2024.

[244] Awais Khan, Chomyong Kim, Jung-Yeon Kim, Yunyoung Nam, et al. Sleep posture classification using rgb and thermal cameras based on deep learning model. *CMES-Computer Modeling in Engineering & Sciences*, 140(2), 2024.

[245] Yuxizi Zheng, Zhaocheng Yang, Bing Luo, Ping Chu, and Jianhua Zhou. Continuous respiratory rate estimation approach based on phase features using array radar in home sleeping monitoring. *IEEE Sensors Journal*, 2024.

[246] Charles Dickens. *The posthumous papers of the Pickwick Club*. Carey, Lea and Blanchard, 1838.

[247] Christian Guilleminault and Vivien C Abad. Obstructive sleep apnea syndromes. *Medical Clinics*, 88(3):611–630, 2004.

[248] William C Dement. History of sleep physiology and medicine. *Principles and practice of sleep medicine*, pages 3–15, 2011.

[249] Christian Guilleminault, Frederic L Eldridge, Ara Tilkian, F Blair Simmons, and William C Dement. Sleep apnea syndrome due to upper airway obstruction: a review of 25 cases. *Archives of Internal Medicine*, 137(3):296–300, 1977.

[250] W Whitelaw. Characteristics of the snoring noise in patients with and without occlusive sleep apnea. *Am Rev Respir Dis*, 147:635–644, 1993.

[251] Helen Bearpark, Lynne Elliott, Ron Grunstein, Stewart Cullen, Hartmut Schneider, Wilma Althaus, and Colin Sullivan. Snoring and sleep apnea. a population study in australian men. *American journal of respiratory and critical care medicine*, 151(5):1459–1465, 1995.

[252] Amy Veenstra and Emylene Untalan. Implications and interventions related to obstructive sleep apnea. *Critical Care Nursing Clinics*, 26(4):499–509, 2014.

[253] A Jay Block, Philip G Boysen, James W Wynne, and Lynn A Hunt. Sleep apnea, hypopnea and oxygen desaturation in normal subjects: a strong male predominance. *New England Journal of Medicine*, 300(10):513–517, 1979.

[254] Kingman P Strohl and Susan Redline. Recognition of obstructive sleep apnea. *American journal of respiratory and critical care medicine*, 154(2):279–289, 1996.

[255] Dirk A Pevernagie, Barbara Gnidovec-Strazisar, Ludger Grote, Raphael Heinzer, Walter T McNicholas, Thomas Penzel, Winfried Randerath, Sophia Schiza, Johan Verbraecken, and Erna S Arnardottir. On the rise and fall of the apnea- hypopnea index: A historical review and critical appraisal. *Journal of sleep research*, 29(4):e13066, 2020.

[256] Kiran P Maski, Louella B Amos, John C Carter, Ellen E Koch, Uzma Kazmi, and Carol L Rosen. Recommended protocols for the multiple sleep latency test and maintenance of wakefulness test in children: Guidance from the american academy of sleep medicine. *Journal of Clinical Sleep Medicine*, 20(4):631–641, 2024.

[257] Ahmed S BaHammam, Mahadevappa Hunasikatti, and Seithikurippu R Pandi-Perumal. Current clinical perspective of adult obstructive sleep apnea: Symptomatology, clinical features, and different phenotypes. In *Sleep Apnea Frontiers: Pathophysiology, Diagnosis, and Treatment Strategies*, pages 85–99. Springer, 2024.

[258] Richard B Berry, Rohit Budhiraja, Daniel J Gottlieb, David Gozal, Conrad Iber, Vishesh K Kapur, Carole L Marcus, Reena Mehra, Sairam Parthasarathy, Stuart F Quan, et al. Rules for scoring respiratory events in sleep: update of the 2007 aasm manual for the scoring of sleep and associated events: deliberations of the sleep apnea definitions task force of the american academy of sleep medicine. *Journal of clinical sleep medicine*, 8(5):597–619, 2012.

[259] Brett Duce, Jasmina Milosavljevic, and Craig Hukins. The 2012 aasm respiratory event criteria increase the incidence of hypopneas in an adult sleep center population. *Journal of clinical sleep medicine*, 11(12):1425–1431, 2015.

[260] Madeleine M Grigg-Damberger. The aasm scoring manual four years later. *Journal of Clinical Sleep Medicine*, 8(3):323–332, 2012.

[261] David NF Fairbanks, Samuel A Mickelson, and B Tucker Woodson. *Snoring and obstructive sleep apnea*. Lippincott Williams & Wilkins, 2003.

[262] Winfried Randerath, Johan Verbraecken, Stefan Andreas, Michael Arzt, Konrad E Bloch, Thomas Brack, Bertien Buyse, Wilfried De Backer, Danny Joel Eckert, Ludger Grote, et al. Definition, discrimination, diagnosis and treatment of central breathing disturbances during sleep. *European respiratory journal*, 49(1), 2017.

[263] Raman K Malhotra. Aasm scoring manual 3: a step forward for advancing sleep care for patients with obstructive sleep apnea. *Journal of Clinical Sleep Medicine*, 20(5):835–836, 2024.

[264] Luigi Fiorillo, Giuliana Monachino, Julia van der Meer, Marco Pesce, Jan D Warncke, Markus H Schmidt, Claudio LA Bassetti, Athina Tzovara, Paolo Favaro, and Francesca D Faraci. U-sleep's resilience to aasm guidelines. *NPJ digital medicine*, 6(1):33, 2023.

[265] Christian Guilleminault and Anstella Robinson. Central sleep apnea. *Neurologic clinics*, 14(3):611–628, 1996.

[266] Jeremy E Orr, Indu Ayappa, Danny J Eckert, Jack L Feldman, Chandra L Jackson, Shahrokh Javaheri, Rami N Khayat, Jennifer L Martin, Reena Mehra, Matthew T Naughton, et al. Research priorities for patients with heart failure and central sleep apnea. an official american thoracic society research statement. *American Journal of Respiratory and Critical Care Medicine*, 203(6):e11–e24, 2021.

[267] Shahrokh Javaheri, David M Rapoport, and Alan R Schwartz. Distinguishing central from obstructive hypopneas on a clinical polysomnogram. *Journal of Clinical Sleep Medicine*, 19(4):823–834, 2023.

[268] Willis H Tsai, W Ward Flemons, William A Whitelaw, and John E Remmers. A comparison of apnea–hypopnea indices derived from different definitions of hypopnea. *American journal of respiratory and critical care medicine*, 159(1):43–48, 1999.

[269] G Ernst, M Bosio, A Salvado, E Dibur, C Nigro, and E Borsini. Difference between apnea-hypopnea index (ahi) and oxygen desaturation index (odi): proportional increase associated with degree of obesity. *Sleep and Breathing*, 20:1175–1183, 2016.

[270] Atul Malhotra, Indu Ayappa, Najib Ayas, Nancy Collop, Douglas Kirsch, Nigel Mcardle, Reena Mehra, Allan I Pack, Naresh Punjabi, David P White, et al. Metrics of sleep apnea severity: beyond the apnea-hypopnea index. *Sleep*, 44(7):zsab030, 2021.

[271] Mehran Baboli, Aditya Singh, Bruce Soll, Olga Boric-Lubecke, and Victor M Lubecke. Wireless sleep apnea detection using continuous wave quadrature doppler radar. *IEEE Sensors Journal*, 20(1):538–545, 2019.

[272] Ståle Toften, Jonas T Kjellstadli, Stig S Tyvold, and Mads HS Moxness. A pilot study of detecting individual sleep apnea events using noncontact radar technology, pulse oximetry, and machine learning. *Journal of Sensors*, 2021(1):2998202, 2021.

[273] Jae Won Choi, Dong Hyun Kim, Dae Lim Koo, Yangmi Park, Hyunwoo Nam, Ji Hyun Lee, Hyo Jin Kim, Seung-No Hong, Gwangsoo Jang, Sungmook Lim, et al. Automated detection of sleep apnea-hypopnea events based on 60 ghz frequency-modulated continuous-wave radar using convolutional recurrent neural networks: A preliminary report of a prospective cohort study. *Sensors*, 22(19):7177, 2022.

[274] Sun Kang, Dong-Kyu Kim, Yonggu Lee, Young-Hyo Lim, Hyun-Kyung Park, Sung Ho Cho, and Seok Hyun Cho. Non-contact diagnosis of obstructive sleep apnea using impulse-radio ultra-wideband radar. *Scientific reports*, 10(1):5261, 2020.

[275] Masayuki Kagawa, Hirokazu Tojima, and Takemi Matsui. Non-contact diagnostic system for sleep apnea–hypopnea syndrome based on amplitude and phase analysis of thoracic and abdominal doppler radars. *Medical & biological engineering & computing*, 54:789–798, 2016.

[276] Jonas Alexander Gross-Isselmann, Torsten Eggert, Alina Wildenauer, Sarah Dietz-Terjung, Martina Grosse Sundrup, and Christoph Schoebel. Validation of the sleepiz one+ as a radar-based sensor for contactless diagnosis of sleep apnea. *Sleep and Breathing*, pages 1–9, 2024.

[277] Zhijing Wei, Jiahuan Xu, WenYang Li, Xingjian Wang, Zheng Qin, Jiawei Zhou, and Wei Wang. Evaluation of a non-contact ultra-wideband bio-radar sleep monitoring device for screening of sleep breathing disease. *Sleep and Breathing*, pages 1–8, 2022.

[278] Masayuki Kagawa, Hirokazu Tojima, and Takemi Matsui. Non-contact screening system for sleep apnea-hypopnea syndrome using the time-varying baseline of radar amplitudes. In *2014 IEEE Healthcare Innovation Conference (HIC)*, pages 99–102. IEEE, 2014.